Thermal and Residual Stress Analysis of Welded Joints in Cladded Pipelines

A thesis submitted for the degree of

Doctor of Philosophy

By

Bridget Enoba KOGO

Department of Mechanical, Aerospace and Civil Engineering
College of Engineering, Design and Physical Sciences
Brunel University London, Uxbridge
United Kingdom

April 2021

Abstract

The approach employed in this research in resolving the challenge of welding induced stresses on the dissimilar material joints of cladded pipes and the aftermath of weld is unique in approach compared to other researchers in that the transient heat recorded with high temperature thermocouples (positioned at strategic points) and Pico logger uncovered the trend and rate of heat transmitted throughout the dissimilar material welded joint during welding. This further revealed that the rate depended on the nature of the material, the distance from the weld line, weld axis, weld start, the thermal conductivity of material, phase change and not just the assumed proximity to the heat source. Hence the thermocouple closest to the heat source was not necessarily the first to receive the heat neither received the highest amount of heat compared to the rest of the thermocouples, most especially those placed farthest. This was further validated with the aid of finite element analysis of the welded joint of dissimilar materials and was confirmed for different clad thicknesses.

Butt welding of two dissimilar materials: stainless steel of grade AISI 316 and mild steel of grade CR4 was carried out with the aid of the tungsten arc weld at a voltage of 240v using metal filler elements of A15 copper wire and 304/316 SS filler metals for the carbon steel and stainless steel sections of the weld, at the Brunel University laboratory.

In this thesis different thicknesses (2mm and 12mm) of stainless steel clad in the dissimilar material clad joints has been investigated using scanning electron microscope (SEM), EBSD, XRD and EBSD to examine the dissimilar interface region and carbides in adjacent clads to generate the diffusion interface occurring in the dissimilar welded joint in order to guarantee the structural integrity of the structures for improved product quality and reliability. This resulted in generation of diffusion representation of the microstructural occurrences by reason of the results obtained from the microscopic and macrostructural analysis which stands out from all other authors.

The approach of resolving the thermally induced weld stresses using the Gaussian theorem also differs from the approaches of other researchers and proved effective in the FEA of modelling and validation of both thermal and stress models and with respect to the weld direction. It was discovered from the weld induces direction, the radial and axial shrinkage effects radial shrinkage increase with increasing angle of inclination whereas the axial shrinkage at lower increments differs from those at higher increments of the axial length – cause of creep effect experienced at higher shrinkages.

List of Publications

JOURNAL PAPERS PUBLISHED

1. Kogo, B., Wang, B., Wrobel, L. and Chizari M., Microstructural Analysis of a Girth Welded Subsea Pipe. (2018) *Engineering Letters, 26:1, EL_26_1_23*, 1-10, pp. 193-200.

2. Kogo, B., Wang, B., Wrobel, L. and Chizari M., Thermal and Stress Analysis of Girth Welded Joints of Dissimilar Metals in Clad Pipes: Experimental and Numerical Analysis. (2018) Journal of Offshore and Polar Engineering (IJOPE, OA-22)

3. Guo, Wei; Zhang, Li; Xu, Chao; Chai, Rong; Gao, Zhong; Kogo, Bridget; Mahmoud, Chizari; Zhang, Chuanwei; Wang, Bin. Study on the Wear Resistance of Effects of Laser Cladding Iron-base Alloy by Heat Treatment. (2018) Materials Research Express MRX-110000.R1

BOOK CHAPTER

1. Kogo, B., Wang, B., Wrobel, L. and Chizari M. Residual Stress Simulations of Girth Welding in Subsea Pipelines, (2018) Springer.
2. Kogo, B., Farr M., Wang, B. and Chizari M. Mechanical Modelling of Cylindrical Rings versus Hollow Spheres under Impact Loadings, (2020) Springer.

CONFERENCE PAPERS PUBLISHED

1. Kogo, B., Wang, B., Wrobel, L. and Chizari M. 3D Simulation of Stress in Girth Welding of Pipeline, Thermal Analysis of Girth Welding in Pipeline. Proc of the Third Intl Conf. Advances in Civil, Structural and Mechanical Engineering – CSM 2015 26-27 May 2015 Copyright @ Institute of Research Engineers and Doctors, USA. All rights reserved. ISBN: 978-1-63248-062-0 DOI: 10:15224/978-1-63248-062-0-56.

   Best Student Paper Award *at the International Conference of Mechanical Engineering at the World Congress of Engineering (WCE 2017), Sept 2017, London.*

2. Kogo, B. Wang, B. Wrobel, L. and Chizari, M. Assessment of Weld Overlays in a Cladded Piping Systems with Varied Thicknesses. ASME OMAE – International Conference on Ocean, Offshore and Artic Engineering, OMAE 2019, June 9-14, 2019, Glasgow Scotland, UK, OMAE2019-96348.

3. Bridget Kogo, Bin Wang, Luiz Wrobel and Mahmoud Chizari. Authentication in Welded Clad Plates with Similar Material and Thicknesses Proc of the Eight Intl. Conf. on Advances in Civil, Structural and Mechanical Engineering – CSM 2019 Copyright

 ISBN: 978-1-63248-170-2 DOI: 10:15224/978-1-63248-170-2-01.

4. Kogo, B., Wang, B., Wrobel, L. and Chizari M. Thermal Analysis of Cladded Pipe at a Joint Connection; Proceedings of the UKHTC2017 - 15th UK Heat Transfer Conference, Brunel University London, 4th – 5th September 2017

5. Kogo, B., Wang, B., Wrobel, L. and Chizari M. Thermal Analysis of Girth Welded Joints of Dissimilar Metals in Pipes with Varying Clad Thicknesses. Proceedings of the ASME 2017 Pressure Vessels and Piping Conference ASME PVP 2017-66272; July 16-20th, 2017 at Waikoloa, Hawaii, USA.

6. Kogo, B., Wang, B., Wrobel, L. and Chizari M. Residual Stress Simulations of Girth Welding in Subsea Pipelines, Proceedings of the World Congress on Engineering 2017 Vol II, WCE2017, July 5-7, 2017, London, U.K. pp. 861-866.

7. Kogo, B., Wang, B., Wrobel, L. and Chizari M. Thermal Analysis of Girth Welded Joints of Dissimilar Metals in Clad Pipes; Experimental and Numerical Analysis; Proceedings of the Twenty-seventh International Ocean and Polar Engineering (ISOPE) Conference San Francisco, CA, USA, June 25 – 30, 2017, ISBN 978-1-880653-97-5; ISSN 1098-6189.

8. Kogo, B., Wang, B., Wrobel, L. and Chizari M. Experimental and Numerical Modelling of Metal Rings Subjected To Fixed-End Crush Loading, And Comparisons with Hollow Spheres; Proceedings of the World Congress on Engineering 2019 Vol II, WCE2019, July 3-5, 2019, London, U.K.

9. Kogo, B., Wang, B. and Chizari M. Clamping effect on the Welding Deformations in Dissimilar Welded Pipes (Joints) with Varied Thickness: Axial and Radial Shrinkage ASME OMAE August 3rd – 7th, 2020 (Virtual Conference OMAE2020-18897)

10. Kogo, B., Wang, B., Wrobel, L. and Chizari M. Verification of Stress Model in Dissimilar Materials of Varying Cladded Pipes Using A Similar Cladded Plate Model PVP 2020, July 20th – 24th, (Virtual Conference PVP2020-21694)

Dedication

I hereby dedicate this thesis to GOD the Father, GOD the Son and GOD the Holy Spirit for His invaluable gift of life, health and resources used to commence and finish this research. To GOD alone be all the praise and glory both now and forevermore, Amen.

Acknowledgements

I sincerely wish to express my profound gratitude first of all to the Almighty GOD for Life he's given me for grace and strength to persist in carrying out this PhD as well as for surrounding me with the right people who have made invaluable inputs into this work.

I want to appreciate my Supervisor Dr. Bin Wang for his distinguished supervision, constantly inspiring and motivating me on this research. I also want to thank my second supervisor Prof. Luiz Wrobel for his immense contributions and impeccable mentoring.

At this point I acknowledge Dr Chizari Mahmoud for his tireless effort in seeing to the success of the projects alongside his motivation and for believing in me. Thank you very much.

To my husband Dr Kogo, for standing by me throughout this journey, always calling, providing, and being on the move, believing in me and for his encouragements.

My children Tehila and Emmanuel, for being the best children one could ever wish for. Thanks for your prayers and love and for believing in me. You inspire me to want to do more. I love you and am proud of you. I want to thank friends and family for doing a fantastic job of child minding while I worked on my research.

My Father, Mr C.U Agada, my siblings Mrs Adedoye, Mrs Ejeh, Miss Linda and family, Misters Fidelis, Ode, Abraham and Samuel for your prayers, encouragements and care. I also appreciate My Uncle and his wife Mr & Mrs Ugwoke and family and Mr & Mrs Ejah and family; also Mrs Ayeni, Mrs Okuniyi, Mr Ogah, Mrs Okoye and family and my in-laws too.

All the Lab technicians in the Civil and Mechanical Labs/ workshops: Keith, Guy, Costas, Chris, Paul, Andrew, Ali and constant relentless assistances in the lab work. I also want to appreciate the teams at Experimental technique Dr Lorna, Ashley, Safiyah, and BCAS Prof. Hari, Steve, Sam, Kawther, the computing office for your ingenuity and my colleagues.

Appreciations go to my sponsors: Petroleum Technology Development Fund PTDF for providing the funds with which to carry out this research. To Brunel University London and NSIRC at TWI, Granta Park for the resources and conducive atmosphere to research in.

I would like to acknowledge the Winners Chapel International and my Pastor, Brethren and

Winners Satellite and Campus Fellowships. You have been a blessing and a family.

Table of Content

List of Tables

List of Figures

Glossary and Abbreviations

Symbol	Description
A	Cross Sectional Area of Column (mm^2)
As	Surface Area (mm^2)
α	Co-efficient of thermal expansion (per degree) ($^oC^{-1}$)
a_f	Length of front ellipsoidal of heat source (mm)
a_r	Length of front ellipsoidal of heat source (mm)
b	Half width of heat source (mm)
CMn	Carbon Manganese
б	Stress (MPa)
$б_L$	Longitudinal residual stress (MPa)
$б_1$, $б_2$, $б_3$	Three principal stresses (MPa)
$б_{bol}$	Stefan-Boltzmann constant (5.6703×10^{-8} $Wm^{-2}K^{-4}$)
бh	Anticipated hoop stress in MSR treatments (MPa)
$б_o$	Weld induced residual stress (MPa)
$б_p$	Tensile stress (MPa)
σ/γ	Interphase boundary
σ_s	Sigma phase
$б_r$	Residual stress after MSR (MPa)
$б_y$	Yield stress (MPa)
$б_T$	Transverse residual stress (MPa)
$б_v$	Von Mises stress (MPa)

c	Penetration depth of heat source (mm)
C	Specific heat
D	Material Stiffness
ΔT	Difference between the reference temperature and actual temperature (^oC)
ε	Total strain
ε^{et}	Elastic strain
ε^{th}	Thermal strain
ε_S	Strain components
E	Young's Modulus of Column (MPa)
F	Circumferential Force
F^a	Acceleration force vector
f_f	Fraction of heat in front ellipsoidal of heat source
fr	Fraction of heat in rear ellipsoidal of heat source
h_{total}	Combined convection and radiation heat transfer coefficient ($Wm^{-2}K$)
$h_{convection}$	Convective heat transfer coefficient ($Wm^{-2}K$)
H	Enthalpy of Material (J/Kg)
HFL	Heal flux vector ($W.m^{-2}$)
I	Current (amperes)
K	Stiffness of Column
Kg	Kilogram (kg)
L	Length of Column (m)
L	Plate length (m)

M	Bending Moment (Nm)
mm	Millimetre (mm)
M(r,z)	Scalar multiplier as a function of axial and radial position
m^3	Cubic metre (m^3)
ɳ	Area efficiency (%)
NT	Nodal temperature (^oC)
Θ	Angle from instantaneous arc heat source position (^{o})
Ø	Outer Diameter of Cylinder (m)
Pí	Required internal pressure for MSR
Po	Required external pressure for MSR
ρ	Density of material (Kgm^{-3})
Ǫ	Shear Force (MPa)
q (0)	Maximum flux at the centre of the heat source (Wm^{-2})
q(r)	Surface flux at radius *r* (Wm^{-2})
$q_{convection}$	Heat loss by convection
q_{loss}	Total heat loss
$q_{radiation}$	Heat loss by radiation
Ro	Outer radius of cylinder (mm)
r	Cylinder mean radius (mm)
r_i	Cylinder inner radius (mm)
r_o	Cylinder outer radius (mm)
S	Stress components
Tc	Current temperature at cylinder surface (^oC)

T_{amb}	Ambient temperature (^oC)
TEMP	Element temperature (^oC)
Tm	Melting Point Temperature (^oC)
Tp	Plate thickness (mm)
t	Cylinder Wall Thickness (mm)
V	Voltage (volts)
W	Plate width (mm)
WS	Weld Speed (mms^{-1})
w	Displacement vector of a general point

Abbreviation	**Meaning**
ABAQUS	Modelling Software for Analysis
AE	Energy of the Arc
AISI	American Iron and Steel Institute
API	American Petroleum Institute
AWS	American Welding Institute
AWST	Annealing + Welding + Solution + Temperring
ASME	American Society of Mechanical Engineers
ASTM	American Society of Testing and Materials
ASTM A 106 Gr B Steel	ASTM Specification for Seamless carbon steel pipe for High temperature
BCC	Body Centered Cubic
BM	Base Metal

BS 7910	British Standard code of practise for the assessment of flaws (weld defects) using fracture mechanics
CAE	Computer Aided Engineering
CES	Cambridge Engineering Selector
CM	Clad Metal
CO_2	Carbon dioxide
CONV	Convection
CR4	Cold Reduced Steel
DBTT	Ductile to Brittle Transition
DP440	Dual Phase Steel 440
DP590	Dual Phase Steel 590
EBSD	Electron Backscatter Diffraction
ECA	Engineering Critical Assessment
EDAX	Energy Dispersive X-ray Analysis
EXP	Experimental
FCC	Face Centered Cubic
FCAW	Flux Cored Arc Welding
FDS	Full Data set Correlation
FE	Finite Element
FEA	Finite Element Analysis
FEM	Finite Element Modelling/Methods
FLW	Fine Line Welding
FM	Filler Metal
FZ	Fusion Zone

GB	Gigabyte
GDP	Gross Domestic Product
GGHAZ	Grain Growth Heat Affected Zone
GMAW	Gas Metal Arc Welding
GTAW	Gas Tungsten Arc Welding
HAZ	Heat Affected Zone
HI	Heat Input
hkl	Lattice spacing
HSW	Heat Sink Welding
HSLA	High Strength Low Steel
LME	Liquid Metal Embrittlement
MIG	Metal Inert Gas
MMAW	Manual Metal Arc Welding
MP	Melting Point
MS	Mild Steel
MSR	Mechanical Stress Relieving
MSSS	Mild Steel Stainless Steel Weld
ND	Neutron Diffraction
NPL	National Physics Laboratory
NSIRC	National Structural Integrity Centre
OD	Outer Diameter
PC	Personal Computer
PJP	Partial joint penetration

PM	Parent Metal
PWHT	Post Weld Heat Treatment
PTDF	Petroleum Technology Development Fund
RAM	Random Access Memory
RO	Root Opening
RSW	Resistance Spot Welding
TC	Thermocouple
TEM	Transmission Electron Microscopy
TIG	Tungsten Inert Gas
TWI	The Welding Institute
TZ	Transition Zone
WA	Weld Axis
WCO	World Corrosion Organization
WE	Weld Edge
W_L	Weld Line
WP	Weld Pool
WPP	Welding Process Parameter
WS	Weld Start Position
WSA	Weld Start Axis
WZ	Weld Zone
SAE4130	Type of heat treatable and high strength low alloy metal
SAW	Submerged Arc Welding
SEM	Scanning Electron Microscope
SS	Stainless Steel

TEM	Transmission Electron Microscopy
USA	United States of America
UT	Ultrasonic
UTS	Ultimate Tensile Strength
XRD	X-Ray Diffraction

1 INTRODUCTION

Welding is a fundamental joining technology which has been widely used for joining pipelines in the oil and gas industry. The weld joints are amongst the most vulnerable parts in the structural integrity failure assessments arising from such a system. The thermal and mechanical loading in the process has a profound impact on the integrity of the pipeline over its service life. An accurate and thorough assessment of the process on the associated residual stress and its effect on the structural properties of the pipeline is necessary since the dynamic stress analysis carried out in this research resulted from thermal heating. This primarily calls for understanding the thermal distribution within such a system, even at the time of weld in order to appreciate the changes and stresses induced in the body or such system.

Pipeline failure has been a frequent and severe occurrence around the world as a result of several factors such as ageing pipelines, environmental assisted cracking, corrosion of pipelines and fatigue. All these have posed a great challenge to pipeline operators and there is therefore the need for better design scenario to withstand all these factors. Single walled pipelines do not have sufficient strength to withstand the pressures from the environment, especially in deep offshore operations and also from the flowing fluid within the pipes. One way of solving this problem is to enhance the strength of the pipes with clad. The cladding of pipelines involves technology which enhances the mechanical properties of pipelines, enabling them to perform under stable conditions and prolong their life by improving the operating performance of the pipelines.

As emphasis on health, safety, environment and security issues increases, pipeline operators will need to broaden their focus from the initial feasibility stage right through to operations. A major technical goal of these companies is managing the integrity of pipelines for incident-free

operation. Achieving this will allow them to continue the safe and reliable transportation and supply of oil and natural gas to their customers without adversely affecting people or the environment. Cladding is also used in other industrial practices such as nuclear industry to house fuel pellets and retain fission products, preventing direct contacts between coolant and fuel (Rajan, 2016).

The safety and reliability of subsea pipeline in high consequence/impact areas is a flow assurance and pipeline integrity related project which aims at making the transportation of gas and oil feasible and convenient in all circumstances, if possible.

The ability of man to harness/ optimize the situation begins with the investigation of welding and the aftermath of phenomenal occurrences (thermal and residual stress) which is key to the stability and duration of any pipeline because firstly, no pipeline is designed to be infinitely long in original length and secondly, if a structure is to fail, it will commence from the weakest point - the joint, which in this case is the welded joint.

1.1 Background of Research

Welding is a joining technology used in the fabrication and manufacturing process. The several benefits of welding as a joining technology include cost effectiveness, flexibility in design, enhanced structural integrity (by optimized design as a result of optimized weld parameters, reduced rate of failure and improved product life), and composite weight reduction. However, thermal stress is usually initiated on the weld and the base metal (Lampman, 2001; Goldak, 2005; Youtsos, 2006; Muhammad, 2008). Poorly welded joints result in leakages, pipe failures and bursts, which lead to possible environmental hazards, loss of lives and loss of properties.

The integrity of welded joints in pipelines and structures is crucial whether in the atmospheric environment or the marine environment, as encountered on the seabed of both shallow and deep offshore operations. The welding of cylindrical objects is complex and poses a source of concern in manufacturing processes. There have been attempts made in the past to investigate the weld induced imperfections at research centres and prestigious institutions however, majority of these emphases were placed on prediction of weld induced imperfections such as deformation and residual stresses in plates/ sheet welds and T-joints structures. Limited work and significant contributions (Javadi, 2015; Javadi et al, 2013; Yaghi et al., 2006; Jiang et al, 2011; Sinha et al, 2013; Dar et al., 2009; Feli et al, 2011; Ren, 2016; Ren et al., 2018) were carried out for welding residual stress field distribution and effects on the structural integrity and performance of sheets rolled circumferentially welded thin-walled cylinders and the critical study of these structures is yet to be explored. This calls for immediate attention of complex phenomenon in these types of structures. The optimized design as a result of optimized weld parameters reduced rate of failure and improved product life of cylindrical welded shell structures that are cladded with dissimilar materials – these are the major contributions of this research. Two different thicknesses of the clad are considered and comparison of the performance with respect to the welded joint is explored in this research.

Residual stresses are the internal stress distributions confined within the body of a material. Invariably, they are the stresses remaining in a body after all external forces have been removed. Although there are elastic residual stresses, and residual stresses without plastic deformations such as thermal misfit strains in parts with more than one material or chemically induced misfit strain, because of constraints in the deformation which can be elastic constraint or plastic constraint. In this research, stresses within the body are induced by plastic deformation within the immediate environment of the weld as a result of the heating and subsequent cooling of the clad metal, the filler material and base metal in a quick succession.

Research has shown that when weld-induced residual stress is of same magnitude as the yield stress of a material; it leads to deformation, thereby reducing the reliability of the welded structures (Dar et al., 2009). The issues concerning welding as a joining technology are many and varied. Variables that affect welding such as the weld type, temperature, component thickness and weld travel speed; all impact on the residual stress distributions. The impact of these variables is of key interest to researchers, as they continue to pose challenges to the industry. This is particularly true in regions close to the point of weld, where induced thermal stresses are most sensitive. Other operating factors affect the residual stress distribution in welded joints during service life such as thickness of the parent plate, boundary restraint applied during welding process, heat input supplied by welding (kJ/mm) and post weld heat treatment (Bate et al., 1997).

Many experiments have been carried out in times past to enable a better knowledge of the relationships that exist between the residual stress distributions and weld factors such as melting point of metal, thermal conductivity, coefficient of thermal expansion, reactivity, surface condition and electrical resistance (Ebert, 1974; Frith & Stone, 2015). These experiments can be time-consuming and expensive thereby limiting the level of information that could be obtained about residual stress distributions. Advances made in numerical analysis especially Finite Element Analysis (FEA) or Finite Element Method (FEM) have made it possible for computational evaluations of residual stress distributions relevant to the weld factors either in conventional or intricately shaped engineering materials. In computational schemes it is possible to deploy known physics to bear on the determination of the effects of the above weld variables for most engineering materials towards the total design of structures. In effect, it is possible to properly evaluate residual stresses of welded joints using computational methods, provided it has a RAM of 32GB upwards, storage space of 250 GB upwards for storing and resolving complex geometries, and links to routine libraries of the

relevant physics. This means that the requirement for the computing facility is not fixed but dependent on the size and nature of the model and number of degrees of freedom, whether it is linear or non-linear. It has evolved into more developed platforms which enable most engineering designs to be resolved, such as ABAQUS software.

1.2 Research Motivation

All over the world, the issue of oil spillage on land and marine environments are common occurrences that affect the economic use of land as well as aquatic lives. In the Gulf of Mexico, there are over 17,000 miles of subsea pipelines gathering and carrying oil and gas from offshore wells to platforms and facilities offshore which are regulated by the Office of Pipeline Safety of the U.S. Department of Transportation (under code of Federal Regulations 49 CFR) and Minerals Management Services of U.S Department of the interior (under code of Federal Regulations 49 CFR) which regulates subsea pipelines. The potential significance of leaks in offshore pipelines gives rise to continuous efforts in documenting and reporting as well as analysing failures. Statistics shows that approximately 1000 incidents occurred between 1960 to 1990, out of which 49 % were offshore pipelines due to corrosion and the corrosion induced failures have cause 2% of pollution with no fatalities. On the other hand, failures from maritime traffic accounted for 14% of the failures causing 90% pollution damage and several fatalities. In continued search for cost-effective safety and risk informed criteria design (in a particular case) four limit states are defined – serviceability (normal operation), ultimate (leak tightness), fatigue (crack propagation) and accident (rupture) (Antaki, 2005).

Pipeline Hazardous Materials Safety Administration (PHSA) in 2010 reviewed several projects constructed in 2008 and 2009 with 20-inch or greater diameter grade X70 and higher line pipe in which the metallurgical testing results of failed girth welds in pipe wall thickness transitions

revealed pipe segments with misalignment of the pipe weld, improper bevel and wall thickness transitions, improper back welds and improper support of the pipe and appurtenances (Pipeline and Hazardous Materials Safety Administration, 2010).

The restoration of ecological balance after oil spillage is normally associated with high cost of the clean-up operation and soil remediation. In Nigeria, pipeline bursts, oil spillage and consequent fire outbreaks have taken its toll on human lives, destroyed properties and have had a profound effect on the natural ecology. These pipeline bursts include those carrying refined petroleum products to the upper regions of the country and numerous incidents in the Niger Delta area carrying crude oil. Table 1.1 shows some notable pipeline disasters witnessed in Nigeria and the casualty figures (Newswatch, 2006). The majority of these oil pipeline bursts are traceable to defects in welds and or corrosion. It is possible that relative matters of pipeline integrity relative to the variables that affect weld joints may not have been properly considered *ab initio*.

The prevention of these kinds of disasters is only possible through the curious determination of all variables that are involved in the design of pipeline integrity. This study is focussed on pipeline integrity with the aim of looking at two extreme design scenarios of thick and thin clads of pipeline welds. Improvements in pipeline integrity have been developmental, particularly with the availability of design software using digital computers. This enables structural shapes to be correctly evaluated using relevant physics prior to welding. Given that most of the pipelines in operation are ageing and could have been victims of poor weld design considerations, it is of research interest that weld design variables be properly considered through simulations and correlated to experimental works to see agreements in failure occurrences. Due to confidentiality of court cases currently ongoing with regards to failed welds, evidence is kept confidential. Weld temperature and weld thickness are considered to have a profound effect on the integrity of welds because they affect the strength of the material.

Depending on the heat intensity of the weld, it can affect the material property. Weld consumables have significant effect in determining the level of strength and integrity of the weld.

Table 1.1 Some Notable Nigerian Pipeline Disasters – Failures

	Date	Location and Estimated Casualties
1	May 2006	At least 150 killed in Lagos
2	December 2004	At least 20 killed in Lagos
3	September 2004	At least 60 killed in Lagos
4	June 2003	At least 105 killed in Abia State
5	July 2000	At least 300 killed in Warri
6	March 2000	At least 50 killed in Abia State
7	October 1998	At least 1, killed in Jesse

Secondly, stress from welding is one of the bases for cracking and fracture in welded pipes. Prior to determining the crack propagation factor, it is expected that the stress should be determined and known, that is where this research finds relevance.

There is the need for better design factors and enhanced weld scenario, as well as cladding to withstand a corrosive environment. Statistics from the International Energy Agency (IEA) show that over 50% of the world's gas fields are very corrosive and up to 70% of the residual oil reserves comprising of crude oil contains a significant amount of carbon-dioxide (CO2) and sulfur which is corrosive, hence the need for long lasting pipes with six times its original life span (Miller, 2013).

1.3 Aims and Objectives

The aim of this research project is to achieve a good knowledge of the relationship and the variations between the thermal effects and residual stress distribution in cladding pipes.

In carrying out this research the following objectives are being pursued:

To resolve the intricacies of the heat transmission in the welded joints of dissimilar materials during Narrow gap GMAW welding of thick section materials.

To resolve the modelling problem for multiple (seven) weld passes of narrow gap welding of thick sections of dissimilar materials joints by developing different models of the thermal weld passes. The modelling problem is interpretation and representation of thermal heat and residual stresses in the dissimilar material joints of the welded blocks and geometries using simulation since every modelling is unique according to the perception and understanding of the researcher and the approach to resolving the simulation is also unique.

To resolve the modelling problem for residual stress distribution in (multiple) seven weld passes of Narrow gap welding of thick sections of dissimilar materials joints by developing different models of residual stress profiles of the welded joint in 3D pipe strip, 2D Plates, 3D clad pipe and clad plates.

To gain better understanding of the effect of heat input on the mechanical properties and microstructures evolution of welding of dissimilar material joint with recurring reheating.

Understanding the effect of solid-state phase transformation on the residual stresses of the dissimilar material joints of weld with respect to two different clad thicknesses.

In summary, the above objects will be practically carried out via the following procedures:

I. Studying the effects of weld in order to understand the thermal analysis – especially in clad pipes

II. Discovering the effects of thermal and residual stresses in dissimilar joint welds of clad pipelines

III. Studying and discovering the occurrences on the HAZ of the welded joints of dissimilar materials – to investigate the reheating occurrences at the weld zone.

IV. Determining the weakest point of burst of the welded dissimilar material joint

V. Carrying out Finite Element Analysis (FEA) and Simulation of weld by the:

a) Developing of 2D axis symmetric and 2D finite element models of pipes and plates for thorough examination of the thermal and residual stresses of the welded structure.

b) Creating of a 3D Strip model of the Pipe for the studying of the thermal and residual stress analysis and distortions.

c) Creating of a full 3D Pipe model and 3D Clad pipe and plate model for further analysis of the thermal and residual stress distributions.

VI. Understanding the heat distribution during the welding process and its influence on the thermal stress formation via weld experiments and mechanical testing and laboratory investigations as well as FEA simulations.

VII. Understanding the effect of microstructure on the mechanical performance of welds – recognizing the microstructural differences at the various weld regions: Heat Affected Zone (HAZ), Fusion Zone (FZ) and Parent Metal (PM) via examining the microstructures under different laboratory tests such as Electron microscope; SEM analysis XRD, EBSD and EDAX.

1.4 Research Methodology

The research methodology employed in this research is combined FEA simulations of the various welds listed above and experimental welding backed up by mechanical tests and laboratory analysis as reported in this thesis. This entails a traditional arc weld process for joining two plates of differing thickness and materials together, carried out in the departmental laboratory at Brunel University, London. Two mild steel plates of 150 mm by 100 mm of 10 mm thick, and two same sized stainless-steel plates of 2 mm thick were welded together along the 150mm line in multiple passes of 4 with a specific filler element: 304/316 filler wire for the Stainless Steel and A15 copper wires for the mild steel. Heat thermocouples are placed at different positions away from the point of welding according to the thermal results and plot of thermal analysis. Measurements are taken at 10, 20 and 30 mm from the weld line in both the stainless steel and mild steel plates.

1.5 Main Contribution of this research work

In spite of the fact that welding is one of significant processes of fabrication in the engineering industries, there is limited scientific understanding currently in productivity measurement and evaluation of welding processes. Since it is a manufacturing technique, welding provides a number of technical challenges to the welding community specifically the shop floor engineers involved in manufacturing of structures integrated through welding such as cladding. While joining components of structure together, via welding, the highly localized thermal gradients from welding result in high amount of stresses of the order of yield strength of the material within and around the weld vicinity causing significant deformation of the structures to be welded which in this case are dissimilar material clad. The weld residual stress and deformation can significantly affect and hinder the performance and reliability of the welded cladded

structures. Welding of clad pipes can result in a variety of complex microstructures due to the presence of dissimilar alloys. The difference in chemical composition and thermal properties will influence the integrity of the welded joint and can result in a crack susceptible microstructure. This calls for the need to critically investigate the residual stresses from the welding of these cladded dissimilar metals during the design and manufacturing phases in order to guarantee intended in-service use of the welded structures (Dar et al, 2009; Javadi, 2015; Javadi et al, 2013; Yaghi et al., 2006; Jiang et al, 2011).

The contribution of this research is the investigation of the thermal phenomenal occurrences and stresses induced in the welded joint of the dissimilar material clad (double layer) as compared to same material joints and also the single weld layer of pipe welds which is the predominant manner of welding in pipeline industries – with respect to different clad thickness and especially examining the effect at the heat affected zones of the dissimilar welded joints. The need to investigate the recurrent reheating which takes place within the base metal and clad metal during the welding is very key. Investigating the recurrent reheating of the weld layers, intricately unveiling the occurrences at the dissimilar welded joints microscopically and macroscopically in order to explain how the findings enhance the performance of the welded joints. The approach utilized in carrying out the FEA modelling is unique from other authors; the FEA design of the welded joint is also different from previous authors. The high temperature thermocouples employed alongside pico-logger used for measuring the thermal responses and the thermal representation of transient heat which is synonymous to the rate of heat transfer during the welding process as well as the validation using the experimental data. There is the diffusion representation of the microstructural occurrences by reason of the results obtained which stands out from all other authors.

Efforts have been made in the past to examine weld induced weld imperfections in different universities across the globe and the emphasis have been on the determination of weld imperfections such as deformations and residual stresses in sheets single layer, T-joint structures, single layered pipe and same cladded material. Few significant contributions towards weld residual stress distribution and its effect on the performance and structural integrity of dissimilar material cladded pipes and the thorough investigation of this structure has not been fully discovered. As a result, the complex phenomena of welding and after math of welding in these types of structures both at macroscopic and microscopic scale requires urgent attention and focus of researchers to guarantee the structural integrity of the structures for improved product quality and reliability. It is expected that the method of approach using FEA, optimized weld parameters, reduced failure rates, improved product life are the major contributions from this research.

In this thesis different thicknesses (2mm and 12mm) of dissimilar material clad joints has been investigated using scanning electron microscope (SEM), EBSD, XRD and EBSD to examine the dissimilar interface region and carbides in adjacent clads to generate the diffusion interface occurring in the dissimilar welded joint to guarantee the structural integrity of the structures for improved product quality and reliability.

High corrosion resistant materials such as stainless steel possess good strength and are tough. Cladding provides corrosion resistance. The use of a clad layer on a base metal helps reduce the cost enhancing manufacturing outcome (TWI, 2007).

The thickness of a clad layer usually varies from 2mm to 20mm and finds use in different welding techniques such as Gas metal arc welding (GMAW), manual metal arc welding (MMAW), submerged arc welding (SAW), flux cored arc welding (FCAW), laser deposition and gas tungsten arc welding (GTAW) (Smith, 1992; Smith, 2012; Davies, 1994; Frenk et al., 1997, TWI, 2016). The clad (which in this case is a stainless-steel layer in the interior of the

pipe) provides the required resistance to abrasion, corrosion and oxidation, whereas the carbon steel is the base metal of the outer pipe and supplies the strength, increased thermal conductivity of the overall structure as well as ‘fabricability’. Refer to Figure 1.1 below.

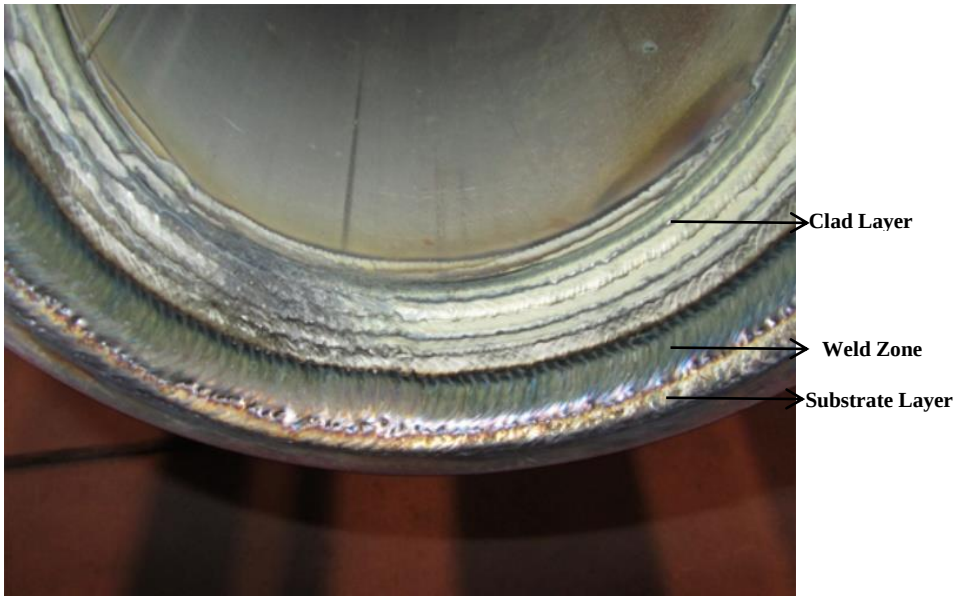

Figure 1.1Cladded Pipe Weld (TIP TIG, 2019)

The contribution of this research is seen in addressing the welding between two dissimilar material joints. It is obvious that the demand for reliable long-lasting and very safe engineering facilities, mode of operation and working environment are in high demand in every industrial application. This spurs the need for joining dissimilar metals with the main aim of achieving enhanced and improved components with better mechanical and thermal properties (qualities), lightweight and outstanding performances, as well as prolonged in-service life for such facilities (Kah & Martikainen, 2014). An outstanding and effective weld between dissimilar metals therefore is one in which the strength of the weld equals the weaker of the two metals being joined. This invariably means great tensile strength and ductility to prevent failure in weld joint. This kind of desirable weld output can be achieved via several welding procedures, which will be discussed in-depth in chapter two (Materia, 2006).

It is of great importance to guarantee the integrity of the HAZ and the clad metal while ensuring the material properties of the base metal. Invariably, the metallurgy of the clad metal and base metal must be clearly understood. Since dissimilar metal joint is a major contribution to research at the fusion zone (FZ) and (HAZ), there is change in the structure and array of grains and chemical composition of the clad metal and base metal as well as the introduction of new elements from the filler metals. This then alters the chemical composition of the newly formed structure even more. All the above occur by reason of the increase in heat supplied to the weld metal in the course of welding, which subsequently alters the chemical composition, hence producing new compounds with different properties and microstructural array. In this research, the clad metal is the stainless steel AISI 316 and the base metal CR4 is carbon steel. The filler metals are 304/316 filler wire and A15 Copper wires respectively.

There is the tendency for the base metal (also known as substrate layer) to dilute the clad metal (clad layer) therefore altering the corrosion resistance of the cladding. This calls for care while carrying out the welding. The age of low-cost and residual oil is gone. An account by the International Energy Agency states that seventy percent (70%) of the world's reserve is made up of crude oil (consisting of high CO_2/ CO_2 or sulphur levels), which demands the use of corrosive material of a very high quality and standard. Data also shows that over fifty percent (50%) of the world's gas reserves are very corrosive, which calls for the use of clad pipelines for transportation. (Miller, 2013). From a world economic view and analysis, corrosion costs a huge sum of money to treat. The World Corrosion Organization (WCO) last quoted it at $2.2 trillion (roughly 3 percent of the world's GDP). One trillion dollars which is equivalent to 45 percent of the annual cost of corrosion is allocated to the petrochemical, oil and gas sectors. There is a huge request for material that can withstand challenging operating environments such as greater corrosion, higher pressures, greater tear and increasing temperatures. The use

of corrosion resistant clad pipes with higher strength and toughness is the best option in such cases.

Advanced clad techniques in pipelines not only enhance the life span of the pipelines but reduce downtime and expensive repairs. This in turn saves several hundreds of thousands of dollars in hourly lost profits. Finally, it decreases emission to a minimal rate hence elongating the life span of the pipe by a factor of six times its original (Miller, 2013).

1.6 Significant contributions and gaps covered in this research

In carrying out this research additional information has been obtained in uncovering the fact that further understanding on the continuous reheating at the welded joint is required. Also investigating the trend of transmission heat and confirming that the welding is independent of the path travelled. Finally, new, and more specific systems have been developed which are applicable to both pipe and plate. (Kursun T., 2011; Sun, 2012; Jiang, 2013; Steel, 2016; Acar, 2017; Roa, 2004; Shin, 2012; Dean, 2006; Bate, 2005; Di Gioacchino, 2015; Lakshminarayanan, 2010; Das, 2016; Feli et al, 2012).

Ren (2018) investigated the residual stress in narrow-gap multi-pass X65 pipe steel girth weld in as welded condition and after global and local post weld heat treatment procedures using neutron diffraction technique. While Yao focussed on the post heat treatment of only one material configuration and compared results with 2D FEA model of the weld (Ren, 2018), this research focussed on 3D FEA model of the weld investigating the fact that recurrences of re heating took place via the different clad thicknesses and also studied that over two different clad thicknesses of dissimilar material welded joints.

The suggestion for further work no 4 in the research above, stated as follows: The work can be extended to a wider scope. As only one material configuration was studied in this work, the findings regarding the residual stress distributions and magnitudes in narrow-gapped multi-pass pipe spool before and after furnace/local PWHT weld were not sufficient to be standardized for general (narrow-gapped weld) cases. It is suggested to perform large numbers of residual stress evaluation on girth welds with various thicknesses or R/t ratio values to provide related residual stress profiles in BS7910 and R6.

The above has been carried out in this research. The neutron diffraction measurements of residual stresses will be considered as future work to be done on different clad thicknesses.

In order to verify the outcome of the PWHT carried out at the welded joint, neutron diffraction measurements of residual stress were employed (Ren, 2018). To further verify and prove the existence of continuous reheating occurring within the welded zones of the dissimilar material joints in this research, further microscopic lab investigations of the weld macrostructures were carried out and the results truly confirmed the fact that continuous reheating took place throughout the welding process and at the welded joints of the dissimilar materials. This was also confirmed from past findings of researchers on reheating occurrences for post welds.

If there exists continuous reheating at the welded joints and of interest in this research, within the dissimilar material joints of the weld; it calls for the need to investigate the manner, nature and especially trend of the distribution of heat that was transmitted during the welding of the dissimilar welded joints (how that it was dispersed within the joint) especially because heat input will introduce residual stresses at the welded joints.

As recommended in the R6 procedure, in order to obtain representable analyses, it is preferable the material properties up to melting point (Tm) are measured instead of using literature values. This can be applicable for both temperature-dependent thermal and mechanical properties.

With the aid of FEA modelling, factors such as transient heating and cooling curves were developed and compared with the measured values and it was discovered that a good agreement existed to verify the trend of heat distribution within the welded joint. Also the 3D FEA model of the stress distribution in the different clad thicknesses of the dissimilar welded joints were simulated in a model to predict the post-heat treatment residual stress and this had similar stress distribution both in the pipes and through the thickness models of the post-heat treated samples.

Due to the limited availability of material, equipment and cost, the study on local reheating in the dissimilar material joints cladded only examined the effect of (heating) and weld macrostructures as well as 3D FEA simulation (Kursun T., 2011; Sun, 2012; Jiang, 2013; Steel, 2016; Acar, 2017; Roa, 2004; Shin, 2012; Dean, 2006; Bate, 2005; Di Gioacchino, 2015; Lakshminarayanan, 2010; Das, 2016).

In the FEA simulation, the reading and stress distribution along the weld direction have been shown to be independent of the order in which the weld is carried out unlike the findings obtained in past literature such as (Feli et al, 2012).

1.7 Outline of Thesis

This thesis is divided into six chapters as listed below:

CHAPTER 1: Introduction

This chapter illustrates the significant contributions of the research alongside the relevance of the research. It points out the thermal effects of welding as it concerns the HAZ and also the residual stress induction and distortions which occur in plates and circumferentially welded pipe joints or cylinders as well as the factors that inspired the research. If a pipe is to fail, it begins at the weakest point, which is the welded joint. This is fundamentally the inspiration

behind this research – the failure of pipeline welded joints. The aims and objectives of the research are clearly pointed out alongside the layout of the research.

CHAPTER 2: Literature Review

Work that has been previously done is discussed in this chapter. It portrays findings and contributions to the situation and shows the challenges that arise with pipeline failure, clad and weld joints. The evolution of FEA in this trend of research and findings is also highlighted. The effects of weld parameters on the Fusion Zone (FZ) and HAZ are also enumerated, as well as live cases of pipes bursting. They have been thoroughly studied and highlight the key factors behind the failures.

CHAPTER 3: Experimental Studies

This Chapter describes the experimental laboratory work carried out in this research. Ranging from the actual welding processes right through to clarifying the approach to tackling these challenges encountered in welded pipeline joints and clad joints. This was further followed up by undertaking some mechanical tests such as the Charpy impact, indentation and tensile, as well as laboratory analyses on SEM, XRD and EDAX. All the tests and microscope analyses are discussed under the three major subheadings of methodology, results and discussions. The experimental setup for welding, precautions taken (safety standards) and array of thermocouples as well as heat recorded. The results obtained from the above experiments described in chapter three were clearly presented in tables and with figures, charts and graphs. Special care was given to details of how the different results complement each other and further verified the findings and expectations from the research. It is important to note here the practical demonstration of how the weld parameters affect the (FZ) and especially, the (HAZ).

CHAPTER 4: Thermal Analysis (FEA)

The thermal effect of welding is discussed in this chapter. The result of the FEA thermal analysis of the pipeline and plate are discussed and plots of transient thermal cycles and axial temperature distributions displayed. The plots of temperature versus time are also plotted. Beginning with the FEA Simulation carried out with the Abaqus software the comparison of the FEA thermal cycles and those of the weld experiments carried out in the laboratories and weld parameters are displayed and further analysed.

The geometries were considered, as well as the material properties and choice of meshing.

CHAPTER 5: Stress Analysis (FEA)

The technique of structural analysis, as well as boundary conditions applied, are discussed. Contains the plot of the residual axial stresses at different cross sections both on the external and internal surfaces of the pipe strip, pipes and plates. Validation of simulated residual stress results using measured stress results in plates and pipelines. Welding distortions are mentioned briefly. Welding residual stress fields and axial stress fields are displayed using FEA.

CHAPTER 6: Discussion and Conclusion

Discussions and interpretations of both experimental findings and FEA results (to prove the validity of thermal and residual stresses within clad pipes and plates), a summary of key findings within the research, suggestions for further work, and conclusions are all highlighted here.

2 LITERATURE REVIEW

2.1 Introduction

The chapter on literature review discusses the heat effect of welding and microstructure, advancement in high strength steels and their relevance both in offshore operation - subsea pipelines and structures in general. It also expatiates on the different techniques of joining with particular focus on welding of high strength steels, residual stresses and the techniques involved in its measurements, cases of weld failure and finite element analysis, simulations of welding in both clad and non-cladded plates and pipes as well as contributions by this research. It further uncovers the failure scenarios and the experimental and numerical simulation in plates and also in pipes; dissimilar material which is the research focus, alongside the deformation in welding and welding techniques, will also be discussed. The advantages in the choice of weld utilised was also discussed, as well as the principles governing the different techniques and choice of methods employed both in experimental and simulated stages of this research.

The need for clean energy and transportation of higher volumes of oil and natural gas via high pressure steel pipelines have resulted in demand for large quantity of steel for fabrication and installation of many pipelines all over the globe (Hwang et al, 2005; Zhao et al, 2011). Pipelines have also been in extreme conditions and environments like the artic, seismic regions and permafrost where high performance line-pipe steels with high strength, good weldability, superior corrosion resistance and low temperature toughness are promising candidate materials for fabricating pipelines (Shin et al., 2007; Hashemi & Mohammadyani, 2012; Kolhe & Datta, 2008). As a result, HSLA line-pipe steels have evolved from X60, X70 to currently X80 and X100 grades (Asahi et al., 2004;Yan et al., 2009; Fairchild et al., 2004; Koo et al., 2004; Asahi et al., 2004) in the last decades. These pipelines undergo internal pressures up to 15 MPa and higher in low ambient temperature of -40 ^{o}C and lower (Hwang, 2005). These applies to X70

steels with wall thickness up to 40 mm and for X80 and X100 line pipe with wall thickness of 25 mm and below (Bai & Bai, 2005; Koo et al, 2004). Increasing the operating pressure while using thinner pipelines implies reduction in fabrication and transportation costs (Shin et al., 2007; Hashemi & Mohammadyani, 2012; Hwang, 2005; Kolhe & Datta, 2008).

With the progress in mechanical properties of steel and methods of production such as thermo-mechanical control processing, quenching and tempering processes, high strength steel structures have found variety of applications because the properties of high strength steels and high-performance steels have availed engineers innovative solutions to fabricate enhanced and economical steel structures.

Examples of high strength steel which have been utilized in building notable structures in different geographical locations include Sony Centre in Germany which employed the S460 having a nominal strength of 460 MPa and S690 having a yield strength of 690 MPa; the Beijing Bird's Nest Olympic Stadium using steel with yield strength of 460 MPa and the Star City hotel and Latitude building in Sydney Australia employed steel products with the yield strength of 690 MPa (Shi et al., 2014). Other structures around the globe include Freedom Tower in New York French cable-stayed road bridge Millau Viaduct (Qiang et al., 2012; Kitada et al., 2002; Gao et al., 2009).

2.1.1 Offshore Pipelines

The current trend in onshore pipelines is towards line pipe such as grade X70 with a wall thickness of up to 40 mm, this is however too thick for offshore applications because installation will require bending and deforming of the pipe. The thickness of pipe wall ranges from 15 – 25mm in the North Sea because the water depth is partially low. Also, in the North Sea, a large offshore pipeline project in grade X70 is operated by Statoil which connects Karsto,

Norway with Dornum, Germany being 600 km long and having a dimension of 42 in. OD and 25 mm to 30 mm wall thickness. In 1990s Europipe finished the development of grade X80 pipe 48 in. OD and 18.3 mm to 19.4 mm wall thickness for offshore pipelines and the use of commercially manufactured large diameter X80 pipe for long transmission pipelines has been verified (Bai & Bai, 2005).

Series of pipes in offshore application have been supplied for qualification testing with regards to laying of pipe and with the help of a joint industry project referred to as EXPIPE, the engagement of X80 line pipe for export pipelines was approved (Bai & Bai, 2005).

Low alloy steel pipelines such as X65 is the current material employed for operating in sour service (Bai & Bai, 2005), therefore with the aid of chemical composition during the fabrication of the steel, the formation of nucleation sites for hydrogen-induced cracking (HIC) is prevented. Currently, the trend in production depicts great potential for the development of higher grades up to X80 for slightly sour conditions (Bai & Bai, 2005).

Grade X70 is being utilized for high transmission lines in several countries even for high pressure transmission lines on land. Suppliers include Sumitomo for Canada, Malaysia and Bangladesh; Nippon Steel for USA, UAE, Columbia and Malaya and NKK for Canada and Vetco Gray. In addition to the above, a pipeline project installed in July 1997 for BP in the North Sea, entailed laying grade X70, subsea pipeline 74 km long and 24-in. OD pipeline having a wall thickness of 25.8 mm (Bai & Bai, 2005). Britannia also laid a subsea pipeline in the North Sea same period having dimensions of 190 km in length OD of 28 in. and wall thickness of 17.5 both of which were welded using the Passo GMAW (Bai & Bai, 2005). Passo is the latest development of automatic GMAW/FCAW welding system designed for both onshore and offshore pipeline construction (S and J lay) and the main highlights and advantages of this is high weld quality and repeatability controlled by a customized software in real time all welding parameters (Bai & Bai, 2005). Shell Oil Mensa installed an offshore subsea pipeline

in the Gulf of Mexico in 1997 having dimensions of 100 km long and an OD of 12 in. with wall thicknesses of 19, 21 and 32 mm which was installed using phoenix mechanized GMAW with shaw mechanized UT and likewise the subsea Norfra pipeline in the North Sea has an OD of 42 in. and is 840 km long (Thorbjornsen et al, 1997; Bai & Bai, 2005).

The density of the structure determines the weight which is vital in ascertaining weightlifting structures such as crane since there is a strong drive in the crane manufacturing industry to increase the loading capacity. High strength steels which are suitable materials for cranes enables lighter and more slender structures which reduces the dead weight of cranes efficiently enhancing loading capacity and economic consumption of fuel (Shen et al., 2012; Khurshid et al., 2012). The use of high strength steel also contributes towards cost savings on design of lighter cranes with less material consumption and utilization hence reducing fabrication costs (Siltanen et al., 2015; Zhang et al., 2012).

2.2 Manufacturing Processes of Cladded Pipes

In dissimilar material clads, two major type of bonding are being employed – metallurgical bonding and mechanical bonding. The former entails the use of chemical bonding between a substrate and a coating area that a close proximity and contact or diffused evenly example laser cladding (Xu et al., 2015). Heat treatments by post spraying dispersions are employed to augment this bond. Metallurgical bonding can further be grouped into Ferrous metallurgical bonding and non-ferrous metallurgical bonding. While Ferrous bonding incorporates the technique and alloys that are iron-based and is responsible for 95 % of worldwide metal production known as black metallurgical bonding; non-ferrous metallurgical bonding comprises of alloys and processes based on varieties of metals and is referred to as coloured metallurgy. Metallurgical bonding establishes the balance between the two different materials

being bonded together using the following specific properties – strength, corrosion resistance, toughness, fatigue resistance, weight, hardness, performance in extreme temperatures and cost. Cladded metal pipes are manufactured via techniques that entails joining of a tube blank and a coaxially disposed pipe section received therein and subsequently the combination of an extrusion of resultant tube blank pipe to create an internally clad pipe of required specification. With internally directed pressure the pipe section inserted into the tube blank is radially expanded simultaneously, following the application of axial force in order to maintain the expansion of pipe section after the extraction of the applied internal pressure, and axial force. A completely fabricated pipe is formed via a combination of mechanically joined tube blank pipe hence it is fully fabricated to form a finished pipe of exact specification containing diffusion bond in between material layers consisting the internally clad pipe which refers to both pipe section and tube blank.

There are several processes of manufacturing cladded metal pipes and internally clad metal pipes. These include extrusion, centrifugal casting, roll welding and internal-pressure plating.:

1. Extrusion – involves inserting a metallic inner pipe known as clad into a metal pipe such that an alloy which possesses low melting-point is plated onto the internal circumferential surface of the outer pipe acting as a bonding device. Next is the evacuation of the bonding surface by heating intermediate space between both pipes to 1100 ^{o}C such that the bonded metal alloy melts and diffuses between the two pipes. The pipe combination is then hot-extruded (U.S. Pat No. 4,744,504, November 4, 2003).

2. Centrifugal casting – entails the casting of molten metal into a metal pipe mounted on bearings which rotates about its axis, distributing the molten metal evenly across the internal circumference and along the length of the metal pipe during its rotation.

3. Roll welding – This technique entails the bending of roll-clad metal plates to form a pipe which is welded together along the longitudinal axis (USA Patent No. 5,940,951, August 24, 1999).

4. Internal-Pressure plating – This is the insertion of an internal thin walled pipe known as internal cladding into a metal pipe and by reason of internal pressure, this is further pressed onto the inner circumferential surface of the outer pipe German patent 4,406,188 (Rhoden, 27 October 1943)

In each processing there are several manufacturing stages which makes the overall cost of fabrication expensive and less competitive when compared with the costly conventional cladding, however the ultimate goal is to simplify the fabrication procedure for cladded pipes such that corrosion resistant solid monowall pipes in order to attain an affordable price and also to ensure that the fabrication of clad pipes and internally cladded pipes is fundamentally alloys of metal and metals. Cladding usually entails the interior conveys the end product or fluid and it is corrosion resistant stainless steel or nickle based alloy while the exterior is made up of material such as carbon steel or low alloy steel and in some cases similar material. Cladding can be double layered or more, although best practise entails cladding is a single layer. There are some cases where cladding in pipe is made of low material such as carbon steel; it is advisable that the interior of the pipe be made of higher quality material such as stainless steel. There is therefore the application in fabrication whereby a cladded pipe is a single layer internally clad pipes and the procedures for this fabrication of clad metals are as follows (USA Patent No. 5,940,951, August 24, 1999):

1. Pipe section having shorter length and greater wall thickness in comparison with the final product which eventually becomes the coating of the clad is inserted into a tube blank of equal length with the pipe section and having an external diameter which corresponds to the internal diameter of the tube blank and also of equal great thickness as the final product. It is observed

that the pipe section fits accurately after matching the opposite circumferential surfaces of the tube blank and the pipe sections to be metallically bright.

2. Placing the pipe section subject to internal pressure such that it fits flush on the inner circumferential surface of the tube blank, dispelling the air between the tube blank and pipe section so that the pipe section is also (upset) in the axial direction.

3. The combination of the pipe formed from the tube blank and the upset and expanded section of the pipe is heated in one motion to the ultimate and required specification. (USA Patent No. 5,940,951, August 24, 1999)

2.3 Heat Effects of Weld

The process of carrying out welding using an arc welding process entails melting down the base metal. In this research, it also involves melting down the clad metal. During the course of carrying out the welding, filler metals are also melted, such that the solution formed by heating up all these materials and holding them at that range of temperature long enough to permit the diffusion of constituents into this molten solution and cooling down rapidly in order to maintain these constituents within the solution. The aftermath of this procedure generates a metallurgical structure positioned in-situ the material which supplies superior tensile strength. The bulk of the material immediately after the fusion zone which has its characteristics altered via the weld held is termed Heat Affected Zone, denoted as HAZ. Figure 2.1 (below) shows how the volume of material within the HAZ undergoes considerable change. This can be advantageous to the weld joint, but also non-beneficial in some circumstances.

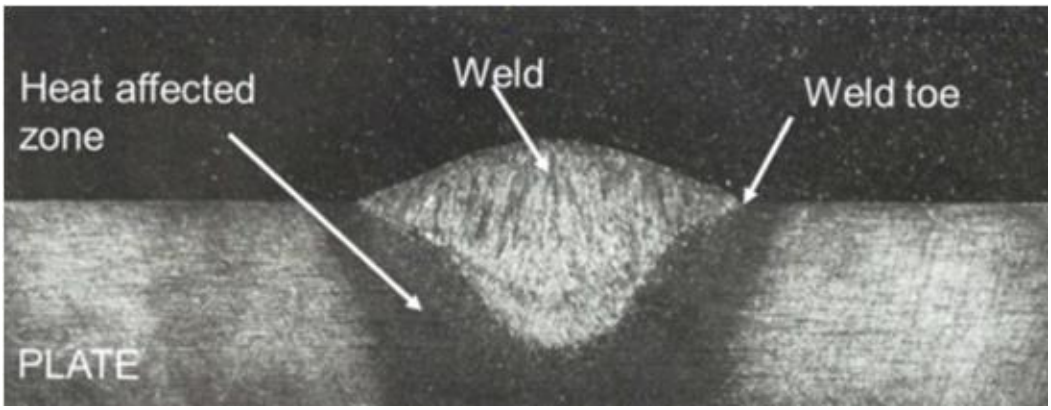

Figure 2.1 Heat affected zones as viewed under an electron microscope. This a single layer weld and shows a cross-section of the HAZ (Menon, 2017)

The findings and relevance are focussed on the heat affected zone and the effects of the thermal analysis on the heat affected zone, as well as the effect of the thermal and residual stresses on the heat affected zone. The heat-affected-zone (HAZ) is a region of the base metal which undergoes alteration in its metallurgical properties even though not melted, by high thermal energies during welding or high heat cutting. The HAZ which has differing lengths, depths and widths also differs in areas of severity (affected by heat), undergoes the heating and cooling cycles, which in turn generates the changes in the HAZ. These changes could be metallurgical in which case; they induce stresses that subsequently reduce the strength of the material, or generation of nitrides within the HAZ affecting the weldability. The profile of hardness varies across the HAZ and the microstructure and consequently, corrosion resistance or cracking (Milella, 2013; Du Toit et al., 2006; Lau et al, 1985; Taniguchi & Shigesato, 2015; Mithilesh et al, 2013; Lu et al, 2011). During welding the precipitation of carbides at grain boundaries in a stainless-steel or alloy causes it to become susceptible to intergranular corrosion. This is known as sensitization. When certain alloys are exposed to temperature (sensitization temperature), they become particularly susceptible to intergranular corrosion. The characteristics of weld such as high localized stresses and hardness can be enhanced by

regulating the pre- and post-weld heat treatment conditions (Lee et al, 2014; Leggatt, 2008; Olabi & Hashmi, 1996).

The physical attributes of HAZ can also be altered. The extent to which the physical and metallurgical properties are altered is dependent on factors such as the filler metal, the quantity of heat imputed into the weld and the base material. The size of the HAZ is controlled by parameters such as time of exposure to heat, the welding speed and Ampere of current used in carrying out the welding (Yousefieh et al., 2011; Karimzadeh et al., 2005; Mourada et al., 2012; Inspatguru, 2016; Insectioneering 2016).

Furthermore, the nature of the weld type utilized is that of a narrow band gap, which is not only a new technology in welding but finds great relevance in welding thick sections between pipelines, especially in oil and gas transmission lines. If an engineering structure is going to fail, it will start from the point of the weakest joint which is the welded joint. This calls for the need to pay close attention to the weld joint and minimize failure to as low as possible. This means that the weld root which is the beginning point of the weld needs to be narrowed in size as is the case with the Narrow gap weld.

2.3.1 Weld Induced Residual Stresses and Distortions

Local plastic deformations produce residual stresses which are in turn caused by the sudden heating up and gradual cooling of defined regions within metal. More often than not, these regions are restricted domains within the metal. The weld region cools down to solidify rather quickly generating residual tensile stress in that region, while consequently maintaining the remaining parts of the metal at residual compressive stress.

Figure 2.2 illustrates the transverse and longitudinal residual stresses present in centre cross sections of a rectangular plate. Longitudinal stress decreases with increase in distance from the centre of weld; having been generated from a successive heating and cooling series constrained by the metal within its immediate environment. It further diminishes (zero value) along the longitudinal path and tends towards compression in the transverse path.

Welding is basically the localised heating of edges of joints to form a new structure. Stresses are generated which are not uniform in nature within the material by reason of the heat introduced thereby causing expansion and contraction of the material. Compressive stresses are induced in the parent material with low temperature by reason of the hot weld pool which heats up the immediate environment known as the HAZ. When the weld pool cools down, tensile stresses are formed because the parent material then resists the contraction of the weld pool and the adjoining HAZ (Lucas et al., 2016).

The amount of thermal stresses introduced into the metal is determined by the change in the volume of the weld on cooling to room temperature. A typical example could be seen from the welding of carbon manganese (CMn) steel which shrinks on cooling down by 3%. This also impacts on the volume of the HAZ which shrinks further by 7% as it approaches room temperature. When the amount of stresses from the weld which is in form of thermal expansion and contraction; surpasses the yield strength of the parent metal, deformation sets in within the immediate environ of the weld zone, the HAZ (Lucas et al., 2016). This deformation can take the form of longitudinal shrinkage, buckling, angular distortion, bowing and dishing, as well as twisting.

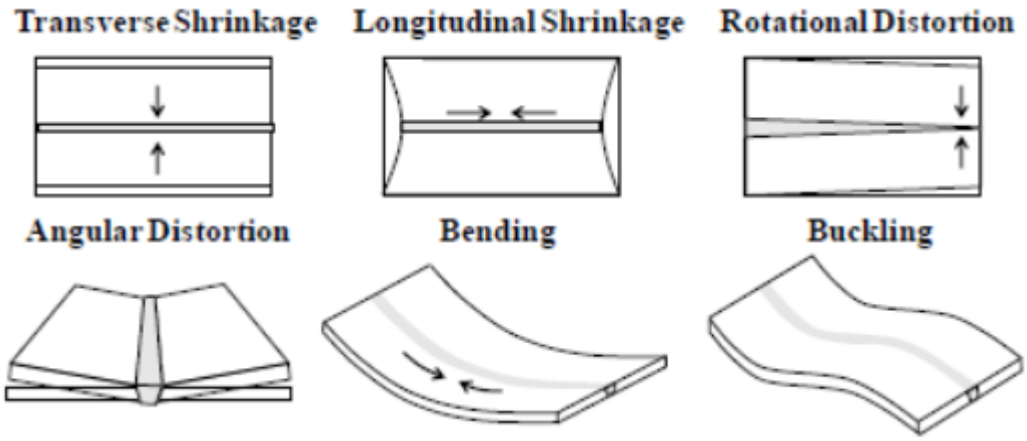

Figure 2.2 Schematic of Deformation in Weld (Soul & Hamdy, 2012)

When a structure is subjected to a weld process, its structure changes, subsequently altering its dimensions (Kovacevic, 2012). If this occurs when all external thermal forces are absent, it is referred to as welding induced distortions - an alternative distortion caused by the welding process, (Masubuchi, 1980) as illustrated in Figures 2.2 and 2.3.

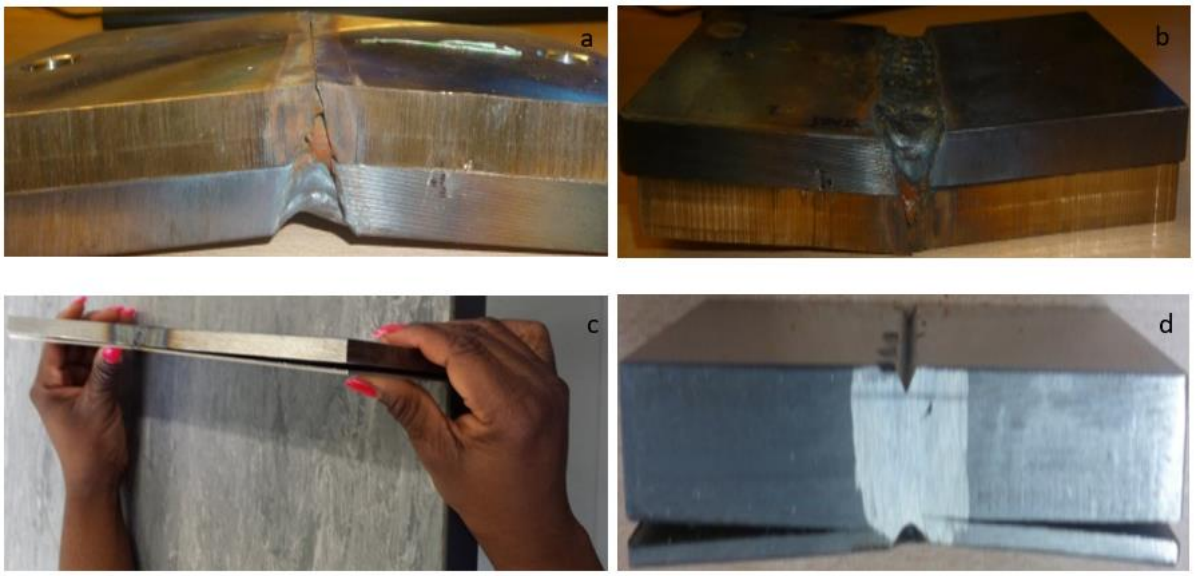

Figure 2.3 An experiment showing weld deformations. (a) and (b) show the side view of a deformed 12 mm clad weld not properly clamped into position. (c) and (d) show the same deformation, but with a 2mm clad weld.

Input heat and weld gives rise to deformation. It is possible to measure the heat input into the system from the heat source. The stress in the longitudinal direction is generated by the contraction in weld length. The stress in the transverse direction is caused by the contraction of the weld width and the angular stress is generated from the geometry of having more weld in the cap than in the roots and as a result, there is more concentration which gives rise to the bending of the material (Leggart et al, 2008; Leggatt, 2008; Teng et al, 2001; Radaj, 2002, Long et al, 2009; Changa & Teng, 2004; Colegrove et al, 2013; Rossiniab et al, 2012, Chang & Lee, 2009; Nowegian, 2012).

The factors responsible for distortion in the welded sample shown in Figure 2.3 are as follows: the technique of welding, design of joint, characteristics of the parent material, part fit-up and quantity of restraint. The welding technique impacts directly on the quantity of heat inputted into the system, thereby affecting the extent of distortion caused within the weld system. The criteria for the selection of welding technique is dependent on suitability of weld purpose, and the meeting of the required demands, as well as the delivery of quality. The welder is limited in his control over the distortion. The design of the joint is an important factor in determining the distortion in a weld system. Wide gaps such as fillet and butt joints allow for distortion. In order to avoid or reduce this distortion, a different type of joint such as a double-sided fillet is employed which brings the thermal stresses at equilibrium throughout the plate thickness (Hicks, 1999; Lancaster, 1992; TWI, 2016).

Characteristics of the parent material, such as specific heat in a unit volume and coefficient of thermal expansion also impact on the distortion of the weld system. The coefficient of thermal expansion induces stresses and distortions into the weld system via repeated expansion and contraction of the system during the course of the welding. Since the coefficient of thermal expansion in stainless steel is higher than that of mild steel, it has a greater chance of

undergoing more distortion. The greater the restraint the more the residual stress and likelihood of cracks being introduced into the weld metal and HAZ.

Part fit-up is expected to be at same elevation, so as to minimise deformation to only permissible limits. It is best practice to reduce the size of the weld gap as wide gaps will require a greater quantity of weld metal to fill it, thereby increasing the extent of distortion. Light spot welding of the joints in place or tacking of the weld joints is necessary to limit movement.

The level of restraint is an important factor to consider, because the more the restraint on movement of the weld system, the less the residual stresses caused by distortion. The weld components are held in place by whatever possible means (spot welding of surfaces and G clamps etc.) to minimise displacements while welding and especially the distortion of the base and clad metals while cooling, as observed in Figures 2.3 (a and b).

2.3.2 Weld Failure and Weld Imperfections

There are several weld defects such as porosity, cracking, inclusions, lack of penetration, lamella tearing, lack of fusion and undercut. The most common weld imperfections are poor weld bead, porosity and cracking. Each one poses a threat as it results in high stress intensity which leads to abrupt failure after less load cycles than expected in the case of cyclic loading or failure below the design load.

Porosity can be traced to the trapping of gasses in the microstructure of the filler area. The HAZ material consists of several regions which experience thermal cycles with progressively decreasing peak temperature from the fusion boundary. The Fusion Zone is created by heating above the melting point. Porosity is fundamentally caused by the presence of absorbed hydrogen in the weld pool which produces visible pores within the weld metal on cooling.

Hydrogen is present in water vapour in the shielding gas (air) which absorbs moisture from the surface contaminants of filler wires and parent metals as well as the surrounding area.

Figure 2.4 Failed weld 2mm clad

The consolidation of the weld metal and the parent metal via heating, results in diverse distortion arrangements (Conrardy et al, 2006; Abid & Siddique, 2005; Dong et al, 2016; Rammerstorfer et al, 1992; Ikeagu, 2007) as shown in Figures 2.3 and 2.4. Residual stress and distortions in circumferentially welded thin-walled cylinders vary from the conventional cylinder, in that the projected distortions radial deflection and axial shrinkage play very key roles in the deformation of the welded pipe. When the welded pipe undergoes shrinkage in the circumferential direction, this produces a bending moment M, a circumferential force F and a shearing force Q to the cylinder (Ueda et al, 1986). The combination of these three forces generates a stress state which is different from that of a welded plate (Vaidyanathan et al, 1973; Xiangyang, 2002). The diameter of a pipe, welding sequence and procedure, thickness of the pipe wall as well as the geometry of the weld collectively affect the residual stress orientation within that pipe (Lee & Chang, 2008; Malik et al, 2008).

2.3.3 Heat effect on mechanical properties and microstructure of welded joints

Since welding is a process that generates spontaneous heating and cooling within a component by reason of molten heat and solidification the heat given off from the source creates thermal cycles which in turn gives rise to the heat affected zone. The rate of cooling is a vital factor which affects the evolutions in microstructures in the HAZ or FZ (Gianetto et al, 2012). Thermal cycles possess certain traits such as high temperature, minute retention time at peak temperature and quick heating and cooling successions which generates changes both in the mechanical properties of the weld component such as strength, toughness and hardness; and within the weld microstructures in the fusion zone and HAZ (Poorhaydari et al, 2006; Harrison & Farrar, 1989). Slow rate of cooling is influenced by increase in the heat inputted into the weld zone and likewise faster cooling rate is also determined by reduction of heat input. The mechanical properties of the HAZ and FZ are influenced by the amount of heat inputted during the weld (Ravi Shankar et al, 2009; Murti et al, 2009; Shi et al, 2004). The input heat is in turn regulated by the input power (current and voltage) as well as the speed of welding and is expressed by the equation 2.1:

$$\text{Heat input [J/mm]} = \frac{\text{current [A] x voltage [V] x efficiency [\%]}}{\text{welding speed (mm/s)}} \qquad \text{Eqn (2.1)}$$

In Laser welding the heat inputted into the welding can be obtained from the expression in equation 2.2:

$$\text{Heat input [J/mm]} = \frac{\text{laser power [w] x efficiency [\%]}}{\text{welding speed (mm/s)}} \qquad \text{Eqn (2.2)}$$

Weld efficiency for laser welding is 80% (Benyounis et al, 2005; Fuerschbach, 1996) when considering the heat lost via conduction and mean efficiency for consumable electrodes such as GMAW is 80% (DuPont & Marder, 1995). The characteristics of the HAZ regulates and controls that of the welded joints (Piccini and Svoboda, 2012; Bonner & Smith, 1996) and as

such, a heterogenous microstructure in the HAZ determines the deteriorating mechanical properties of the welded joint of high strength steels (Lan et al, 2012; Piccini & Svoboda, 2012); but could these be the case in all weld microstructures?

The effect of heat input and welding speed on the microstructure, mechanical property and quality of welded joints carried out by Viano et al using four wire – double tandem, submerged arc welds in high strength steel (X 80) revealed the fact that as the heat input is increased, a reduction in the rate of cooling is observed which gave rise to coarser acicular ferrite laths, larger cellular dendritic cell spacing and reduced ferrite in the weld microstructure. Mohandas and Madhusudhan (1997) examined the effect of chemical composition of high strength low alloy steels.

2.3.4 Finite Element Analysis (FEA) of welding and welds

There are different Computer Aided Engineering (CAE) software systems used to carry out simulation such as Ansys and Abaqus. In welding, Finite Element Analysis (FEA) is carried out in two steps or phases. The first is the thermal analysis where thermal variations are depicted by colour bands and the heat distribution is clearly observed, Figure 2.5. The geometry of the structure is considered alongside the material selection which is key to the output generated. The thermal conductivity, specific heat, latent heat, coefficient of expansion and density are part of the material properties fed into the thermal analysis. There is also meshing and the application of boundary conditions of convective and radiative heats.

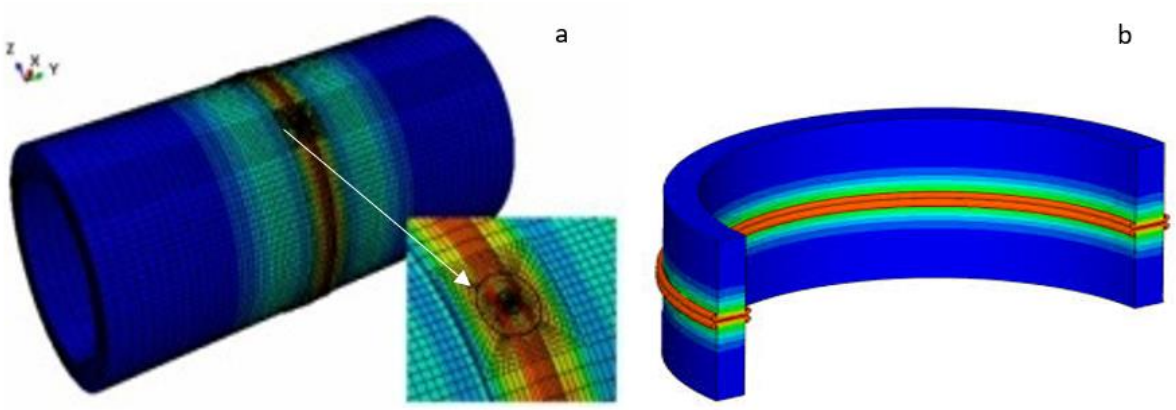

Figure 2.5 FEA Analysis of weld in pipelines (a) Exterior and (b) Interior view of weld (Hossain, 2018)

The second is stress analysis in which the output from the thermal analysis forms the input. The thermal and mechanical loading in the process has a profound impact on the integrity of the pipeline over its service life. An accurate and thorough assessment is needed on the associated residual stress and its effect on the structural properties of the pipeline. 3D simulations of stress in girth welded pipe sections have been carried out using Abaqus CAE software in two steps, the first being thermal modelling with a moving hot spot and added mass and the second being stress or mechanical analysis. The research presented in this thesis is fundamentally on 3D finite element modelling of residual stresses in a stainless-steel clad girth welded x65 Carbon steel pipes; in which the modelling procedures for universal residual stress characteristics are clearly demonstrated. The different kinds of weld induced residual stress fields which the weld joint undergoes are hoop and axial and the differing types of distortion trends are radial and axial shrinkage. The 3D finite element model of the simulated gas tungsten arc welding is captured to depict the residual stresses and deformation.

2.4 Well Known Cases of Weld Failure

The relevance of this research can be appreciated in the weld failure scenarios discussed below. The failure examination investigates the fundamentals and techniques used in structural pieces and bodies, as well as test specimens via a physical examination through to microscopic examinations such as SEM and EBSD and TEM. A great analysis is the product of the expertise of the engineer, as well as the depth of knowledge in materials and metallurgy. The following cases of weld failure occurred in 2011, 2015 and 2016 and were documented by Bernasovsky, Wang and The Welding Institute (TWI) (Wang, 2016).

2.4.1 Gas Pipeline Failures

Background: The city of Slovakia is situated in a country which has the highest system of pressurized gas transmission pipelines, traversing it with the oldest in service for well over three decades. Four of these pipelines had 720 mm outer diameter and 7mm wall thickness; the fifth being completed and was at the last stage of completion, did not need to be inspected as frequently as the others (Bernasovsky, 2013).

2.4.1.1 The First International Gas Pipeline

The first case of Pipeline failure was the First International Gas Pipeline which was constructed in 1965 and composed of L380n Russian Steel (with its reputable toughness and low ductility) with Silicon alloy (which posed a threat to corrosion protection). A crack, 1.8m in length ran along the spiral welded pipe with an Outer Diameter OD of 720mm and a thickness of 8mm, caused by Liquid Metal Embrittlement (LME) of liquidized copper (incorporated from the copper electric contact rods) embedded in spiral welds during the manufacturing process. The

crack is shown in Figure 2.6 (a) whereas the spiral weld portrayed poorly aligned weld runs – both linear and opposite as shown in Figure 2.6 (b) (Bernasovsky, 2013).

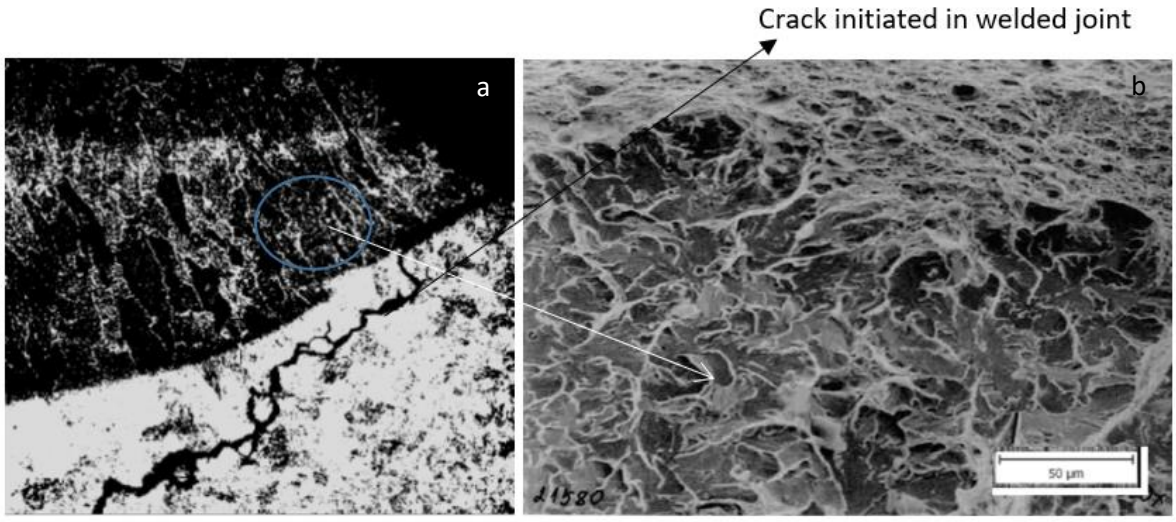

Figure 2.6 (a) and (b)Hydrogen Induced Crack along the misaligned spiral weld as a result of liquidized copper embrittlement and Surface of Transcrystalline Cleavage fracture (Bernasovsky, 2013)

Table 2.1 Mechanical Properties and Chemical Constituents [%] of 15 G2S steel

C	Mn	Si	P	S	Cr	Ni	Cu	Ti
0.14 -0.15	1.37 – 1.45	1.07 – 1.08	0.014	0.029	0.06	0.05	0.08	0.032
Re [MPa]		**Rm [MPa]**		**A5[%]**	**ChV FATT (50 J.cm^{-2})**		**Upper shelf**	
387 - 404		591 - 612		22 -27	+ 14°C		55 j.cm^{-2}	

The mechanism responsible for the Cu-induced hot cracking in the weld is sourced from the liquid-metal embrittlement of Cu contaminating the surfaces of the Fe- and Co-based FCC (Face centred cubic) alloys. The quantity of Cu contaminant required to cause the cracking is 0.003 mil which is equivalent to 7.62 x 10^{-5}mm in thickness metal (Savage et al, 1978). This is slightly less than the value given in Table 2.1 for Cu. The hot cracking in the weld which occurred as seen in Figure 2.6 shows that little quantity of Cu or Cu-alloy were transferred to the work surface near the weld form the weld rods. As the heat of the weld melts the Cu hot cracking by liquid embrittlement results. The path of a liquid-metal embrittled crack is usually

intergranular as observed from Figure 2.6 where the ductility and stress of the fracture is sensitive to temperature, liquid composition, thermomechanical history, size of grain, composition of solid, temperature and strain rate. Three criteria were met based on the interaction with the solid-liquid metal couple which includes joint solubility between the solid metal L380n Russian Steel and liquid with no formation of intermetallic compound and a barrier to plastic flow in base metal which is inContact with the liquid metal (Savage et al, 1978). .

Lack of proper heating of the metal joint can result in a weak weld. Cracking is one common defect that occurs in welded joints because of the stress build up that accumulates when a heated-up material is rapidly cooled. Weld also fails due to longitudinal cracking by reason of high shrinkage stresses particularly on the last passes. It can also be caused by hot cracking mechanisms. Root cracks commence from the weld root and extend midway into the weld. They are the most occurring longitudinal crack type due to the small. In order to avoid weld failures, it is important to properly match the filler metal and base material strength. The cladded metal strength needs to also be properly matched with the filler metal as is the case in this research. There is the need for an overmatching scenario rather than undermatching scenario in the welded joints of the dissimilar material clad.

2.4.1.2 Fourth Transmission line

In the report by Bernasovsky (Bernasovsky, 2013), this failure incident occurred during the pipe laying of the fourth X-70 steel welded grade transmission line with an outer diameter (OD) of 1420 mm and thickness of 18.6 mm; and not in-service. He further stated that a few of the pipes cracked along the spiral welds as illustrated in Figure 2.7 (a) while the pipes were bent on site, refer to Figure 2.7 (c). This was illustrated in the schematic diagram that cracks

propagated up to 1m lie the same distance from the pipe end along the spiral weld as shown in Figure 2.7 (e). (Bernasovsky, 2013) The crack was propagated along the heat affected zone (HAZ) refer to Figure 2.7 (b) also termed 'cold impressions' of the weld region which indicates that the steel rollers meant for reinforcing the furnace and shielding the pipe, were wrongly fitted, refer to Figure 2.7 (b)

Typically, furnace pipes are heated to a temperature of 300 ^{o}C and insulated with polyethylene (PE) insulation after which they are rotated spin on the rollers up to 70 revolutions. As a routine, pipe inspections are carried out before installation of the furnace pipes. During a particular workover – a pair of faulty rollers were taken out for repair, leaving the remaining pair to support the pipe weight of 12 tons within a distance of 11.5 m. The increase in temperature favoured the impressions as observed from Table 2.2. The impression was not detected because inspections of all pipes were carried out prior to insulation. In order to unravel the cause of this failure, ultrasonic inspections of all bent pipes constructed within that time period, were carried out which revealed that the pipes in question were already distributed in the section up to 150 km long, and hence already buried under the soil. The relevance of huge weld reinforcement angles and cold impressions were examined in the result of the particular impact test. There is the effect of weld angle on fracture that was carried out along the weld direction with mean fracture angle for specimens being 14^{o}, 28^{o} and 32^{o} for the transverse weld and 45^{o} and the longitudinal welds. The two most common locations of the weld fractures were interface between weld passes and at shear leg. Results shows that mean fracture angle of 14^{o}, 23^{o}, 27^{o} and 32^{o} generates a mean fracture strain of 0.164, 0.202, 0.272 and 0.472 for steels such as T20, T26 L1 and L2 (Deng et al, 2003). The weld stress being determined from the measured fracture surface area and theoretical throat sourced from mean leg sizes of the welds. The fracture angle shows that weld failed at the shear leg there-by providing significantly larger surface compared to specimens that failed near the weld throat under combined shear and

tension. These cannot be compared with the strength of the longitudinal welds which also failed in the shear. The strength of transverse welds is similar to mean strength for longitudinal welds which requires no toughness. Over here it is neither the filler metal nor toughness level that has significant effect on the transverse fillet welds strength. The failure experienced at the shear leg as compared with the weld throat is a function of the quantity of the weld face reinforcement as additional weld face reinforcement can lower the fracture angle (Deng et al, 2003). Typical Butt weld is 60^{o} 1mm to 2mm root gap and a zero to 1.5 mm thick root face as seen from section 2.6.1.

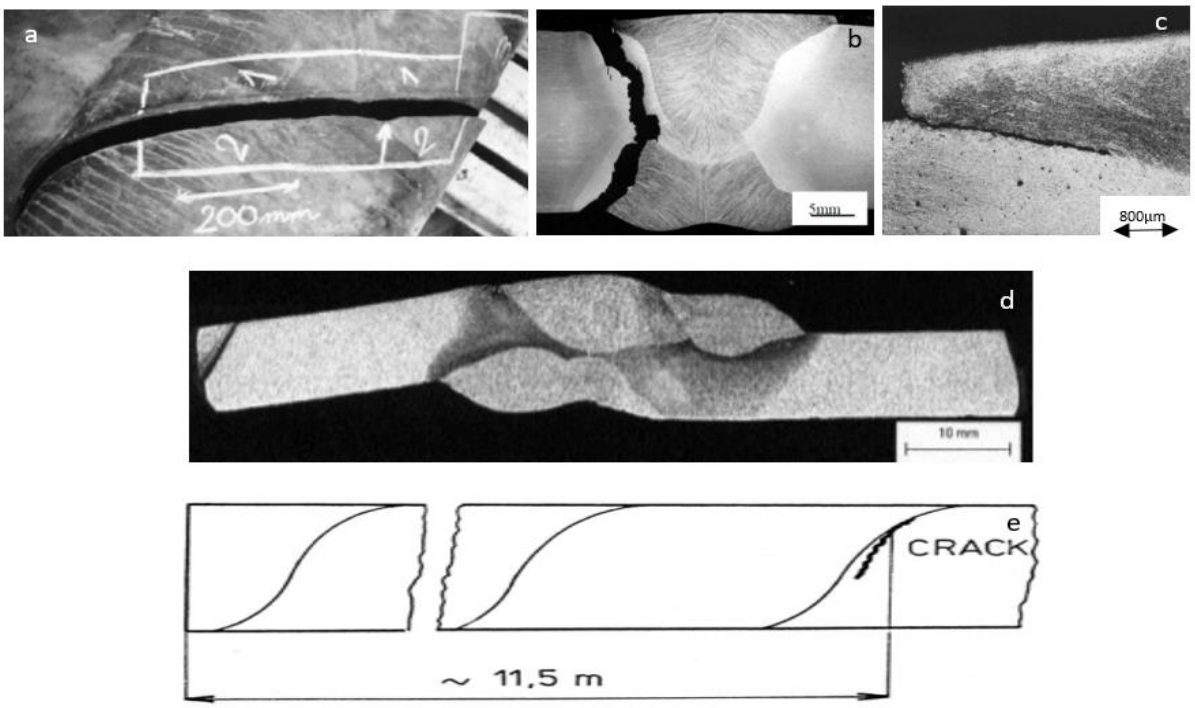

Figure 2.7 (a) crack along Spiral weld; (b) fracture spiral weld wall (HAZ); (c) overlapping due to impression of weld (d) poor workmanship revealing linear and opposite weld runs and (e) sketch of fractured pipes (Bernasovsky, 2013)

Table 2.2 Impact energy (J) of HAZ of Spiral weld with natural notches and ISO-V notch (Bernasovsky, 2013)

T[°C]	ISO-V notch	Natural notch				
		real impression	artificial impresion	cold 1ap	α =90°	α =55°
0	51.5	51.3	13	46	48	120
20	83	63	35	68	122	124

2.4.2 Weld Joint of Carbon Steel pipe fitting and Stainless-Steel Panel of Tank

A 439 stainless steel oil tank was circumferentially welded to a pipe fitting made up of carbon steel at the panel of the tank as shown in Figure 2.8 (a) (Wang, 2016). It was later heated through high temperatures while in service, as a result, a through the thickness crack was located on the circumferential weld joint which was Gas Tungsten Arc Welded (GTAW) with a consumable 309L stainless steel rod and argon gas shield, refer to Figure 2.8 (b). According to (Wang, 2016); the tint of the crack when examined revealed that it originated from the weld joint of the seam tank and pipe fitting and secondly, that the thorough penetration of the weld joint was not reached. Energy dispersive X-ray spectroscopy and SEM analysis carried out to detect immediate chemical constituents of the fracture as shown in Tables 2.3 and 2.4 further revealed a deposit of chromium oxide on the channel of the weld which signifies the presence of plasma cut induced impurity prior to welding (poor weld hygiene), in addition to the high percentage of oxygen found present in the weld. He further stated that the results of the microstructural examination also showed duplex microstructure at the stainless-steel side of the foot of the weld crack. Microstructural evaluation such as weld foot micrograph of austinite and ferrite duplex microstructure (as seen in Figure 2.8 (a and b)) revealed a ($\boldsymbol{\Upsilon + \delta}$) duplex microstructure at the toe of the cracked weld at the stainless-steel panel side. The interesting truth about this discovery is the fact that thermal expansion coefficients of ferrite and austenite greatly induce stresses within the immediate weld environment. In summary, the investigator concluded that the crack was initiated by the presence of chromium oxide which could have been cleansed with light grinding; and secondly, the significant amount of residual stresses generated within the austenite/ ferrite duplex further propagated secondary cracking. First of all, comparing the chemical compositions of the stainless steel (SSP) and carbon steel pipe (CSP) with in Table 2.3 with those of the local surface of fracture in Table 2.4; there is a very conspicuous increase in Nickle, Oxygen Chromium, Carbon and slightly in manganese. Oxides

in steel metal can initiate fracture which is the case in the failure scenario or improve toughness by influencing the development of beneficial microstructures (Terashima & Bhadeshia, 2006). According to He et al, 2018, the effect of oxygen in molten pool and keyhole can increase weld penetration and supress porosity as well as reduce the weld width as well as improve the laser energy (He et al, 2018). However, metal oxidation takes place when ionic chemical reaction occurs on the surface of the metal in the presence of oxygen. Electrons are transferred from the metal to the oxygen molecules and negative oxygen ions are generated which penetrates the metal creating oxide surface. This occurs in the presence of air (atmospheric moisture) or when the metal is exposed water or acids. Ni, Ca, Mn and N enhances austenite and Cr alongside Si, Mo and niobium encourages formation of Ferrite. Although Cr and Ni enhance the strength and hardness of the steel and Ni increases corrosion resistance, promoting elasticity whereas Cr and Mo promotes corroding at high temperatures with the later improving the creep resistance of steel at elevated temperatures; it is important to note that these elements were in less quantity compared with oxygen. The quantity of oxygen in Table 2.4 which is more than the constituent parent metals in Table 2.3 by 21, and likewise Ni by 2, Cr by 12 (for the CSP value) and carbon by 9, clearly revealed that oxide played a significant role in determining the fracture. Increase in carbon content increase hardness and strength of the steel thereby increase hardenability however it decreases the weldability making the weld more brittle susceptible to martensite formation.

Since cracking occurs in welded joints because of the stress build up that accumulates when a heated-up material is rapidly cooled, the choice of the filler metal should be compatible with the base and clad metal for strength and other properties (matching the tensile or yield strength of the filler metal to the base metal) so as to obtain the required overmatching scenario. For thorough penetration not being reached, it implies partial joint penetration (PJP) where under matched strength of the filler metal to base metals was carried out. As a rule of the thumb,

when welding a lower strength material to a higher one, ensure matching the filler metal to the lower strength metal to allow for greater ductility and to prevent the risk of cracking.

It is also vital that grinding is not compromised when planning to weld components. In the current research grinding is vital to the good contact and bond between the dissimilar materials to be welded (the stainless-steel cladded metal and the carbon steel base metal) so as to ensure strong weld and to eliminate the likelihood of weld crack or failure. Prior to that the surfaces were cleaned with solvent to eradicate impurities. In order to avoid filler metals from picking up debris oil, moisture or dust that could lead to contamination and consequently, weld failure, it is important to follow proper storage procedures. Filler materials should be stored in their original packaging until when needed and stored in dry condition with same temperature as weld cell to prevent condensation which takes place when transiting from cold to warm temperature thereby causing the filler metal to absorb moisture (which contains oxygen and or hydrogen). The advantage of filler metal acclimating to the temperature protects it against hydrogen pickup which could lead to cracking or weld failure. Welding hygiene entails wearing hand gloves to protect it from moisture from the hands and covering open spools with plastic bags (when not being used) prevents accumulation of contaminants from the air may lead to poor weld quality and/ or failure. Because the presence of oxygen in weld leads to oxidation, corrosion and eventuality weld failure, that is why arc welding employs inert gas such as helium to create the arc shield, which is used to shield the molten weld and weld zone from impurities within the environment – refer to section 2.5.1 on arc welding.

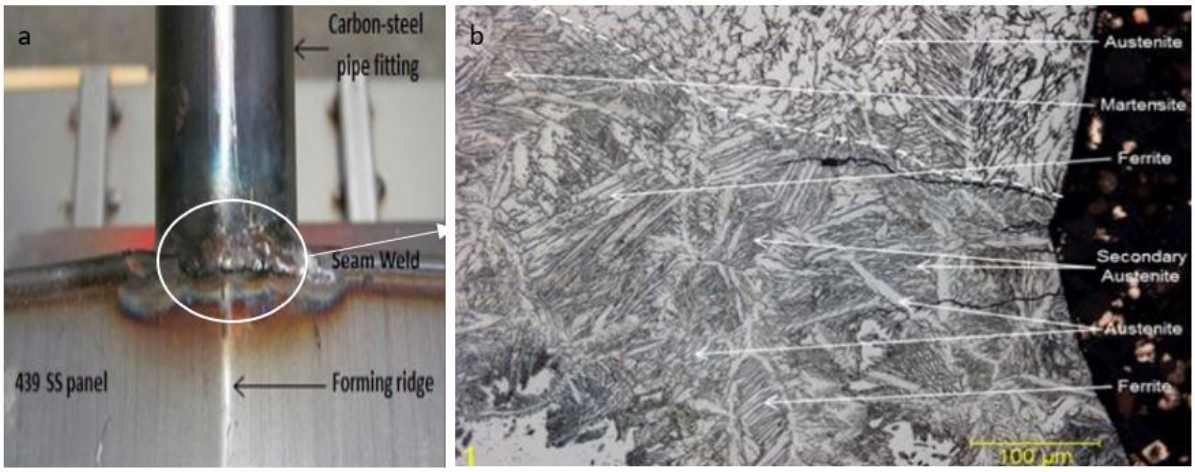

Figure 2.8 (a) weld joint between carbon steel and stainless-steel tank panel and (b) weld foot micrograph of austenite and ferrite duplex microstructure (Wang, 2016)

Table 2.3 Chemical compositions of carbon steel pipe (CSP) and stainless-steel panel (SSP) in percentage weight (%) (Wang, 2016)

Material	C	Mn	Si	P	S	Cr	Ni	Mo	V	Cu	O	N	W	Ti
CSP	0.049	0.15	0.016	0.009	0.005	0.016	--	0.002	--	0.009	0.006	0.004	--	0.001
SSP	0.010	0.19	0.31	0.024	0.001	17.6	0.27	0.028	0.05	0.16	0.003	0.011	0.04	0.15

Table 2.4 Local Chemical composition on surface of fracture in percentage weight (%) (Wang, 2016)

C	Mn	Si	Cr	Ni	O	P	Ca
9.12	0.38	0.29	12.18	2.26	31.82	0.21	0.24

2.4.3 Weld Cases Presented by The Welding Institute (TWI)

2.4.3.1 HAZ Liquation cracking

This is a failure analysis that occurred by short intergranular fractures (grain boundary crack) situated within the high temperature zone of the Heat Affected Zone (HAZ) (Holmes, 2015). These same cracks were initiated during a subsequent weld run in the previously deposited metal weld as shown by Holmes (2015) in Figure 2.9. Grain boundaries were formed from the liquid films at temperatures below the alloy melting temperatures. On solidifying, because this

liquid is not able to withstand the tensile strain which sets in on contraction, cracks are generated as shown in Figures 2.9 (c) (Holmes, 2015). The three conditions that were satisfied as a result of the interaction with the solid-liquid metal couple includes joint solubility between the solid metal and liquid with no formation of intermetallic compound and a barrier to plastic flow in base metal which is in contact with the liquid metal (Savage et al, 1978). High strength steels with high carbon content and or high alloys tends to susceptible to weld failures due to cracking because they are less ductile and therefore tend to generate residual stresses along the base metal and the finished weld while cooling. Lack of proper heating of the metal joint can result in a weak weld. Pre heating such materials for recommended time and temperature in accordance with the weld procedure is vital to enable adequate and uniform heat soak takes place throughout the material. Where necessary post weld treatment (PWHT) should be implemented. One of the key purposes of this research is to investigate the occurrence of reheating which takes place at the top and bottom layers of the welded passes in the dissimilar material joints while welding, it is therefore vital to note that pre heating the material prior to welding prevents rapid cooling which helps in maintaining a more ductile internal grain structure (pearlite) in the heat affected zone (HAZ) of the weld.

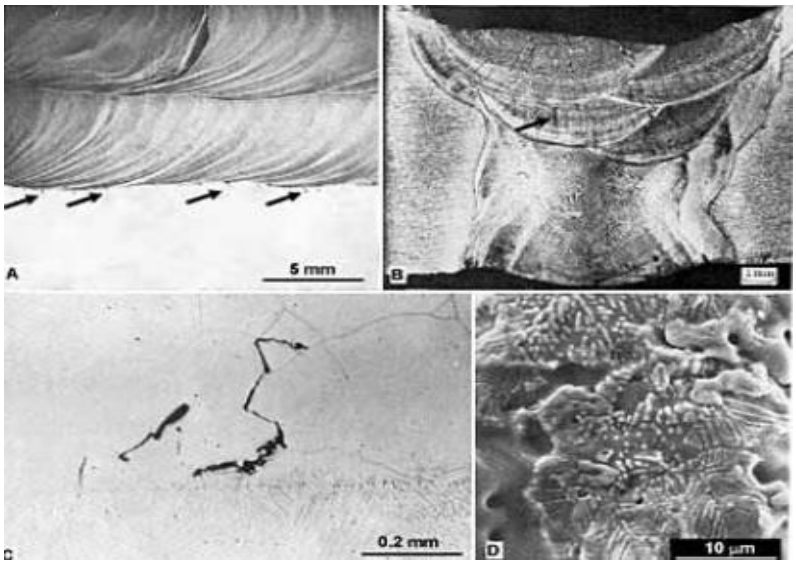

Figure 2.9 Photomicrographs of HAZ liquefaction cracking in austenitic stainless steel clad with a nickel alloy weld metal. The location of the liquation is depicted by arrows (Holmes, 2015)

2.4.3.2 *Duplex Stainless Steel*

This is a case study of failure in stainless steel which entailed embrittlement via intermetallic precipitation. The brittle failure occurred in the duplex stainless steel due to sigma phase because of incorrect heat treatment of forging and tensile stress seen in the residual stress and applied stress during hydrotest. The Dye penetrant reveals the crack located on the heat affected zone of the weld metal, as shown in Figure 2.10 (a). As a result of the sigma phase which can been seen from the result of the steel microstructure in Figure 2.10 (b) and 2.11 (b) and the EDX spectrum analysis in Figure 2.11 (a) which reveals the composition of the phases present in the weld metal, brittle fracture sets in. The results of the test analysis revealed that the causes of failure are the duplex stainless steel, the sigma phase precipitation rich in Chromium and Molybdenum as shown in Figure 2.11 (a), incorrect heat treatment of forging and tensile stress seen in the residual stress and applied stress during hydrotest. For weld failure to occur in the residual stress results, it shows that the stress exceeds the yield strength of the steel.

The residual stress is not supposed to exceed the yield strength of the material otherwise failure set in. The yield strength is one of the most common material properties that the designer needs for majority of the rules in the design code and for this research it is the R6 and BS 7910. It is the magnitude of the stress at which the transition occurs representing the limit of the elastic behaviour.

Super duplex stainless steel is one of the family of steel that is known for its excellent corrosion resistance and high strength properties (Fellicia et al, 2017). This resistance of the super duplex can be reduced by reason of precipitation of sigma phase which is formed at high temperatures. Sigma phase is a non-magnetic intermetallic phase compound that is made majorly of chromium which is consequently produced in austenitic and ferritic stainless steels when exposed to a temperature of 560^{o} – 980 ^{o}C (Hsieh & Wu, 2012). The sigma (σ_s) phase

precipitates readily at the σ/γ phase boundary which is rich in Cr. At the formation of high Cr region, the depleted Cr forms causing a reduction in the corrosion resistance at same time. The σ/γ interphase is also a high energy interphase sight which means that several defects hibernates there and concentrate – it is beneficial site for the heterogenous nucleation of the σ_s phase. As the later phase nucleates at the σ/γ interphase boundary, some of the defects disappear releasing free energy of the materials. This subsequently reduces the activation energy barrier to forming a coherent interface. In the current research the selection of the filler material and the clad and base metals were vital to enable proper matching and eliminate incompatibilities where necessary especially those that arise from different materials (Hsieh & Wu, 2012). Molybdenum (Mo) is known to enhance the resistance to pitting corrosion as an alloying element in duplex stainless steel (DSSS), however, it also increases the precipitation of the harmful phase such as sigma phase. The acceleration of the sigma phase by Mo is due to the increase in the solvus of sigma phase because the sigma phase does not always grow rapidly (Ogawa & Osuki, 2019).

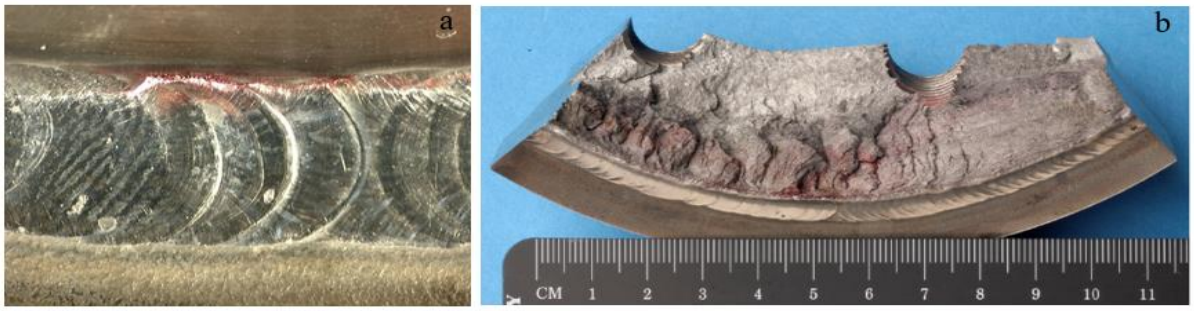

Figure 2.10 (a) Dye penetrant weld metal/HAZ crack and (b) Brittle fracture due to sigma phase (Holmes, 2015)

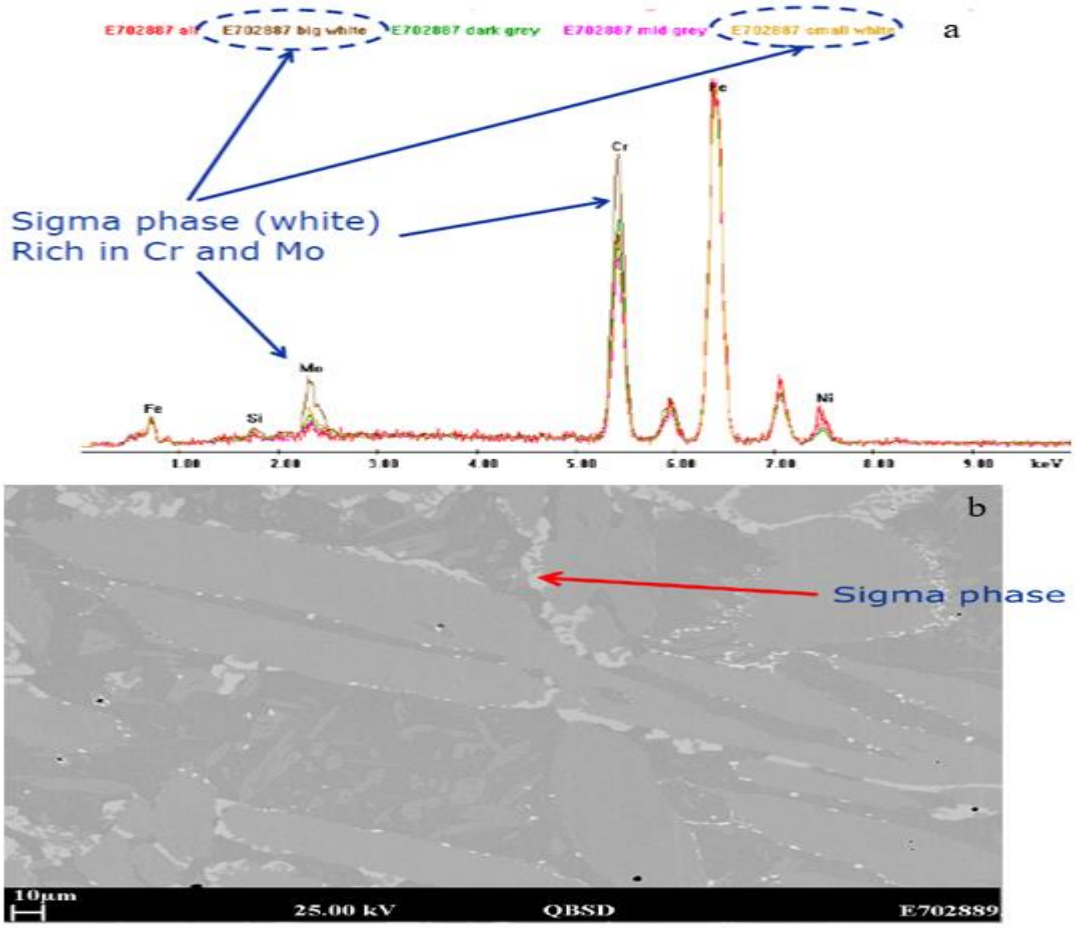

Figure 2.11 (a) Composition of Phases in EDX Spectrum and (b) Microstructure of Duplex Stainless Steel (Holmes, 2015)

2.5 Existing traditional welding techniques for high strength steels

Large structures are assembled in components using joining techniques such as welding. The more common welding technique for welding HSLA steels and assembling large and complex structures include resistance spot welding (RSW), submerged arc welding (SAW), gas metal arc welding (GMAW) and gas tungsten arc welding (GTAW).

The effect of thermal refining on mechanical properties of annealed SAE 4130 using the multi pass GTAW was examined by Lee et al and it was discovered that the AW (annealing + welding) and AWST (annealing + welding + solution + tempering) occurred with minimum hardness value at grain growth heat affected zone (GGHAZ) due to coarse grain growth; the

hardness occurred with sudden drops between the multilayer welding, although it was bigger than the minimum value at HAZ. SAE 4130 alloy steel is heat treatable and high strength low alloy (HSLA).

Mohandas and Reddy (Mohandas & Madhusudhan, 1997) compared continuous and pulse rate current GTAW of AISI 4340 high strength steels whose heat input was ~ 1.3 kJ/mm for each pass and welding speed was 0.15 m/min. Their examination brought to light the continuous current welds which revealed columnar grain morphology, whereas pulse current welds displayed equiaxed grain morphology. The grain size of the average fusion zone was smaller in pulsed current welds and consequently displayed superior mechanical properties. ASTM A 106 Gr B steel tubes having a dimension of 101.6 mm OD and thickness of 6.6 mm was welded together by Silva and Farias using GTAW technique with heat input of ~ 1.4 kJ/mm and a welding speed of ~0.03m/mm.

A comprehensive study was undertaken on high cycle fatigue behaviours of butt weld joints in 2 mm thick advanced high steels having diverse levels of strength and bead geometries by Ahiale and Oh using GMAW technique on dual-phase steels (DP440 and DP 590) and martensitic steel (MS) possessing tensile strength of 440, 590 and 1500 MPa respectively (Ahiale & Oh, 2014). The heat input employed was ~0.32 kJ/ and speed of welding was 0.6 m/min. The outcome revealed that the microstructures with the lowest hardness were located at the base metal, the subcritical HAZ and fusion zone for DP440, DP590 and MS welded specimens respectively. It was discovered that at the points of lowest hardness, fatigue failure of specimens without weld beads reinforcements occurred and fatigue life exhibited in the order of MS > DP590 > DP440 which is similar to the order of value of lowest hardness in each welded specimen.

Some of the benefits of submerged arc welding (SAW) include high rate of deposition, ease of automation and operation (requiring less skills), minimum welding fumes, excellent weld joint quality and extensive industrial usage for fabrication pressure vessels, pipelines, marine vessels wind turbines and offshore structures (Kathleen, 1993; Shen et al, 2012; Almqvist, 1978).

Arc welding techniques are employed for joining high strength steels (Piccini & Svoboda, 2012; Murti et al, 1993) but due to their high heat inputs, which results in softening of the heat affected zones, slow cooling rates of weldment and grain growth, the mechanical properties of the high strength steels are depreciated (Zhang et al, 2012; Bayley & Mantei, 2009). It can therefore be implied that the use of high strength steels in structural integrity minimizes the usage of materials and component size as well as weight of structure without compromising the integrity of the structure (Abedrabbo et al, 2009; Shi et al, 2008). The weldability, strength and toughness of high strength steel have made it possible for its vast application in line pipes, automotive industry, pressure vessels, offshore construction, lifting and handling as well as shipbuilding (Yang et al, 2008; Zhao et al, 2002).

The versatility of laser welds in structural integrity applications is majorly due to the fact that it is mechanized with the aid of robots, has significantly low distortion when compared with arc welding techniques and the aspect ratio with narrow HAZ is high. Laser weld also has the benefit of being operated with optical fibre delivery of its beam and can be carried out without a filler metal which is the case with single pass autogenous laser welding (Li et al, 2014). The later technique is prone to cracking, porosity, mis-tracking of weld seams and dropout of molten material especially in thick and medium component sections (Bachmann et al, 2014). It is also not compatible with tight joint fit up and functions with restricted laser power in commercial applications (Elmesalamy et al, 2013) hence not capital intensive. The solution to

the above is to combine bot conventional arc welding techniques with laser welding in a process known as hybrid laser welding which has several benefits.

The effect of welding speed on the weld bead, leading and trailing wire current on the weld bead dimensions and mechanical properties in single pass two-wire tandem submerged welding of 12 mm thick typical HSLA steel plate was carried out by Kirana and De (Kiran et al, 2012) and it was observed that the yield strength, ultimate tensile strength and elongation were 497 MPa, 662 MPa and 27.9% respectively. Two-wire tandem submerged arc welding process entails deposition from two electrode wires simultaneously, the leading wire being connected to direct current (DC) power supply whereas the trailing wire to alternating current (AC) source of power. The profile of the weld bead and mechanical properties of tandem submerged arc welding were significantly affected by the leading and trailing wire current transients and the speed of welding such that the leading wire current affected the weld bead penetration whereas the trailing wire current pulses affected the width of the weld and height of reinforcement.

The impact of thermal cycles on the characteristics of the coarse-grained heat affected zone in X80 HSLA steel plate was considered by (Monifera et al, 2011) using four wire tandem submerged arc welding (TSAW) system to weld 17.5 mm thick X80 HSLA steel plate (Monifera et al, 2011). The four-wire TSAW process with different heat input on ~ 3-4 kJ/mm for each weld pass and welding speed was 1.7 m/min. Optical micrograph of weld cross section for the selected sample was obtained and it was discovered that the martensitic/ austenite constituent was revealed in the microstructure of the heat affected zone region for all the specimens along the prior austenite grain boundaries and between the bainitic ferrite laths. The fractional area of martensite/ austenite particles due to different rates of cooling was the major contributing factor for increase in hardness values in the coarse-grained heat affected zone.

Multi-pass laser welding with filler wire is a feasible technique to weld medium and thick section material using the limited laser power at hand. In addition, the introduction of a filler

wire into the welding groove can improve the metallurgy and the properties of the weld. Joining of thick plates is accomplished by using filler materials to fill the prior prepared welding groove (Koo et al, 2004) Usually a “Vee” groove is prepared. However, the thicker the plate, the wider the groove is, which results in lower productivity and more consumption materials. Over the last few years, the multi-pass narrow gap laser welding technique has been demonstrated. Multi-pass narrow gap laser welding technique can be applied to weld medium and thick section materials with a filler wire using relatively moderate laser powers. This technique has many advantages, including increase productivity, saving consumption filler materials, releasing precise fit-up requirements, improving the metallurgical properties of the welds, improving the melt sagging problem, and reducing residual stress and distortion (Fairchild et al, 2004).

Elmesalamy et al. (Fairchild et al, 2004; Elmesalamy et al, 2013) successfully welded 20 mm thick 316L stainless steel plate to a 10 mm plate using a 1 kW IPG single mode fibre laser with an ultra-narrow gap (1.5 mm gap width) and a taper of 6° groove angle from double sides using multiple-pass narrow gap laser welding approach. Shi et al. Tata Steel has developed an advanced low carbon, low alloy S960 steel with a minimum yield strength of 960 MPa. This steel is a promising high strength steel for application in the heavy crane sectors due to its high specific strength, good impact toughness and formability. Ruukki Metals (Pande & Imam, 2007) are also developing Optim 960 QC steel with strength of 960 MPa. The Optim 960 QC strip steels are made by modern hot strip rolling and direct-quenching processes, which is similar to the method employed by Tata Steel.

It can be found from the above reviews on the narrow gap laser welding technique, most of these investigations are just focused on the welding technique and welding parameters optimisations. Studies on the microstructure evolution and mechanical properties of the narrow gap laser welded materials are scarce.

So far, there is a knowledge gap in the trend of heat distribution within these welded joints of dissimilar material studied. In this present work, a comparative study on the heat distribution during the traditional gas metal arc welding (GMAW) was carried out on the CR4 and API S16 grade steel.

2.5.1 Girth Weld

Girth welding can be applied to a wide variety of manufacturing and maintenance solutions. The equipment is portable and the cost as well as maintenance of the equipment is affordable compared to some of the other welding processes. The cost of the welding gasses, supplies and operator's time depends on the materials being joined and size, shape and position in which the weld must be made. The rate of heating and cooling is relatively low and favours some weld cases, however, in situations where rapid heating is required, the oxyacetylene welding process is not appropriate. The quantity of heat fed to the joint can be regulated by a skilful welder which is advantageous; however, there is the need to separate the oxygen and nitrogen in the atmosphere from reacting with the metal in order to prevent formation of harmful oxides and nitrides. Girth welds are the type of joining process which entails welding two pipes along the circumference during pipe fabrication subject to environmental factors and convenience. It involves several passes in order to complete the welding procedure and seal the joint. The start of the weld proper is the root weld which requires a definite speed and is the most challenging part of the weld, followed by the hot pass that increases the thickness of the fill and then last of all, the fill and cap pass used for finishing and covering the joint. Gas tungsten arc TIG is the style of application, taking into consideration the strength of the welded pipe joint, environments surrounding the pipe, the expertise of the welder, the pipe fabrication technique and the pipe dimension, as well as diameter and wall thickness of the pipeline.

2.5.1.1 Gas Metal Arc Weld (GMAW)

The gas metal arc welding makes use of an electric arc in between the metallic piece to be welded and the weld rods, known as solid electrode wire, as shown in Figure 2.12 below. This arc heats up the weld metal and base metal along with the rods thereby melting them altogether. All these procedures are shielded from impurities in the environment with the aid of the shield gas introduced into the system. The current conductor conveys power of regulated voltage which powers up the whole process by channelling the solid electrode wire to the accurate position per time. The metallic pool can be transferred via spray, globular, pulsed spray or short circuiting as required. The welding gun has a Gas nozzle, current conducting cable, a wire guide and contact tube made of copper. The wire guide ensured that the electrode is kept on course.

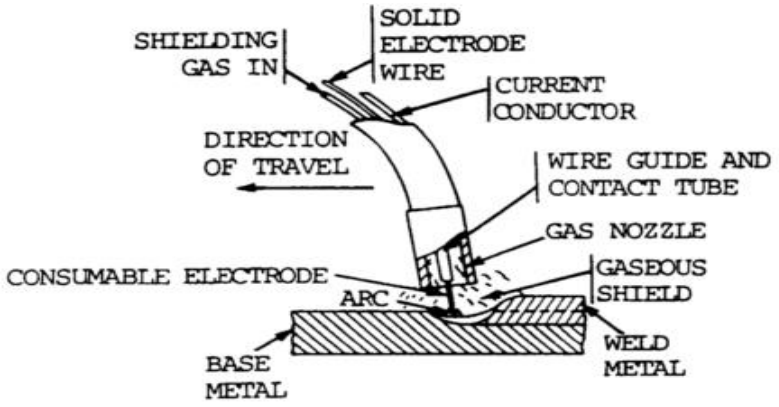

Figure 2.12 A schematic diagram of a typical Gas Metal Arc Weld (MWC, 2016)

2.5.1.2 Gas Tungsten Arc Weld (GTAW)

The tungsten Inert Gas (TIG) weld is the specific Gas Tungsten Arc Welding which uses a tungsten electrode to generate the weld. (Minnick William, 1992) It is similar to the MIG (Metal Inert Gas) in the sense that an arc is used to shield the molten weld and weld zone from impurities within the environment. An inert gas such as helium is used to create the arc shield.

The current carrying conductor generates enough power to the system which together with the filler metal, base and weld metals produces the molten weldment. This power is transmitted through the arc in the form of a charged cloud. Unlike GMAW, GTAW is used to produce stronger welds with greater integrity; as a result, it can be manoeuvred solely by the welder. It has the following advantages: It enhances the speed of welding, it is affordable and readily available at little or no cost, it can be carried out within limited space, it is used for different purposes and also makes it convenient to use with a broad range of electrodes. It also has flexible welding styles which makes the welding of any geometric position feasible. Also, it is straightforward and does not involve complexity in the welding process, it can be remotely monitored and sustained, the resultant weld is of significant integrity and improved finishing and this is specifically suited for sensitive or particular demands workpiece and weld sections that are not too bulky.

2.5.2 Limitations in Girth Welding

In considering the assessment of stress below the specified minimum yield strength of the pipe, as applied in BS 7910, the assessment procedure permits evaluation of flaw in relation to failure prevention by fracture and plastic collapse while embracing the fatigue crack growth and stable crack extension via ductile crack growth known as tearing. The technique includes the effects of welding residual stresses in assessment of fracture and because the specific profile distribution of residual stresses via the wall thickness of the pipe is not known, the technique presumes that a uniform residual stress equal to the value of the yield strength exists transverse the to the weld. It further presumes an overmatching scenario of the parent pipe yield strength whenever the weld metal strength over matches that of the parent pipe. This presumption of yield stress is questioned by some as conservative, which is the case and intention, notwithstanding the technique permits the relaxation of the residual stress pending the stress

applied and size of flaw to a minimal value (Hadley, 2013; Andrews et al, 2014; Wang and Liu, 2004; Wiesner at al, 2000; Withers, 2007; BSI, 2013; BSI, 2015; British Energy, 2014; Budden and Sharples, 2015; Budden and Sharples, 2017; Frost, 2009; Feng et al, 2019; Milne et al, 1988; Sharples et al, 2003; Zhang et al, 2012). The technique allows the inclusion of the precise value of the residual stress distribution when evaluated and guidance are made available to evaluate a conservative distribution once the conditions for welding are determined. The presence of residual stresses aggravates the driving force for fracture; hence it cannot be overlooked and future revisions of BS7910 will be explored for a comprehensive guidance on girth welds (TWI, 2011).

The misalignment of girth welding known as 'hi-lo' is another feature addressed by BS 7910 and it is regarded as bending stress derived from stress concentration factors equations. Misalignment increases the driving force derived from FEA undertaken at TWI. Increasing misalignment from 0 to 3 mm implies that the CTOD condition is doubled at applied strains close to yield (0.5% strain), hence the gap increases for larger strain values. Bending stresses are regarded and evaluated as primary stresses because it is not stated clearly in the BS 7910 how misalignment should be assessed, which consequently implies that the bending stress imparts on both axes of fracture (Kr) and plastic collapse (Lr) in the failure analysis diagram (FAD), which is also a conservative technique. Based on current research carried out at TWI, for materials induced with gentle slope stress strain curve with applied strains below the yield, misalignment can be considered and assessed as secondary stress – which implies that it considers only fracture axis (Kr) not plastic collapse (Lr axis of the FAD) hence it is regarded as a local stress concentration. Misalignment becomes relevant to both primary and secondary stress when the value of the strains is above yield strain. This criterion also applies to weld components samples having discontinuity in yield known as L*ü*ders plateau where the applied strain is below 3% and regarded as secondary for misalignment criteria.

2.6 Weld Joints

There are five basic types of joints used in arc welding namely Tee Joints, Lap joints, Butt joints, Edge joints and Corner joints are shown in Figure 2:13. The T-joint is used to join parts of an angle to each other and are either made with single, double or groove fillet weld combination. Corner joints although similar to T joints because they are made of sheets and plates in component parts, they are used in groove welds and fillet welds. They are better used for heavier metals to avoid buckling in thin metals. Edge joints are used for welding adjacent and parallel-placed edges of plates or sheets. Lap joint is single fillet, plug slot, double fillet or spot welded. Bridging fillet weld need to be utilized where component parts are not in close contact to each other. For cylindrical parts, interface fit eliminates this problem. The type of weld used for the experimental work at the Laboratory in Brunel University London is the Girth weld using the Butt Joint. Butt joint is required for high strength and can withstand stress better when compared with other weld joint types. For pipes, butt joint is preferred to lap joint because the lap joints would lead to contours on the pipes (Hicks, 1999).

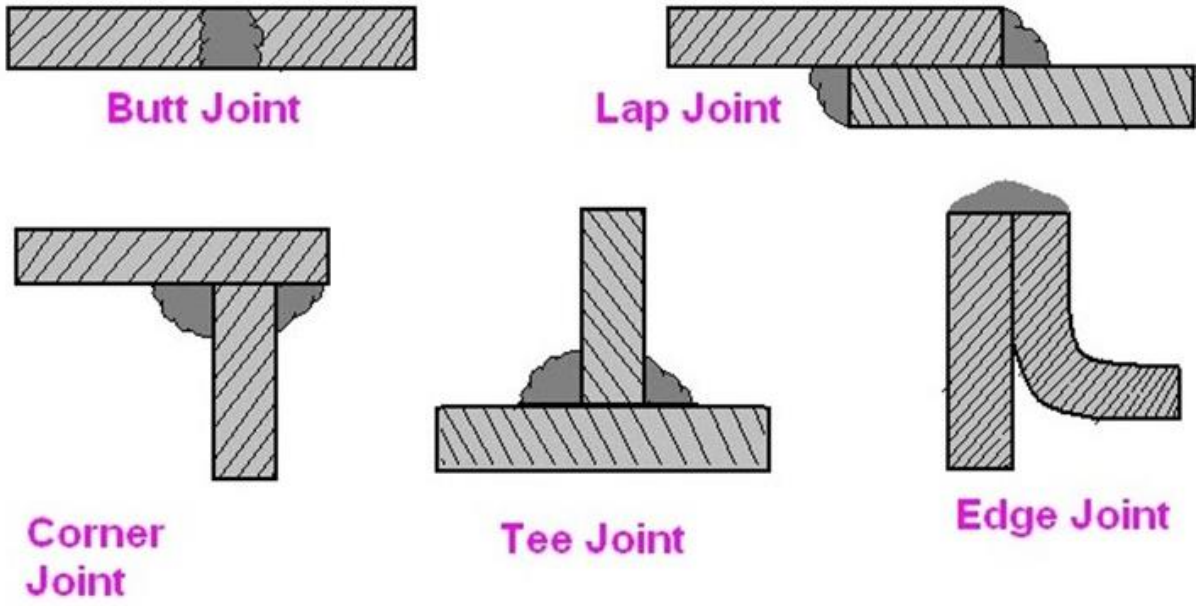

Figure 2.13 Types of Weld Joints (Hassan, 2010)

2.6.1 Butt Weld

Butt welding is a technique used in joining two parts that do not overlap, and that are parallel to each other. In this joint, the weld metal is contained within the planes of the surfaces being joined and the weld throat are either full section thickness, full penetration joint or a partial penetration joint (TWI, 2019). There are different types of Butt weld such a square, V U, J, as shown in Figure 2.14 (Advance Steel Forum, 2016). Welds are either single sided or double sided. It is very economical both in terms of cost and usage of additional constituents (TWI, 2019). Two ends of the weld metals are heated up (prior to joining) under certain pressure and the welding is sustained continuously in contrast to restarting each time with fresh sets of metal (Groover, 2010). The choice of bevel angles and root gaps depend largely on procedures used to fabricate joint and thickness of materials (TWI, 2019). Root opening, the separation between components to be welded enhances accessibility of the electrodes to the base or root of the

joint. The smaller the angle of bevel, the harder to obtain the root fusion hence necessitating the use of smaller electrodes thereby prolonging weld time. Large root opening requires more weld metal consumption and increases welding cost and distortion (ASME, 1910). Narrow bevel angle is economical but difficulty in access risks welding defects. Wide gap on the other hand results in loss of control of weld pool and melt generating irregular and excessive penetration bead, however back strip could be used to overcome this (TWI, 2019).

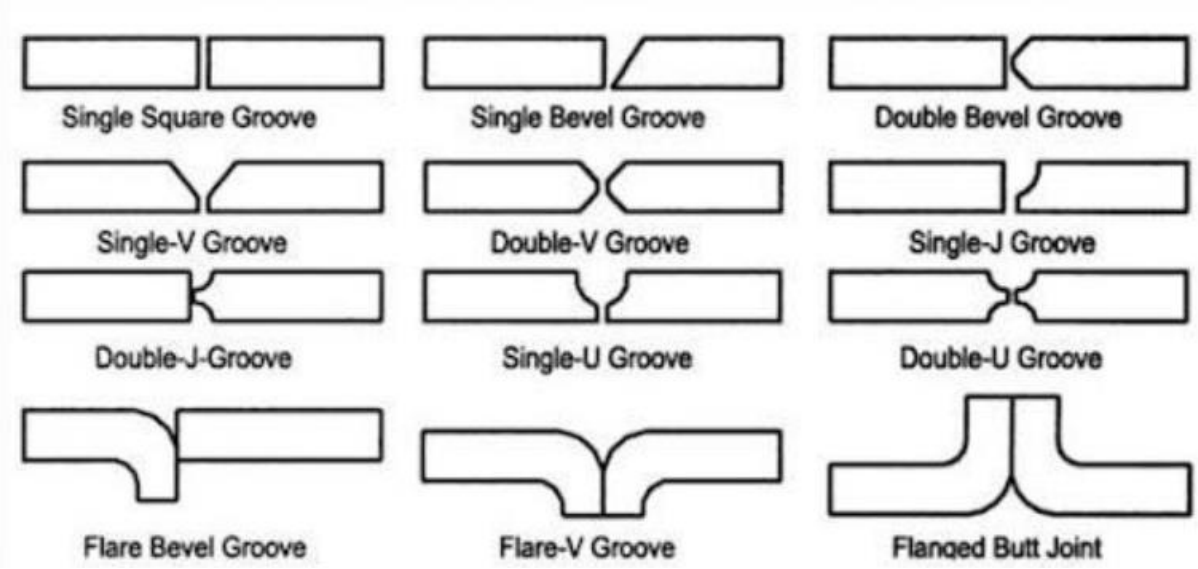

Figure 2.14 The different types of Butt Joints (Advance Steel Forum, 2016)

To weld full plate thickness and obtain weld throat thickness, cut away enough metal along weld joint using either flame or plasma cutting or machining. Reduction in weld volume is achieved using the J preparation unlike straight chamfer of the V preparation. Typical Butt weld is 60^{o} 1mm to 2mm root gap and a zero to 1.5 mm thick root face (TWI, 2019).

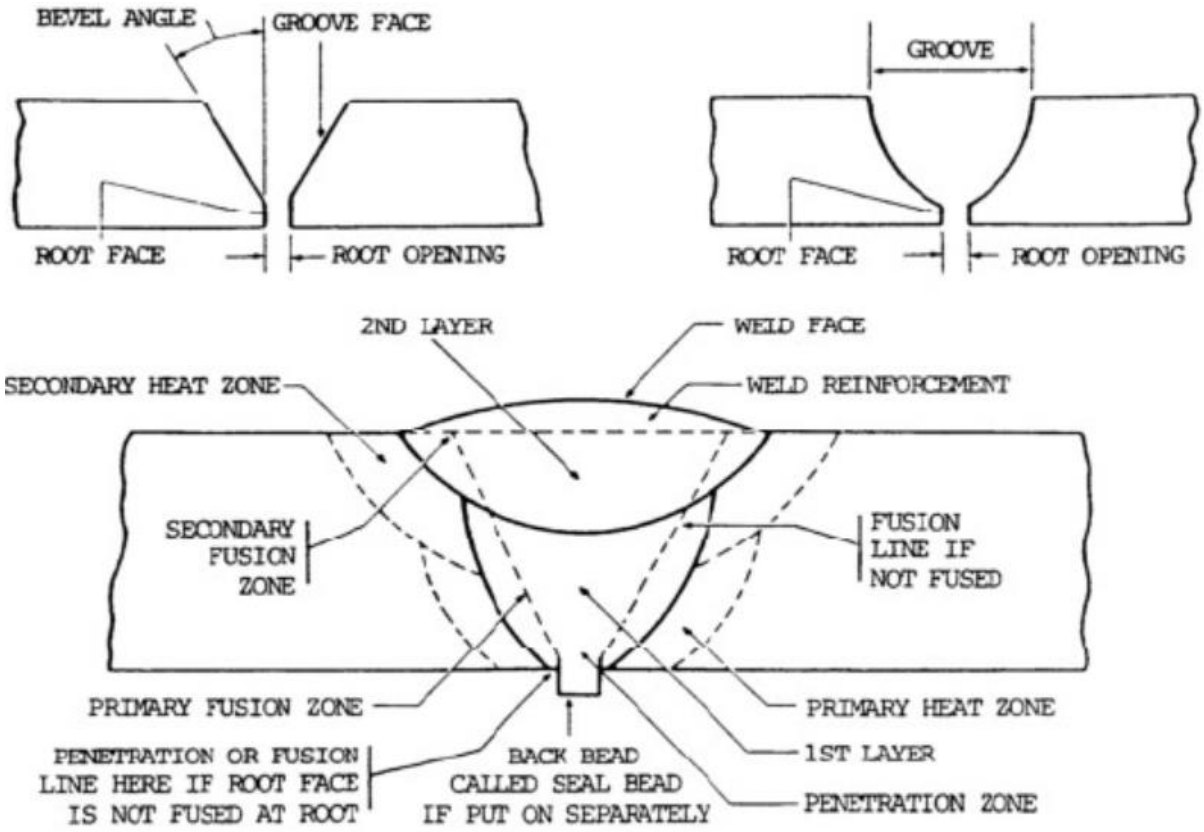

Figure 2.15 Reinforcement on Butt Weld (ASME, 1910)

Nominal reinforcement of the weld is vital as shown in the Figure 2.15 in which there is the back bead known as seal bead, first layer, second layer and weld face. There is also the weld reinforcement, primary heat zone, secondary heat zone, primary fusion zone, secondary fusion zone, penetration zone and penetration of fusion line. The width and height of the weld must be adhered to and be kept to the minimum since increase in reinforcement becomes an additional cost. Double groove joint is preferred to single groove joint since it reduces the quantity of welding in half, hence reducing distortion and enables alternating weld passes which further help reduce distortions. In design and fabrication of pressure vessels and pipelines, the safety of the public is considered in order to minimise the danger of catastrophic and permanent failure. Codes and specifications are written by Government, professional organisations, companies and trades regarding applications on type of material, size,

fabrication, inspection and testing, heat treatment and service limitations requirements. They further detail the expectations for specification for operators and welding procedures. Among the major national organizations involved in writing codes regarding arc welding are American Society of Mechanical Engineers (ASME), American Welding Institute (AWS) and American Petroleum Institute (API) to mention but a few (ASME, 1910).

2.7 Experimental Studies in Welding - Circumferential and Plates

Weld tests include both destructive and non-destructive tests. The latter is carried out in the laboratory and workshop because of its non-destructive effects on the sample and subsequently the samples can be reused several times. The types of tests that can be carried out in the workshop include tensile, bending, impact, fatigue, cracking and hardness tests. Laboratory tests are the test types that can be carried out with the aid of specialized and advanced microscope investigations and include chemical, microscopic (such as optical microscope, SEM, XRD, EBSD and EDAX), corrosive and macroscopic examinations.

2.7.1 Mechanical Testing

2.7.1.1 Tensile Tests

Tensile tests are carried out chiefly to obtain materials for engineering duties and functions. The tensile behaviour of a material being loaded under other types of loading - apart from uniaxial, can be predicted from tensile response. These tensile qualities are built into material design in order to meet the required standard. Tensile characteristics are regularly obtained at developmental stage of each new material and procedures in order for comparison of different materials and procedures.

The main focus here is the strength of a material, which could be determined as stress required to generate a plastic deformation or the overall quantity of stress the material can bear. These stress forms are expressed as safety factors in design engineering. Another key factor is ductility, the degree extent to which materials deforms prior to fracturing. More often than not ductility is included in specification of material than design inn order to maintain toughness and integrity. When the resistance to fracture under other forms of loading is low, it clearly reveals that the ductility level in a tensile test is low. Elasticity is another significant characteristic; however, measurements were carried out using unique methods. More information on tensile tests can be found in chapter 3, under sub-section 3.4.2.

Tensile testing in Plate Welds

The Material to be tested is machined with the edges rounded of in order to avoid cracking. In order to appreciate the elongation, either an extensometer is affixed the Instron machine or punch marks made into the specimen. It is possible to have rolled steel plate that exhibits varying tensile characteristics in the transverse direction, through-the-thickness and vertical path. For tensile specimens less ductile in nature, a vertical cut is preferred as shown in Figure 2.16, especially to reveal the tensile property of the HAZ. For specimens - brittle in nature, the HAZ cracks and does not propagate into the parent metal. It also does not stretch into parent metals. The specimens require high temperatures for undertaking the tensile tests because strength of a metal rises with fall in temperature. Standards include PD 5500 and ISO 15614-1.

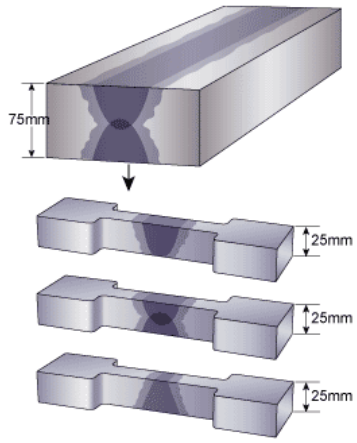

Figure 2.16 Tensile Test Specimen from single layer welded plates Reinforcement (TWI, 2004)

Tensile Testing in Pipe Welds

Tensile tests are applied to pipes considering extensive segments of the whole pipe diameter using mandrels which were positioned into the finishes of the pipes in order to hold the pipe sample in place within the test machine. Alternatively, the ends of the pipes could be flattened as shown in Figure 2.17. If the pipe thickness is required, then the specimen is pipe diameter or cylinder. If only the length of the complete pipe is required for the test, the specimen is designed so as to exclude the diameter of the pipe.

The most important rule of thumb is to note that the axis of the test specimen is cut such that it is situated halfway the thickness of the pipe. Broader diameters of pipe, cylindrical samples at right angle to axis can be used, similarly flat samples (Krishna, 2014). Punch marks drawn on the specimen to reveal the elongation caused in the specimen.

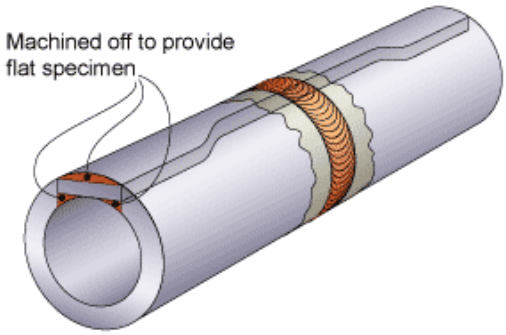

Figure 2.17 Flat Tensile Specimen cut out from Tube (TWI, 2004)

2.7.1.2 Hardness Tests

Hardness test depicts the capability of the metal to resist wear and abrasion and resistance to indentation. Four different hardness type tests are Scleroscope, Rockwell, Brinell and Vickers diamond pyramid.

Vickers Hardness Test is carried out to reveal the hardness of the weld profile refereeing to Heat Affected Zone and Fusion Zone and well as to reveal the hardness profile of the parent metal. Details about this test are discussed in chapter three – subsection 3.4.3 Hardness tests.

2.7.1.3 Charpy Impact Test

With the insert of a v-notch as shown in Figure 2.18 and temperature differences, the Charpy determines the toughness and shock loading of the material. More information on Charpy test

is presented in subsection 3.4.5 under chapter 3. It invariably determines the amount of energy expected to split a sample with a v-notch of 2 mm at an angle of 45 degrees or a U-notch

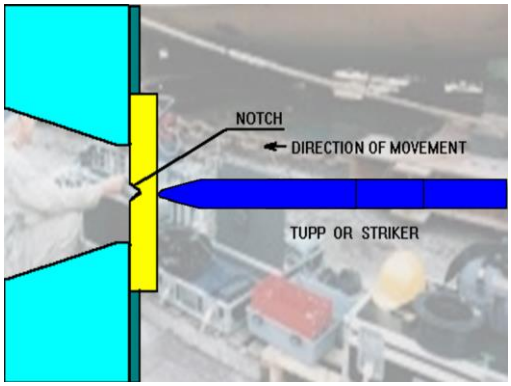

Figure 2.18 Charpy Sample (TWI, 2004)

2.7.2 Laboratory Testing of Welds

Laboratory tests include chemical, microscopic, corrosive and macroscopic examinations. While welding it is typical for defects to take place which could alter the toughness or feature of the plate. Some other defects are as a result of the welder's skill. Etching is needed to reveal interesting and relevant structures within the microstructures of welded specimens. Nitric acid is one of the most widely used etchant and 1 to 2 % of nitric acid is diluted in distilled water or alcohol whereas Aluminium solution is used by diluting 10 to 12% of caustic soda in water.

2.7.2.1 XRD

X-Ray Diffraction is a special process of identifying the degree of structural order of a material. This is crucial because in every atom, there is a unique order of array of the crystals that make up that atom or material and this crystallinity directly affects the density, diffusion hardness or transparency of that material or metal. Since each metal has a peculiar signature, XRD finds relevance in the following:

1. Quantifying the crystallinity of a material or metal
2. Uniqueness of the polymorphic types that there are.
3. Categorising the crystalline from the amorphous crystal types
4. Verifying the crystalline nature of the material.

The characteristics of a crystalline nature are: Accuracy in its solubility, Intrinsic Dissolution Rate (IDR) and melting point. The dissolution rate alongside the IDR determines the rate of release of crystal into solution, which is known as the rate of dissolution. This is key with respect to the weld zone and heat affected zone in vivo since it can determine the sizes at which the particles sets, evaluation of solubility and form the basis of comparison for the different HAZ and weld zones formed using different weld parameters, standards and conditions. (Analytical, 2016)

The diffractogram displays the diffraction angle as it varies in proportion to the intensity as shown in the figure below. When the material displayed is positive, it means there is coherence in the angle of diffraction of the sample being analysed and a reference material, displayed in the diffractogram.

Principle of Measurement

The fundamentals and phenomena of XRD is essentially the intrusion and combination of X-rays in such a manner as to reinforce the displacement of the radiation of equal wavelength in a crystalline sample. The source of the x-rays is a cathode ray tube which selectively releases monochromatic waves of high intensity, focused with the aid of a collimator, at the sample. When Bragg's Law is satisfied, the rays are incident on the weld sample; a diffracted ray emerges, and the superimposed interference is generated. Braggs Law is expressed as:

$$n\lambda = 2dsin\theta \qquad \text{Eqn (2.3)}$$

Where: λ is wavelength of electromagnetic radiation

θ is the diffraction angle

d is lattice spacing in a crystalline sample

n is an integer

X-ray diffraction has a pattern produces a 'signature' of crystals situated in sample which enables the element of interest to be distinguished when the matched with regular reference measurements and distribution trend. More information is presented in section 3.9.

2.7.2.2 SEM

X-rays are generated when fast moving electron strike their target. When the primary beam interacts with the atoms inside the sample resulting in shell transitions, it gives rise to emission of x-rays similar in energy as with parent element. Depicting and detecting the energy generated analysis of the element, is a detection technique that measures the elemental quantitative analysis at a depth of 1-2 microns in every sample. The emitted x-rays also display the distribution of elements present in a sample in form of line profiles or maps.

The secondary electrons are electrons emitted from the top surface atoms yielding meaningful results and imageries in return. The nature of the surface distribution of a sample informs the image contrast. This means that a tiny width of the primary electron beam can generate high quality images.

The backscattered electrons are electrons reflected from atoms within the solid (not surface as in secondary electron). The atomic number of elements within the sample informs the quality of imagery produced which reveals the spectrum of the varying chemical phases in the sample. The quality of images generated from the procedure and is low because the electrons are radiated from within the sample at a depth. More information presented in section 3.7.

2.7.2.3 EBSD

EBSD is the characterisation of crystals on a microstructural level. The material phase and the array of the crystals are taken into consideration, as well as the structure of the test specimen. (Electron Backscatter Diffraction, 2016) The atomic layers in the crystalline test specimen diffract the excited electrons in the primary beam of the scanning electron microscope. (Swap, Electron Backscatter Diffraction (EBSD)) A phosphor screen (inside the sample chamber of SEM, positioned at right angle to the pole piece) radiates clear lines called EBSP (electron backscatter patterns) or Kikuchi bands when the diffracted electrons fall on them. (Swap, Electron Backscatter Diffraction (EBSD)) The individual bands can be indexed using the Miller indices of the parent-diffracting plane. These lines are an extension of the array of the lattice planes therefore, they transmit the details of the crystalline arrangement grain alignment of particular phases via software (Team). Essentially 3 planes or bands intercept are sufficient

to provide distinct information to the crystal in the lattice. The study is practically determining the positioning of atoms within solids is termed as crystallography. More information in section 3.8.

2.7.2.4 EDAX

Energy Dispersive X-ray spectroscopy often referred to as EDX or EDS or even XEDS is a method for chemical representation or fundamental investigation of the elements within a material specimen. Every element has a specific array of atoms within its configuration; this informs the manner of display of the peak energy distributions on interaction with x-ray. A beam of x-rays of maximal energy is directed at the specimen, this excites certain type of x-ray distributions. An unexcited electron is one at the ground state. When an atom is bound to the nucleus in defined energy levels, it is said to be at rest. This further means that when x-rays are directed at the atom within a sample, it transfers energy to the electron in the inner nucleus of the atom and mobilizes it, thus leaving behind holes, which are filled up by electron from a higher energy level. The difference in energy levels of the atoms is radiated as x-rays. The instrument used to measure the quantity of x-ray released in this radiation is the energy dispersive spectrometer. Of significance is the fact the EDS measures the elemental configuration of the sample understudied using the principle that the energies of the x-rays are a direct measure of the variation in energy between the two shells and atomic structure of the element radiating it. Further information is provided in chapter 3 section 3.10.

2.8 Measurements of Residual Stresses

Residual stresses are stresses that are left in a body when all external forces are removed (Withers & HKDHB, 2001). This implies that forces residing in a body at equilibrium with its surroundings or kept stationary. Sources of residual stresses in any material include heat treatment joining technologies such as welding, abrasion, machining forming (Kartal et al, 2008). The combination of residual stresses and service stresses has led to adverse effects such as shortening of component life and failure (Radaj, 1992). Tensile residual stress in the surfaces of components and structures reduces fatigue life and strength, increasing crack propagation and thereby reducing the resistance to environmentally assisted cracking (Hornbach & Prevéy, 2002; Murugan et al, 2001). On the other hand, compressive residual stress in the surface of a component retards the formation and growth of cracks subjected to cyclic loading thereby enhancing fatigue life of a structure (Kartal et al, 2008). Welding initiates localised rapid heating and cooling cycles within the components and structure which produces regions of thermal cycles with the weld region and also fusion zones in the weld (Murugan et al, 2001). An inhomogeneous expansion and contraction in the weldment is generated by reason of the non-uniform heating and cooling cycles within the material component such that upon solidification, the welded region applies a pull on the surrounding region and which holds back via constraints thus inducing misfit strains in the regions of the weld (Francis et al, 2007). Depending on the degree of strains applied, it can either be sustained elastically or localised plastic deformation set in generating residual stresses within the structure (Elmesalamy & Francis, 2014). Usually, the misfit strains are usually close to the yield tensile strains of the material at room temperature especially in the welding direction (Francis et al, 2009).

This implies that within the welded joints and vicinity, there exist substantial tensile stresses when the component has attained thermal equilibrium (Radaj, 1992; Francis et al, 2007). The regular residual stresses exist within the welded zone and HAZ; however, the compressive are

induced in conditions where solid state phase transformation occurs during welding, volumetric expansion as a product of solid-state transformation generates compression stresses (Francis et al, 2007).

The understanding of residual stress is crucial because it not only exists in structures and complicated in nature but enables the prediction of the strength of any engineering structure or component (Withers, 2001). It is therefore vital to employ reliable techniques to in carrying out the measurement of these residual stresses and thorough interpretation of the data or trend of distribution generated (Pagliaro et al, 2009). There are two major ways of measuring the residual stress – Non-destructive and destructive methods (Lu, 1996). The destructive methods are primarily based on the principle of strain measurement in a material that have either been removed or sectioned such as contour method, hole drilling and layer removal. Non-destructive techniques are based on altering the physical characteristic of the component such as lattice spacing or magnetic properties by reason of residual stresses examples are neutron diffraction and x-ray diffraction methods (Withers & Bhadeshia, 2001).

2.8.1 Contour method

This technique is used in measuring residual stresses in two-dimensional stress profiles with the aid of displacement maps and it consumes less simulation time, computing cost and is destructive in approach (Mahmoudi et al, 2009). It does not require advanced tool for measurement and the stress-free lattice parameter, and it is independent of the weld microstructure (Prime, 2010). The drawback of this technique is that it does not measure effectively the residual stresses in the near-surface region of the weld joint or structure and when the yield strength of the material equals the measured stress of the component, it is

subjected to errors in the plasticity induced stress measurements (Traore et al, 2011). As a result, it obtains reading (of 2D stress profiles) in only one stress direction (Prime, 2001).

This technique of residual stress measurement is based on the Beukner's elastic principle of superposition (Bueckner, 1958) which measures residual stresses perpendicular to the reference plane. In sectioning the parts of a component for evaluation of residual stress, first there is the part of the component preserved with the residual stresses, which is further split in two on the x=0 plane such that it undergoes deformation as the residual stresses are released. Next is the surface contour from the half piece of component retaining the partially relaxed stresses and finally the evaluation of the stress-free body analytically by displacing the cut surface to its original flat shape. The original residual stress contained in the component can be calculated by superimposing the partially relaxed stress state with the change in stress at the final state for an elastic medium and this can be expressed as follows:

$$\boldsymbol{\sigma^A}_{(x,\,y,\,z)} = \boldsymbol{\sigma^B}_{(x,\,y,\,z)} + \boldsymbol{\sigma^C}_{(x,\,y,\,z)} \qquad \text{Eqn (2.4)}$$

$\boldsymbol{\sigma^A}$ is the original stress, $\boldsymbol{\sigma^B}$is the remaining stress and $\boldsymbol{\sigma^C}$ evaluates the changes the stress undergoes in terms of relaxation from sectioning and is therefore referred to as the change stress, whereas $\boldsymbol{\sigma}$ is the overall stress tensor. Contour technique entails cutting the specimen evaluation the stress profile, smoothening of the data and FE Analysis (Prime, 2001).

2.8.2 Deep hole drilling methods

This technique is very effective for measuring residual stresses in very thick sections components and structures and it is semi destructive in nature and measures stress in one-dimension map (Hosseinzadeh et al, 2011). It measures residual stresses through-the-thickness by evaluating the strain via stress relief in a small material (Mahmoudi et al, 2009) and this can be carried out in four ways.

Step one involves placing two reference bushes on both front and back surfaces of the materials to generate references void of stress and prevent drill bell-mouthing. Next, a tiny reference hole is drilled into the component and diameter determined from different angular location and at along the axis of the hole at similar intervals. Thirdly, some part of the component is trepanned coaxial to reference hole thereby releasing the residual stresses. Fourth step involves evaluating the diameter of the already measuring the hole at similar angular locations and intervals as previous. The difference in the diameter of the reference hole gives the distortion of the hole in the radial direction. The principle behind the trepanned holes can be compared to those of plates positioned separately each with a tiny hole that is brought under to constant uniaxial stresses (in same direction). There is usually change in the diameter $\triangle d(\theta, z)$of a tiny hole placed in an elastic plate when the plate is subjected to an isolated and constant stress fields ($\boldsymbol{\sigma_{xx}}$, $\boldsymbol{\sigma_{yy}}$ and $\boldsymbol{\sigma_{xy}}$) and is dependent on angle θ roundabout the hole and via the plate thickness z. The perpendicular distortion in the radial direction denoted by $\boldsymbol{U}_{\Upsilon\Upsilon}$, round about the hole is proportional to the residual stresses in the plane of the component, and expressed as follows (Smith et al, 2000):

$$\overline{\boldsymbol{U}}_{\Upsilon\Upsilon}(\theta) = \frac{\Delta dy(\theta)}{d(\theta)} = \frac{1}{E}\left[(1 + 2cos2\theta) + \boldsymbol{\sigma_{yy}}(1 - 2cos2\theta) + \boldsymbol{\sigma_{xy}}(4sin2\theta)\right] \quad \text{Eqn (2.5)}$$

The local stresses can be determined where there is no hole present by determining the difference in the diameter of the reference hole before and after trepanning using the following expression.

$$\Delta d(\theta) = d'(\theta) - d(\theta) \quad \text{Eqn (2.6)}$$

The $d'(\theta)$ and $d(\theta)$ are the reference hole diameter after and prior to trepanning. For every depth z along the axis of the hole, these readings are taken repeatedly at m different angles from the reference hole such that there is a linear distortion in the stresses within the plane normal to the reference hole axis, expressed as:

$$\overline{\boldsymbol{U}}_{\Upsilon\Upsilon}(\theta) = \frac{\Delta dy(\theta)}{d(\theta)} = -\frac{f(\theta)\boldsymbol{\sigma}_{xx} + g(\theta)\boldsymbol{\sigma}_{yy} + h(\theta)\boldsymbol{\sigma}_{xy}}{E} \quad \text{Eqn (2.7)}$$

The above holds true if the stress in out of plane direction is zero which implies that the normal radial distortion at a location along the reference hole is given as:

$$\overline{\boldsymbol{U}}_{\Upsilon\Upsilon}(\theta) = \frac{1}{E}\boldsymbol{M_{2D}\sigma} \quad \text{Eqn (2.8)}$$

E is the young's modulus whereas $\boldsymbol{M_{2D}}$ is the matrix of angular functions. For m angles of readings taken, the pseudo inverse matrix of the least of squares line of best fit for the diametral strain can be expressed as (Smith & Bonner, 1994):

$$\widehat{\boldsymbol{\sigma}} = E\boldsymbol{M^{*}_{2D}}\overline{\boldsymbol{U}}_{\Upsilon\Upsilon} \quad \text{Eqn (2.9)}$$

And

$$\boldsymbol{M^{*}_{2D}} = (\boldsymbol{M^{T}_{2D}}\,\boldsymbol{M_{2D}})^{-1}\boldsymbol{M^{T}_{2D}} \quad \text{Eqn (2.10)}$$

Where $\widehat{\boldsymbol{\sigma}}$ is the optimum stress vector that best fits the diametral distortions, $\boldsymbol{M^{*}_{2D}}$ is the pseudo inverse of matrix $\boldsymbol{M_{2D}}$ and $\boldsymbol{M^{T}_{2D}}$ is the matrix transposed (Hosseinzadeh, 2009).

2.8.3 Diffraction method

Both X-ray and Neutron diffraction are techniques employed in the measurement of residual stresses in a non-destructive approach by penetrating multi-crystalline ceramics and metals at varying beam levels to the order of tens of microns (James et al, 1999). For atomic spacing in some engineering components applications, the wavelength of neutrons penetrates as far as centimetres unlike those of x-rays methods (Withers & Bhadeshia, 2001). Unlike X-ray diffraction technique which measure the residual stresses on the surface, Neutron diffraction techniques measures residual stresses deep within welded structures and joints although there are some limitations by reason of spatial variations in the lattice of the reference structure which involves chemical changes or microstructural gradients and textures of the weld zone and surrounding (Krawitz & Winholtz, 1994). It is observed that such structures and welded joints

are too thick for effective measurements of the residual stresses using neutron diffraction technique which require the measurement of stress-free lattice parameter d_0, unlike the contour technique.

2.8.3.1 Neutron Diffraction method

This technique depends on elastic deformations inside a multi-crystalline component or structure which alters the spacing of lattice planes from their stress-free state. The detector moves round the sample identifying the locations of diffracted beams with high intensity. They are able of measuring bulk penetration depths of 100 mm for (aluminium), 0.2mm near surface depths and can also generate three-dimensional strain amps with high spatial resolution via rotational and translational motion of their accessories. The two approaches for neutron diffraction techniques – time of flight and conventional $\theta/2\theta$ since neutron beams are either pulsed from a spallation source or continuous from a reactor source. The continuous beams utilize the $\theta/2\theta$ scanning in which phase changes $\triangle\theta$in a single $'hkl'$ diffraction peak are regulated by the relationship:

$$\epsilon = \frac{\Delta \mathrm{d}}{\mathrm{d}} = Cot\theta \triangle \theta \triangle \theta \qquad \text{Eqn (2.11)}$$

Where θ is Bragg scattering angle and $\triangle\theta$ is difference in the Bragg scattering angle

The pulse beam utilizes the time-of-flight approach which entails a variable incident wavelength λ and constant Bragg angle of the order of $2\theta = 90^{o}$ due to large range of energies contained in each pulse of neutrons exiting the target, the very energetic arriving prior to the slower neutrons. It is possible to calculate the wavelength and energy of each neutron from the time of flight that is the time duration from the release of the neutron and the strain can be expressed as:

$$\boldsymbol{\varepsilon} = \frac{\Delta t}{t} \qquad \text{Eqn (2.12)}$$

Where t is the time of flight

Detectors with higher resolution measures longer flight path compared with other detectors because the resolution of the strain is a function of accuracy of the measurement of time of flight which is greater than a hundred meters (Withers & HKDHB, 2001).

2.8.3.2 X-ray diffraction method

This technique measures the strains inherent in the atomic planes using the Bragg's law which expresses the criteria for diffraction as (Fitzpatrick et al, 2005):

$$n\lambda = 2dsin\theta \qquad \text{Eqn (2.13)}$$

Where d is the interplanar spacing, λ is the wavelength of the incident x-rays, n is the order of reflection represented by n = 1, 2, 3 … and θ is angle between the incident beam and reflected beam. The interplanar spacing d can be calculated when θ and wavelength λ are known. Residual stress measurements are carried out when the monochromatic beam incident on the atomic planes and the reflected beam from the atomic planes are displayed, the inherent residual stresses within the weld sample (or component) provokes a shift in the interplanar spacing so that x-ray diffraction peak changes giving rise to the quantity of residual stress measured.

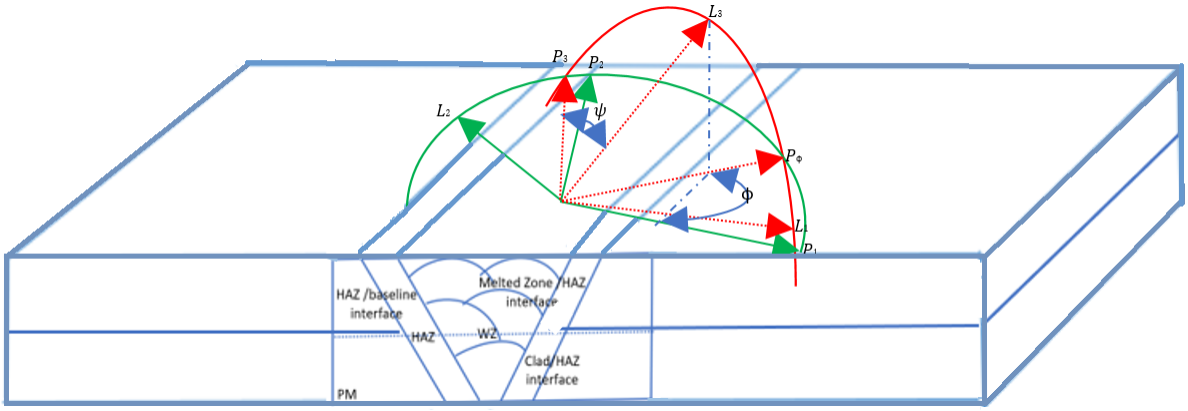

Figure 2.19 X-ray diffraction measurement technique for Residual Stress using Axial System

In Figure 2.19, L_1, L_2 and L_3 are the frame of reference given in the lab in line with the line detectors, whereas P_1, P_2 and P_3 are the three perpendicular directions to the sample being examined. Angles φ and in some cases $\emptyset$ are the relationship between Pi and Li axes where φ is the angle between the measured strain direction L_3 and the normal to the surface P_3. This strain along L_3 is obtained from the equation if $d\emptyset\varphi$ is the interplanar spacing from the diffraction peak for a given 'h k l' plane, in direction of angles $\emptyset$ and φ.

$$(\boldsymbol{\varepsilon_{33}})_{\emptyset\boldsymbol{\varphi}} = \frac{d_{\emptyset\varphi} - d_{\emptyset\varphi=0}}{d_{\emptyset\emptyset=0}} \qquad \text{Eqn (2.14)}$$

Where $\emptyset$ is the angle between one of the principal stress axes P_1 and the projection of the measured strain direction L_3 to the surface of the sample and $d\emptyset\varphi = 0$ is the value of the stress-free interplanar spacing. The $Sin^2\varphi$ approach underpins the measurement of residual stresses in X-ray diffraction technique as shown in Figure 2.19 where diffraction methods are carried out at some tilt angles φ.

For two tilt measurements at angles 0^o and the residual stress at the surface can be derived from the following:

$$\boldsymbol{\sigma}_{\emptyset\varphi} = \frac{E}{1-\nu}\frac{1}{Sin^2\varphi}\frac{d_{\emptyset\varphi} - d_{\emptyset\varphi=0}}{d_{\emptyset\emptyset=0}} \qquad \text{Eqn (2.15)}$$

The term E/ (1 - ν) is constant with ν as Poisson's ratio and E Young's modulus. The curve of the difference in d given by $\triangle$d/d versus $Sin^2\varphi$ results in a straight line with a slope being a function of E, ν and $\boldsymbol{\sigma_{\emptyset}}$**.** The stress at the surface $\boldsymbol{\sigma_{\emptyset}}$ can be calculated for varying tilt angles from the slope of the least square of the best line fit (Francis et al, 2007; Murugan, 2001; Elmesalamy, 2014).

2.9 Simulations of Welding Phenomenon – Numerical

Several works have been carried out on numerical simulation which is evident in published literature with regards to computational work. This involves the simulation of non-linear heat flow generated from the welding of a plate with a single pass or multiple. The majority of the concerns generated during the weld processes are as a result of non-linear heat flow which refers to the moving heat model or the weld torch. This same work began as an experimental investigation from as far back as 1960 right through to 1970, with limited finite solutions for the non-linear transmission of transient heat analysis prior to 1970 (Qureshi, 2008). Computer coding of the multifaceted heat flow process via weldments unto the base material were being advanced from the mid1970s (Qureshi, 2008). A three-part comprehensive evaluation on welding simulation was assembled by Lindgren recently (Lindgren, 2001; Lindgren, 2001) as well as Adib Becker and Anas Yaghi (Yaghi & Becker, 2004).

Rosenthal in 1946, was the first to simulate the welding system using the moving heat source to resolve the transient thermal distribution in arc welding using a 2D and 3D solid heat flow with limited boundaries (Rosenthal, 1946). The moving heat source is the physical states when the thermal excitation changes its location in a more or less regular manner with reference to the body analysed for the heat conduction phenomena.

He further authenticated his findings with experimental results obtained from thermally distributed welded plates of varying sizes and thickness. Following Rosenthal's discoveries, other researchers discovered that although his model gave a detailed estimate of the temperature from a distance; the close-range values were quite high. Debicarri (Debiccari, 1986) and Rybicki (Rbicki et al, 1978) along with other scientists created multiple point heat sources which produced an accurate evaluation of the transient thermal distribution from a weld torch. In addition to using a predefined temperature at certain points, Goldak (Goldak et al, 1984; Goldak, 1996) developed a heat source model known as Double Ellipsoidal Heat Source having a Gaussian distribution to overcome the previous limitation. Currently this is the most common model utilized with the ability to make amendments whenever necessary. Other heat models in use today include Sabathy et al (Sabathy et al, 2001) and (Ravichandran et al (Ravichandran et al, 1996).

Finite element methods in welding simulation were developed by Habbitt and Marcal (Habbitt & Marcal, 1973) and Ueda and Yamakawa (Ueda & Yamakawa, 1971) but with limitations; which spurred subsequent scientists such as Anderson, Friedman and Rybicki et al to provide welding simulations - having fundamentally clear and precise step by step procedures for analysis (Anderson, 1978; Friedman, 1975; Rybicki 1978). This same model took into cognisance the thermal variant material properties and dormant heat related with liquid solid phase transformation. Rybicki developed an enhanced model which was capable of simulating the pipe girth weld of a pipe in a rotational and planer point of view as well as sequentially combining the effect of 28-point sources corresponding to the thermal field. Butt Welding using Plates and simple strain illustration was developed by Friedman and Andersson, the thermo-mechanical uncoupled modelling of the weld was carried out using only half of the cross section (Anderson, 1978).

ABAQUS provides options to carry out coupled and uncoupled simulations. As the former poses higher demand to computing capacity, with only a single core desktop available for this research, the uncouple option was chosen in which the thermal analysis was conducted first, followed by the mechanical analysis using the thermal analysis output as the input.

The Finite Element technique was also utilized for a series of several simulations with a good number of experimental works carried out towards verifying numerical analysis and procedures such as the type of element used in model design, the concentration of the mesh, choice of filler material, method of modelling and the nature of simulation software all playing crucial roles (were employed). The inherent characteristics of different materials were keenly observed with their influence on the thermal and stress analyses closely monitored. The type of computational modelling invented by (Mc Dill, 1915, 1999) and other scientists (Qureshi, 2008), proved to be most effective yielding qualitative results – he established the different element types that could be used while meshing a model; however, for parts of the model, having high stress and temperature differences meant that a default mesh was employed to resolve complexities. As a result of the different mesh styles available for meshing, the number of elements was concentrated. The consequence of this saw a reduction of simulation time. A good number of inventors among whom were the likes of Hyun (Runnemalm & Hyun, 2000) and Lindgren, Runnemalm and others (Lindgren, 2001) (Lindgren, 2001), modified the existing methods of re-meshing. Some of the synopses outlined by Lindgren (who is quite vast in the field of welding and a specialist), are:

Moving heat source is better used in modelling welds compared to the axisymmetric model because it yields less distortion when compared with the latter since the latter takes into consideration the overall circumference of the pipe/cylinder welded. When observing the arc at close range, the immediate environ for the double ellipsoidal model is more effective in representing the heat inputted into the model. The important assumptions made in the choice

of linear elements for meshing is keeping the temperature value invariant in the stress analysis as well as ensuring a consistent overall strain to eliminate locking. While carrying out the stress analysis the extent (amount) of movement/ displacement in any and all directions should be a step above thermal analysis because the latter results in the former. By reason of the unstable nature of ferritic steels during phase conversion which is obvious in the yield stress and thermal expansion, the growth of their microstructure is embedded into the material library. Numerical analysis of a temperature field distribution is more direct compared to the analytical solution. Quite a significant number of weld experiments carried out with the aid of thermocouples are required to generate the appropriate amount of data which can be fed back into the Finite element analysis model to verify computational findings, such as the overall amount of heat inputted into the model prior to analysing the effect of varying weld parameters and design parameters.

2.9.1 Thermal and Stress Analysis of Welded Plates

FEA of thermal stress analysis in rectangular plates was carried out to solve controlling heat equation thereby generating FE equation for thermos-elastic stress analysis using classical theory of thermos electricity. Since temperature was conveyed in the middle of the plates, the temperature increases with time, it increases in middle of plate whereas decreases at edge of plate maintained at constant temperature. Dislocation is highest at insulated edges and maximum temperature and lowest at surface. Thermal stresses were observed at insulated edge and central section of plate (Verma et al, 2014).

In 2D and 3D model developed by Xu in 2014, 3D model provides prediction of heat flow and stress distribution within the model using Goldak double ellipsoidal heat source via DEFLUX interface of Abaqus. This because order than the 2D Axisymmetric model, a 3D model provides

a more realistic picture and detailed information regarding the model compared to 2D. It is observed that greater amount of residual stresses occurred at regions near the weld and corners of weld plates and residual stress responded faster to heating time compared with other weld parameters such as weld path and cooling time. The ability of the software to integrate and clearly interpret specific and combined data such as heating time and weld path as well as cooling time will depend on the computing power of device available, version of the software employed and modelling ability of the user to intricately include and factor all these factors into the Abaqus software. Would this same distribution of residual stresses be displayed in a 3D model of dissimilar material clad having different clad thicknesses? It was observed however that the 2D FE models were suitable for weld because they give inaccurate solutions of residual stresses which could possibly mean that not all details were depicted in the stress profile of the 2D model as compared with the 3D hence the curved profile of residual stress appeared accurate due to approximations in the 2D model by reason of iterations carried out. It is therefore inferred that the 2D axisymmetric models provides as much detailed information as a 3D plate analysis compared with 2D model.

In analysing the stresses in a welded joint, a change in the welding condition definitely impacts on the nature of residual stresses obtained. For instance, residual stress encountered in well clamped system will be less than that in a non-clamped setup. In the 'Investigation of Clamping Effect on the Welding Residual Stress and Deformation of Monel Plates by Using the Ultrasonic Stress Measurement and Finite Element Method', 3D thermomechanical FE was carried out by Javadi in 2015 and it was revealed that longitudinal axial residual stress measured up to 240 MPa whereas ultrasonic measured 230 MPa and hole drilling method measured 250 MPa as shown in Figure 2.18. The difference between the residual stresses measured by the ultrasonic method and those obtained from the FE simulation did not exceed 25 MPa which is about 10% of the yield strength of the Monel plate which implied that

ultrasonic and FE simulation have reasonable agreement. This is commendable because provided the yield strength is not exceeded, failure does not set in and FEA residual stress model is validated by the experimental model. The evaluation of residual stress and deformation in the Monel plates was used to investigate the clamping effect on the residual stresses and deformation by employing the Ultrasonic stress measurement L_{CR}, angular shrinkage measurement, FE simulation and hole-drilling method in Figures 2.20 and 2.21. It was discovered that the angular shrinkage of the clamped plate 2 is less than one-quarter of unclamped plate 1 as shown in Figure 2.20. Ultrasonic stress measurement distinguished the clamping effect on longitudinal stresses with the aid of L_{RC} waves. The process of welding in Monel plates with the aid of clamp yields an increase of 10% in longitudinal stress. By reason of the close agreement obtained between the ultrasonic stress measurement and FEA, it reveals the fact that the former can be used in measurement of residual stress.

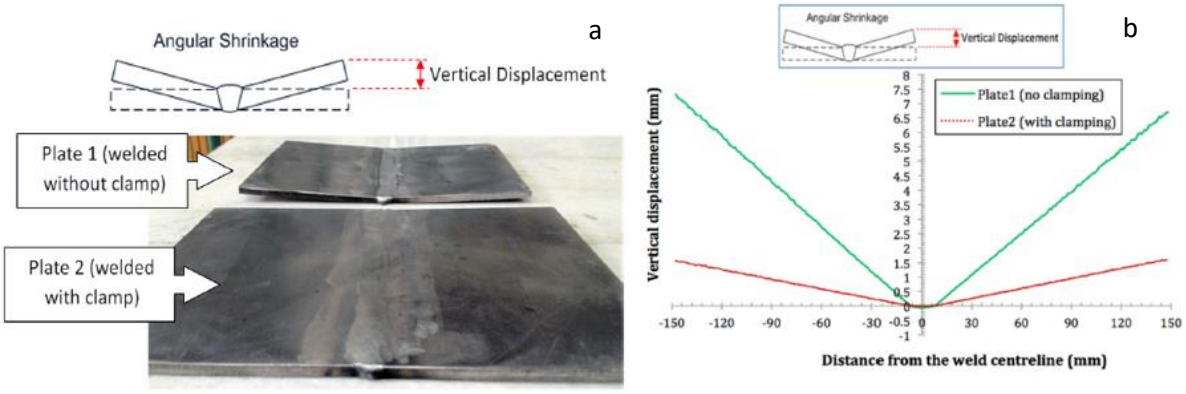

Figure 2.20 (a) Clamping effect on the welding deformations and (b) Angular shrinkage produced after the welding of Monel plates (Javadi, 2015)

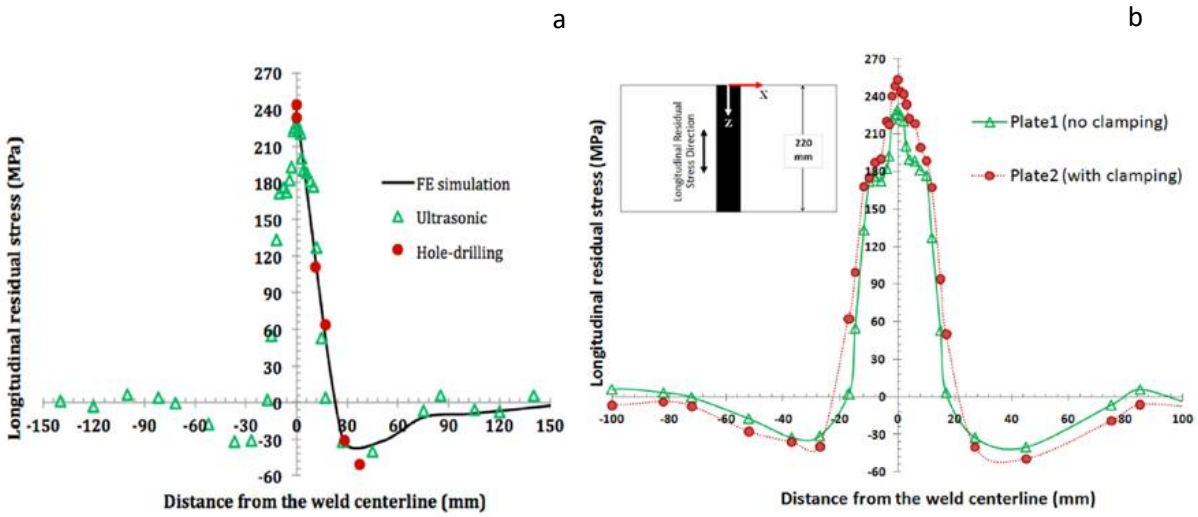

Figure 2.21 Figure (a) Longitudinal Axial Stress FE, ultrasonic and (b) hole drilling Clamping effect on the longitudinal residual stress (Javadi, 2015)

2.9.2 Thermal and Stress Analysis of Welded Dissimilar Materials

The stress behaviour and response in a welded structure has been carried out with the discussion on single plates and pipes layer (monolayer) however in double layer not much has been done.

Ultrasonic residual stress measurement can also be used to verify through the thickness welding residual stresses of dissimilar steel pipes as seen in (Javadi et al, 2013) but not without its drawback such as the complexity in the residual hoop stress which is sensitive to the distance from weld centreline on outer pipe surface as shown in Figure 2.22. Increase in frequency increases the similarity between the residual stress so the outer pipe surface and hoop stress although in close proximity to the surface is increased. There exists an inverse proportionality between the tensile stress and the frequency and by reason of high yield stress; the peak residual stress in the stainless steel exceeds that of carbon steel side of the weld as shown in Figure 2.22. Hence Ultrasonic is suitable for measurement of residual stress difference of two dissimilar pipes at positions faraway from weld line, would the difference be greatly appreciated in two different clad thicknesses of dissimilar material joint? This difference is appreciated at higher frequencies of transducers.

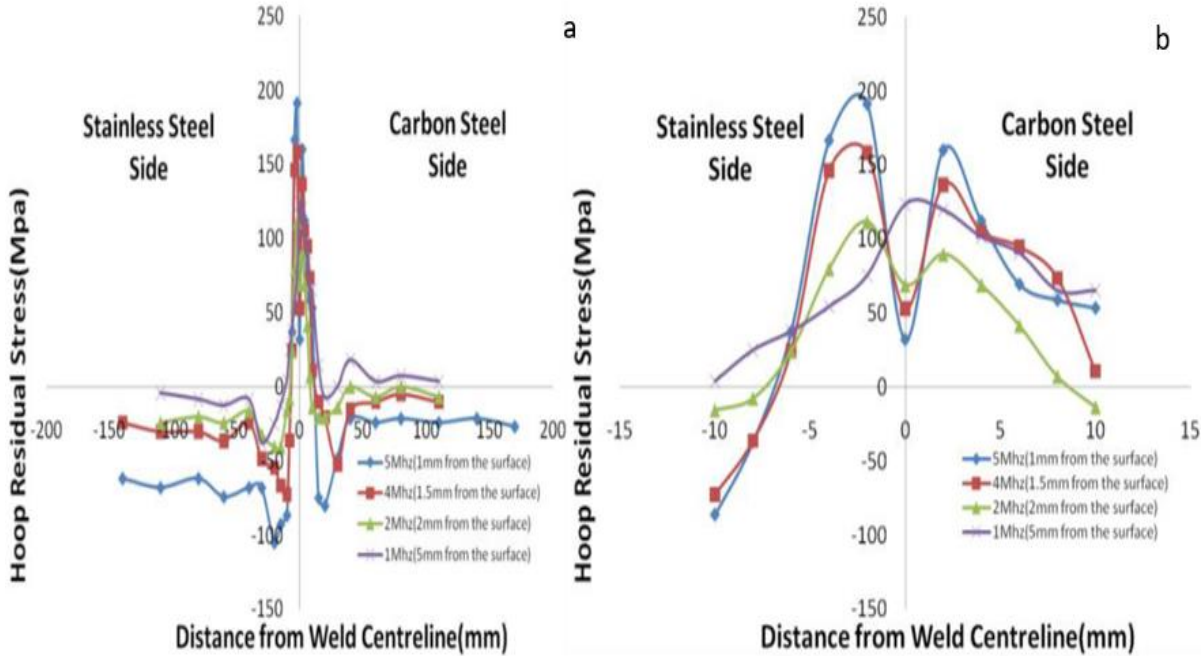

Figure 2.22 (a) Ultrasonic stress measurement results and (b) Residual stress on the weld centreline (Javadi et al, 2013)

(Yaghi et al, 2006) revealed that the residual axial stresses in a thin-walled pipe of 4-pass FE model are tensile at the pipe interior for low Ri/T (bore –thickness ratio) value and at exterior, it is compressive, and in between the wall of the pipe, peak axial stress do occur. The tensile stresses within the interior of pipe decreases from 100 MPa to zero, with increase in Ri/T even up to the value of 100; hence increasing the default compressive stress of the outer pipe surface towards becoming more tensile ranging from -350 to -100 MPa. This is expected for stress distribution within pipes, however does this hold for dissimilar materials clad and what would be the trend in varying dissimilar materials clad thicknesses? This brings about an equivalent of crossover via the wall thickness at an approximate Ri/T ratio of 0.6-0.7. Similar trend is observed for the hoop stress even though higher stresses of the order of -300 to -400 MPa are experienced for Ri/T of 1.0 having a compressive stress of -100 MPa at the outer surface of the pipe. Cracks occur by reason of hoop stress for relevant fluid conditions within surface. At HAZ, Figures 2.23 a and b and 2.24 below, similar trend of tensile axial stress occur at the

interior of pipe which eventually decrease as Ri/T increases and likewise, compressive axial stresses at pipe exterior with Ri/T decreasing compared to the WCL position. Hoop stress distribution is similar to that of axial.

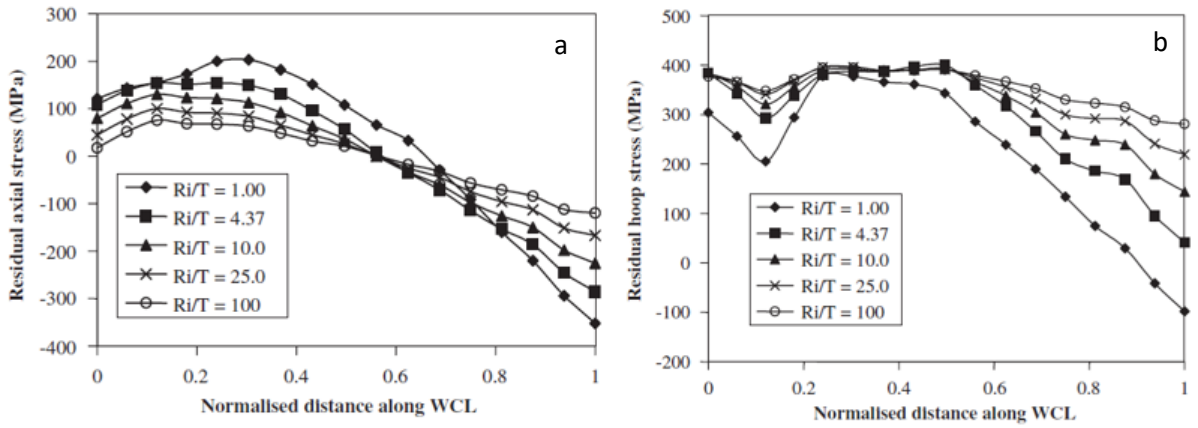

Figure 2.23 (a) Residual axial stress curves for 4 pass model (b) Residual Hoop stress for 4-pass model (Yaghi et al., 2006)

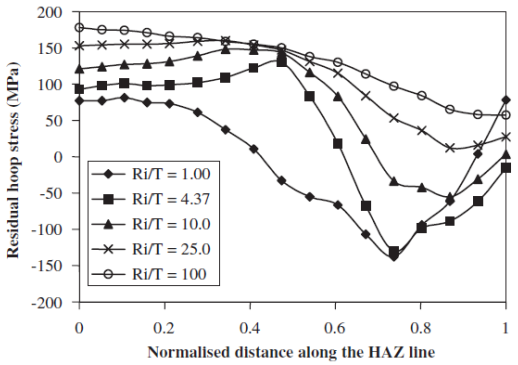

Figure 2.24 Residual Hoop Curve for 4-pass model (Yaghi et al., 2006)

The thick-walled pipe of 36-pass FE model revealed a more complex situation because of the increased weld beads as shown in Figure 2.25; could this condition be the case with thick-walled cladded pipes of dissimilar material weld? For the two position HAZ line and WCL, there exist peaks through the thickness which suggest that the interior of the thicker pipe is less

sensitive to cracking and sensitivity increases with increase in Ri/T, the effect being less than in the thinner walled pipe.

Currently there are no recommended profiles for axial residual stress in restrained material in Engineering Critical Assessment (ECA) procedures. This is because the tensile stress on the un-yielded material would spread outwards. Weld beads with small depth-to-width ratio similar to one formed when bridging a wide gap with a thin and broad bead are more susceptible to solidification cracking because the centre on the weld being narrow has negligible resistance to cracking. Welding techniques and parameters are also key to creating weld bead which has acceptable depth to width ratio (minimum 0.5:1) hence guaranteeing adequate resistance to the solidification stresses. Large depth to width ratio (>2:1) results in segregation and excessive transverse strains in controlled or restricted joint and solidification cracking.

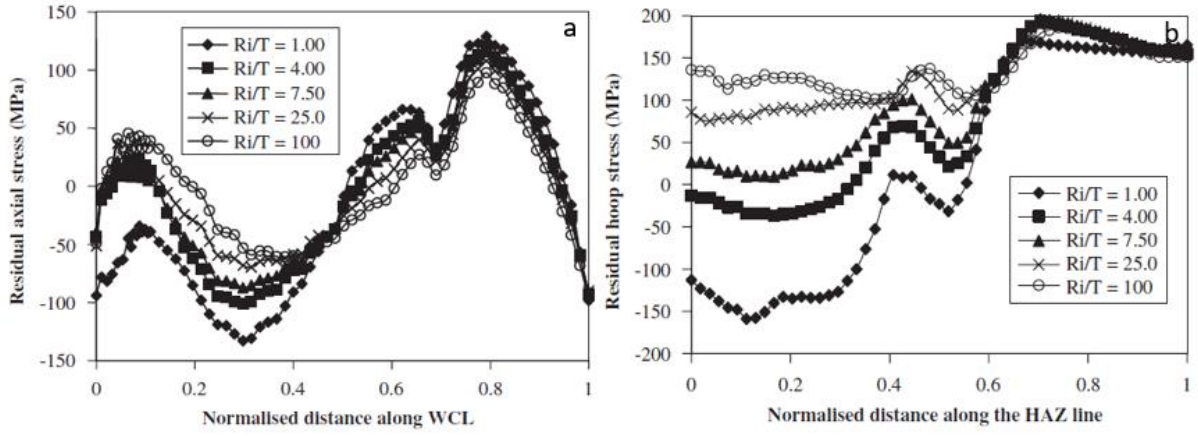

Figure 2.25 (a) Residual hoop stress for 36-pass model (b) Residual axial stress for 36-pass model (Yaghi et al, 2006)

(Jiang et al, 2011) carried out research on "Effects of Clad and Base Metal Thickness on Residual Stress in the repair Weld of a Stainless-Steel Clad Plate". The FE technique shown in Figures 2.26 (a -b) was used to determine the residual stresses which emanated from the repair weld of a stainless-steel clad plate – refer to Figures (C-D) – which embraced the effect of the depth of clad metal, as well as the effect of the depth of the base metal. High residual stress

was induced in the heat affected zone (HAZ) and the weld metal. The thickness of the base metal and that of the clad metal both had a direct impact on the residual stresses (Jiang et al, 2011). The greater the thickness of the clad metal, the more the plastic strain as shown in Figure 2.26 hence deformation increased in order to balance out (relax) some of the residual stress hence reducing the residual stress, however can this be applicable with joints of dissimilar materials in pipes? The structure to be repaired possesses an angular deformation for the weld shrinkage, but this is curtailed since the base metal is of higher strength than the clad metal. Increase in the thickness of the base metal, however, increases the constraint on the weld shrinkage thereby increasing the residual stress. Weld cladding and dissimilar material joints generally create substantial discontinuity stresses at the interface refer to Figures 2.26 and 2.27 such that the subsurface is prone to fatigue cracking.

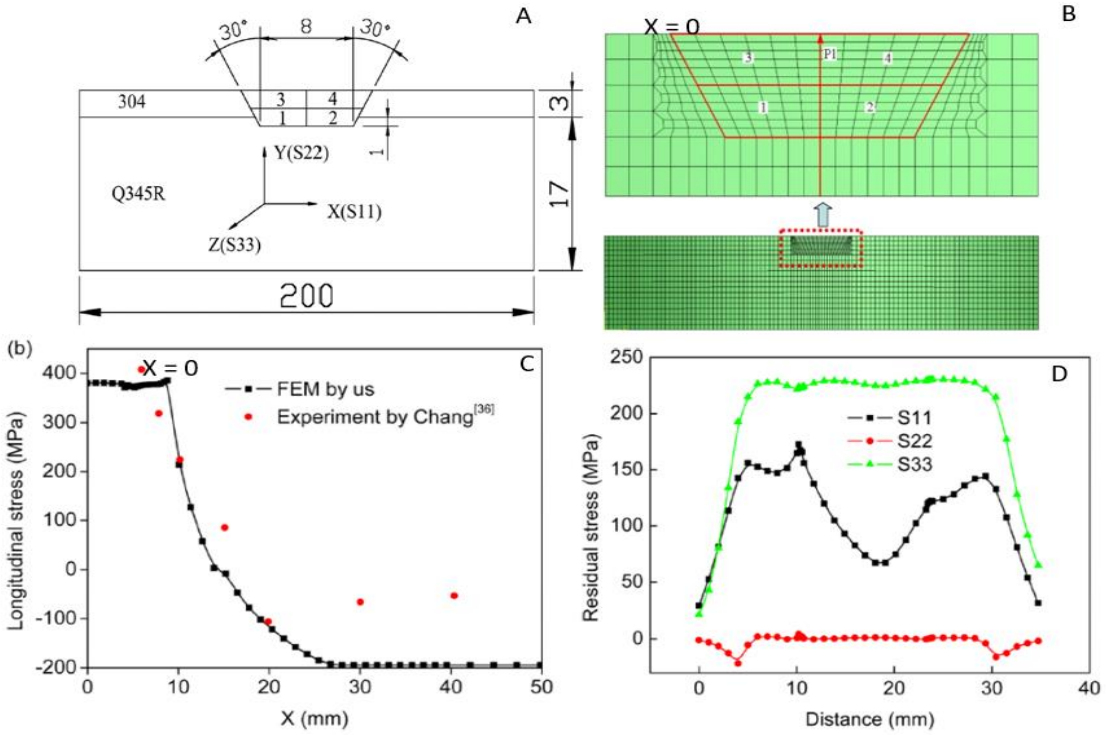

Figure 2.26 (A) Geometrical Model of Clad plate repair weld (B) FE Meshing (C) Comparison of Transverse by Us and Chang (D) Residual Stress along top surface (Jiang et al, 2011)

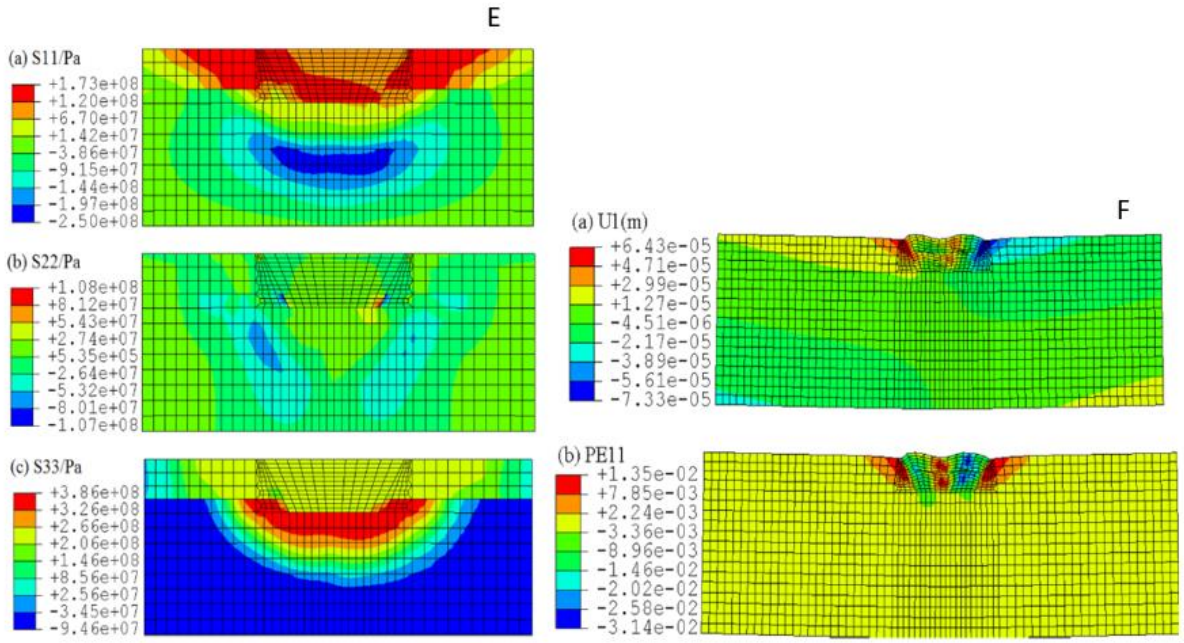

Figure 2.27 (E) Residual Stress Contours in S11 (a) S22 (b) and S33 (c); (F) Contour deformation (a) and Plastic Strain (b) (Jiang et al, 2011)

It was observed that during the repair weld of the clad plate, high residual stresses were induced on the HAZ and weld metal alongside angular distortion on the weld metal by reason of weld shrinkage as seen in Figure 2.27. This can be accounted for by the fact that distortion in a weld is sourced from heating and cooling circles of expansion and contraction in the weld metal adjacent the base metal while welding, and local plastic deformation as a result of weld thermal cycles which is generated as a decrease in the yield strength and elastic modulus as thermal expansion and specific heat increases. This affects the shrinkage and deformation of the material alongside the flow of heat and uniform distribution of heat inducing stress at the weld joints as shown in Figure 2.27.

2.9.3 Thermal and Stress Analysis of Welded Pipes

The stress behaviour and response in pipes has been carried out with discussion on single pipes however in double layer (cladding and with dissimilar material), research is currently ongoing.

(Sinha et al, 2013) in 'Analysis of Residual Stresses and Distortions in Girth-Welded Carbon Steel Pipe' constructed a sequentially coupled 3D FE model of a carbon steel pipe using girth weld in order to comprehend the features of the distortions and residual stress that there are when using tungsten arc welding. Transient, non-linear thermal solution based on heat conduction, convective and radiative boundary conditions is solved in the first part to obtain the nodal temperature history refer to Figure 2.28 (b). Since thermocouples were employed in Figure 2.28 (c) at 4 different locations to take the thermal reading, it is critical to understand the functions undertaken by each of the thermocouples in the nonlinear thermal distribution at the welded joint and the order in which each contributed to the overall distribution in transmission and conveyance of the transient heat. Further still is the fact that it would be well appreciated to compare these heat distributions in different clad thicknesses of dissimilar material joints. The temperature fields are further utilized as thermal loads in subsequent elastoplastic structural analysis to obtain the transient and residual stress fields and distortions, see Figures 2.29 (a-d). This model comprises of a 'V' groove as shown in Figure 2.28 (a) in a 300 mm OD pipe having wall thickness of 3mm. Experimental validation of the thermal and stress models were carried out via temperature distribution, residual stress and distortion measurements. There was a good match between the measured and simulated results refer to Figure 2.29 (b). The result also showed that close to the weld area, the axial stresses are compressive in the outer surface of the pipe as shown in Figure 2.29 (f) and tensile within the internal surface of the pipe as observed in Figure 2.29 (a); this however contradicts the residual stress distribution in (Dar et al., 2009) which reveals compressive stresses within the internal surfaces of the pipe and tensile stresses within the exterior surfaces of the pipe; whereas hoop stresses are tensile outside and inside the pipe – refer to Figure 2.29 (c and d) (Sinha et al., 2013). If this is the stress distribution in 3mm cladded pipe what will be the profile for higher clad thicknesses of dissimilar material joint? The angles 50, 90, 150 and 250 are four different

angles at which the readings of the residual axial stress distributions were taken to reveal the stress distributions.

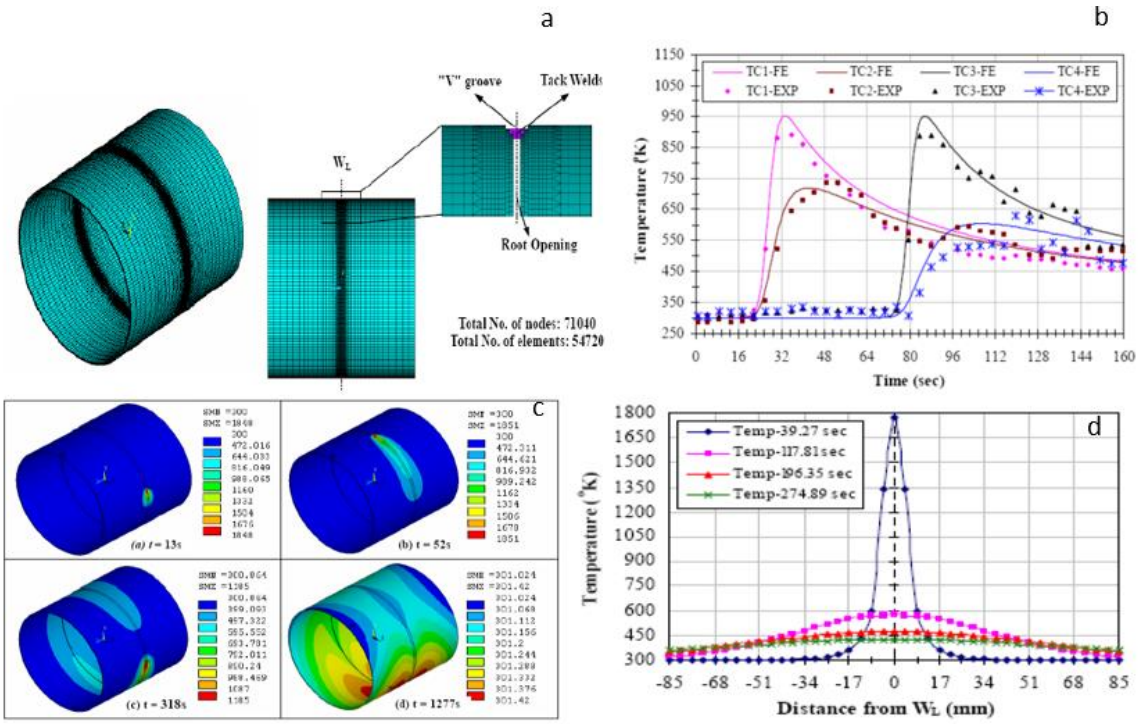

Figure 2.28 (a) 3D FE mesh sensitivity analysis (b) Computed and measured transient temperature profiles on pipe outer surface. (c) Temperature profiles at four different time steps (d) Axial Temperature distributions for four different cross-sections (Sinha et al., 2013)

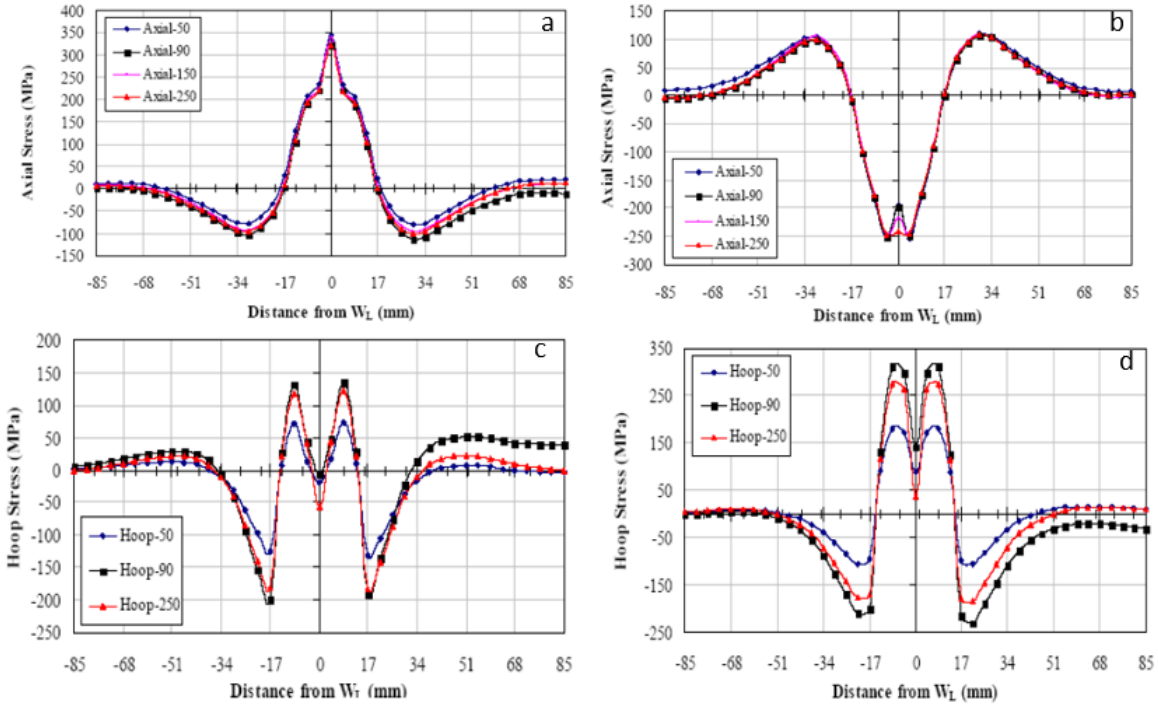

Figure 2.29 (a) Axial residual stresses on inner surface (b) Axial residual stresses on outer surface (c) Hoop residual stresses on outer surface (d) Hoop residual stresses on inner surface (Sinha et al., 2013)

The wall thickness has a direct impact on the residual stress profile in a girth welded cylinder in that higher wall thickness gives rise to reduced residual stress and greater residual hoop stresses. Close to the line of weld the highest values of radial deflection and axial deflections are observed, this is because the characteristic axial residual stresses are compressive near the weld. In BS 7910, there is currently no guidance on the residual stress distributions along the pipe length showing how residual stresses fade away from the weld centre-line outwards. Far away from the weld line, the shrinkage in radial direction reduces steadily and approached a near zero value at the restrained end. There is a face tilt seen at the non-restrained end of the cylinder. This difference in the angular distortion is due to deviation of the radial deflection of the end of the pipe.

(Dar et al, 2009) worked on 'Analysis of weld-induced residual stresses and distortions in thin-walled cylinders' in 2008. The research entailed computational simulation of 3D FE models

of thin layered cylinders using TIG welding to demonstrate the distortions and residual stresses using ANSYS with subroutines and material properties except yield stress. The model used is the Gaussian distribution for circumferential welding and has features of power and density distribution control in the weld pool and HAZ. The geometry of the butt weld was carried out on a 300 mm outer diameter cylinder having a wall thickness of 3mm and having a V shape. The procedure was carried out with the aid of a non-linear thermos-mechanical analysis and the results of the mechanical and thermal analysis are confirmed via experiments for residual stresses, thermal responses and distortions. High tensile and compressive axial residual stress exists on inner and outer surfaces of the cylinder. One way to reduce the residuals stresses without external constraint is to reduce the weld shrinkage which is typical in most welds, however with proper weld grove design and welding procedures parameters as well as edge preparation for conventional narrow grooves in pipes, it can be minimised. For the examination of residual stress states in the pipe, current ECA procedures were introduced in which distribution and magnitude of the stress were recommended for certain thicknesses. Although the guidance was developed for general case with wide groove welds, the degree of conservatism could be evaluated. Narrow grooved joints have proved effective for residual stress reduction compared with GMAW and pulsed PGMAW according to (Giri et al, 2014). Hoop residual stresses on external and internal surfaces vary at different cross sections (Dar et al., 2009).

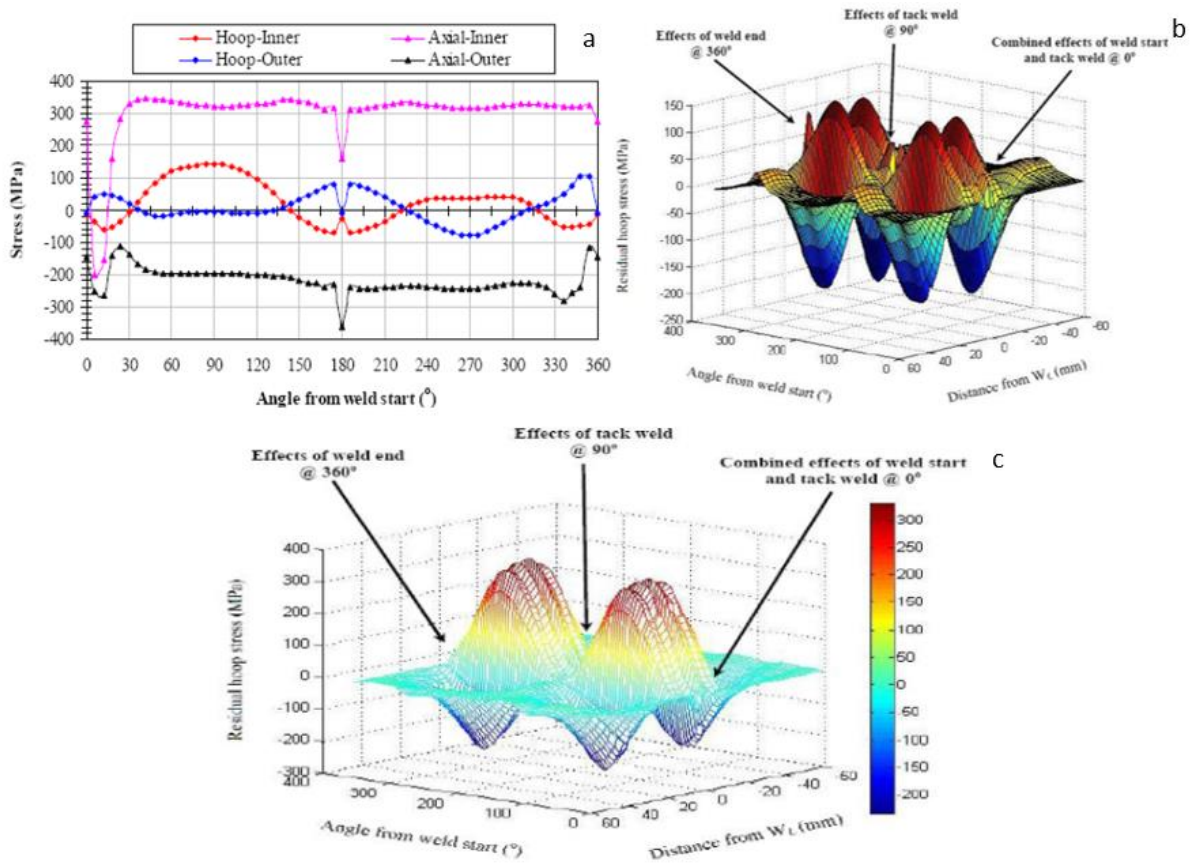

Figure 2.30 (a) Axial and hoop residual stress distributions on outer and inner surfaces of cylinder (b) Hoop residual stress fields on cylinder outer surface (c) Hoop residual stress fields on the cylinder inner surface (Dar et al., 2009)

They observed that the residual axial stresses vary slightly with the circumferential positions from the start of the weld, similarly the hoop stresses also vary with the circumferential positions as shown in Figure 2.30 (a). The profiles of the axial residual stresses are as good as homogenous in the circumferential direction exception of the weld start position – refer to Figure 2.30a). There is a conspicuous protuberance underneath the crest of the weld which signifies the discrepancy in stress as observed in Figure 2.30 (a-c).

(Feli et al, 2011) carried out research on 'Finite Element Simulation of Welding Sequences Effect on Residual Stresses in multipass butt-welded stainless steel pipes'. In the research 3D model and 2D axisymmetric FE models, pipes were developed using the Abaqus software in order to analyse the temperature history as shown in Figures 2.31 (a and b) and residual stress

– refer to Figures 2.32 (c and d) conditions in multi weld passes in stainless steel. They employed the Goldak and Akhlaghi double ellipsoidal heat source model for moving heat source for both front and back heat source using the DFLUX (used to define nonuniform distributed flux in a heat transfer or mass diffusion analysis) subroutine provided by ABAQUS. User subroutine FILM (is a subroutine in Abaqus used to define non-uniform film coefficient and associated sink temperatures for heat transfer analysis) was employed to simulate the overall heat boundary conditions. When the outcomes of both 2D axisymmetric and 3D simulations were compared with experimental results, it was discovered that there was good agreement and that the hoop and axial stresses in both models have similar distributions in all locations apart from the weld start position as shown in Figures 2.33 (a-d). High values of final axial and hoop residual stresses in the weld zone is as a result of high yield strength of weld metal and the residual axial stress profile inside and outside the pipes are opposite as shown in Figure 2.33 (a and d). In BS 7910, there is currently no guidance on the residual stress distributions along the pipe length showing how residual stresses fade away from the weld centre-line outwards. Mechanical analysis according to (Ahmed et al, 2019) is hinged on the fundamental principles of thermal-elastic-plastic equations because the material is strained while welding by reason of weld thermal cycle such that the total strain comprises of elastic strain, thermal strain, plastic strain, volumetric strain and transformation-induced plastic strain which produces residual stresses and deformation. The plastic deformation induced is associated with von mises criterion so that equivalent stress is expressed as field (Dai et al, 2019; Ahmad et al, 2019; Yupiter et al, 2013; Ahmad et al, 2019):

$$\boldsymbol{\sigma_p} = \frac{\boldsymbol{\sigma_y}}{\frac{\mathbf{1}}{\sqrt{\mathbf{2}}}[(\boldsymbol{\sigma_1}-\boldsymbol{\sigma_2})^{\mathbf{2}}+(\boldsymbol{\sigma_2}-\boldsymbol{\sigma_3})^{\mathbf{2}}++(\boldsymbol{\sigma_1}-\boldsymbol{\sigma_3})^{\mathbf{2}}]^{\mathbf{1/2}}} \qquad \text{Eqn (2.16)}$$

Where $\boldsymbol{\sigma_1}$, $\boldsymbol{\sigma_2}$ and $\boldsymbol{\sigma_2}$ are the principal stresses in the and total strain which is the sum of the individual strain components can be expressed as (Ahmad et al, 2019):

$$\boldsymbol{\varepsilon_{total}} = \boldsymbol{\varepsilon_e} + \boldsymbol{\varepsilon_p} + \boldsymbol{\varepsilon_T} + \boldsymbol{\varepsilon_V} + \boldsymbol{\varepsilon_{T_r}} \qquad \text{Eqn (2.17)}$$

Where is $\boldsymbol{\varepsilon_{total}}$ is the total strain, $\boldsymbol{\varepsilon_e}$ is the elastic strain, $\boldsymbol{\varepsilon_V}$ is volumetric strain, $\boldsymbol{\varepsilon_T}$ is the thermal strain, $\boldsymbol{\varepsilon_p}$ is plastic strain and $\boldsymbol{\varepsilon_{T_r}}$ is transformation-induced plastic strain.

If the effects of volumetric strain change and transformation induced plastic strain can be neglected, then the stress field and displacement field can be obtained from the following expression:

$$\{\mathbf{K_1}\}\{\boldsymbol{U_e}\} - \{\mathbf{K_2}\}\{T_e\} = \{\boldsymbol{R}\} \qquad \text{Eqn (2.18)}$$

Where $\{\boldsymbol{R}\}$ is temperature loads of each node, $\{\boldsymbol{K_1}\}$ and $\{\boldsymbol{K_2}\}$ are stiffness matrix, $\{T_e\}$ is the temperature and $\{\boldsymbol{U_e}\}$ the displacement field (Dai et al, 2019; Ahmad et al, 2019; Yupiter et al, 2013; Ahmad et al, 2019).

(Feli et al, 2011) also studied the consequences of the order of welding on the thermal and mechanical analysis; having taken into cognisance four different type of weld order. It was discovered that for the four type welding sequences employed, FE analysis predicted that order than the start point of weld, residual there are no significant variations in the profile of the residual axial and hoop stresses with the amplitude varying slightly. However, could it be that it is possible to obtain similar distributions of residual stresses irrespective or the sequence in which the weld direction is taken, especially for different clad thicknesses of dissimilar material weld?

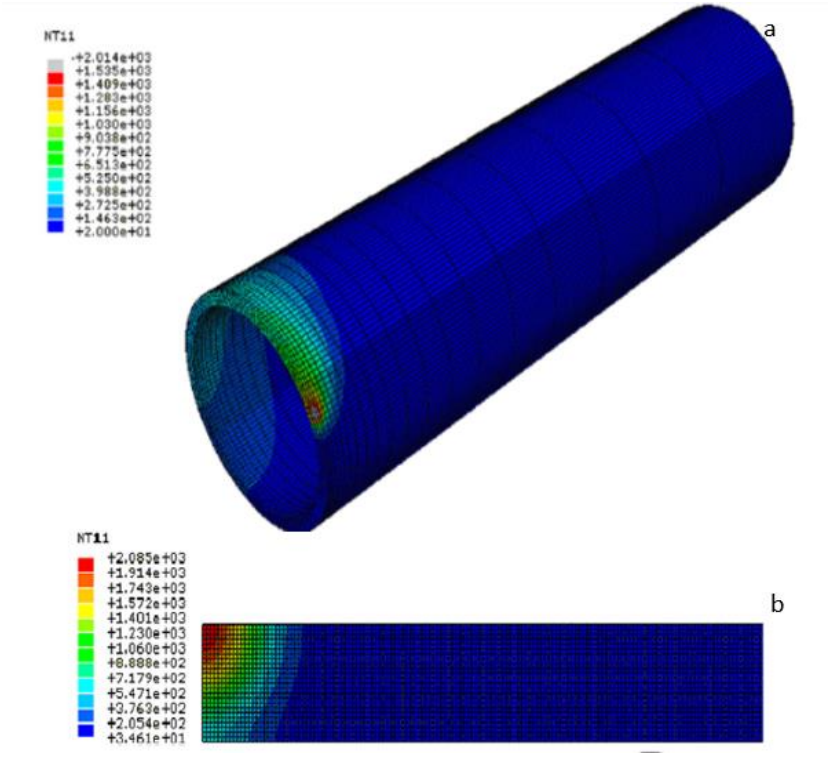

Figure 2.31 (a) Temperature distribution in 3D FE simulation (b) Temperature distribution in 2D FE simulation (Feli et al, 2012)

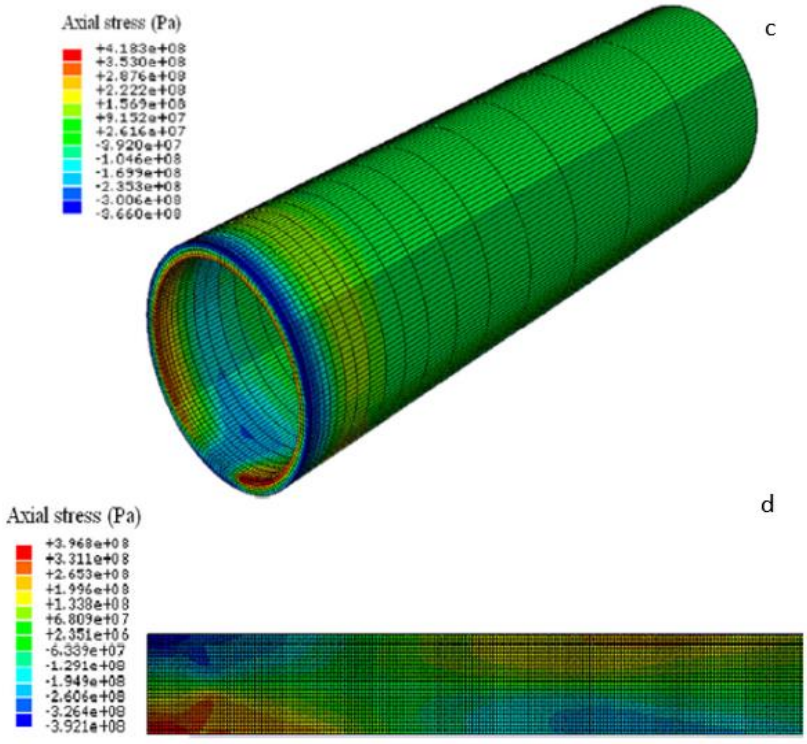

Figure 2.32 (c) Axial stress distributions of the welded pipe in 3D FE simulation (d) Axial stress distributions of the welded pipe in 2D FE simulation (Feli et al, 2012)

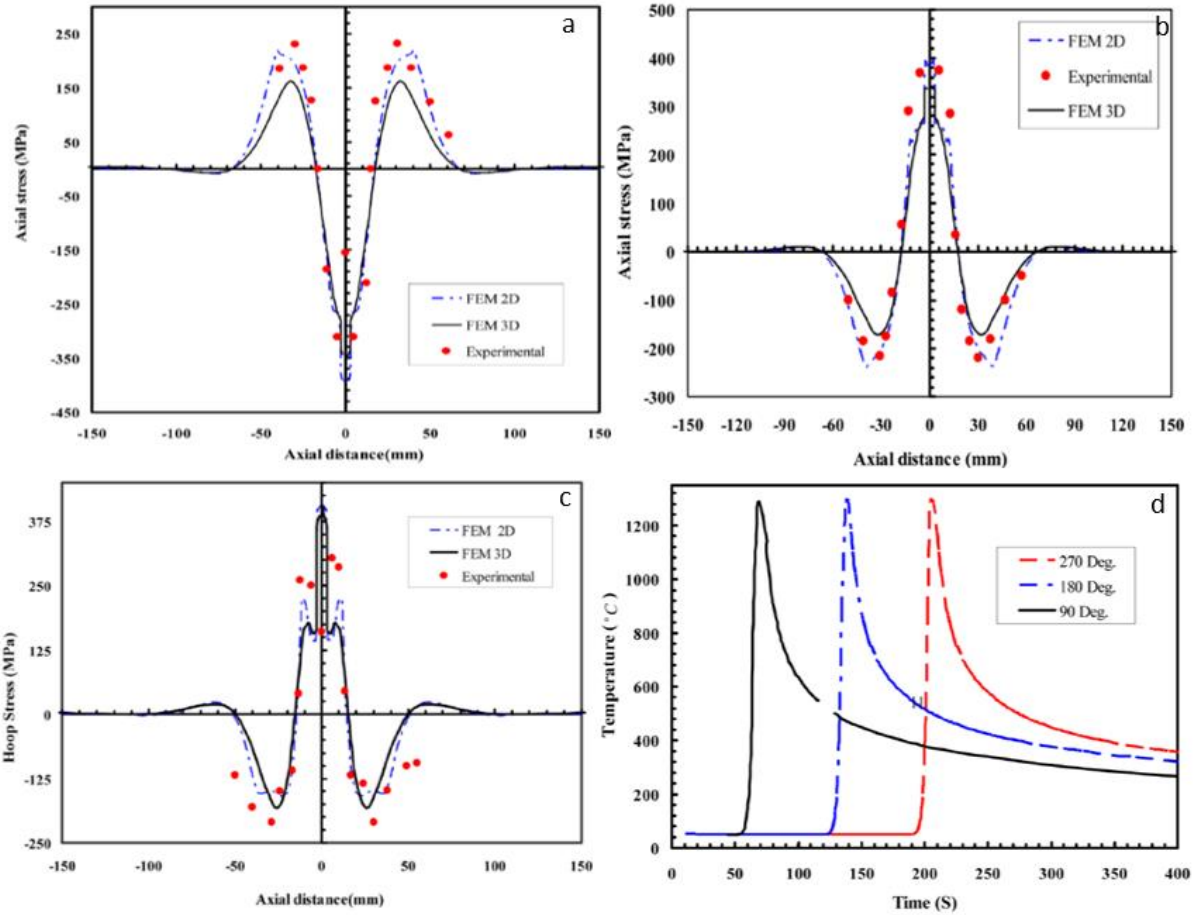

Figure 2.33 (a) Axial residual stress at 180° on outside surface (b) Axial residual stress at 180° on inside surface (c) Hoop residual stress at 180° on the inside surface (d) Thermal Cycles at 3mm of weld centreline in 90° deg, 180° and 270° (Feli et al, 2012)

It was found that opposite distribution exists between the residual axial stress on the inside and outside surfaces and both stresses are similar irrespective of weld start point because of high yield strength of the weld metal. Metallurgical factors were not taken into account in the numerical models.

Smith et al, 2000 carried out work on "Measurement and Prediction of Residual Stresses in Thick-Section Steel Welds". Thick sections of weld generate substantial quantity of residual stress and a few researchers were able to predict the distribution via the depth. They employed the deep-hole technique to measure the residual stress in the thick sections by gathering the outcome of the experiment on different welded steel components and finally compared it to the

outcome with FE simulations of residual stress in a welded cylinder in order to validate it. A good agreement was discovered.

The residual stress through thickness was generated for components with a wall thickness that ranged from 35 mm to 108 mm and can be obtained using FE simulation. DH is effective in measuring stress to different thick sections of welded steel components such as plates, pipes and cylinder nozzles.

Engineering Critical Assessment (ECA) procedures such as BS7910 and R6 recommend through wall residual stress profiles to be used in the assessment of structures containing flaws in the absence of residual stress measurements and or simulations.

Current ECA procedures are widely used for the evaluation of residual stresses in conventional wide-gap weld. Stress profile recommended in these standards did not consider the profiles measured from non-destructive neutron diffraction in the narrow-gap weld in as-welded and after PWHT conditions. (Ren et al., 2016) considered the challenges of measuring residual stresses in large girth welded pipe spools using neutron diffraction technique (Ren at al., 2016) in as-welded and local post weld heat treated conditions. Choice of stress-free lattice spacing value is key to accurately measuring the residual stress. Using the hkl specific material properties for the measured planes as established on the DECal software of the Kroner model on a sample of dimension 95 mm long and 6 mm thick. Residual stresses are reduced in as-welded condition when compared to the yield strength of the material and significant relaxation is observed in PHWT samples.

When using BS7910 or R6 procedures for the evaluation of the residual stresses, recommended stress profiles should be obtained by applying correct value of the component thickness and understanding the level of heat input locations, but also provided information such as the time required to complete a set (stress component at each direction) of measurement on large scale and complex geometry components (Ren et al., 2018).

Yao Ren also researched on the Residual Stress State of X65 Pipeline Girth Welds before and after local and Furnace Post Weld Heat Treatment (PWHT) and investigated the local post using identical pipeline production manufacturing multi-pass narrow gap welds. Pipe sections fixed horizontally without clamps during welding using two mechanically and electrically controlled welding torches with short time period between each pass for cooling, inter-pass temperature range of 80 – 160^{o}C. Hoop stress at the exterior surface of pipe closer to weld toe is 40% of room temperature yield strength of parent metal and same stresses occur at this weld toe too signifying that the stress distribution from measurement are below the upper bounds advised in the codes and standards. Also considering 3mm underneath the exterior pipe surface the axial and hoop stress distributions are similar for the two as-welded pipes with hoop stress in weld being 75% of yield strength and >30% in toe and zero further 15mm from weld centre line. Axial residual stresses are tensile up to 55% of the material yield strength at 3mm below pipe exterior surface and reduced to 20% after PWHT. Since the recommendations of R6 in yield zone are conservative (Ren et al., 2016) it implies that there is the need for reduced residual stresses via smaller HAZ and reduced heat input in the narrow gap weld procedure. The weld centre line has reduced stress 20% for PHT1 locally heated pipe and approximately zero for PHT2 1. Hence, PWHT is effective stress reducing means in pipe spools (Ren at al., 2018). In all the researches considered, the possibility that there could be continuous reheating of a previously laid weld pass while the new weld pass is being laid has not been considered nor investigated; not even at the macrostructural level, not to mention different clad thicknesses of dissimilar material weld – with the aim of finding out evidences to prove that indeed fully reheated weld sample can in fact have interesting and similar findings with the continuous reheating which takes place during the laying of the weld passes.

2.10 Conclusion

Through reviewing and researching of literature and past work, the gaps of knowledge and need for this research were uncovered. The major gaps that there are in knowledge include: transient heat intricacies (via the array of thermocouples), reheating occurrences at the welded joints, welding path and developed systems. There is therefore the recommended to perform large numbers of residual stress evaluation on girth welds with various thicknesses or R/t ratio values to provide related residual stress profiles in BS7910 and R6 which were the standards employed in this research.

Development for the local content is also seen in the relevance of this research since the residual stress measurement in cladded pipes in TWI is not clearly stated. There is no standard guidance for predicting the residual stress distribution profiles across the parent metals and weldment along pipe length. Typical approach would be to conduct measurement. This is the build up as a first step to the instructions given in coding and industrial standards. In reference to Nigeria and with due respect to PTDF, this research feeds into the knowledge gained to the local industry.

Previous works have been carried out primarily on welding in single layer pipes for the thermal and stress analysis and experimental work, and although some work has been carried out on cladding, there still is the need for improvement in understanding the welded joints. Cladding is carried out mainly for the purpose of enhanced corrosion resistance and structural integrity. Since two metals of different chemical constituents are welded together what will the newly formed weld joint be in terms of chemical composition, strength, corrosion resistance etc? It is important to find out if these properties are enhanced or reduced.

Since welding is carried out on two dissimilar materials – stainless steel and mild steel, there is the need to investigate what occurs in the Heat Affected Zone of the welded joint since the

chemical component of the HAZ is altered via high weld temperatures in the course of welding. Because there is continuous reheating of the thick clad section during the course of the weld, there is the need to discover the weakest point of burst because if a structure is to fail it first begins at the weakest point of joints; therefore, occurrences and discoveries at the microstructural level are very important.

There is also the need to capture the temperature responses (transient) from the welded joint with the aid of thermocouples positioned at strategic points on the welded joints with the main aim of understanding and justifying the reasons for the thermal responses is vital. It is not enough to presume the distribution of heat through the weld metal but detailed study on the temperature profile and heat distribution is needed in order to uncover any peculiar trends and being able to account for the peculiarities discovered.

NOTE: The first page of published papers both in international conferences and journals are given in appendix 1.

3 EXPERIMENTAL STUDIES OF DISIMILAR MATERIAL WELDED JOINTS IN CLAD

3.1 Introduction

This chapter presents the experimental technique of sample preparation and the step-by-step procedure for mechanical testing in order for mechanical characterisation of dissimilar weld joints samples. The research carried out in the laboratory comprise of weld using gas metal arc welding (GMAW) which entailed welding of two dissimilar materials – 316 stainless steel API Grade and CR4 mild steel grade – carried out on two different clad thicknesses of 2 mm and 12 mm. Section 3.2 discusses the sample preparation which include the choice of filler metals, the weld parameters and welding procedures. Section 3.3 is thermal measurements carried out with the aid of thermocouples placed at strategic positions. Prior studies have been carried out in welding without due attention given to the intricacies of the transmission of heat within the welded joint, so the need arises to obtain and record the data of the transient heat within the welded structure in order to uncover the trend of heat transmitted within the welded joint because this transient heat curve will be compared with the transient curves of the FEA thermal analysis in chapter 4. Section 3.4 is the discussion of the mechanical testing of the welded joints using tensile, Charpy and indentation tests with the intent of finding out the strength and hardness as well as point of the joint most susceptible to crack initiation – in the weld, while section 3.5 is the optical microscopy which is the grinding of sample surfaces for laboratory examinations of macrostructural evolutions. Sections 3.6 -3.9 comprised of the different electron microscopy and laboratory examinations such as SEM, EBSD XRD and EDXA which were carried out in order to investigate the occurrences in the weld microstructure with the intent of verifying the evidence of reheating which took place at the welded joints while welding. Finally, section and 3.10-11 summarises and concludes the

achievements in the fabrication of the welded joints using girth welding. The HAZ is of relevance because the melting and fusion of both parent material and clad metal alongside the filler material takes place here resulting in modification in the chemical properties (metallurgical), which occurs via high thermal energies during welding. The HAZ also determines the life and duration of a pipe because that is the portion of the pipe most susceptible to rust, pitting and cracks, which eventually could lead to it bursting, or failing. It therefore plays a vital role in determining the integrity of the pipe and ensures a longer in-service life.

3.2 Welding of Samples

3.2.1 Material Preparation

The compositions of elements present in the parent metals - stainless steel and mild steel as well as the filler metals for both stainless steel (304/316 filler wire) and mild steel (A15 Cu-coated filler wire) were obtained using SEM and are contained in Tables 3.14 through 3.18 under the EDAX section. The 304/316 filler wire is compatible with the clad metal – stainless steel (grade 316) while A15 Cu-coated filler wire is compatible with base metal – mild steel (CR4), the compositions are displayed in Table 3.14 and 3.15. Compatibility is very important for the welded joint in order to produce an appropriate matching scenario.

For the first set of weld experiments, a mild steel plate of thickness 10mm and dimension 150 mm by 100 mm of grade CR4 was mounted on a stainless steel 316 grade plate 2 mm thick, of dimensions 150 mm by 100 mm and then welded with a 60-degree V-groove for butt weld, see Figure 3.1. The design of this narrow gap weld using GMAW is important because the base of the clad is 2mm in line with the narrow gap specification. The base metal was positioned adjacent to the other base metal at varying angles of 50 and 60 degrees. The plate surfaces were scraped with an electric brush and thoroughly cleaned with isopropyl alcohol, after which carbon steel plates were mounted on top of the mild steel and clamped into position with the aid of G-Clamps, as well as spot welded to avoid movements and enhance stability. Spot welding was used to fix the thermocouples into position prior to welding, as shown in Figure 3.2 (d).

For the second set of weld experiments, a mild steel plate of thickness 10 mm, dimensions 75 mm by 100 mm and of grade CR4 (British BS 970: 1991) (Acton Bright Steel, 2018). It was then mounted onto a stainless-steel grade AISI 316 plate that was12 mm thick and the dimensions were 75 mm by 100 mm. It was then welded with a 50-degree V-groove for butt weld (see Figure 3.2 (b)). A similar procedure was again used in the first set of welds, as shown in Figures 3.2 (a and c). The thermal conductivity of stainless steel is 16 [W/mK] whereas that of mild steel is 36 [W/mK]. The linear thermal expansion coefficient of stainless steel is 1.34mm/m and 1.00mm/m for carbon steel or mild steel.

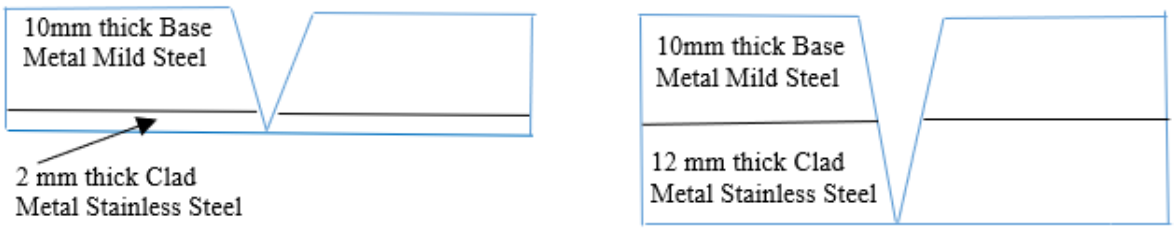

Figure 3.1 A schematic diagram of a weld set up for (a) mild steel (10 mm) and 2 mm stainless steel (b) mild steel (10 mm) and 12 mm stainless steel

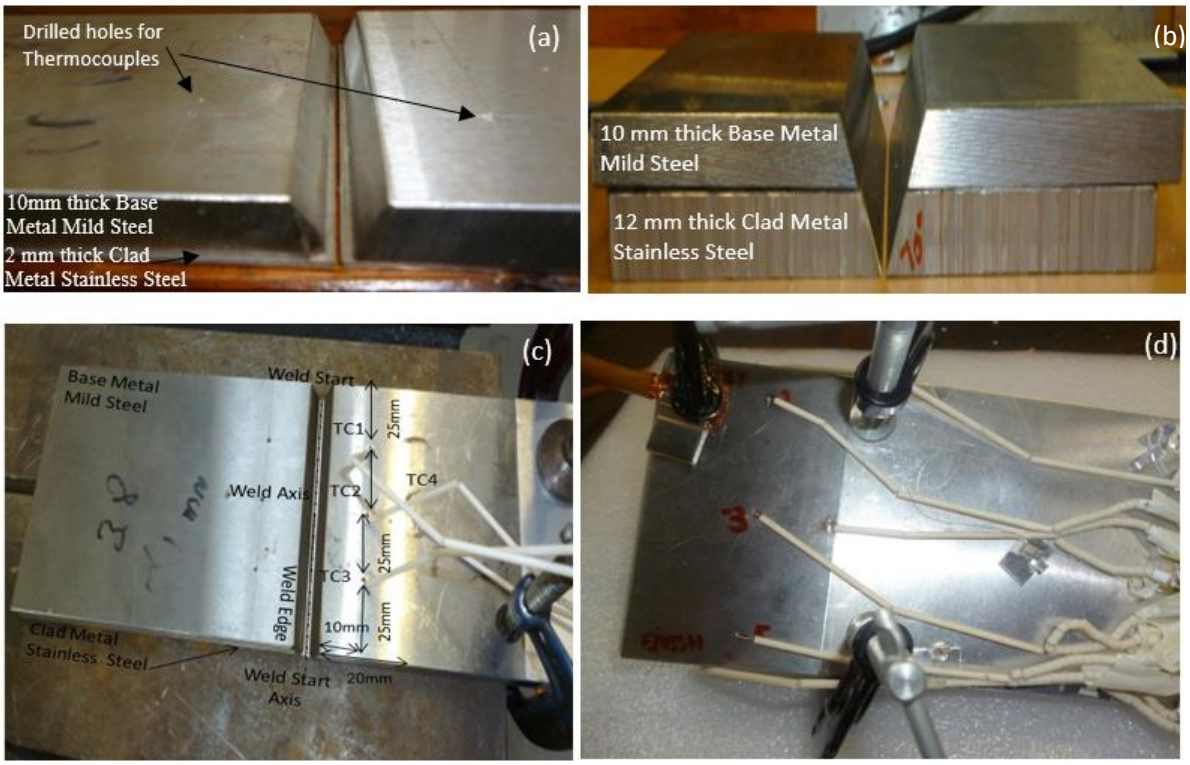

Figure 3.2 (a) Weld set up showing drilled holes for thermocouples. (b) Weld set up on mild steel (10 mm) and 12 mm stainless steel (c) Positions 1 to 4 of 10 mm mild steel and 2 mm stainless steel clad with thermocouples (d) Marked positions 2 to 5 of weld block

NB Drilled holes (2 mm) on the steel plates indicate the position of the thermocouple in order to feed into channels 1 to 4 on the data logger. NB the red dot indicates position 6 for the thermocouple to feed into channel 6 the input of Pico logger. Although the angle was marked 70 degrees with a permanent marker before cutting, it was actually angle 50 degrees that was cut, not 70 as shown in Figure 3.2. Connecting wires and plugs were also used for the weld experiment. The data logging device was chosen to record the temperature variations during the weld, see Figure 3.4.

3.2.2 Experimental Set-up

Table 3.1 Variables used for welding – weld parameters

Variables	Unit	Low level (-1)	High level (+)
Arc Voltage	Volts	230	240
Arc Current	Amperes	5	45

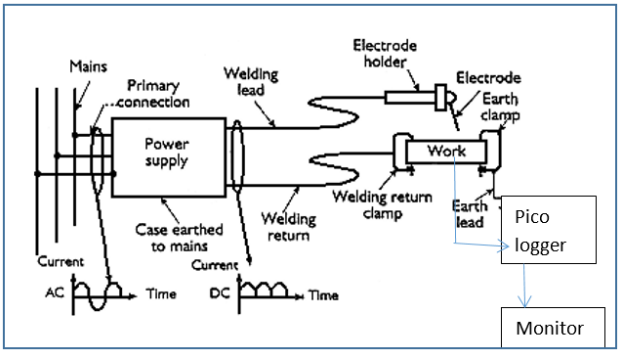

Figure 3.3 Schematic diagram of weld circuit diagram

The experimental set-up is shown in the schematic diagram Figure 3.3. The power supplied to the weld set-up, which is displayed in Table 3.1, is transmitted via the weld lead and through the Electrode holder and onto the weld plates and joints. The thermocouples positioned on strategic locations of the weld plates record the response to the thermal variation of heat transmitted onto the plates at different time intervals of 10 seconds and are positioned away from the heat source. These thermal values though transient are received via an electrical signal and into the channels of the pico logger – a data logging machine connected to the monitor of a laptop as shown in Figures 3.3.

The Weld plan shows the position of the thermocouples from the top, side and bottom of the stainless steel-mild steel block array. Different weld angles of 50° and 60° were utilised, as well as different distances from the weld line to determine the heat response from the weld touch to the thermocouples. One of the objectives is to determine the speed and rate of heat transmission from the weld line to the thermocouples while carrying out the weld. A thirteen-

amp fuse was used, and sixteen (16) fuses altogether were used for welding. In the 2mm cladded joints, 2 weld passes for the stainless steel and 6 weld passes for the mild steel.

3.2.3 Weld Parameters

Filler metals: A15 Cu-coated filler wire of thickness 2.37 mm was used for welding the mild steel section whereas a 304/316 filler wire of thickness 1.56 mm was used for the stainless-steel segment of the weld, which invariably is the TIG root. Argon pure shield gas was used and the nozzle type being N0 5 nozzle ceramic. The weld set up was suspended on the workbench using the G-Clamp (as seen in Figure 3.4.) The weld time was 15 minutes in total after which the metal was left to cool. Welding, was carried out within the permitted zone (weld arena) and the recording of the data, was carried out on the laptop. Welding was carried out in a loop format from the weld start position to the weld end position as shown in Figure 3.4 (a).

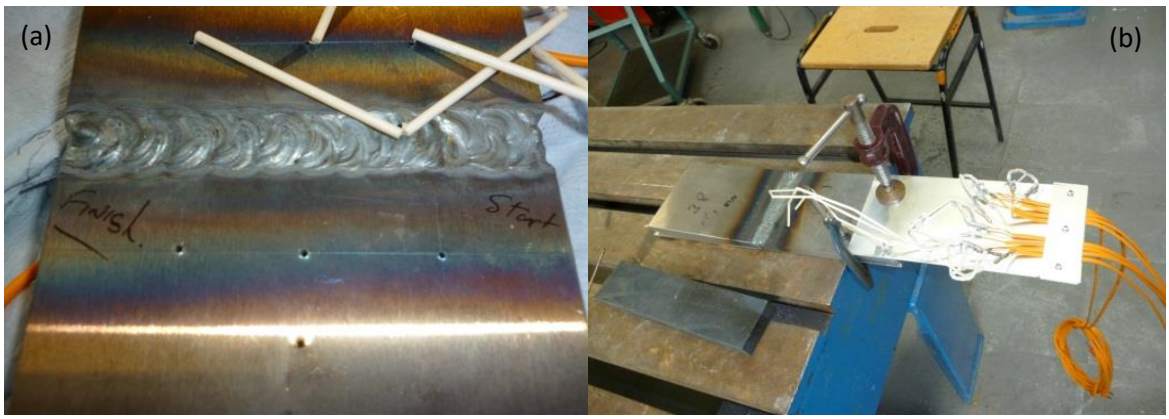

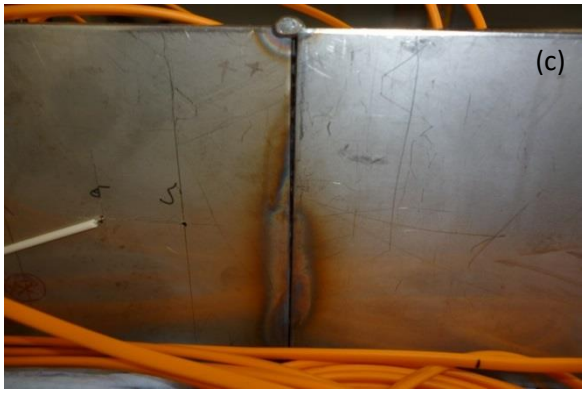

Figure 3.4 Sequence of TIG weld in laboratory at Brunel University London a) fully welded 2 mm clad plates, b) welded plates suspended from work bench with thermocouples attached, c) stainless steel/mild steel plate showing thermocouple points 5 and 6 under plate

3.2.3.1 Factors Affecting Heat input and Energy of Arc

The amount of heat inputted into a welding process is an expression of the energy fed into the workpiece to generate the weld, known as the Energy of the Arc (AE). These are expressed in kJ/mm as follows: (TWI, 2016) using the ISO/BS Standard

$$AE = \frac{60VI}{1000v} \qquad \text{Eqn (3.1)}$$

Where v is the speed of travel of the weld torch given in distance (mm) per minutes, I is the supplied current in ampere, V is the measure of voltage supplied in volts, Heat input (HI) is expressed as:

$$HI = \eta AE \qquad \text{Eqn (3.2)}$$

Where η is the process efficiency and is unique for every arc welding procedure. 0.6 for TIG and 0.8 for GMAW. For this experiment, the speed is 10 mm in 4 minutes which comes to 2.5 mm in 1minute.

3.3 Thermal Measurements

3.3.1 Thermocouples

High temperature (1700^{o}C) thermocouples were purchased from a company and dealer in thermocouples known as TC-Direct (Thermocouple Couple). There are two types of high temperature thermocouples available in the market namely R-type ad S-type and they are both made up of platinum / rhodium wires. While the former has one of its conductors composed of 13% rhodium/87% platinum and the other conductor of pure platinum, the latter has one of its conductors composed of 10% rhodium/ 90% platinum and pure platinum for the other conductor. The type of thermocouple used in carrying out this experiment is the R-type thermocouple because it delivers 15% more mV than the S-type. The R-Type was spot welded at strategic positions on the dissimilar metals, so as to have a thorough spread of the temperature distribution within the dissimilar materials surfaces and joint, as well as to determine the speed of heat transmission within the base and clad metals while welding. Figures 3.5 and 3.6 show the array of the thermocouples on both the stainless steel and mild steel plates. Each terminal was fed into the Pico-logger with the aid of the Platinium-Rodium compensating cables (made up of copper and copper nickel), wires of 1mm in length and high thermocouple plugs of type R and orange in colour, as seen in Figure 3.4.

Thermocouples were positioned in 8 different positions for the 12 mm clad thickness and 6 different positions for the 2 mm clad thickness. The distance of each thermocouple from the weld start (WS) position (first point of weld) was recorded as indicated in Figures 3.5 and 3.6. The distance of the thermocouples from the weld edge (WE), weld line (WL) and weld axis (WA) respectively for the 2 mm and 12 mm clad thicknesses, were noted so that the time taken, as well as the weld speed required for each thermocouple to attain its peak value was recorded

by the Pico logger. These values would be compared in the transient temperature curve with the simulated values from the Abaqus thermal simulation in chapter four – thermal analysis.

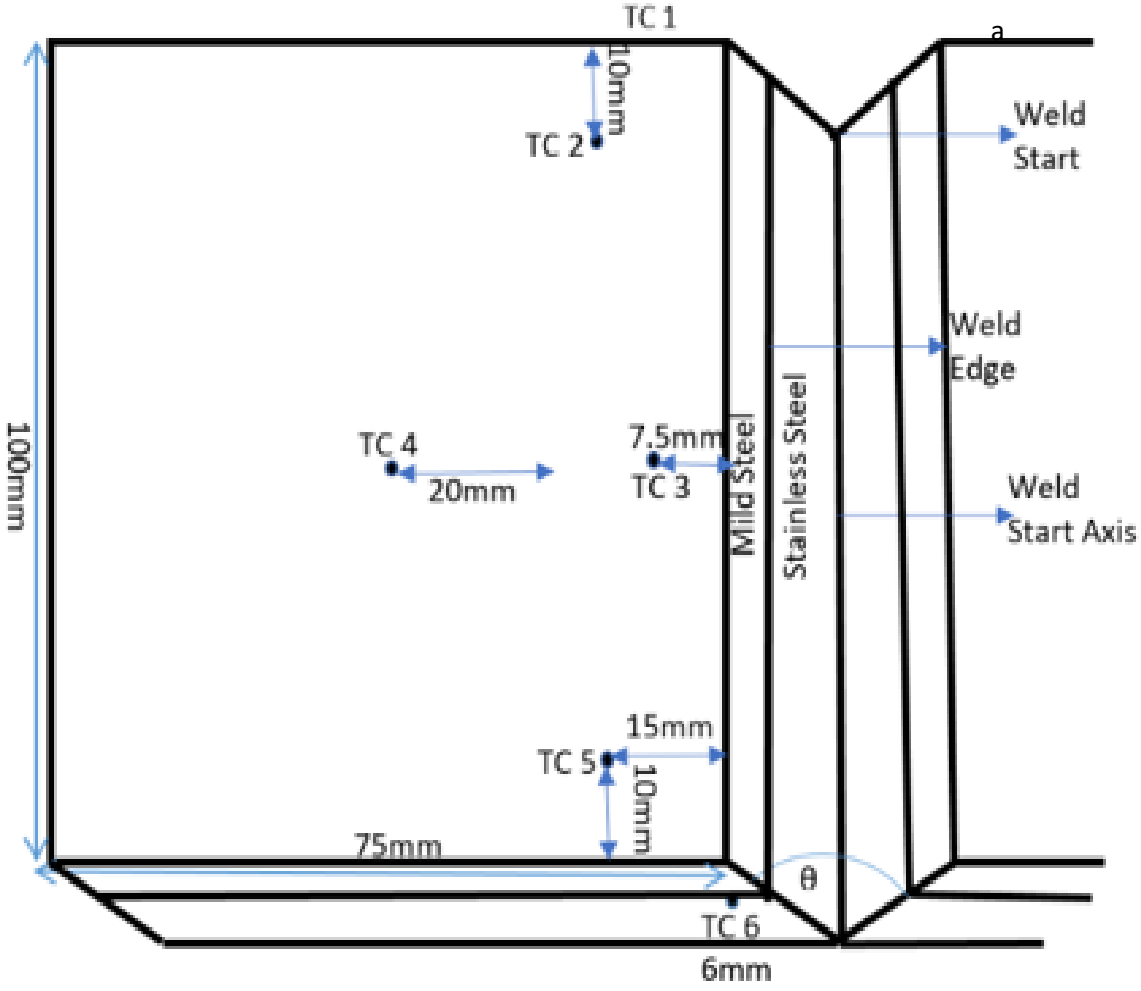

b

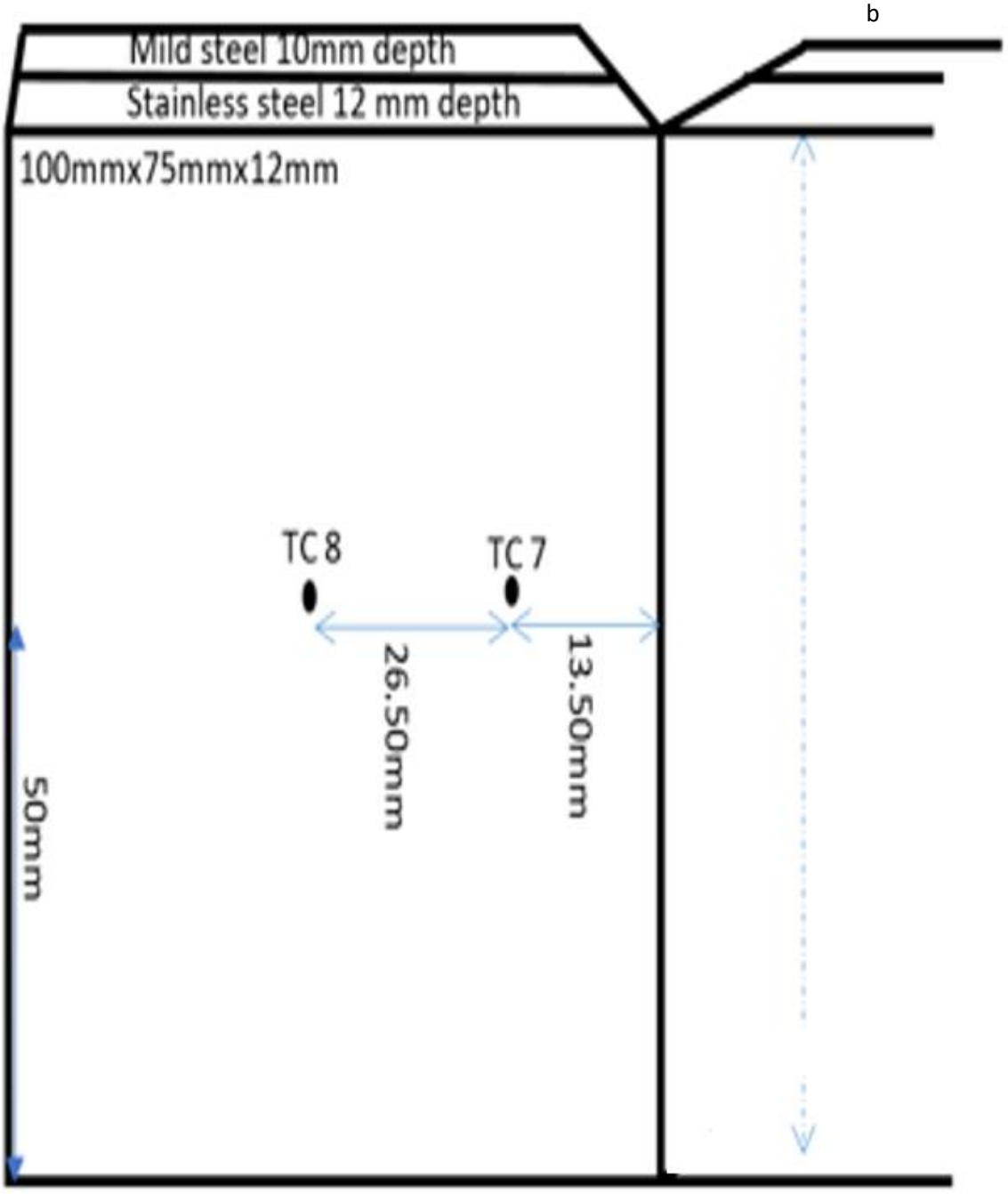
Mild steel 10mm depth
Stainless steel 12 mm depth
100mmx75mmx12mm
TC 8
TC 7
26.50mm
13.50mm
50mm

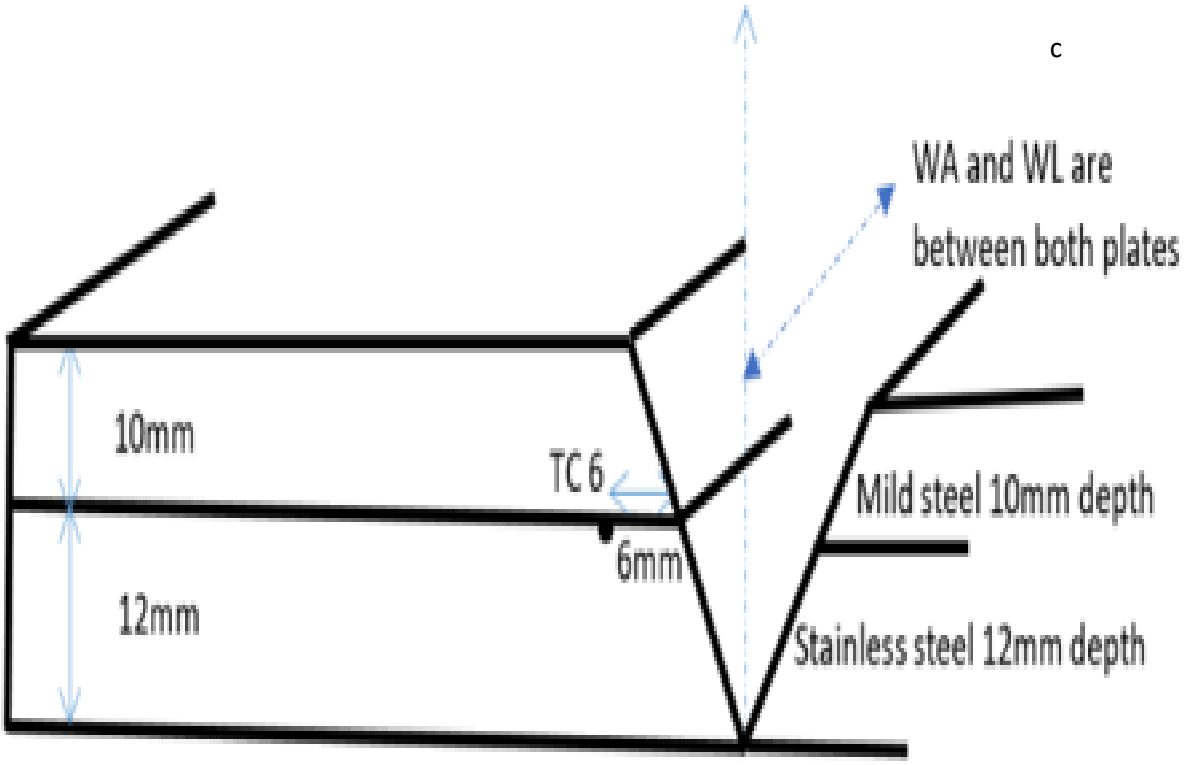

Figure 3.5 (a) Top view of weld plan and thermocouple positions 2-6; (b) Bottom view of weld plan and thermocouple positions 7-8 and side view of weld (c) Side view of weld plan and thermocouple positions 6 and 1 on the opposite end of 12 mm clad weld steel blocks

With reference to Figures 3.6 (a) and (b), the initial dimensions of stainless steel and mild steel were 100 mm by 150 mm for the 2 mm stainless steel clad weld, whereas dimensions for the 12 mm stainless steel clad weld were 100 mm by 75 mm as seen in Figure 3.5. The reason being that after the first weld was carried out, the weld block was cut out and the remaining part of the stainless steel and mild steel were assembled for the second set of weld experiments, as shown in Figures 3.2 (b).

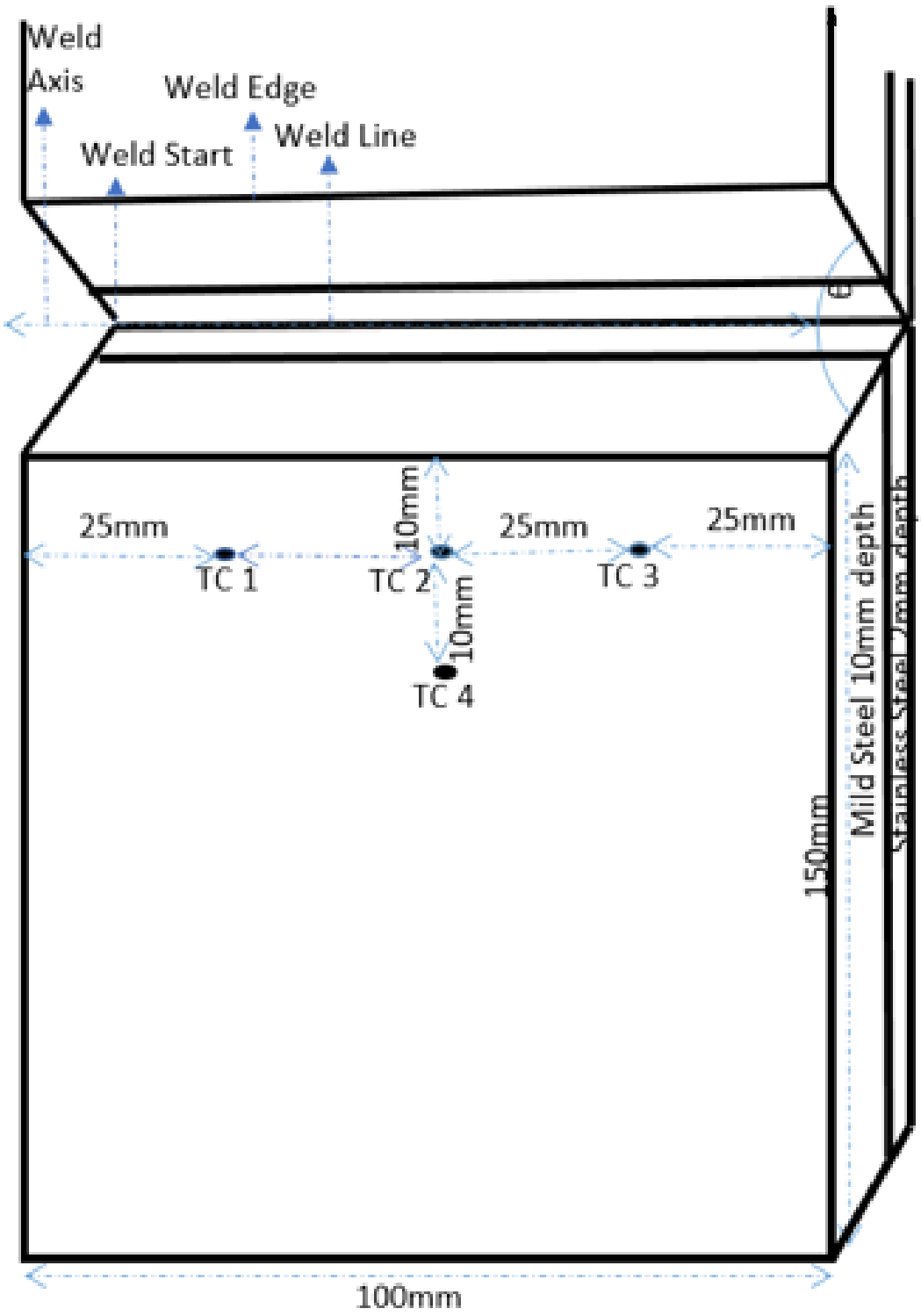
Weld
Axis
Weld Edge
Weld Start
Weld Line
θ
25mm
TC 1
10mm
TC 2
25mm
TC 3
25mm
10mm
TC 4
150mm
Mild Steel 10mm depth
Stainless Steel 2mm depth
100mm

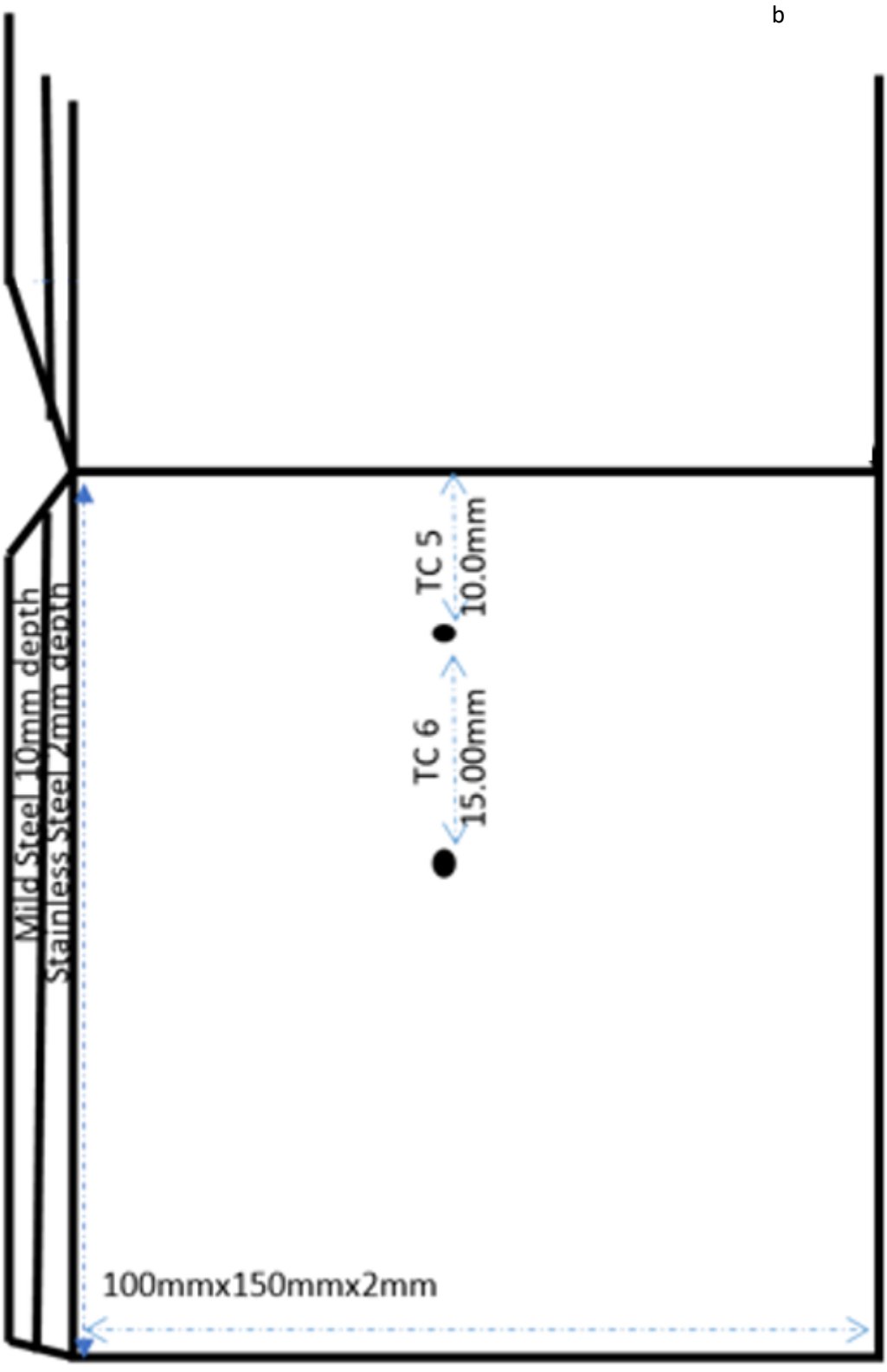

Figure 3.6 (a) Top view of weld plan and thermocouple positions 1-4 and weld side view (b) Bottom view of weld plan and thermocouple positions 5-6

Table 3.2 Positions of thermocouples with respect to weld line and weld start of two different clad thicknesses

Positions of Thermocouple	TC1	TC2	TC3	TC4	TC5	TC6	TC7	TC8
Distance from Weld Edge [mm] 2mm Clad	10.00	10.00	10.00	20.00	10.00	25.00	_	_
Distance from Weld Line WL [mm] 2mm Clad	16.93	16.93	16.93	26.93	10.00	25.00	_	_
Distance from Weld Start Axis [mm]	23.86	23.86	23.86	33.86	10.00	25.00	_	_
Distance from Weld Start [mm]	48.86	23.86	98.86	83.86	60.00	75.00	_	_
Actual Distance from Weld Edge [mm] 12mm Clad	13.50	15.00	7.50	35.00	15.00	13.50	13.50	40.00
Distance from Weld Line WL [mm] 12mm Clad	19.75	26.45	18.95	46.45	26.45	19.75	13.50	40.00
Distance from Weld Start Axis [mm]	27.03	39.81	32.31	59.81	39.81	27.03	85.50	112.00
Distance from Weld Start [mm]	27.03	49.81	82.31	109.80	129.81	127.00	135.50	162.00

The respective temperature of the heat from the heat source or weld were recorded with a Pico logger every 10 seconds and displayed on the monitor of the PC using a Picolog recorder. The respective distance of each thermocouple is shown in Table 3.2. The transient temperature is generated and displays the peak temperature for each thermocouple. Electrical noises due to variation in the thermal signals were also recorded. These were filtered out leaving the main heat signals. The transient temperatures are displayed in Figures 3.7 (a and b).

3.3.2 Results

The respective distances of the thermocouple from the weld edge (WE), weld line (WL), weld start axis (WSA) and weld start (WS) positions were measured, as well as the time taken to attain the peak transient temperature values. The rate of transmission of heat is calculated relative to each thermocouple position in Table 3.2 and based on that, the respective speed for each thermocouple relative to the WE, WL, WSA and WS was calculated as also shown in Table 3.2.

Figures 3.7 (a and b) are cumulative transient temperature curves which show the different temperature peaks for the different thermocouples (TC 1-6 and TC 1-8), for the 2 mm and 12 mm clad thicknesses respectively. For the 12 mm clad the highest peak is observed for the thermocouple 1 which corresponds to 453.59 ^{o}C, as shown in Table 3.5 and Figure 3.7 (b). This is because thermocouple 1 is closest to the weld start point and as such is the first to detect the heat from the weld source before other thermocouples. Thermocouple 2 detects a peak temperature after thermocouple 1, as shown in Figure 3.7 (b) and Table 3.4 with a temperature of 378 ^{o}C being the second closest to the weld start position and second to detect heat from the weld source. The next peak is seen in thermocouple 8 which is placed at a distance of 26.50 mm from the weld edge and weld start axis and is 50 mm from the weld start as shown in Figure 3.5 but due to thermal conductivity of steel plate (bottom and clad plate of 12 mm thickness, heat is transmitted faster than the other thermocouples). The first thermocouple (from the left) to depict the peak is the TC7 which is positioned underneath (directly on the 12 mm stainless steel plate) as seen in Figure 3.5 (b). The clad thickness of 12 mm coupled with a thermal conductivity of 16 [W/mK], favours TC7 in attaining the first transient temperature peak within 46.4 seconds. The next thermocouples to attain peaks are TC3, TC2 and TC1 by reason of proximity to heat source and weld start position. TC1 is placed opposite TC 6 at the other end of the weld block array and 13.50 mm from weld start position as shown in Figures 3.5 (a) and (c); whereas TC3 is placed 50 mm from the weld start and 7.5 mm from the weld edge position and TC2 placed 10 mm from the weld start and 15 mm from the weld edge, as observed in Figures 3.5 (a) and (b). The overall order of thermal peaks for the 12 mm clad can be seen in thermocouple 7 followed by 3, then 2 and 1 before 8, 6 and finally 4 in descending order. The channel for thermocouple 5 was faulty; hence no reading was detected for thermocouple 5, Figure 3.7 (b). Thermocouple 6 has the lowest peak due to being positioned

farthest away from the weld start position and weld line and has a reading of 223.7 seconds to detect the peak temperature.

Table 3.3 Peak values of temperature, time, distance and rate of heat transmission data for the different thermocouples 1-6 of the 2 mm Clad

	2mm Clad Distance [mm]						
Thermocouple [TC]	Weld Edge [WE]	Weld Line [WL]	Weld Start Axis [WSA]	Weld Start [WS]	Time [sec]	Rate of transmission [mm/sec]	Temperature [^{o}C]
1	10.00	16.93	23.86	48.86	30.00	0.33	321.00
2	10.00	16.93	23.86	73.86	45.00	0.22	708.82
3	10.00	16.93	23.86	98.86	69.00	0.14	341.00
4	20.00	26.93	33.86	83.86	48.50	0.41	209.68
5	10.00	16.93	10.00	60.00	31.50	0.32	276.00
6	25.00	31.93	25.00	75.00	101.00	0.10	201.75

Table 3.4 Peak values of temperature, time, distance and rate of heat transmission data for the different thermocouples 1-8 of the 12 mm Clad

	12mm Clad Distance [mm]						
Thermocouple [TC]	Weld Edge [WE]	Weld Line [WL]	Weld Start Axis [WSA]	Weld Start [WS]	Time [sec]	Rate of transmission [mm/sec]	Temperature [^{o}C]
1	13.50	19.75	27.03	27.03	69.10	0.20	453.59
2	15.00	26.45	39.81	49.81	67.00	0.22	378.00
3	7.50	18.95	32.31	82.31	63.80	0.12	201.21
4	35.00	46.45	59.81	109.81	225.70	0.16	297.90
5	15.00	26.45	39.81	129.81	_	_	_
6	13.50	19.75	27.03	127.03	223.70	0.07	100.00
7	13.50	13.50	13.50	63.50	46.40	0.29	307.30
8	40.00	40.00	40.00	90.00	180.00	0.22	354.50

Table 3.4 and Figure 3.7 (b) reveals the time taken for the transmitted heat through the weld block to attain the peak value with respect to the distance travelled. For thermocouple 1 the degree of heat transmitted from the weld source at the weld start position – travelling through the clad metal at a rate of 0.20 mm/sec and arriving at the thermocouple position at a distance of 13.5 mm after 70 seconds is 453.59 degree centigrade.

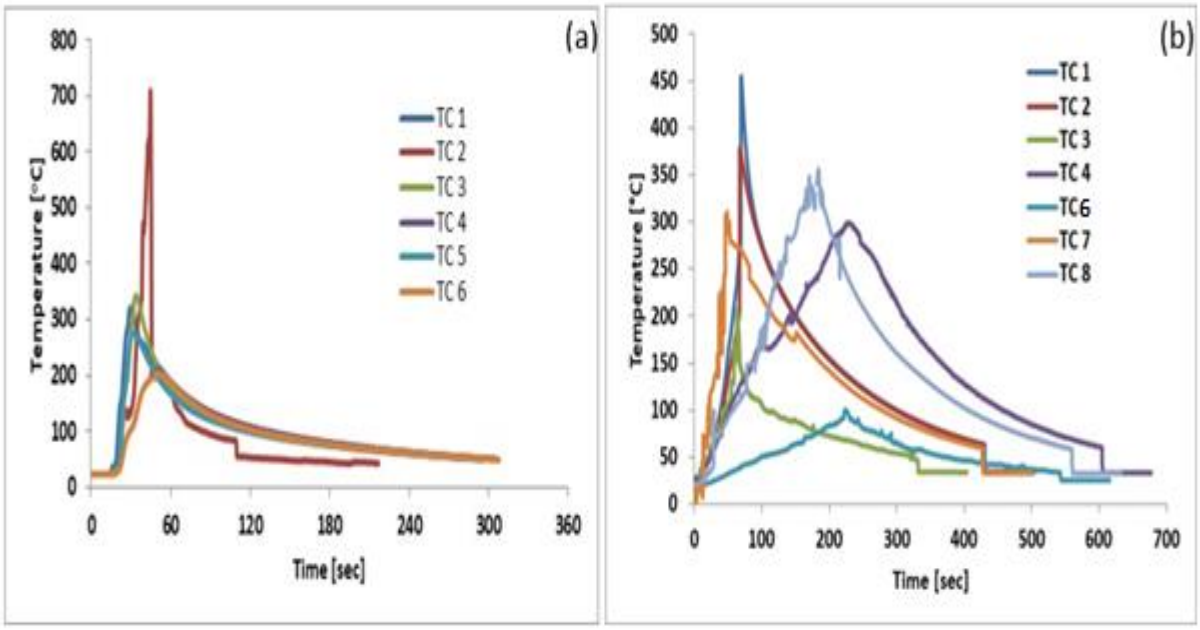

Figure 3.7 Thermal transient curves - thermocouple output by Pico logger (a) 2 mm and (b) 12 mm SSMS clad

By looking at the plot in Figure 3.7 (b), it is evident that high temperatures are involved in carrying out the welding. This is also recognizable from the peaks obtained and the fact that TCs 1, 2, 8 and 7 correspond respectively to the thermocouples position. They experience a peak of the temperatures faster than thermocouples 4, followed by 3 and 6 (which are the last thermocouples). This shows the rate of conduction of the temperatures from the point of weld (weld line W_L) to the respective thermocouples. There is also the gradual cooling down after the peak temperatures were attained.

For the 2mm clad, the respective distances of the thermocouple from the weld edge (WE), weld line (WL), weld start axis (WSA) and weld start (WS) positions are measured along with the time taken to attain the peak transient temperature values. The highest peak is observed for thermocouple 2 which corresponds to 700 ^{o}C, as shown in Table 3.3 and Figure 3.7 (a). This is followed by thermocouples 3 and 1. Although Thermocouple 2 attains the highest peak by reason of its centralized position (10 mm from WE and 50 mm from WS), it slowly dissipates the heat to the surrounding area when compared with other thermocouples placed close to the

edges (TC 3 and 1) - which dissipates heat quickly to the environ. It has been observed that TC2 is not the first to depict a peak in the transient heat curve. The first thermocouple to depict the peak is the TC1 followed by TC5 which is positioned directly underneath the 2 mm stainless steel plate as in Figure 3.6 (b). The fact that 2 mm is negligible, a clad thickness compared with a clad thickness of 12 mm coupled with a thermal conductivity of 16 [W/mK], favours TC5 in attaining the first transient temperature peak. The next thermocouples to attain peaks are TC1 and TC3 by reason of proximity to heat source and weld start position. TC1 is placed 25 mm from the weld start and 10 mm from the WE position, whereas TC3 is positioned at 75 mm from WS and 10 mm from WE respectively, as observed in Figure 3.6 (a). The order of thermal peaks can be seen in thermocouple 5 followed by 4, and 6 in descending order. This shows the rate of conduction of the temperatures from the point of weld (weld line W_L) to the respective thermocouples. There is also the gradual cooling down after the peak temperatures were attained.

Highest temperature peak of 708.8 ^oC followed by 339.8 ^oC and 320 ^oC were observed in the 2 mm clad thickness compared with the 12 mm clad thickness which has moderately high temperatures of 453.15 ^oC, 376.93 ^oC and 353.13 ^oC. This shows that although the 2 mm clad has the advantage of faster thermal conductivity and speed of heat travel via a thin layer (hence the highest peak of 708.8 ^oC being detected), the 12 mm clad thickness also has the added advantage of having a wide spread of moderately high temperatures by reason of the thermal conductivity and thickness of the clad plate. This means that the 2 mm clad thickness favours use in high temperature zones or functions (where ability to withstand high thermal profile is required) whereas the 12 mm clad thickness favours use in moderate temperature zones or functions such as temperate regions.

Electrical noise was present, which is the distortion of electrical signals; these can be clearly seen in some of the charts for thermocouples 3, 6, 7 and 8 in Figure 3.7 (b). Channels 3 and 6

experienced high peaks of up to 1700 degree centigrade, but there were still the electrical noises observed because of the distortion of signals. The use of two-filler materials instead of one compatible filler metal, in welding both parent and clad metals in carrying out the welding was employed in this research.

3.4 Mechanical Testing of the welded joint

Figure 3.8 Welded block of mild steel (10 mm) and stainless steel (12 mm) – to be cut into samples

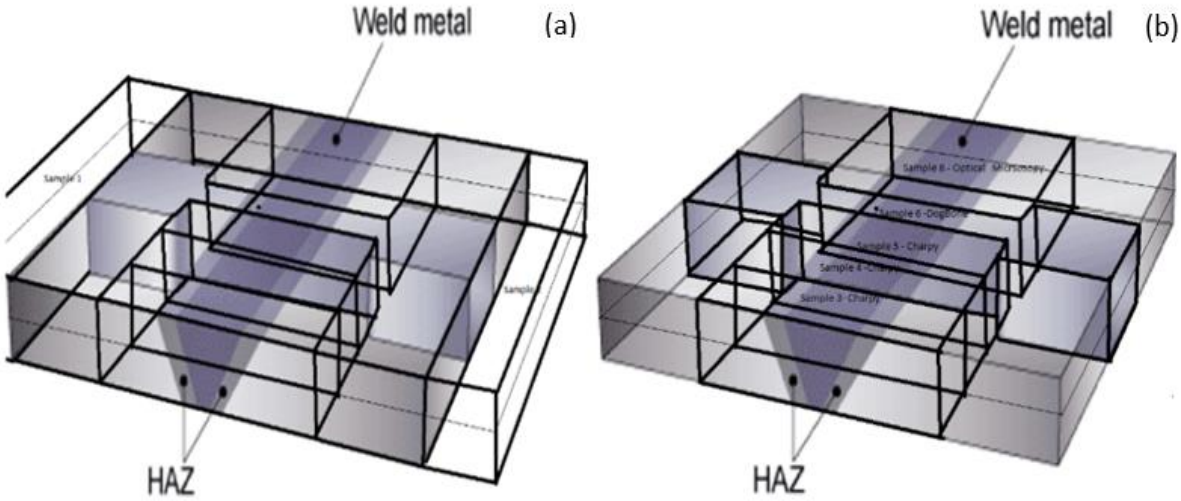

Figure 3.9 Schematic diagram of welded block of mild steel (10 mm) and stainless steel (12 mm) – to be cut into (a) Samples 1 and 2 for tensile tests (b) Five (5) samples: 1 Dog-bone, 3 Charpy and 1 microscopy sample. Specifications are 100 mm x 30 mm x 12 mm. Gauge length is 50 mm and the shoulder length are 20 mm

3.4.1 Preparation of samples for material tests:

The welded Bock of the mild steel and stainless steel as well as the schematic of the block is shown in Figures 3.8 and 3.9. Preparation of the samples entails the following procedures:

Grinding wheel: The top part of the metal block of the weld is milled with the vertical milling machine (surface grind the weld) to produce a flat and even surface. Next, the grinding wheel is employed to grind the surface in readiness for the cutting of samples for various tests such as the charpy, tensile and hardness. A surface grinder is then used to further smoothen the surface – so that the polishing of the surface could be carried out conveniently. Three types of grinding were employed: manual mill machine with standard wheel to get the flat surface, thin wheel to get the slot and finally angle wheeling place for the V angle. For charpy test samples, the machining flat grinding wheel (flip saw) with thin wheel is used to grind all edges to size. Next, the V-notch grinds into place with V-shaped samples carried out on the vertical milling machine. The surface of the weld was ground to produce a flat surface, whereas from the grinding wheel to the angle, the V-notch is created by grinding the V in the sample using grinding wheel with the V.

3.4.2 Tensile Tests

The methodology in carrying out tensile testing follows ASTME 646-98 for machine testing. The machine was used on Instron 5967 screw-driven universal test machine with model number 5967L2134 E2-F1-G1 using a load cell of 30kN capacity. Both base materials of the mild steel and stainless steel were tested along with the weld samples. The loading speed was 2mm/min

3.4.2.1 Results

Figure 3.10 Tensile test sample of (a) 2 mm and (b) 12 mm stainless steel before and after test

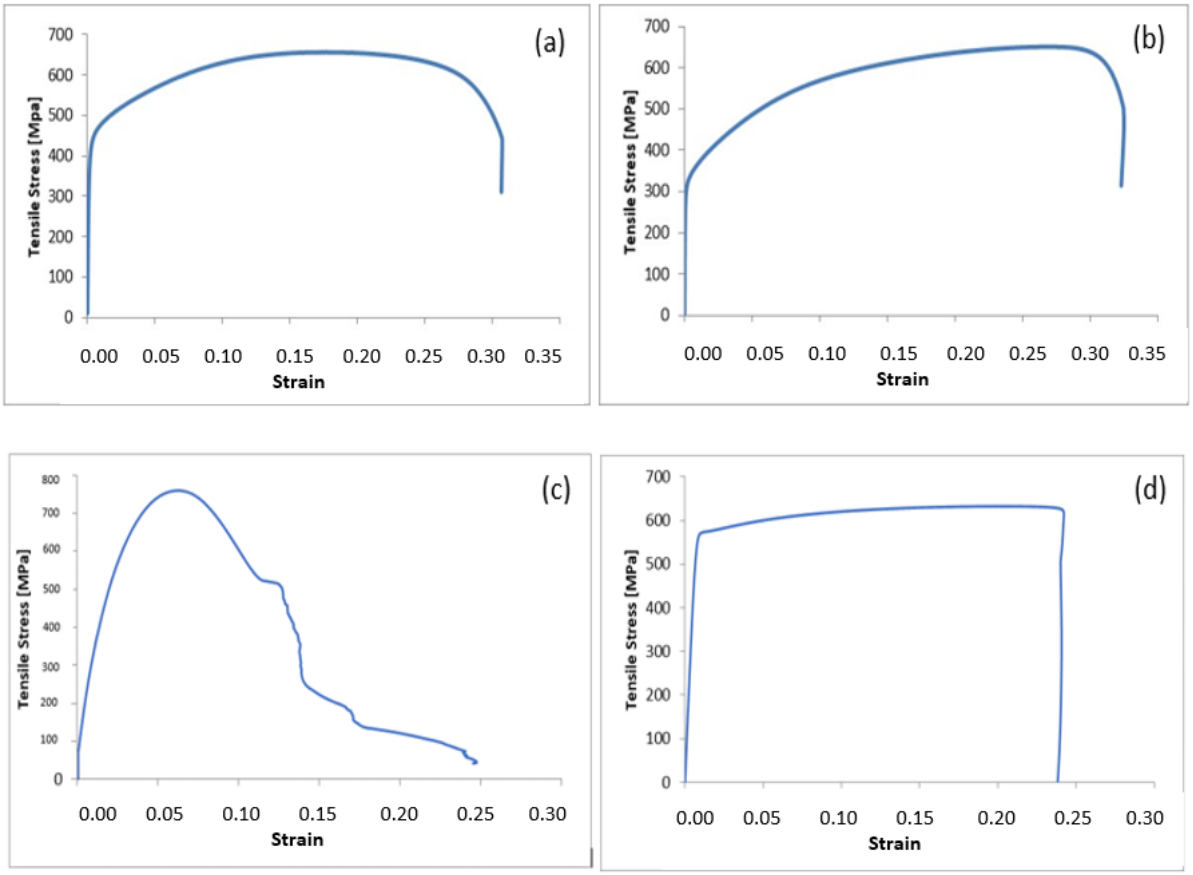

Figure 3.11 Tensile stress – strain curve for (a) 10 mm mild steel dog-bone sample (monolithic base material) (b) 2 mm stainless steel dog-bone (monolithic base material) (c) weld sample 1 (cladded joint sample) and (d) 12 mm stainless steel dog-bone sample (monolithic base material)

From Pipeline designs and Construction, the API 5L grade steel has a minimum yield strength of 448 MPa and Minimum Tensile strength of 530 MPa. The tensile samples elongated, and original are displayed in Figures 3.10 whereas Table 3.5 is the connotations of samples.

Table 3.6 and Figures 3.11 (a) through (d) display the different tensile strength and ultimate tensile strength of the weld metal and parent metal. The respective yield strengths are high and likewise the UTS. The 2 mm stainless steel clad has yield strength of 400, 370 and 470 MPa respectively and corresponding UTS of 760, 720 and 670 MPa (see Table 3.6). The 10 mm mild steel used as a base metal, has a tensile strength of 350, 352 and 370 MPa, which gives rise to a UTS of 650, 670 and 620 MPa accordingly, as seen in Table 3.6. The 12 mm stainless steel (clad) samples have tensile strengths of 580 and 590 MPa respectively which generates corresponding UTS of 630 MPa and 700 MPa.

Table 3. 4 Connotations of Samples used in welding: 10 mm mild steel 1-3, 2 mm stainless steel 1-3, 12 mm stainless steel 1-2, 2 mm mild steel-stainless steel weld and 12 mm mild steel-stainless steel weld

Samples	Connotation
10 mm mild steel sample 1	10 MS-1
10 mm mild steel sample 2	10 MS-2
10 mm mild steel sample 3	10 MS-3
2 mm stainless steel sample 1	2 SS-1
2 mm stainless steel sample 2	2 SS-2
2 mm stainless steel sample 1	2 SS-3
12 mm stainless steel sample 1	12 SS-1
12 mm stainless steel sample 1	12 SS-2
2 mm mild steel - stainless steel weld 1	2MSSS-1
2 mm mild steel - stainless steel weld 2	2MSSS-2
2 mm mild steel - stainless steel weld 3	2MSSS-3
2 mm mild steel - stainless steel weld 4	2MSSS-4
12 mm mild steel - stainless steel weld 1	12MSSS-1
12 mm mild steel - stainless steel weld 2	12MSSS-2
12 mm mild steel - stainless steel weld 3	12MSSS-3

Table 3. 5 Yield Stress (YS) and Ultimate Tensile Strength (UTS) of 2 mm and 12 mm thick stainless steel and 12 mm thick mild steel samples

Samples	YS [MPa]	UTS [MPa]	Mean YS [MPa]	Mean UTS [MPa]
10 MS-1	350	650	357.33 ± 11	646.67 + 25
10 MS-2	352	670		
10 MS-3	370	620		
2 SS-1	400	760	413.33 ± 11	716.67 + 25
2 SS-2	370	720		
2 SS-3	470	670		
12 SS-1	580	630	585 ± 11	665 + 25
12 SS-2	590	700		
12MSSS-1	727	759	663.5 ± 11	729.5 + 25
12MSSS-2	600	700		
	4809	6879		

The weld samples have very high yield strength of 727 MPa and 600 MPa respectively, corresponding to a UTS of 759 MPa and 700 MPa. This means that the weld has a higher strength than the respective base metal (mild steel and clad metal stainless steel) therefore there is good bonding between the weld metals – mild steel and stainless steel – at the dissimilar material joint of the weld. This also implies that the welding is good and consequently, the quality of the filler metals used in carrying out the welding is also good because the quality of parent materials and quality of filler material used in welding and bonding will results in quality welded joints of dissimilar material.

3.4.2.2 Discussion

A number of factors such as temperature, strain rate and anisotropy, affect the shape of the stress-strain curves. The different types of stainless steel (2 mm and 12 mm), mild steel and weld samples for the tensile tests are shown in Figures 3.11. The behaviour of the first weld sample under stress is similar to the behaviour of the parent metals pre-ultimate tensile stress

(UTS), whereas it behaves differently from those of the parent materials – mild steel and stainless-steel post UTS, by reason of a slip occurring after the UTS test. The parent metals have different elongation characteristics and each exhibit this at different rates because of the applied stress under which it is stretched. Similarly, the behaviour of the weld metal under the stress-strain curve in Figures 3.11 (c) is also due to a slip; which is caused by the elongation and failure of the different metals (mild steel and stainless steel) present within the weld samples, since they each have their original UTS. Although the temperature has a first order effect on the microstructure, strain, stress, and formation of defects, the volumetric change and yield strength as a result of the martensitic transformations also have effects on the residual welding stress, increasing the magnitude of the stress in the welded zone. From the EBSD test carried out in the laboratory, (Section 3.8, Figures 3.40 and 3.41) the presence of martensite in the welded zone further verified that, because there were recurrences of reheating taking place throughout the thick 12mm clad section of the weld, as well as changing its sign (Dean & Hidekauzu, 2006). The deformation shape observed in the weld tensile specimen in Figure 3.11 (d) is due solely to the movement of a slip dislocation via a crystal which results in the creation of a step, in which a glide plane criss-crosses (overlaps) the free surface. When several dislocations of that nature tranverse (rotate) on parallel slip planes it produces a macroscopic shear. A slip generates an alteration in shape, but not in the crystal structure. The reason for this is that the Burgers vectors which are responsible for dislocations, are also the same as the lattice vectors. (Bhadeshia, 2001). In Figure 3.11(d), the sharp peaks and bends at the corners of the stress-strain diagram are due to the high strength of the material and brittle nature of the 12 mm stainless steel sample, which leads to sudden failure at the sharp peak. When martensite are formed,the movement of atoms is also involved. This makes the austenite and martensite lattices closely connected. From the results of the EBSD analysis (discussed later on), it has been discovered that there is martensite, austenite and ferrites present in the heat affected zone

and fusion zones of the weld. This means that martensitic transfromation comes into play via deformations that alter the parent metal into the product and has a minimum of one or more lines unaltered, undistorted and unrotated. This is referred to as a one line invariant-line strain (Davis, 2004).

3.4.3 Hardness Tests

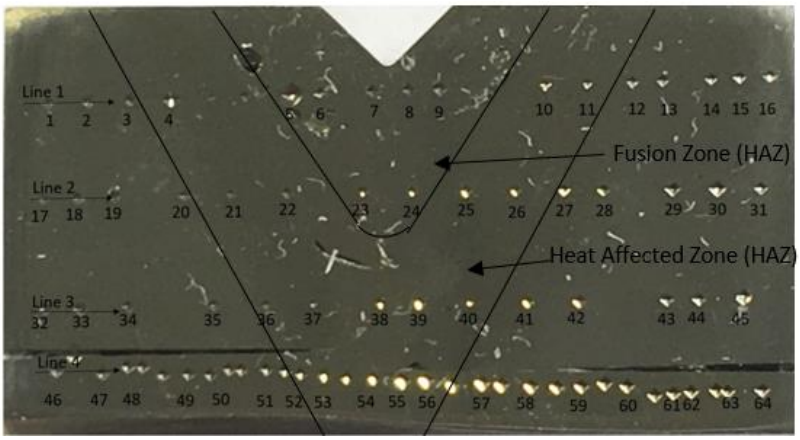

Figure 3.12 Pattern and order for diamond stud imprints across HAZ and welded zone – horizontal display

Hardness is the characteristic of a material which allows it to resist plastic deformation by virtue of penetration. It is also the ability to withstand bending. Vickers hardness was carried out using Vickers Armstrongs Instruments calibrated to B.S. 427/2 having a model number HTM6311 Crayford Kent. A diamond stud pattern was created with the aid of the pyramidal diamond indenter following strictly the pattern in Figure 3.12 across the HAZ and FZ and region close to the welded zones of the weld metals. These were repeated in the second and third lines, as seen in the welded samples. Another type of pattern is carried out vertically across the HAZ. The length of the diagonals of the diamond stud was measured both in the vertical (D1) and horizontal (D2) axes and the average reading recorded. This average value of

the distance was imputed into a standard equation known as the Vickers Hardness equation, as shown below.

$$Hv = \frac{\text{Applied load (kgf)}}{\text{Surface area of impression } (mm^2)} \qquad \textbf{Eqn (3.7)}$$

In the case where an indenter is used as in this research.

$$Hv = \frac{2Fsin(\frac{\theta}{2})}{D^2} \qquad \textbf{Eqn (3.8)}$$

Where F is the applied load in Newton (N) or Kilogram-force (KgF) and has a value of 20N, D is the mean diagonal length in millimetres (mm), θ is the angle and has a value of 136^o and Hv is the Vickers' Hardness measured in Hv

3.4.3.1 Results

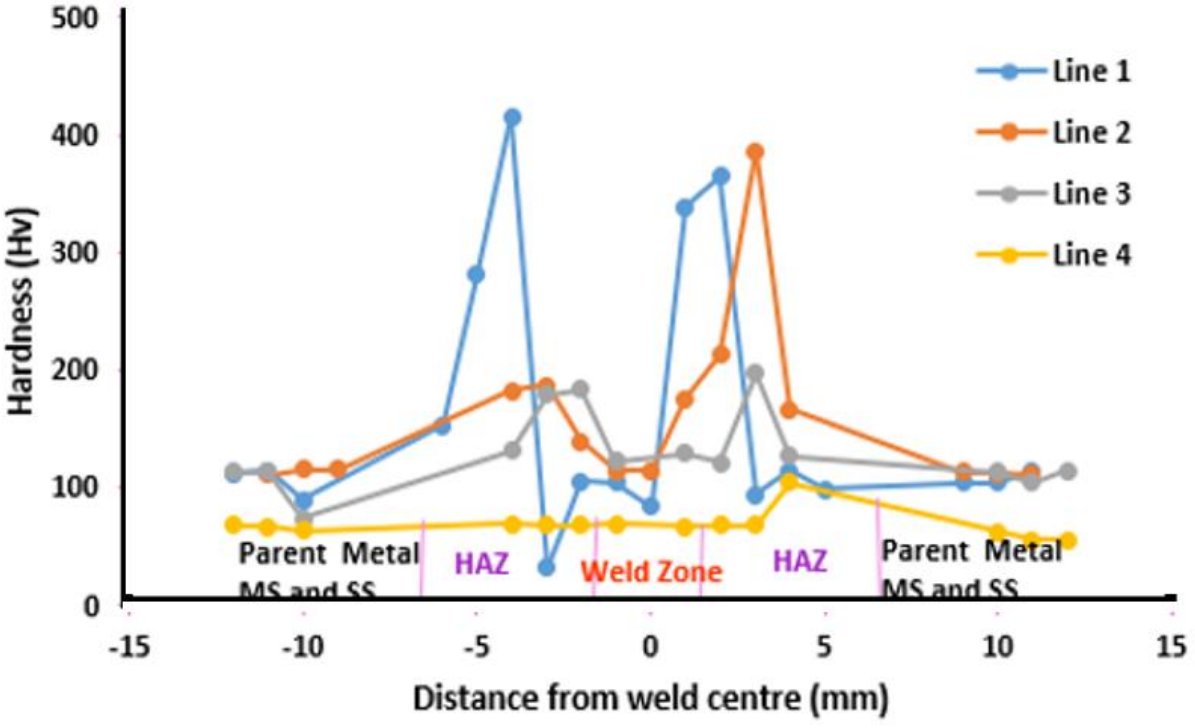

Figure 3.13 Hardness profiles across weld joint for 2MSSS 2

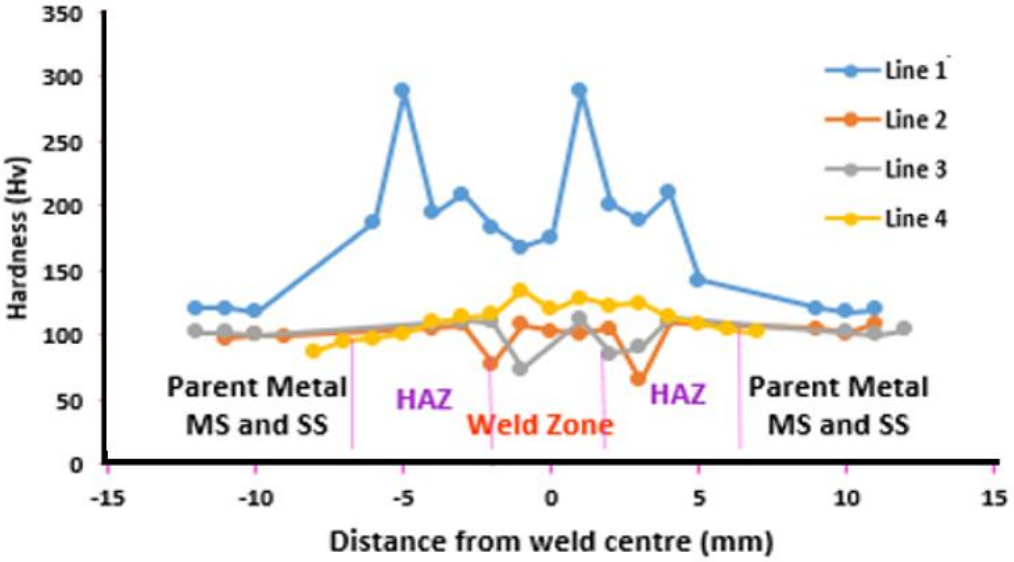

Figure 3.14 Hardness profiles across weld joint for 12 MSSS 3

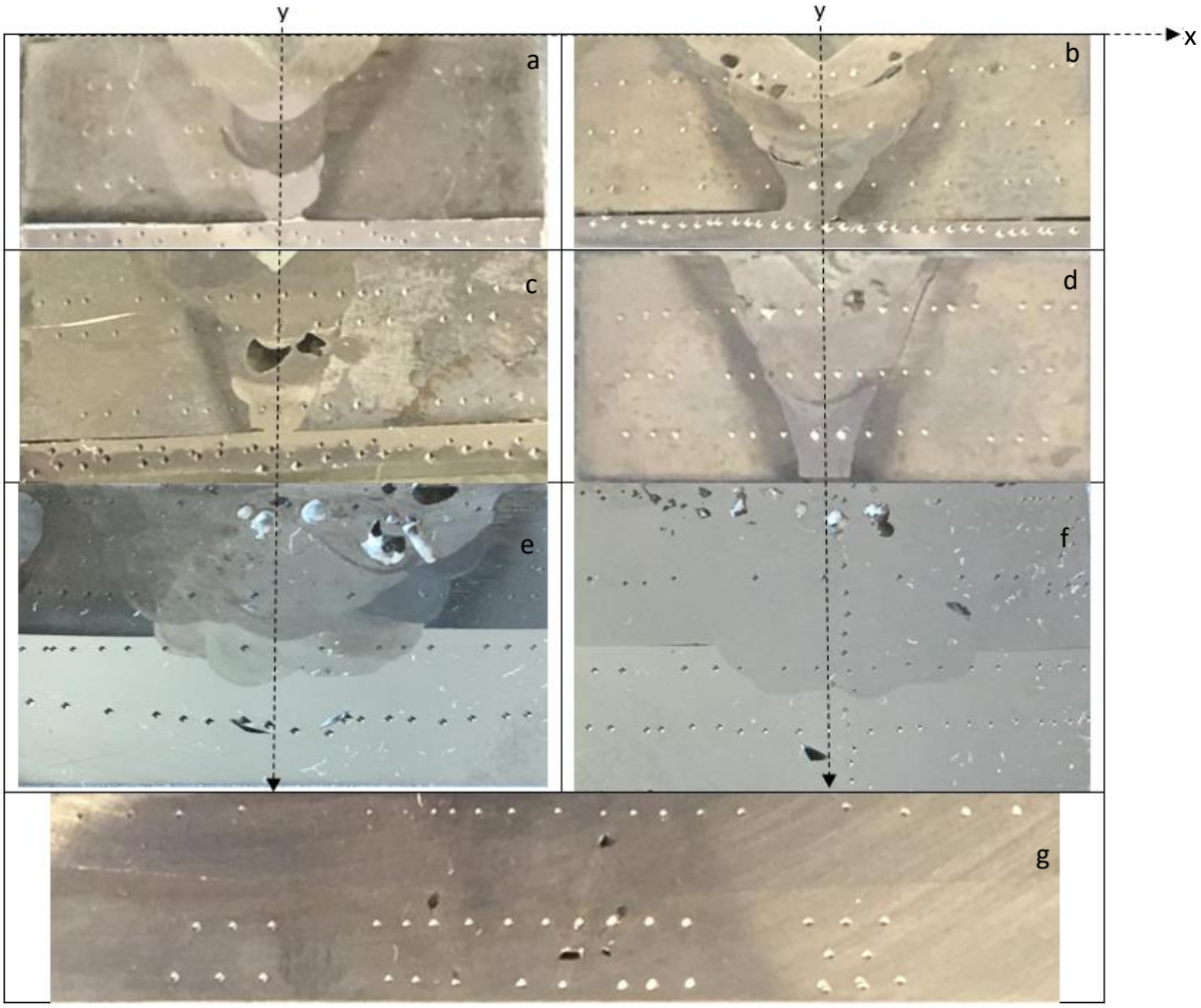

Figure 3.15 (a-g) Indented samples – direction from left to right: (a) 2MSSS-1 (b) 2MSSS-2 (c) 2MSSS-3 (d) 2MSSS-4 (e) 12MSSS-1 (f) 12MSSS-2 (g) 12MSSS-3 (cut into 4mm-6mm)

3.4.3.2 Discussion

It is observed that for the first line of 2MSSS 1 - 4 and 12MSSS 1 -3 that the hardness is very high in both the HAZ and the FZ compared with the parent material as shown in Figures 3.13 and 3.14. The peak values of hardness for 2MSSS 2 from left to right are 219 HV at coordinate -4, 245 HV at coordinate -1, 218 HV at 1, 300 HV at 4 and 243 HV at 5. In 2MSSS 3, it is 415.97 HV at coordinate -4 and 364.98 HV at 2 whereas 2MSSS 4 has the following peak values – 288 HV at coordinate -5, 208 HV at coordinate -3, 288.65 HV at 1 and 209.92 HV at 4.

Of significance, is the fact that hardness is also high in the Fusion zone and HAZ of the second line of 2MSSS 1 to 4, 3.15 (a-d). For the 12MSSS 1, 2 and 3, of Figures 3.15 (e-g), the hardness is higher in the HAZ than other regions. The following hardness respectively from left to right for samples in Figure 3:15, (b) which is MSSS2 has 240.43 HV occurring at coordinate -2 and 209.25 HV at 1 (refer to Figure 3.13); (d) has the following hardness peaks 282.26 HV at coordinate -2, 350 HV at 2, (e) 188.25 HV at coordinate -2 and 187.11 HV at 2 while (f) has the peaks occurring at 127.49 HV at coordinate -2, 156 HV at 1 and 170.75 HV at 3.

From the chart in Figures 3.13 and 3.14, there is a unique trend in the increased hardness profile across the fusion zone and HAZ of the 3rd line in 2 MSSS and the 4^{th} line of 12MSSS.

From the Vickers hardness test, it is obvious that the weld hardness is 30% - 70% greater than the parents' metal. This is due to the very high rate of Martensite formation during rapid cooling of the melt pool. The average hardness of the dilution zone is comparable to that of the clad.

From the hardness plot, it is obvious that the hardness of the HAZ varies linearly from the clad/HAZ interface to the HAZ/baseline interface with values 200 Hv to 420 Hv accordingly.

The reason for the direct variation of hardness in the HAZ is the difference in heating temperature in the HAZ resulting in variation in the growth of grain.

The result of the above is the formation of coarse grain by reason of elevated temperatures leading to coarser microstructures formed close to the Clad/HAZ interface. On the other hand, finer grain sizes are formed as a result of subsiding heating temperatures away from the clad/HAZ interface. Overall, a finer grain size is harder than a coarse grain size.

The hardness of HAZ increases proportionately to 400 Hv which is typical of the hardness observed during heat treatment ranging from 710 ^{o}C to 170 ^{o}C. When A1 (770 ^{o}C) is attained in the temperature range, there is a sharp fall in the hardness at the end of the HAZ which implies that there are no γ transformations occurring (See Phase diagram in Figure 3.16).

A phase diagram is a graphical representation of the physical states of a substance under different conditions of temperature and pressure (Subtech, 2006). Due to continuous heating and reheating of the clad thicknesses (especially 12 mm) and base metals (dissimilar materials), different rates of cooling take place within the weld zone, and consequently different phases are formed at different temperatures which involves austenite and martensite. The face-centred cubic austenite transforms to a highly strained body-centred tetragonal form known as martensite which is supersaturated with carbon. This shear deformation generates a huge number of dislocations, which is fundamentally the strengthening mechanism of steel.

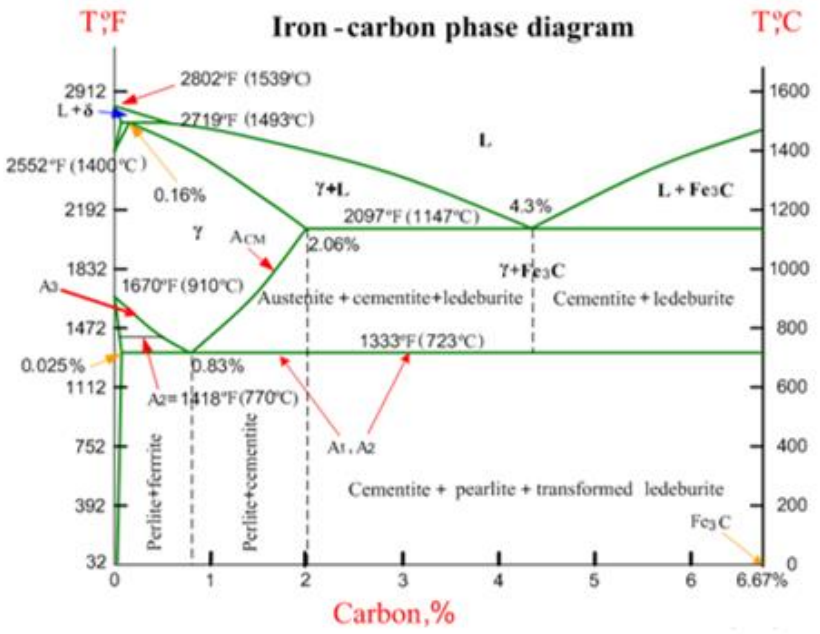

Figure 3.16 Phase diagram showing the position of A1 (Sun et al, 2010)

By reason of heating and reheating occurring throughout the clad thickness and welded zones of the dissimilar material joints, martensite is formed which are of greater hardness compared with austenite, thus increasing the hardness. Since too much martensite leaves the structure very brittle and too little leaves it very ductile, the combination of austenite balances the hardness, such that the strength, hardness and ductility of the welded zone enhances the structural properties for the welded joints.

3.4.4 Hardness of the Weld Line

The next series of tests is the hardness of the overall HAZ from a different position of the weld metal as shown in Figure 3.17. The results are opposite to the pattern obtained in the previous hardness tests displayed above. From Figure 3.18, it is clearly seen that the hardness is highest for the second line compared with the first and third, unlike the trend in the previous charts.

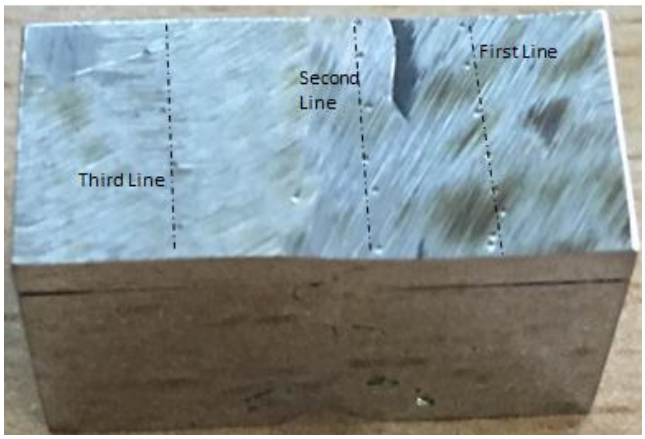

Figure 3.17 2 mm stainless steel mild steel-clad sample - bottom view of weld

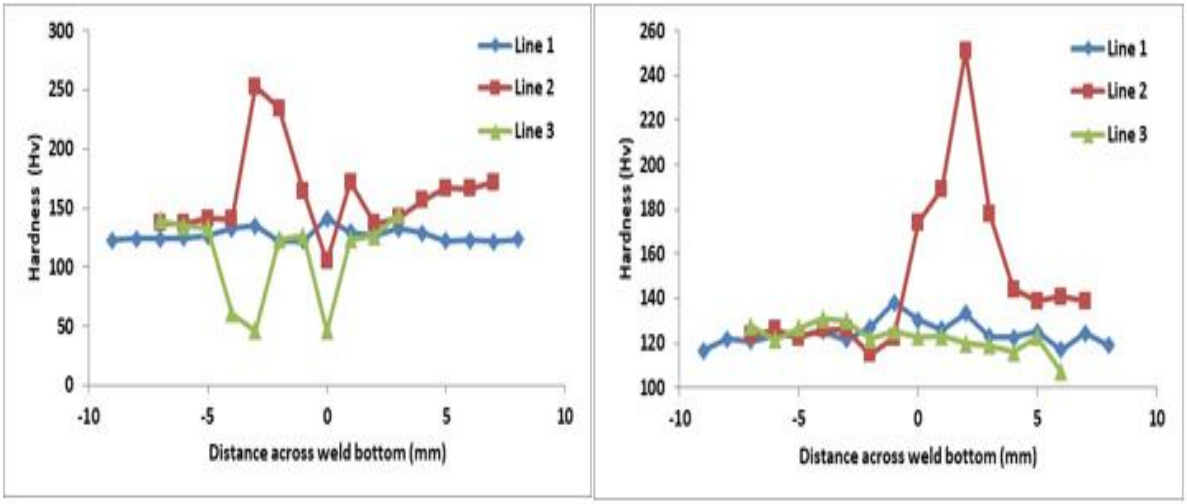

Figure 3.18 Hardness profile for top, middle and bottom (1st 2nd and 3rd) layer of welded joint from the bottom view of (a) 2MSSS3 and (b) 12MSSS1 sample

The above shows the hardness of the weld zone and especially the HAZ, with the highest reading of the test occurring in the second line of both hardness tests, corresponding to the middle of the sample shown in Figures 3.17, which is the welded part of the joint, bonding the stainless steel to the mild steel. It clearly shows the hardness of the weld point in the weld zone. The high hardness peaks in the two Figures 3.18 (a and b) and corresponds to the hardness of the weld point of the welded joint. Of significance is the fact that in both 2 MSSS clad and 12 MSSS samples, high hardness peak occurred around the FZ and HAZ. These both refer to the quality of the weld bond in the FZ and the filler material used in carrying out the weld. At some

other point (a distance) away from the root of the weld, there is no thorough joining, (no effective joining) of the plates as seen in Figure 3. 17 and 3.18 (a and b). This is the reason for the low value of hardness in the first and third lines respectively compared to the weld root (second line). From the plot above, it is observed that the point of joint (or weld), has a hardness of 252.82 Hv in the 12 mm clad sample and 250.86 Hv in the 2 mm clad sample. This is the degree of firmness of the welded joint, a key factor in determining the integrity of the weld joint and projecting the life span of the pipe. The result of the firmness of the weld and the middle weld line is vital to the longevity of clad pipes to avoid corrosion and pitting, which leads to failure in the end. The reason is because the weakest part of the joint (the welded joint) is most susceptible to burst or break, hence good welding ensures longevity of a pipeline.

3.4.4.1 Relationship between Tensile Strength and Hardness

Increase in temperature reduces the yield stress and ultimate tensile stress. From Vickers hardness test, the force perpendicular to the surface of the indenter is given as: (Busby et al, 2004).

$$H_V = \frac{\text{Load}}{\text{Contact Area}} = 0.927\text{P} = 0.927 \text{ x } 2.96\sigma_y = 2.74\ \sigma_y \qquad \text{Eqn (3.9)}$$

The Busby et al. (2005) experimentally derived correlation between yield strength and Vickers' hardness expressed as

$$\sigma_y = 0.364H_V \qquad \text{Eqn (3.10)}$$

Where H_V and σ_y are measured in kg/mm^2, or

$$\sigma_y = 3.55H_V \qquad \text{Eqn (3.11)}$$

Where H_V is in kg/mm^2 and σ_y in MPa.

Gusev et al derived the relationship between yield stress and micro-hardness as (Gusev et al, 2006).

$$\Delta\sigma_{0.2} = k_{\Delta}.\Delta H_{\mu} \qquad \text{Eqn (3.12)}$$

$$\Delta\sigma_{0.2} = 2.96.\Delta H_{\mu} \qquad \text{Eqn (3.13)}$$

Where H_V is in kg/mm^2 and σ_y in MPa, k = 2.96 and $\Delta\sigma_{0.2}$ is the difference in property correlation.

The above equation was derived for both stainless steels irradiated and non-irradiated at high temperatures of 300 ^{o}C, whereas the hardness was carried out at room temperature. This applies to all steel types irrespective of the make-up of the steel. This experimentally derived correlation shows that both hardness tests and tensile tests were carried out at the same temperature which is room temperature. Experimental studies carried out on a larger scale did not factor in the slightest change in composition and possible deposition of ferrite onto the surfaces. Another possibility is also that the brittle nature of the stainless steel at elevated hardening levels could be due to martensitic distortion while carrying out hardness dimensions of the low alloy steel. (Gusev et al, 2006). This universal correlation (k_{Δ}) enables the determination of yield stress from the hardness value, hence improving labour efficiency.

Ductile to Brittle transition (DBTT) varies in different materials, some being more severe than others. However, it can be accounted for via a temperature sensitive deformation process. The procedure and behaviour of a body centred cubic (bcc) lattice is triggered by temperature and responds to the reshuffling of the dislocation core just before a slip. This could result in challenges for ferritic steel in the building of ships. Neutron radiation also influences DBTT, which deforms the internal lattice, hence reducing ductility and increasing DBTT.

The full data set (FDS) correlation expressed as: (Pavlina and Van Tyne, 2008)

Yield Strength = -90.7 + 2.876Hv (Eqn 3.14)

3.4.4.2 Result and Discussion

Table 3. 6 Relationship hardness vs yield Stress for 2MSSS 1-4 and 12MSSS 1-3

Specimen	Hardness *Hv* [kg/mm^2]	Busby et al (2005) Yield Strength [MPa] = [3.55*Hv*]	Gusev et al (2006) Yield Strength [MPa] = [2.96 H*v*]	FDS Pavlina and Van Tyne (2008) Yield Strength [MPa] = [-90.7 + 2.876 H*v*]
2MSSS1	299.79	1064.25	887.39	771.50
2MSSS2	415.97	1476.69	1231.27	1105.63
2MSSS3	317.00	1125.35	938.32	820.99
2MSSS4	307.00	1089.85	908.72	792.23
12MSSS1	320.00	1136	947.2	829.62
12MSSS2	269.00	954.95	796.24	682.94
12MSSS3	288.00	1022.4	852.48	737.59

Since this research focuses on the welding of two dissimilar materials and clad thickness, it is vital to choose the correlation which is applicable to all steels, such as the Busby experimentally derived correlation and the Gusev property correlation as well as the full data set (FDS) correlation. The hardness Hv represented in the second column is the highest peak for the first line of hardness in each sample displayed in Figure 3.15 (a-g). This provides the distribution of hardness across the different weld samples, especially the HAZ which experienced the highest peaks across most samples. For the 12MSSS-1, yield strength is 727 MPa (Table 3.6), the full data set (FDS) correlation gives yield strength of 829.62 MPa as observed in Table 3.7. For the 12MSSS-2, yield strength is 600 MPa (refer to Table 3.6), the correlation gives a yield strength of 682.94 MPa which is quite close a value. Based on the full data set correlation in Table 3.7 the values for the 2MMSS 1-4 samples can be predicted as reliable and higher than those of the 12 MSSS Samples. The strength and hardness of steels cover such a wide range of hardness value and are converted to diamond pyramid hardness known as Vickers hardness in

accordance with ASTM E 140-05 (Pavlina and Van Tyne, 2008) (ASTM, 2005). Average of the highest hardness peak comprising of the 1^{st}, 2^{nd}, 3^{rd} and 4^{th} lines have been taken for 2 MSSS 2 and 3 as well as 12MSSS- 3 and the results are shown in Table 3.8.

The highest hardness (occurs at the region of the HAZ) in Figure 3.19 (a and b). Taking the average across all four lines in point A of 2MSSS-2, results in an average hardness of 415.97 MPa + 170 MPa + 130 MPa + 70 MPa = 785.98/4 = 196.49 MPa

This gives rise to a yield strength of 474.41 MPa when using the full data set correlation and Guzev and Busby correlation in equations generates values of 679.54 MPa and 581.61 MPa for the yield strength.

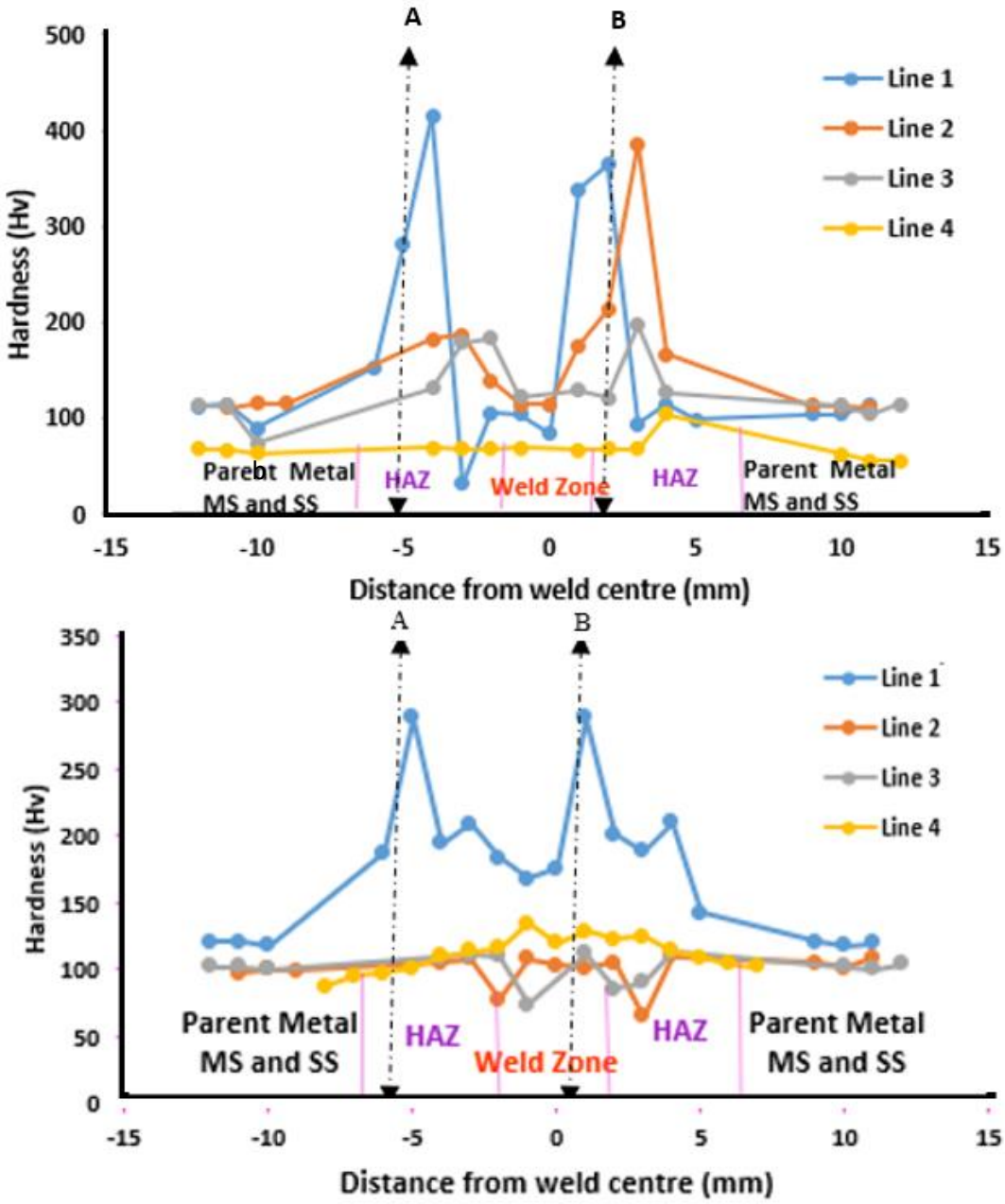

Figure 3.19 Hardness profiles across weld joint for (a) 2MSSS mm and (b) 12 MSSS samples

The average is taken across the line which actually passes through the welded joint cutting across all segments of the dissimilar material welded joints such that only the point where the line first touches the different hardness profile is used.

The hardness needs to be taken across the welded joint and the welded joint which comprise of the fusion zone bordered by the HAZ. From the Figure 3.19 referred to on page 130 the

hardness of the lines cut across the vertical of the welded region which means that it cuts across the welded parent metal and the clad metal.

The reading of line B which is located right in the fusion zone in Figure 3.19 a) has been taken. Figure 3.19 a) also takes into cognisance the reading of line A which gives an idea of the hardness across the HAZ. Each one is relevant and provides useful information giving an idea of the hardness across the weld zone.

Point B average hardness of 375 kg/mm^2 + 210 kg/mm^2 + 120 kg/mm^2 + 50 kg/mm^2 = 755/4 = 188.75 kg/mm^2. This gives rise to yield strength of 452.15 MPa when using the full data set correlation and Guzev and Busby correlation in equations generates values of 670.06 MPa and 558.7 MPa for the yield strength. For the yield strength of 452.15 Mpa for the weld sample MSSS2 compared with the parent metals of 370 MPa (2SS-1) and 352 MPa (10MS-2) from Table 3.6, it shows an appreciable increase in the yield strength which implies that the strength of the weld is higher than those of the parent metals.

The 12MSSS sample, average hardness of point A is 290 MPa + 100 MPa + 110 MPa + 70 MPa = 570/4 = 142.50 MPa. This gives rise to yield strength of 319.13 MPa when using the full data set correlation and Guzev and Busby correlation in equations generates values of 505.88 MPa and 421.80 MPa for the yield strength. Comparing the yield strength of 319.13 MPa with that of the measured value 288.00 MP, there is a good correlation.

Point B average hardness of 290 MPa + 90 MPa + 110 MPa + 180 MPa = 670/4 = 167.50 MPa. This gives rise to yield strength of 391.03 MPa when using the full data set correlation and Guzev and Busby correlation in equations generates values of 594.63 MPa and 495.80 MPa for the yield strength.

Table 3.7 Yield Strength of average hardness across HAZ for 2MSSS 2 and 4 and 12MSSS 1-3

Specimen	Average Hardness *Hv* [kg/mm^2]	Busby et al Yield Strength [MPa] = [3.55*Hv*]	Guzev et al Yield Strength [kg/mm^2] = [2.96 H*v*]	FDS Palvina and Van Tyne. Yield Strength [MPa] = [-90.7 + 2.876 H*v*]
2MSSS2 A	196.49	679.54	581.61	474.41
2MSSS2 B	188.75	670.06	558.70	452.15
2MSSS4 B	280.00	994.00	828.80	714.58
12MSSS1 B	143.75	510.00	425.50	322.73
12MSSS2 A	181.25	643.44	536.50	430.58
12MSSS3 A	142.50	505.88	421.80	319.13
12MSSS3 B	167.50	594.63	495.80	391.03

In Table 3.8, the average yield strength across the HAZ, compares well with the yield strength values measured in Table 3.6. Using the Busby correlation, it is observed that for 12MSS2 A the yield strength of 643.44 MPa compares well with the result of the measured yield strength 600 MPa. Likewise, YS of 12MSSS1 with a value of 510 MPa also compares well with 580 MPa measured in the lab. For the 2MSSS of the weld samples in Table 3.6 the FDS correlation is more appropriate with the values 474.41MPa across HAZ A and 452.15 across HAZ B being comparable with the measured values of 352 MPa from the 10 MS-2 and 370 MPa from 2 SS-2.

Comparing this correlated yield stress with the measured value revealed that the strength of the parent metal being high generates high strength in the weld metal being formed. This means that the yield stress is comparable with the derived correlation. Applying the Busby experimentally derived correlation factor produces an improved value of the yield stress in the 12MSSS samples whereas the FDS correlation produces an improved value of the yield strength in the 2MSSS samples.

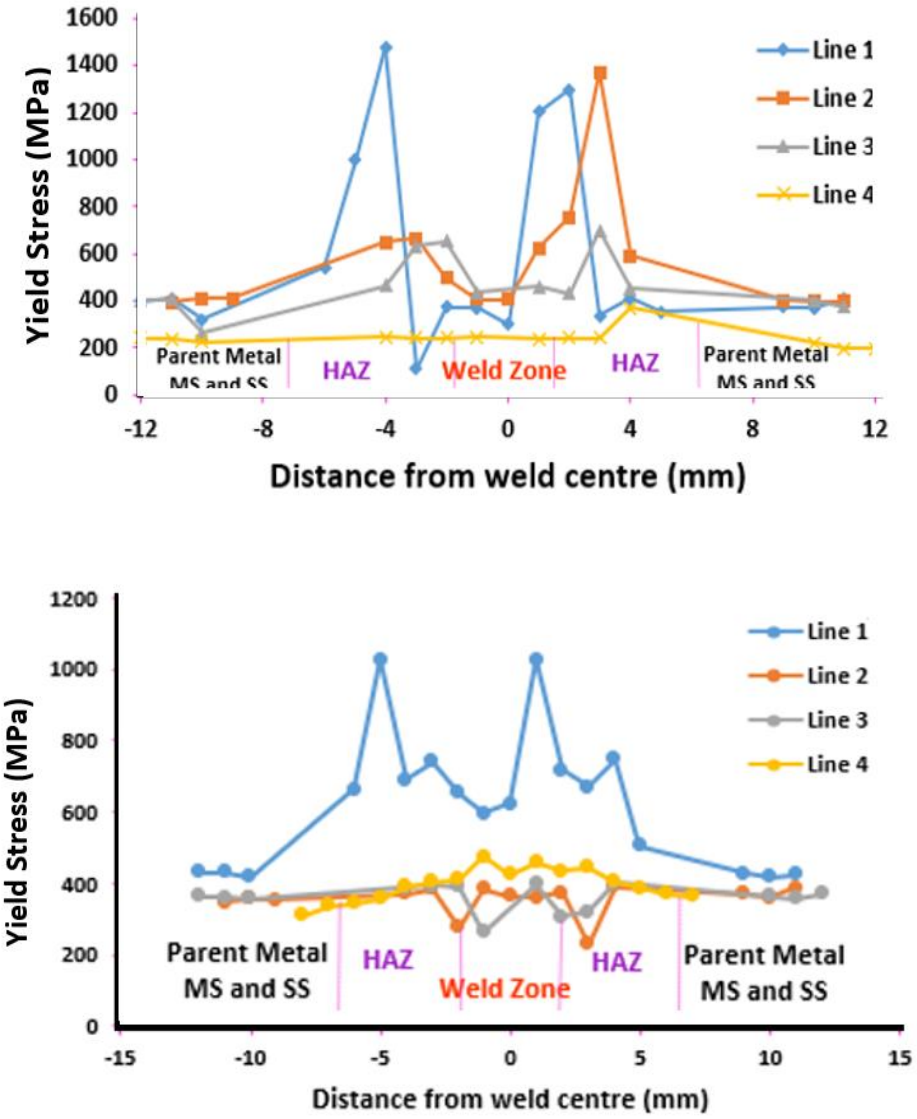

Figure 3.20 Relationship between the yield stress and the hardness of the weld using Busby experimental correlation for (a) 2MSSS-2 and (b) 12MSSS-3

There is a similar trend in the increased yield stress profile across the FZ and HAZ of the 3rd line in 2 mm samples 1 to 4, as well as 12 mm samples 1 and 2. The values of the peak yield stress in Figure 3.20 a) is 546 MPa at -2 and 81for b) 853.55 MPa at -2 and 742.86 MPa at 1; for c) 652.38 MPa at -2 and 697.57 MPa at 3; d) has 1002.03 MPa at -2 and 1242.70 MPa at 2; e) has 668 MPa at -2 and 664.26 MPa at 2 whereas f) has 452.59 MPa at -2, 553.83 MPa at 1 and 606.16 MPa at 3.

The strength is also high in the FZ and the HAZ of the 2 mm sample 1 to 4 of both Figures 3.20 (a-b). For the 12 mm sample one and two, of Figures 3.20, the strength is higher in the HAZ than other regions. It is observed that for the first line of all the samples (2 mm samples 1 to 4; and 12 mm samples 1 to 3), that the yield stress and consequently the Ultimate Tensile Strength (UTS) is very high, both in the HAZ and in the FZ compared with the parents' material as shown in Figures 3.20 (a-b). High thermal gradients were experienced during the butt-welding procedure leading to residual stress and discrepancy in the hardness. By reason of the high concentration of thermal stress in the clad, the presence of residual stresses usually affects the inherent resistance to corrosion and fatigue cracks. In order to improve the mechanical properties of the clad/base metal interface, as well as reduce the residual stresses generated, post heat treatments are carried out.

3.4.5 Charpy Tests

The quantity of energy taken into a material during charpy testing is a function of how brittle the material is and likewise how ductile the materials it. A brittle metal takes in a small quantity of energy whereas the quantity of energy absorbed by a ductile material is high (Charpy Impact Test, 2016; TWI, 2016).

After carrying out a charpy test the surface of the fracture reveals details about the nature of the fracture. When a fracture is brittle the face is bright and crystalline, when a fracture is ductile the face is fibrous and dull. The crystallinity percentage is judged by the quantity of brittle fracture or crystalline on the surface of the fractured sample, this is a measure of the quantity of brittle fracture.

The specifications of a typical charpy v-notch specimen are as shown in Figure 3.21 below – 2 mm deep notch, 55 mm long, 10 mm wide and having a radius of 0.25 mm on the face. The

details of sample preparation are seen under the section on sample preparation of weld samples from the weld block. The charpy test was carried out by Avery machine type 6704 with model number E66234/6. The striking velocity is 5.25 m/s.

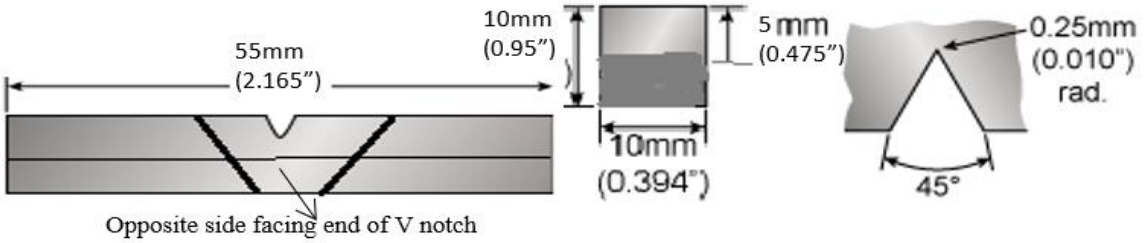

Figure 3.21 Specification of Charpy test samples (a) frontal view, (b) side view and (c) V notch

3.4.5.1 Results

Table 3.8 Absorbed energies of 2MSSS and 12MSSS Charpy specimen

Charpy Notch Test	
Absorbed Energy [J]	
2MSSS	12MSSS
19	94
43	150
60	150
52	128
72	128
100	-

The energy absorbed in the Charpy test samples is a measure of the material toughness and it ranges from as low as 20 Joules to as high as 70 Joules – with the 2MSSS experiencing higher energies of up to 100 Joules with two (2) samples as displayed in Table 3.9. This proves the brittle-ductile transition of the specimen. The test further confirms the reliability of the weld joint structure and components. The striking velocity is 5.25 m/s. The mechanical properties of the weld FZ differs from those of the HAZ and likewise those of the Parent metals (PM).

Stainless steel and mild steel (as observed from the tensile tests and the hardness tests respectively) introduces diverse stress mismatch among these different components of the Charpy sample. This implies that the stress field in the position prior to the notch is greatly proportional to the v-notch position along the weld fusion zone, heat affected zone and base as well as clad metals (Jiang et al, 2013).

Fractured Specimens

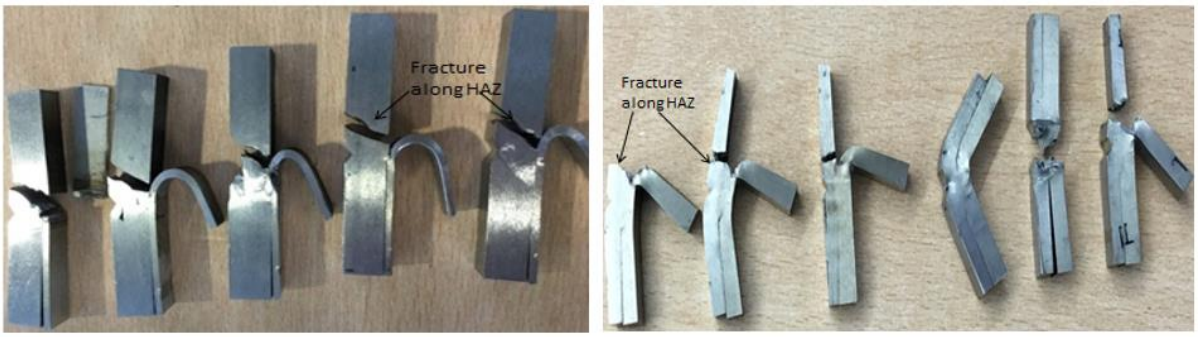

Figure 3.22 Charpy specimen (a) 2MSSS and (b) 12MSSS showing breakage at the border of HAZ

3.4.5.2 Discussion

Examining Figure 3.22 (a) and (b), it is observed that the charpy specimen has been fractured at a point which corresponded with the borderline of the HAZ (which transitions into mild steel on both sides).

3.4.5.2.1 Crystalline nature of the Charpy samples:

This clearly reveals the brittle nature of the heat affected zone and can further be confirmed from figures to correspond to the bright colouration and crystalline nature of the HAZ. Hence brittle fracture has occurred.

On the other hand, however, it is observed that the stainless steel clad is just bent over but did not fracture completely as indicated in the Figure 3.22 (a) and (b). This indicates a ductile

fracture which can further be verified by the dark colouration on the 2MSSS Charpy specimen shown in Figure 3.23.

This is a ductile fracture – the appearance of the surface of the fracture is dark. They were all carried out at relatively the same temperature – room temperature.

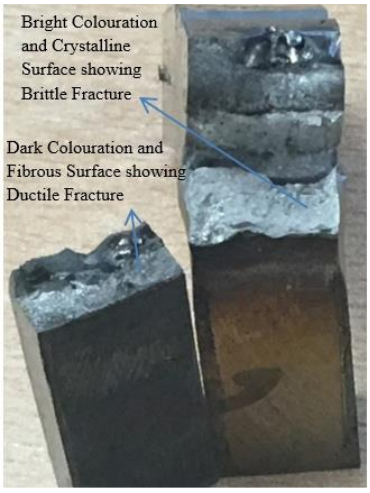

Figure 3.23 Fractured Charpy notch sample showing a brittle and ductile fracture of a 2MSSSS

A further study on the microstructure of the weld reveals that at the base of the clad/ HAZ interface, the transformation of the microstructure is coarser and tends towards a more ferritic, martensitic and austenitic structure when it cools. The martensite formed is brittle in nature as a result of speedily cooling in the air, which makes it less ductile and consequently low when it comes to toughness. In Figure 3.23, the jagged edges show that the fracture was ductile.

3.5 Optical Microscopy

Below are some of the results displaying the weld pattern taken by Olympus Model BX51TRF having serial number 8K16962; and subsequently the distribution of grains precipitating from the weldment during weld are displayed at a magnification of x50 in Figure 3.24. The direction

of the weld is shown in Figures 3.24 (a – f) and illustrated by the flow of grains precipitating from the weldment and when the weld torch direction is from left to right.

3.5.1 Results and Discussion

Weld pattern 1 shown in Figures 3.24 (a and b) reveals the weld pattern at the surface of the weld metal is the end part of the welding process. It has a huge colouration of red signifying iron. There are big grain formations and particle sizes. These were formed upon solidifying. The heat changes occurring within the system causes transition zones which tamper with the natural array of crystals within the lattices of the structure. When a metal is heated in the air, metal impurities such as metal oxides are introduced into the molten weldment or weld system, leading to the formation of voids, in spite of the argon gas shielding. When a metal is heated beyond its boiling point, there is a compound mixture of fluorides, oxides and silicates formed, otherwise known as welding fumes, which condenses on cooling to form smooth elements or crystals. While the vapour of stainless steel has a huge quantity of nickel or chromium present, that of mild steel, holds a huge quantity of Iron. It contains the following: copper, molybdenum, titanium, cobalt, chromium, vanadium and nickel to mention a few.

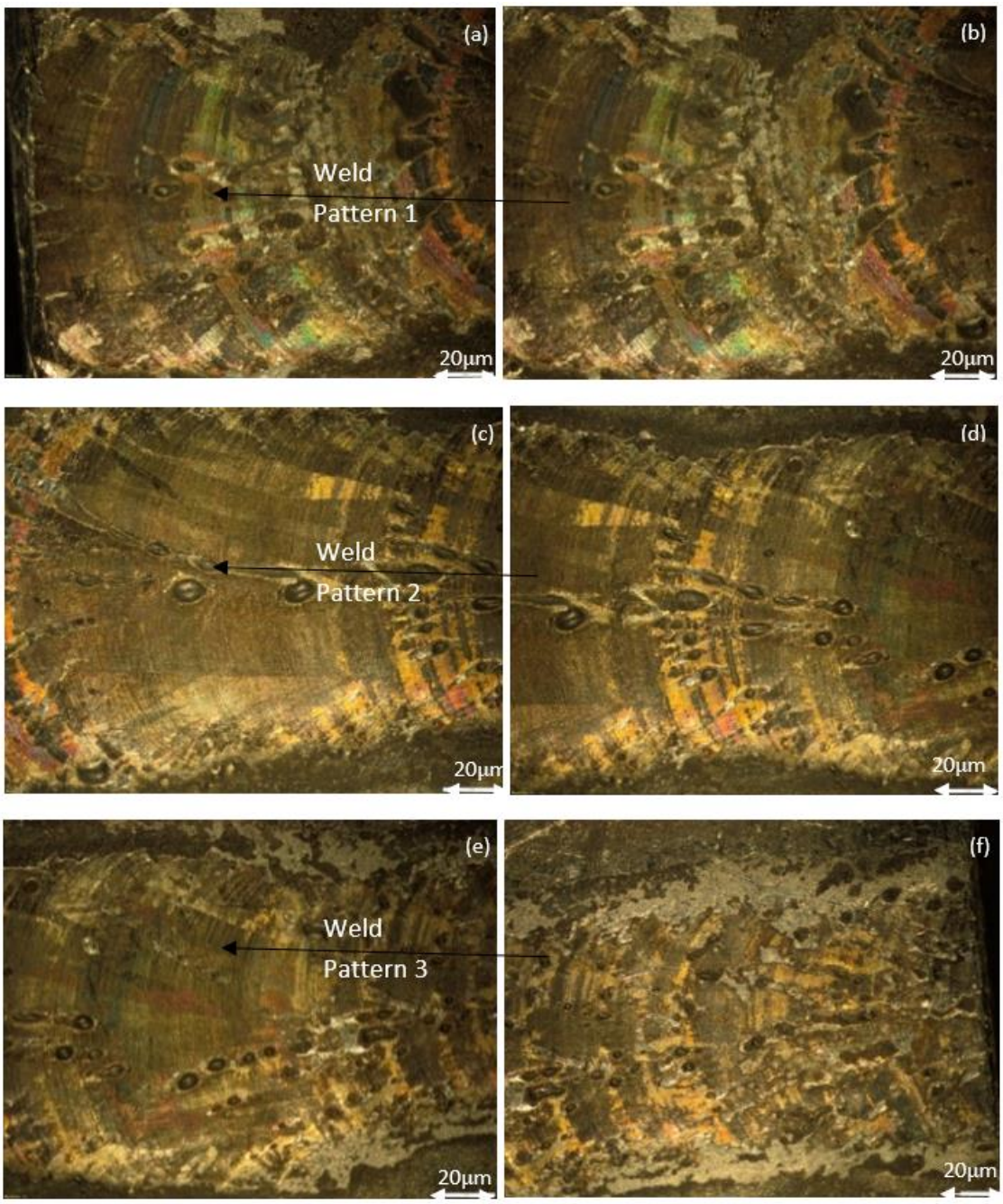

Figure 3.24 (a – b) Weld pattern 1; (c – d) weld pattern 2 and (e – f) weld pattern 3. These are the pattern of the weld surface at the top of the weld zone. Direction of weld is from left to right and the weld particles are also displayed with the larger particles (a – b), average particles (c – d) and the smallest particles (d – f). Magnification of x20

During the process of cooling, a crack is formed or is present on the surface of the weld (Becker et al, 2002; Kelkar, 2019; Lu et al, 2005). The tip faults and the amount of energy at the tip

further propagate the crack leading to failure. This is being controlled as much as possible within the crystal size.

Weld Pattern 2 shown in Figures 3.24 (c and d) shows a smoother interface and top cross section of the weld profile. Large grains precipitated out of the molten solution. The direction of the weld is evident and, in this case, is from right to left. At the point of interest, which is the point of weld, an entirely new compound is being created, not just a mixture as can be explained in the microstructure section below. A solution of one metal in another creates an alloy with new properties in particular at the melting point. This is known as a eutectic mixture as seen in Figure 3.25. That is one material has a melting point and the other material has another melting point. When they form a solution, it has a different melting point at a different level.

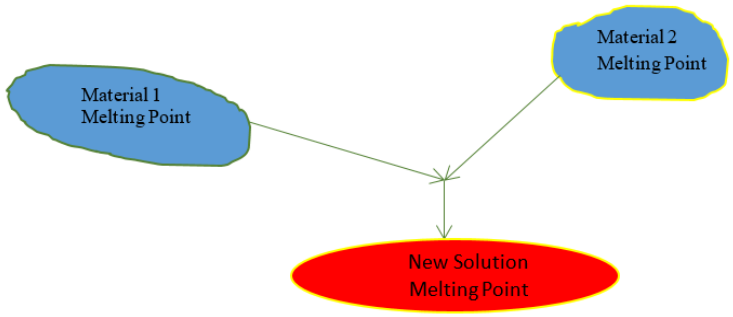

Figure 3.25 New solution melting point (MP) formed from two other solutions with different melting point (MP)

Weld pattern 3 shown in Figures 3.24 (e and f) displays several tiny particles being present in the HAZ. There is also a rough transition into the parent metal bordering the HAZ. If the solution is not a Eutectic mixture, perfect balance of the melting point, there will be crystals precipitated out of the solution (crystallization) as it cools gradually. Therefore, the rate of cooling is very important. Complexity, on the other hand is a paste of some mixture that just set. While scanning the surface of each element in the compound, it is observed that each element has a signature, and each mineral can be identified with.

3.6 Electron microscopy

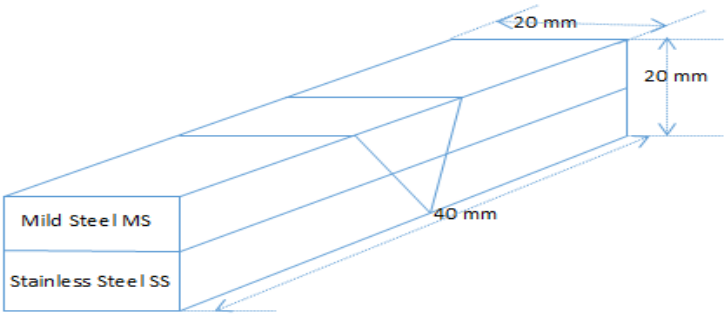

Figure 3.26 New solution melting point (MP) formed from two other solutions with different melting point (MP)

3.6.1 Approach

For the sample preparation samples of weld, with same dimensions as in Figure 3.26, were cut out from the 12MSSS weld. The 2MSSS weld has dimensions of 40 mm by 20 mm by 12 mm. Two samples each of the parent material: (2 mm stainless steel, 12mm stainless steel and 10 mm mild steel) were also cut into dimensions of 4 mm x 4 mm x 2 mm and 8 mm x 4 mm x 2 mm respectively. The parent material samples were formed into a mould using 5 spoonfuls or 2.5 spoonfuls of bakelite S and Struers mount press to enable easy and controlled grinding. The grinding of samples with a manual or automated grinder and silicon carbide papers. The diamond paste and colloidal silica suspension (also called oxidising polishing cloth) was used to attain the mirror surface view of the sample. The surface is dipped in nitric acid to clean and preserve from corrosion.

3.6.2 Results

The polishing made the heat affected zone and weld zone visible as shown in Figure 3.27. However, the peculiar features in the WZ and HAZ were appreciated after etching with Nitric acid as shown in Figure 3.27.

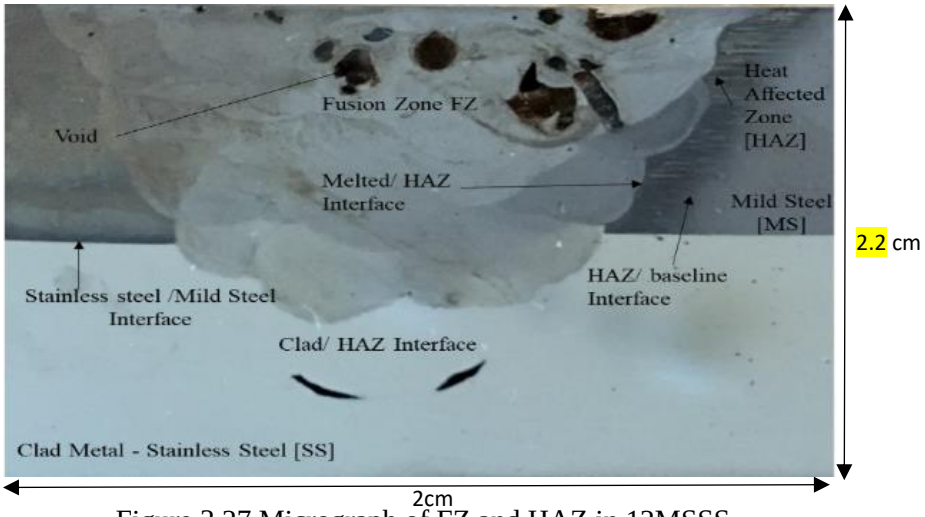

Figure 3.27 Micrograph of FZ and HAZ in 12MSSS

3.6.3 Discussion

The experiment was carried out by following the ASM International standard and Struers metallographic procedures for grinding and polishing stainless steel cladding with mild steel (Bruce & Lawrence, 2004) These clad samples were examined with the aid of an optical microscope to observe the microstructural evolutions within the heat affected zone. The HAZ is as shown in Figure 3.27. The HAZ is the boundary or zone surrounding the welded zone. This area is of paramount interest in this research because of the grain size formed as well as the constituent elements that make up that zone. The result of the charpy tests reveals that the most likely part of the weld most susceptible to crack initiation is the HAZ. High heat input during welding produces lower rate of cooling which results in coarse grain formation and large grain size (if temperature is high enough to promote grain growth prior to transformation). Large grain sizes give rise to poor toughness. The large grain formed in this HAZ (as a result of the austenitic cooling of the martensitic grains) will get oxidized when the pipe is laid on the seabed during deep offshore operations. As this layer – HAZ gets eroded (from the base metal), they expose the layer of the clad pipe, which is beneath the base metal, resulting in pitting. Pitting is crevices located on surfaces of pipes. If not handled properly as a result of

the pressure of fluid within the pipe and the forces acting on the pipe from surrounding environment, the ocean current also contributing, can lead to a leak, which could result in a burst and then complete failure of the pipeline.

In addition to the HAZ, voids are formed in a weld metal as a result of porosity and that is when gasses such as nitrogen, oxygen and hydrogen are absorbed in the molten weld pool which when released on solidification becomes entrapped in the weld metal. Porosity is caused by atmospheric interference with the weld puddle. The weld did penetrate the SS region of the weld, but it is not conspicuous all throughout the thickness of the SS except close to the mild steel region; because it is SS welded to SS and they have similar properties. The filler metal used to weld the SS to SS at the root and lower part of the weld is 304/316 filler metal. They have similar properties with the SS as seen from section 3.10.1 (EDXA of weld rod – filler metals) and are compatible with the SS metal.

3.6.4 Etching

Etching is the phenomena of processing the microstructural details that are intrinsic within a material or metal; the silent features, the ones which are not obvious to the microscope, unless uncovered via a chemical application. The type of metallographic etching carried out in this research is chemical etching and the etchant is nitric acid (HNO_3). Certain features such as the shape of the microstructure including the boundaries of the HAZ and transition zones, size of grain and inclusions, become visible. A seventy percent concentration of nitric acid is diluted with water to form a three percent (3%) solution whose composition is 11.6cc water and 0.5cc Nitric acid. The faces of the weld samples were immersed in nitric acid for 20 seconds and the parents mild steel in one minute resulted in visibility of distinct zones of the welded joints so that the HAZ and FZ – (transition zones) are clearly revealed.

Another methodology could involve taking the picture after each etching. Two pictures of the microstructure of the base metal are taken into consideration, as well as features in the fusion zone. The second image microstructure of the filler metal is also considered. Superimposing the two images either manually or in Photoshop helps to get a perfect image and see the areas of interest. Etching is an inclusion into the microstructure of the sample. The HAZ is of relevance because of the austenite coarse grains formed at the boundary of the HAZ, which could lead to oxidation – rust and could affect the structure of the pipe – leading to a compromise in the integrity of the structure. Pitting (a localized corrosion in chloride environments) (Roa & Rao, 2004; Shin et al, 2012) is then formed which leads to cracks, leaks and bursts and finally a collapse.

3.6.4.1 Results

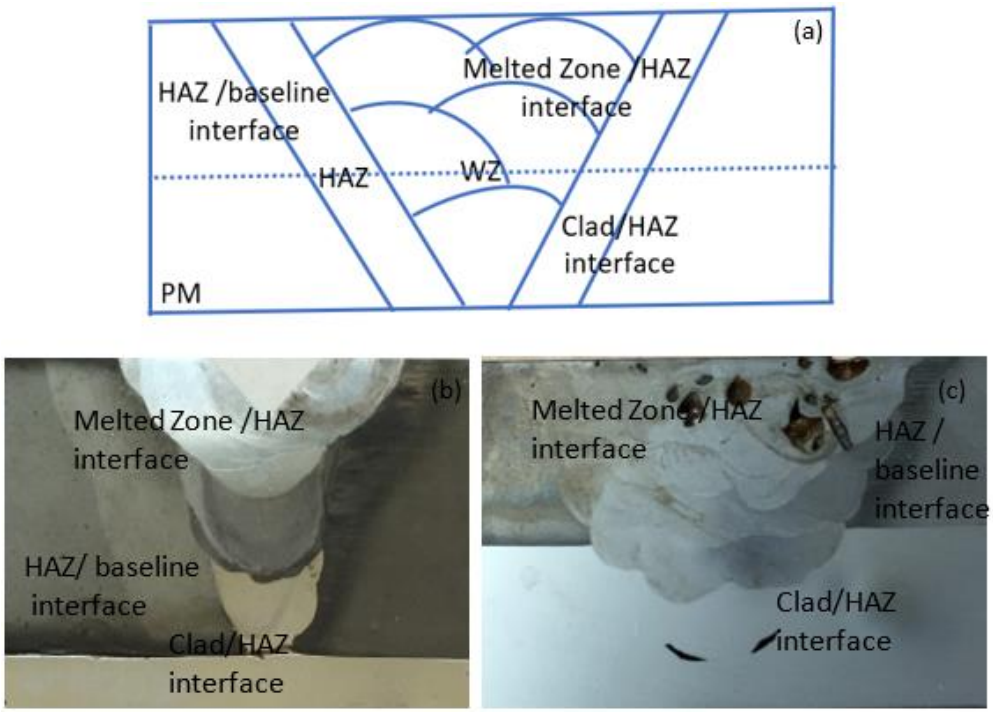

Figure 3.28 (a) A schematic diagram of a weld micrograph of 12MSSS-1, (b) Etched 2MSSS1 and (c) 12MSSS-1 revealing the Clad/ HAZ interface, the HAZ baseline interface and the melted zone/ HAZ interface

The surface of the etched sample reveals the grain boundary and interface of HAZ and Clad; as well as the interface between the baseline and HAZ of the weld microstructure as shown in Figures 3.28 (a, b and c). When comparing these two etched samples with the un-etched versions as shown in Figure 3.12 under Hardness test and in Figures 3.29 (a) and (b) below; the effect of the etching is greatly appreciated as demonstrated in Figures 3.28 (a) and (b).

Figure 3.29 2MSSS samples with the HAZ displayed. NB The boundary and weld features are not as distinct as in the etched samples. (a) without clad (cladded plate detached) (b) with clad

3.6.5 Magnified image of Etched 2MSSS and 12 MSSS at 10 µm 50 µm

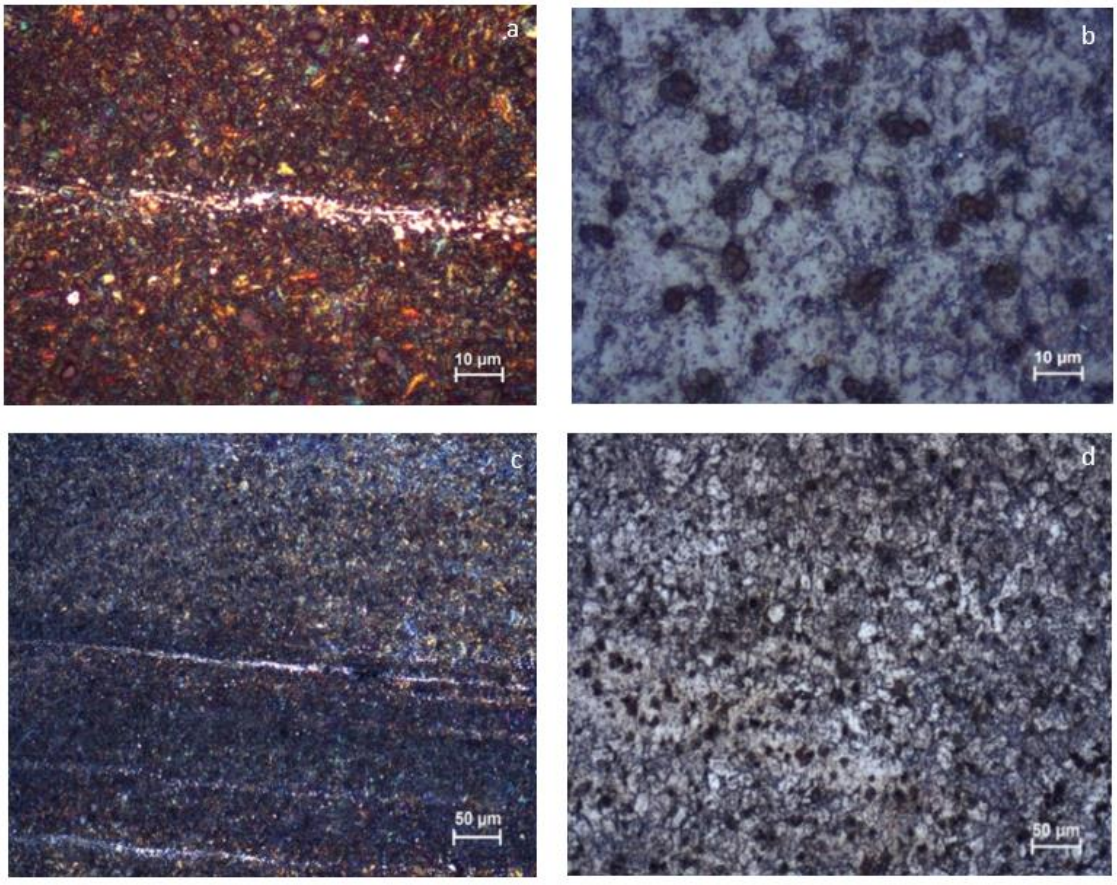

Figure 3.30 Grain sizes for (a) Etched 2 MSSS at magnification of 10 µm (b) Etched 12MSSS at magnification of 10 µm (c) Etched 2MSSS at magnification of 50 µm and (d) Etched 12MSSS magnification of 50 µm

Figure 3.30 shows (a) the grain size of the 2MSSS clad is 4 µm whereas those of the 12MSSS weld in Figure 3.30 (b) is 10 µm at a magnification of 10 µm. The difference can also be seen in the grain sizes at 50 µm from Figures 3.30 (c) and (d), the 12 mm MSSS weld still has bigger grain sizes (10µm) compared with those from the 2 mm MSSS clad weld. The reason is because for such a small quantity of melt in the 2 mm MSSS weld, rapid solidification occurs due to the low volume of the melt. For the 12 mm MSSS clad weld, coarser grain structure occurs due to the slow cooling rate influenced by the higher volume of weld zone and the larger volume of melt and large groove. The volume of fill for the 12 mm clad weldment is larger than that of the 2 mm clad weldment. This implies that it takes a longer time to weld the 12 mm compared with the 2 mm. It also implies that it takes the 12 mm a longer time to cool than it does for the 2 mm clad as seen in Figure 3.8 (a and b).

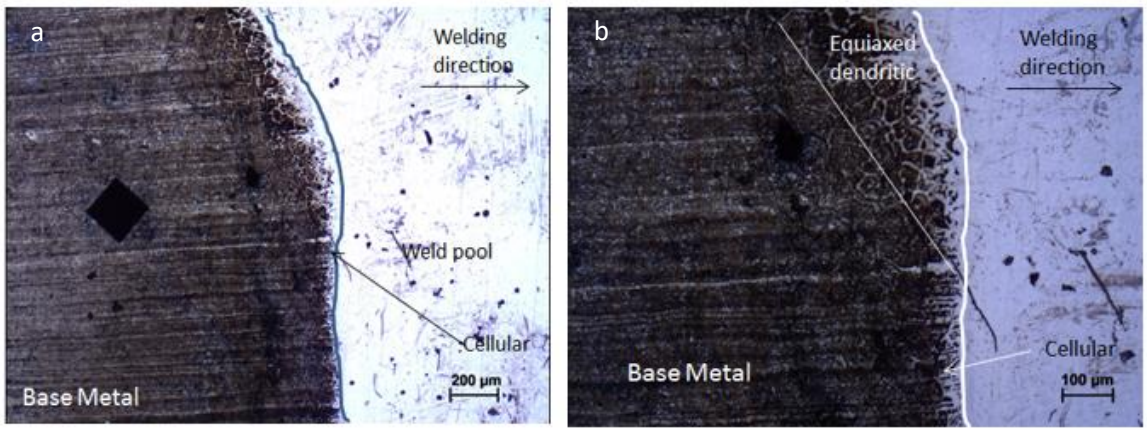

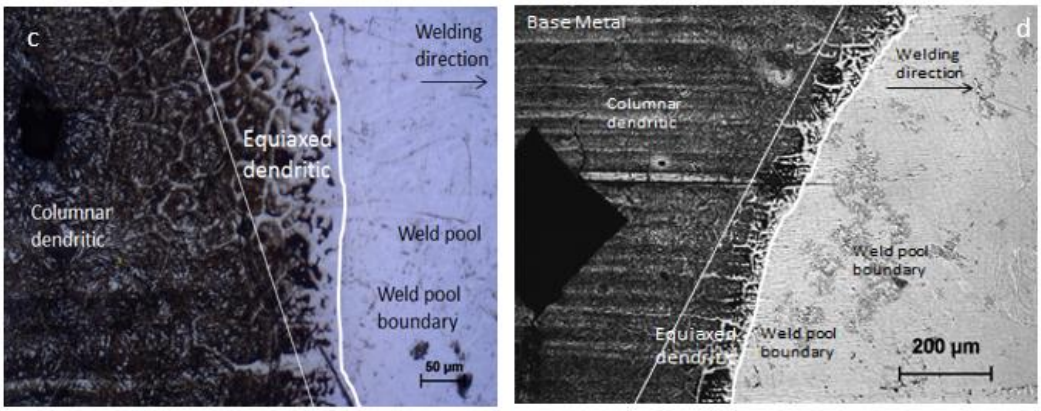

Figure 3.31 Weld pool boundary, columnar dendritic and equiaxed dendritic, as well as the weld direction between the FZ of the weld and HAZ (a-d) etched 2MSSS

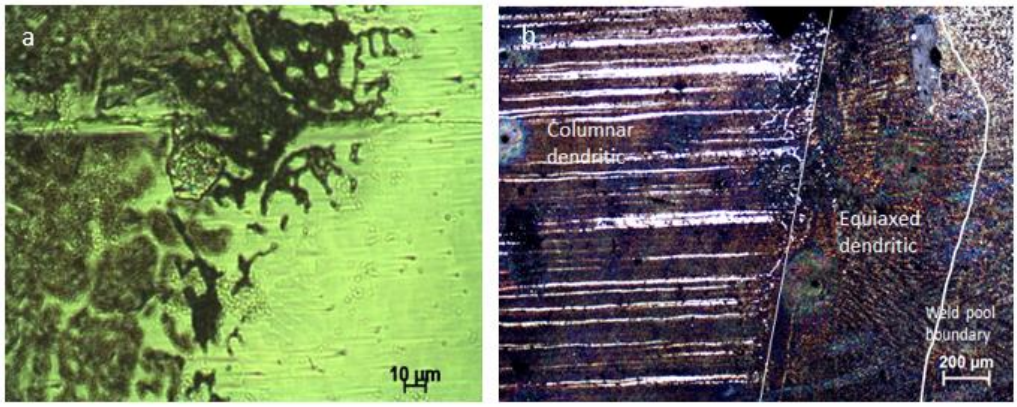

Figure 3.32 Weld pool boundary, columnar dendritic and equiaxed dendritic, as well as the weld direction between the FZ of the weld and HAZ (a) etched 2MSSS and (b) etched 12 mm clad MSSS. The colours (polarized lights) were used to enable visualization of weld growth features

Figures 3.31 and 3.32 reveals an epitaxial growth showing growth sequence and the dendrites present in the weld microstructure of a 2MSSS and a 12MSSS. There is the columnar dendritic (long and narrow in feature) which grows out from the base metal and at the tip of the columnar dendrites is located the equiaxed dendritic just at the boundary of the weld pool showing the direction of the weld pool. The columnar, dendritic and equiaxed growth of the weld grains are in the same direction as the weld pool. This growth occurs at the interface between the base metal and the weld pool. Note that the equiaxed is about same length from all sides, unlike the narrow growth of the columnar dendritic.

3.6.6 Microstructures and Observation of MSSS

3.6.6.1 Microstructure transformation of MSSS

The intermetallic sinter, which came into existence during the course of the welding, broke into pieces under the thermal pressure of the weld touch and reheating process as shown by the weld line (Jiang et al, 2013; Steel, 2016). The ferrite and the pearlite on the stainless-steel side of the structure deformed and transformed into a banded structure, see Figure 3.31. The grains on the HAZ underwent some changes, such as recovery recrystallization. The iron and carbon content of mild steel diffused towards the stainless steel, whereas the chromium, manganese carbon and molybdenum of the stainless-steel mild steel diffused towards the stainless steel (Jiang et al, 2013; Steel, 2016). The microstructure of the steel side was austenite near the interface and as a result of depletion in carbon became austenite as a result of the cooling process.

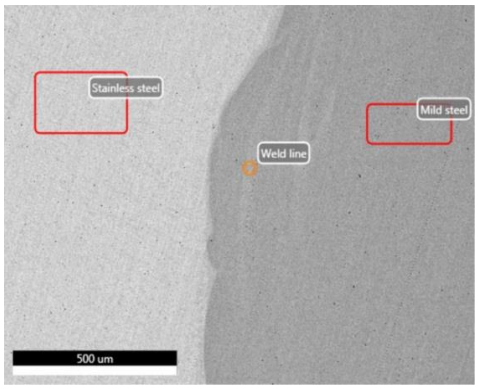

Figure 3.33 Result of SEM images and element distribution profile of the weld interface of MSSS. At the weld zone of the weld microstructure, the carbon element on the mild steel diffused toward the chromium, nickel and molybdenum at the bonding interface of the HAZ

3.6.6.2 Microstructure transformation of interstitial diffusion reaction layer of HAZ and FZ in MSSS

Judging by the results, it is evident that there is an element of carbon in the stainless steel. Refer to the tables under the SEM and EDAX section. It is known in welding that the weakest point

of the weld is the clad/HAZ interface due to inconsistent fusion and reheating, refer to Figure 3.33. During butt welding, there are high thermal gradients experienced during the procedure leading to residual stress and discrepancy in hardness. The presence of residual stresses as a result of a high concentration of thermal stress in clad usually affects the inherent resistance to corrosion and fatigue cracks. In order to enhance the mechanical properties of the clad/base metal interface, as well as to reduce the residual stresses generated, post heat treatments are carried out. The clad zone is the interstitial area, followed by the region between the clad and the weld zone (known as the bonding surface), thirdly some of the weld zone (reflective or bright), are the surfaces where compounds are located and lastly, the other surfaces (or dark coloured regions of the weld zone) are the steel or ferrite layer.

3.6.6.3 Microstructure of the HAZ

The HAZ being a heat-treated area is multifaceted in its make- up because of the quick heating up of the different areas within short intervals of time and the cooling during each pass by air at room temperature. The start of the HAZ is the clad/HAZ interface as seen in Figure 3.34 (a and b) and the peak temperature is just below the melting temperature of the carbon steel. As the temperature continues to decrease along the depth of the HAZ, the material undergoes γ and α phase transformation; γ at above 700 ^{o}C whereas at γ + α at above 727 ^{o}C steadily, until the HAZ/baseline interface is reached, refer to Figure 3.28 for a more visual explanation. Over here, the cooling temperature is usually below the eutectoid temperature of 727 ^{o}C, the lowest temperature for γ transformation. The degree of cooling has given rise to martensite and bainite rate. In Figure 3.34 (a – d), the first part is the interstitial area, the next stage is the bonding surface, thirdly the surface where compounds are located and finally the steel or the ferrite layer.

It is generally understood that the transformation of the microstructure is coarser γ and to ferrite and martensitic and austenitic structure at the base of the clad/ HAZ interface, when it cools (Sun et al, 2012). As a result of speedily cooling in the air, the martensite formed is brittle in nature, which makes it less ductile and consequently has a lower level of toughness. The interface between the clad and the HAZ fusion line is coarse in nature. This is because of high temperature peaks which stimulate the high random movement of the atoms next to the clad HAZ fusion line. The coarsened grain profile of the HAZ stimulated increased grain growth, which transformed into acicular ferrite. Coarsening features observed in clad/HAZ is common with welding which involves elevated temperatures (Sun et al, 2012). Finer grains surface away from the clad/HAZ because of a reduced temperature resulting in a pattern typical of speedily extinguished heat.

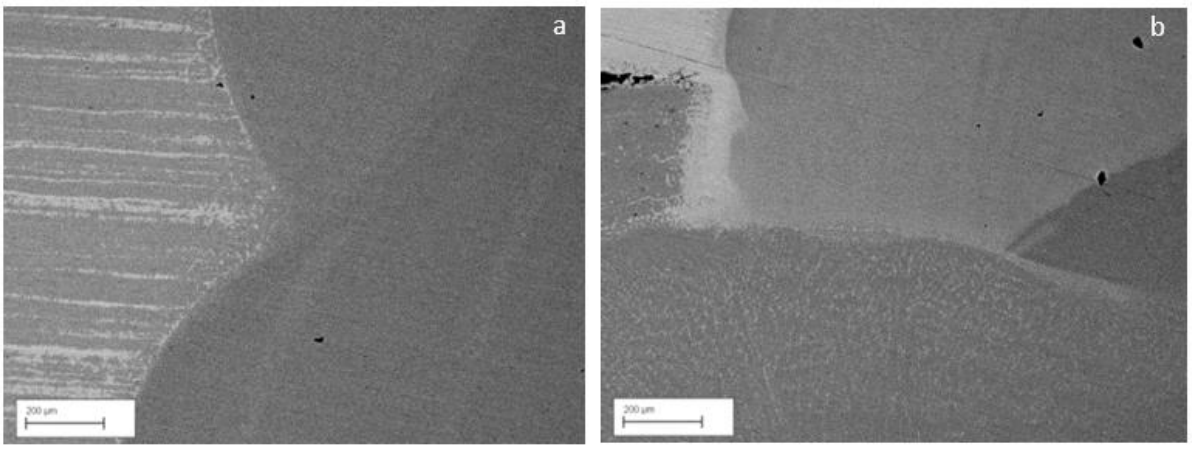

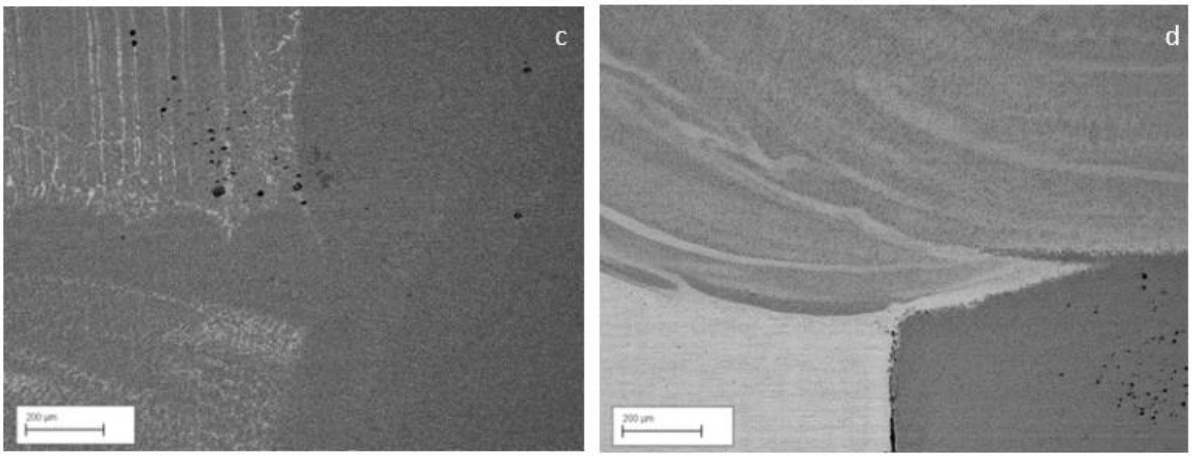

Figure 3.34 (a - d) SEM Images of HAZ and FZ. From Figure 3.32 (b) above the HAZ/ base line interface is the obvious reason why the temperature drops below A1, which is the end for austenitic transformation. There are some dark regions which represent the AISI 316 steel baseline before cladding. In Figure (a) and (c), the heating temperature is slightly greater than A1 which results in white colouration and this is a constituent of α. The transformation is precisely γ+α.

3.7 SEM Observation and Results

SEM identifies the elements present in the weld region and HAZ which favours the dissimilar weld joint and enhances properties the such as high strength, ductility and corrosion resistance of the dissimilar material joint (Goldstein et al, 2018; Vida-Simiti et al, 2004). An interesting feature discovered here is the diffusion of elements across transition zones contributing towards the enhancement of the mechanical properties of the welded joints. In order to carry out the SEM analysis, the sample is prepared in a similar manner to the optical microscopy sample.

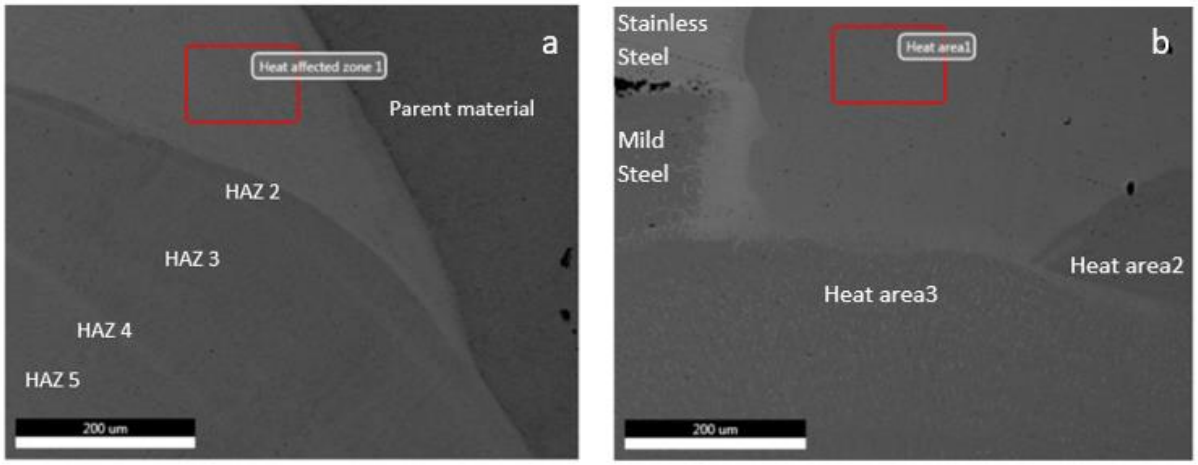

Figure 3.35 Micrograph of transition zone (TZ) (a) 1-5 in 2MSSS and MS (parent metal) (b) 1-3 in 12MSSS and MS (parent metal) and SS (Parent Metal)

Table 3.9 Elements in (a) transition zone (TZ) 1-5 in 2 mm SS/MS clad (b) transition zone (TZ) 1-3 in 12 mm SS/MS clad, (Wt%)

	2 mm clad					12 mm clad		
Elements (Wt%)	TZ 1	TZ 2	TZ 3	TZ 4	TZ 5	TZ 1	TZ 2	TZ 3
Fe	76.65	87.84	88.26	84.27	87.41	90.32	94.65	94.59
Mn	1.35	1.06	0.97	1.07	0.93	0.74	0.66	0.71

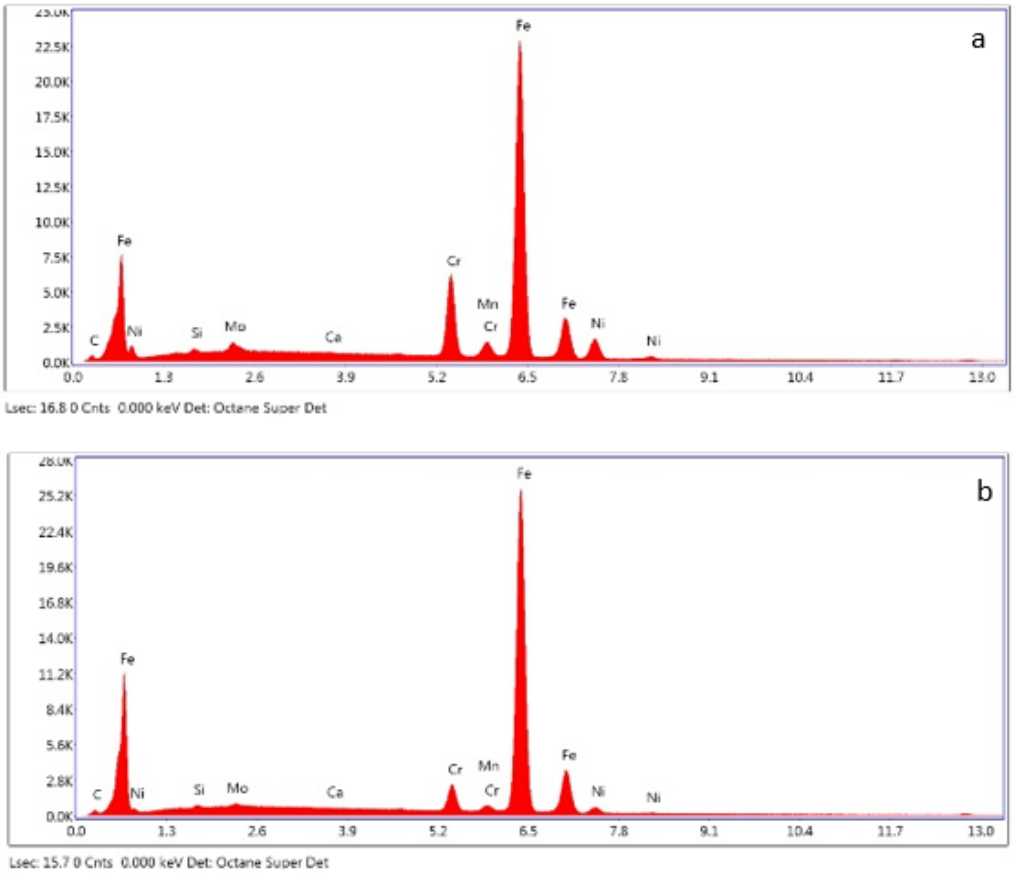

Figure 3.36 Spectrum of transition zone 1 in (a) 2MSSS and (b) 12MSSS

The part of the weld in Figure 3.35 (a) is the base layer of the FZ bordering the parent material – mild steel on one end and the transition zones on the other end. The part of the weld in Figure 3.35 (b) is bordering mild steel and the stainless steel as well as the weld interface end. Some part of the micrograph is brighter in appearance compared to the other parts of the micrograph and similar in appearance to stainless steel. Two of the different constituent elements present in this region are listed in the Table 3.10 and all the elements are displayed in the spectrum in Figure 3.36, which reveal the fact that there is a diffusion of elements not only across the parent metal interfaces but with the filler metal interfaces too. This is illustrated in Figure 3.37 and Table 3.11 gives the elements and interpretations. There is diffusion of elements taking place across the transition zone and the Parent metal as well as the HAZ. Single plus (+) signifies and increases in the elements as a result of diffusion while double plus (++) indicates higher

increase in the concentration of the element across the interfaces by reason of diffusion. It was discovered that the elements that favour corrosion resistance such as Ni, Cr and Mo were diffused from the stainless-steel into the HAZ and FZ likewise higher strength elements such as Fe were diffused from the mild steel into the HAZ and FZ.

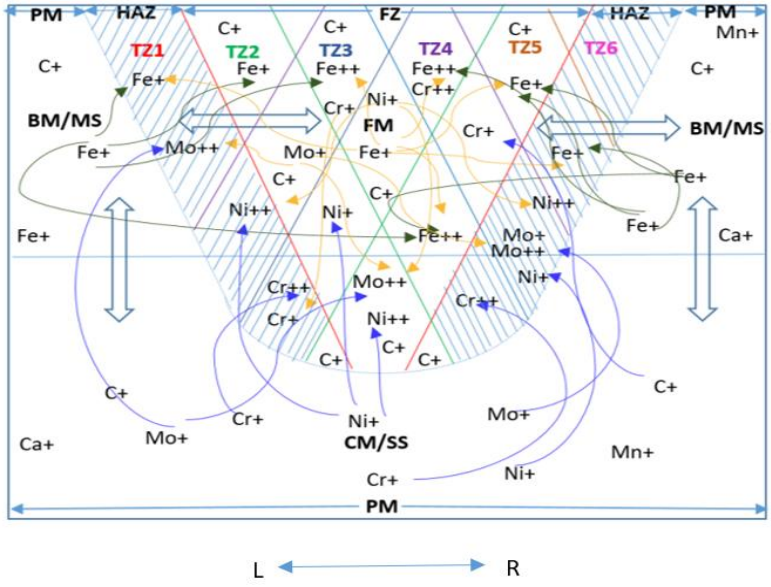

Figure 3.37 Diffusion of elements across PM, HAZ and FM

Table 3.10 (a) Symbols and Meaning (b) Elements and symbols (c) Colours and meaning

KEY

Symbols	Meaning
BM	Base Metal
CM	Clad Metal
FM	Filler Metal
FZ	Fusion Zone
HAZ	Heat Affected Zone
MS	Mild Steel
PM	Parent Metal
SS	Stainless Steel
TZ	Transition Zone

Elements	Symbols
Carbon	C
Calcium	Ca
Chromium	Cr
Iron	Fe
Manganese	Mn
Molybdenum	Mo
Nickel	Ni

Colours	Meaning
Red	TZ1 or HAZ
Green	TZ2
Blue	TZ3
Purple	TZ4
Orange	TZ5
Pink	TZ6 or HAZ
Yellow	Transition from FM
Army Green	Transition fromBM
Royal Blue	Transition from CM
Stripes	HAZ

\+ Normal concentration

++Increased concentration

⟺ Transmission / Diffusion and Dispersion of elements

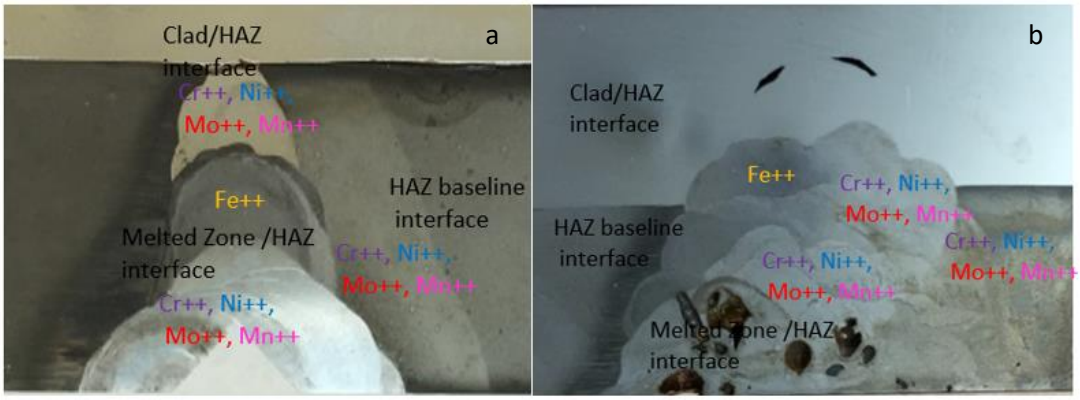

Figure 3.38 Distribution of elements across PM, HAZ and FM of (a) 2MSSS1 and (b) 12MSSS1

Figures 3.38 (a and b) show the actual weld and distributions of elements in the FZ and HAZ. Note that for the first transition zone TZ 1 (or HAZ) in the 2 MSSS, the Iron content is high 76.65% and for the second transition zone TZ 2, the percentage weight of the iron is 87.84%. These are higher than the values present in the parent metal which can be found in Tables 3.16 through 3.18 and also higher than those of the filler metals (FM) in Tables 3.14 and 3.15. Similarly, for the TZ 3, TZ 4 and TZ 5, the percentage weights of Fe are 88.26 %, 84.27 % and 87.41 % respectively (refer to Table 3.10) which are higher than the PM in Tables 3.16 through 3.18 as well as the FM in Tables 3.14 and 3.15.

For the 12 MSSS, the weight percentage of Fe 90.32 %, 94.65 % and 94.59 % in TZ 1, TZ 2 and TZ 3 respectively compared with those of the PM and FM displayed in Tables 3.14 through 3.18 is higher showing that the strength of the welded joint is enhanced through welding of the parent metals and melting the filler metals.

Observing the trend of weight percentage in Manganese Mn across the welded joint in the 2MSSS, reveals an increase in the concentration of Mn across TZ 1, TZ 2, TZ 3, TZ 4 and TZ 5 of the welded joint given as 1.35 %, 1.06 %, 0.97 %, 1.07 % and 0.93 % respectively (see Table 3.10) when compared with the values of 0.52% of the PM in Table 3.16. Likewise, for 12MSSS, there is also increase in weight percentage of Mn across the welded joint across TZ

1, TZ 2 and TZ 3 as seen in the weight percentage of 0.74 %, 0.66 % and 0.71 % when compared with the weight percent of 0.41 % in the PM of Table 3.17. These trends reveal an increase in the concentration of elements being diffused across the welded joint.

A closer look at the spectrum in Figure 3.36 (a) shows the highest peak occurs at 22.5K for Fe at 6.5 keV in the 2MSSS which implies that an energy of 6.5 keV was used to eject a weight percentage of Fe from the K Shell. Another peak occurs at 7.5K for Cr at 5.2 keV and other elements such as Ni having a peak of 2.5K, Mn and Mo at 1.8K, Si at 0.7K and carbon 0.04K. A similar trend of elemental distribution is also observed in the PM and FM in Tables 3.15 through 3.18. This depicts a wide distribution of elements across the welded joints. A higher concentration of Fe is observed in the 12 MSSS as Fe is emitted from the K shell at a peak of 25.2 and at an energy of 6.5 keV, depicting higher strength in the 12 MSSS. The other elements of the 12 MSSS include Cr at 2.8K, Mn and Ni 1.5 K and Cat 0.04K. Similar distribution of elements are also observed in the spectrum of the PM an FM in Figures 3.43 through 3.47.

It is possible to have the same elements on same spectrum because it depends on the energy levels from which the elements are being excited from. The presence of more than one concentration of elements is also dependent on the voltage and beam current used for the analysis. This because the energy of 20 kV might not be enough to excite an electron form the inner L or M shell except the outermost K shell.

The carbon contents for the different layers of the weld zone remains relatively the same irrespective of the varying content of the other elements present in the FZ and HAZs. There are high Cr content and nickel content as well as Mo and Mn. Fe content is also high. Higher peaks are noticed in the spectrum including Mo compared to the fifth transition zone. Of great importance is the very high iron content present in the 2MSSS and 12 MSSS compared to the

PM. The presence of Cr, Ni and Mo in the weld are vital for the preservation (to protect it from corrosion) and the strengthening of the pipe walls.

3.7.1 Discussion

The presence of nickel and manganese in steel decreases the eutectoid temperature lowering the kinetic barrier, whereas tungsten raises the kinetic barriers. The presence of Manganese increases hardness in steel and likewise molybdenum. The stainless-steel part of the microstructures reveals acicular ferrites within the transition zone next to the weld metal in Figure 3.39. When the cooling rate is high in a melting metal surface or material boundaries, the acicular ferrites are formed. The different ferrites are being formed starting from the grain boundary. Such ferrite includes plate martensite, widmanstatten ferrite, lath martensite and grain boundary ferrite. The 12 mm stainless steel and mild steel weld; the section of the macrostructure closest to the weld joints and parent metal interface and melting boundary, has coarser grains being formed. The level of coarsening is proportional to the heat input into the weld system. The rate of cooling and forming of solid is reduced when high heat energy is inputted into the weld system thereby resulting in coarse grain formation (Kursin, 2011). The microstructure of the weld metal displays a dendritic array (Figure 3.37) of solidification of weld grains primarily austenitic in nature and equi-axed in proportion to other grains and those of chromium carbide dispersed with other fine grain boundaries and internal surfaces.

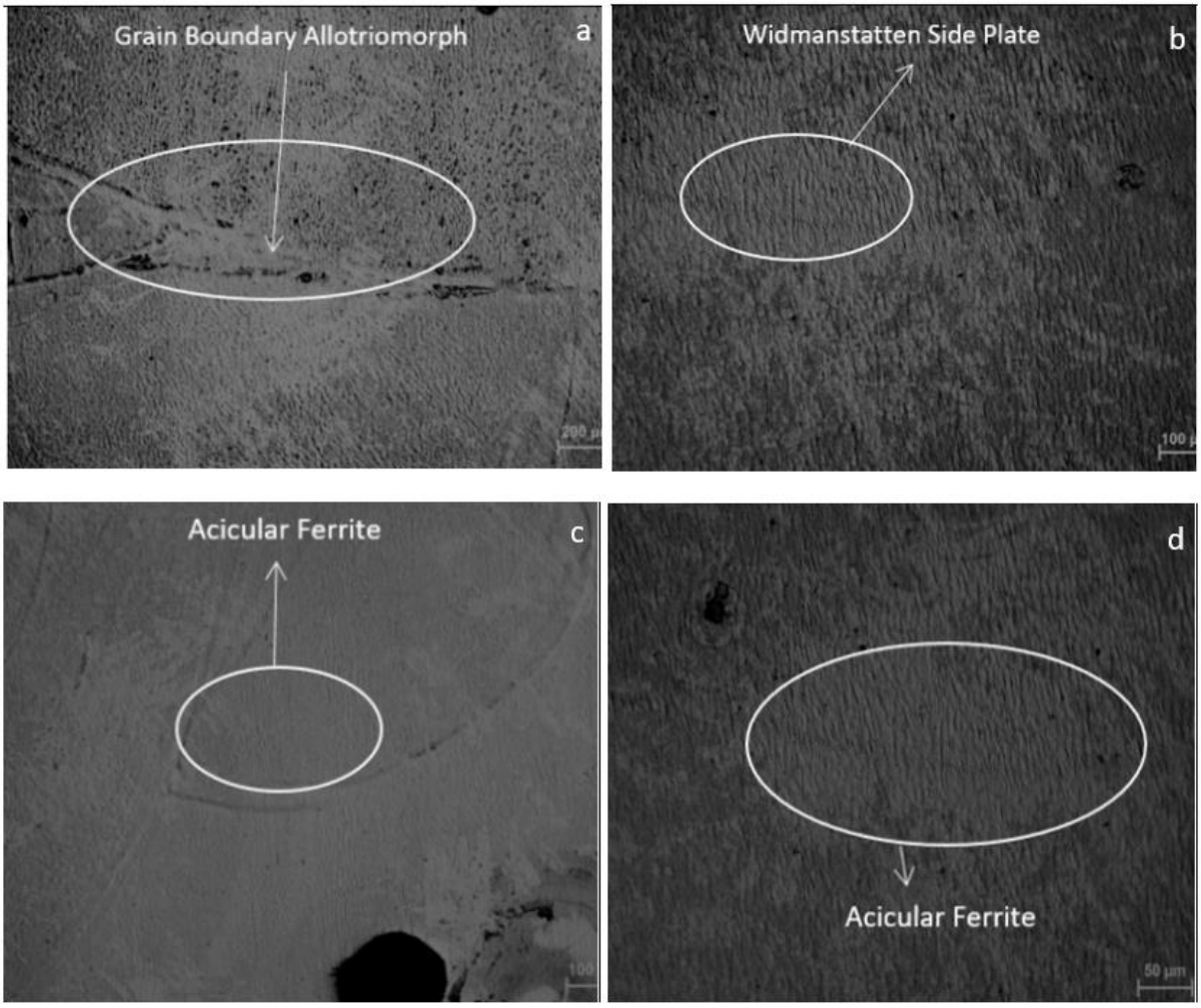

Figure 3.39 Microstructures of (a) to (c) 2MSSS1 and (d)12MSSS 2 showing acicular ferrite and widmanstatten side plates as well as grain boundary allotriomorph

This carbide is hard and provides a hard-wear resistance layer and coating to the other parts of the weld in order to protect it from corrosion and it is also known for increased hardness and increased strength. In the 2 MSSS1 and 12MSSS2 samples of dissimilar weld joint in Figures 3.37 and 3.38 (which has also been analysed using the XRD and the EBSD alongside results from the SEM and EDXA of the weld rods as well as parent metal), it is observed that carbide also diffuses from the parent metals to the weld metal and likewise chromium is also dispersed from the stainless steel to the weld metal as seen in Figures 3.37 and also XRD analysis. In the

EBSD, the austenitic phase was identified, and the phase compounds diffused and identified at the welded joints included Fe_3C, $Cr_{23}C_6$ and Cr_7C_3.

The prominent trend to observe here is the peaks of the first line of weld close to the cap, the middle region of the weld and the lower (root) of the welded joint close to the base metal. The combination of the weld rods and the carbon steel with the molybdenum and manganese elements, and the presence of iron from the filler metals increase the hardness of the welded joints. The quantity of heat also inputted into the welded joints in the GMAW affects the grain nucleation and size of the grain produced on solidification. All these affect the hardness of the weld metal (Kursun T., 2011). In the 2 mm clad, the thickness is smaller compared to the 12 mm clad. The amount of heat applied to such a welded joint compared with that applied to the greater thickness of 12 mm makes it cool down faster, forming smaller sized grains as observed in Figure 3.30 and 3.39 (a) and (c). The reverse is the case for the 12 mm weld joint whereas a result of the bigger thickness a greater quantity of heat if inputted into the weld system and consequently, it takes a longer time to cool consequently forming coarser grain sizes compared with the 2 mm clad welded joint Figures 3.30 and 3.39 (b) and (d).

From the hardness test plot of the 2 mm and 12 mm welded joints, it is observed that the ratio of hardness of the welded joint to the weld seam is high, whereas the ratio of the base metal to the hardness of the welded zone is low. The reason for these differences in the ratio of hardness across the welded zone is primarily because of the diffusion of the carbide from the parent metal (stainless steel) to the weld metal. In the middle region of the welded joint, there are high values of hardness such as HV 300, 320, 420, 288 for the 2 mm stainless steel-clad weld and HV 320 and 270 for the 12 mm stainless steel-clad weld. The transition of the chromium-carbide across the weld parent metal interfaces is responsible for this hardness. The metal rods (A15 Cu coated and 304/316 filler wire) used in welding the base metals and weld metals, has

high molybdenum content which also increases the hardness of the weldment. Molybdenum present in most weld rods generally increases the weld strength and toughness Kursin, 2011).

3.8 Electron back- scattering diffraction (EBSD)

This analysis is used to discover the phases present in the sample and orientation of the crystals of the material (SS and MS) as well as to study the morphology, phase identification and micro-texture of the specimen (Schwartz, 2009), (Randle, 2003) (Chen Z. Y., 2012). The EBSD data was acquired using EBSD with EDAX AMETEK (OCTANE SUPER- A 1.18/195915, VERIOS/G2) systems on a thermal field emission gun with a Four Quadrant Backscattered Electron Detector type. The EBSD mapping data was obtained from a randomly selected 60mm^2 sensor area. The entire aperture is 120.0 micron (μm), current is 0.8901 amperes, scanning - sequence is from bottom to top: right WD = 12.5 and high magnification of 100. Working distance is 9.5 mm, mapping and resolution is for 100 m. Precaution is taken to ensure the detector is brought out before the sample to avoid detector leaks and the return to TV mode.

3.8.1 Result

There are changes in hardness at the weld interface of the weld zone which is confirmed by the presence of porosity in the weld microstructure of the 2mm MSSS Sample. The different phases present in the microstructure are ferrite, martensite and austenite. For the spot 1 the phase identified is ferrite (α), likewise for spot 2. For spot 3, martensite (α′) was identified. Spots 4 to 6 are also ferrite and spot 7 (γ) is austenite. In the microstructure of the 12mm clad, spots 1

and 2 have ferrite (α) phases present in them; spot 3 is austenitic (γ) in nature, while the phases present in spot 4 and 5 are martensite (α′).

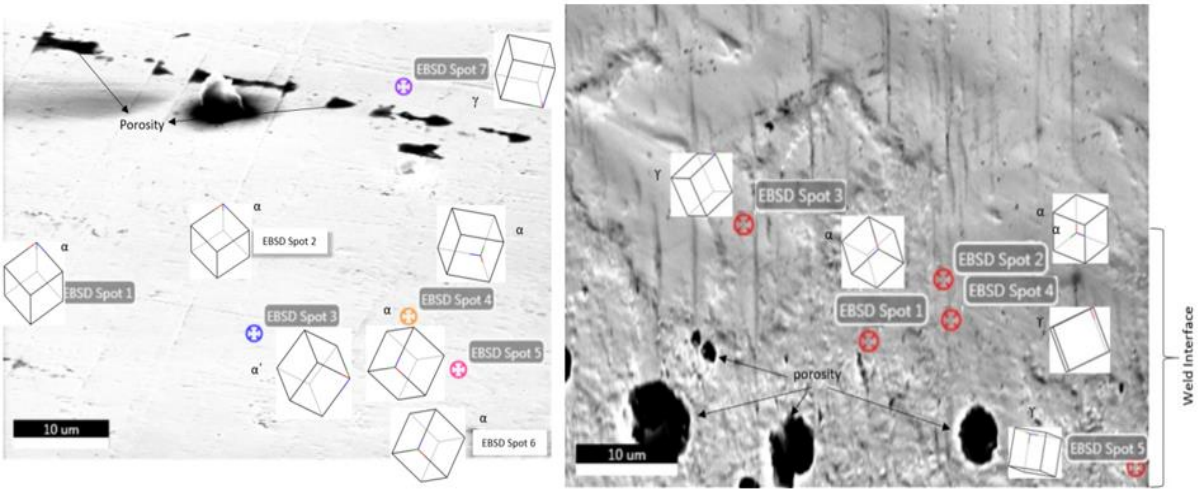

Figure 3.40 (a) Microstructure of 2MSSS-1 and (b) Microstructure of 12MSSS-1; showing the distinct phases present within the welded interface of the welded zone and lattice orientation of each phase – ferrite, austenite and martensite.

3.8.2 Discussion

There is a change in the weld interphase as observed in Figures 3.40 both in the morphology and texture of the weld zone, which is verified by the porosity of the weld microstructure. This is further confirmed by the decrease in the hardness that starts from the line of the transition zone, as observed from the results of the indentation tests and micrographs. This decrease is as a result of repeated thermal cycling causing slight softening in the Mo-free region of the weld. The Mo and the Mn minerals present in the welding electrodes (rods – filler metals) increases in hardness when blended with the carbon steel and is responsible for this increase observed in the hardness of the weld zone (Evans, 1988). The size of the grains formed in the weld metal by virtue of speedy cooling are small and fine in structure due to low heat input of the joints acquired from GMAW (Kursin, 2011).

Depending on the phase changes present in a particular micrograph and sample, the properties of the weld also changes. The change in the orientation of the hkl values also change the properties. The presence of martensite phase change causes a slip, break and fracture. Martensite is a mixture of ferrite and austenite and has lots of residual stress mass as such it is tougher.

Previous tests have shown volumetric change and yield strength, as seen under tensile test curves in chapter 3 by reason of martensitic transformation. It has been shown to have an effect on welding residual stress, by increasing the magnitude of the residual stress in the weld zone, as well as changing its sign. In agreement with the above findings, the results of the simulation in chapter 5 also reveal that the volumetric change and the yield strength change due to martensitic transformation and these have influences on the welding residual stress (Dean & Hidekauzu, 2006). The EBSD scan reveals presence of ferrite, martensite and austenite phases which are cubic structures. Ferrite is body centred cubic bcc; the crystal lattice of martensite is a body-centred tetragonal form of iron in which some carbon is dissolved whereas austenite is face centred.

For Grade 316 stainless steel (and austenitic stainless steel), planar slip is observed, because of its low stacking fault energy, and cross-slip is prevented (Acar & Fitzpatrick, 2017). The grain boundaries act as strong barriers to slip. At the commencement of plastic deformation (<1.5%) dislocations pile up near grain boundaries thereby inducing stress concentration (known as intergranular stresses) near the boundary. Consequently, the plastic strain which is enhanced during the early stages of deformation produces higher stress concentration near the grain boundaries by reason of the high quantity of dislocations in the pile-up. The stress concentrations within the grains of the dissimilar welded joint (Intergranular stresses) begins to decrease with the activation of multiple slip and cross-slip: the intergranular stresses are

therefore relaxed, and the plastic strain compatibility is maintained between the grains. The slip transmission across grain boundaries of the dissimilar welded joint and activation of dislocation sources in neighbouring grains also lowers the intergranular stresses (Acar & Fitzpatrick, 2017).

Any more deformation after the activation of cross-slip and multiple slip generates heterogeneous dislocation structures like dislocation bands and arrays of dislocations inside the grains which subsequently increases the intragranular stresses. It has been discovered from research that the difference between inter- and intra-granular stresses becomes zero at about 6% plastic deformation. Intragranular strains are therefore relevant as the intergranular strains after 6% deformation and cannot be ignored. The residual strain after plastic deformation beyond 6% deformation is said to be made up primarily of intergranular strains which arise owing to the elastic anisotropy of the different hkl planes; and secondly intragranular strains which are generated by reason of the heterogeneous dislocation structures inside the grains (Bate et al, 2005; Di Gioacchino & Quinta da Fonseca, 2015; Acar & Fitzpatrick, 2017; Das et al, 2016).

3.9 X-Ray Diffraction (XRD) Analysis

The Bruker AXS Diffraktometer D8 Erz. Nr. 7KP2025-1LG14-3-Z P02, Serial-Nr 203770, (D 76181 Karisruhe, Germany), was used to analyse the 2mm and 12mm MSSS welded samples and the phase composition, as well as the XRD characterisation being carried out with the aid of the DIFFRAC.EVA, software version 4.0 (32 bit), which was released in 2014. In order to determine the size occupancy and crystal structure as well as the angle, Bruker AXS TOPAS version 5 was used to fundamentally compare the structure of the crystals present in these samples with a standard structure of a crystal already existing in the library (since each metal

has a peculiar signature), so as to obtain the closest similar characteristics or patterns peculiar to it thereby identifying the structure (Cullity, 2001; Pecharsky & Zavalij, 2003; Chung & Smith, 1999; Chung & Smith, 2000; Pecharsky & Zavalij, 2009).

3.9.1 Approach – Sample preparation

The surfaces of the samples were cleansed with ethanol and the weld samples were placed in transparent sample holders; and held in place by plasticine, after which they were placed inside the x-ray detector and the analysis was carried out and monitored via the computer. It is important to remember that since welding is a multifaceted process, and different phases are formed by reason of the change in temperatures during the cooling processes; the properties of the weld change based on the phase changes present in a particular micrograph and sample. Below are patterns of the element distribution, crystallinity, and different phases present within the weld samples as displayed in Tables 3:12 and 3.13 as well as Figures 3.41 and 3.42.

3.9.2 Result

The first crystal size of Chromium Nickel Phase (the yellow phase) in the 12mm MSSS is 411.9 Armstrong. This corresponds to the highest peak in the spectrum. The second Crystal size of Chromium Nickel phase (the yellow phase) in the 12mm MSSS is 411.9 Armstrong, refer to Figure 3:41 and Table 3:12. This corresponds to the next peak of the spectrum in Figure 3.41. The detector also detected a quantity of Chromium Nickel present in the sample at that

wavelength as seen in Table 3:12. There are hkl values for 12mm MSSS weld sample-1, as well as Iron-Nickel (Fe Ni) phase present in 12mm MSSS weld sample-1.

Table 3.11 Percentage Crystallinity and Amorphous present in 2mm MSSS Weld Samples and % present in 12mm MSSS weld samples

Samples	% Crystallinity	% Amorphous	Global Area (μm)	Reduced Area (μm)
2MSSS 1	44.2	55.80%	366.4	161.8
2MSSS 2	54.60%	45.40%	302.8	209.1
2MSSS 3	45.40%	54.60%	328.2	149
2MSSS 4	37.70%	62.30%	1178	444.3
12MSSS 1	9.40%	90.60%	1269	119.9
12MSSS 2	50.1	49.9	343.3	172.1

Table 3.12 Phases present in 2mm and 12mm MSSS Weld Samples and % Quantification present the weld samples

Samples	Phases	Formula	Quantification
2mmMSSS 1	Iron Nickel	Fe3 Ni2	6.70%
	Stainless Steel, Ferrite Iron Chromium	Fe-Cr 410-L	93.30%
2mmMSSS 2	Iron	Fe α–Fe Iron	58.20%
	Chromium Iron Molybdenum Nickel Silicon	Fe6.6 Cr1.7Ni1.2Sil02Mo0.8	41.80%
2mmMSSS 3	Iron Nickel	Fe Ni	90.10%
	Iron Nickel	Fe(0.7Ni0.3)	9.90%
2mm MSSS 4	Iron Nickel	Fe0.7 Ni0.3	28.60%
	Chromium Iron	Cr Fe3	24.60%
	Iron Phosphorus	Fe 0.96 P0.04	34.10%
	Molybdenum Nickel	Mo Ni4	12.70%
12mm MSSS1	Chromium Iron	Cr0.7 Fe 0.3	7.40%
	Iron manganese	Fe19Mn α-Fe19Mn	6.50%
	Stainless steel, Ferrite Iron chromium	Fe-Cr4 10 L	72.30%
	Manganese Nickel	Mn Ni3	4.40%
	Chromium Nickel	Cr Ni	3.90%
	Chromium Iron	Cr0.03Fe0.97 α–Cr0.03Fe0.97	5.60%
12mm MSSS2	Iron	Fe	53.40%
	Iron Nickel (Kamacite (NR))	Fe Ni	46.60%

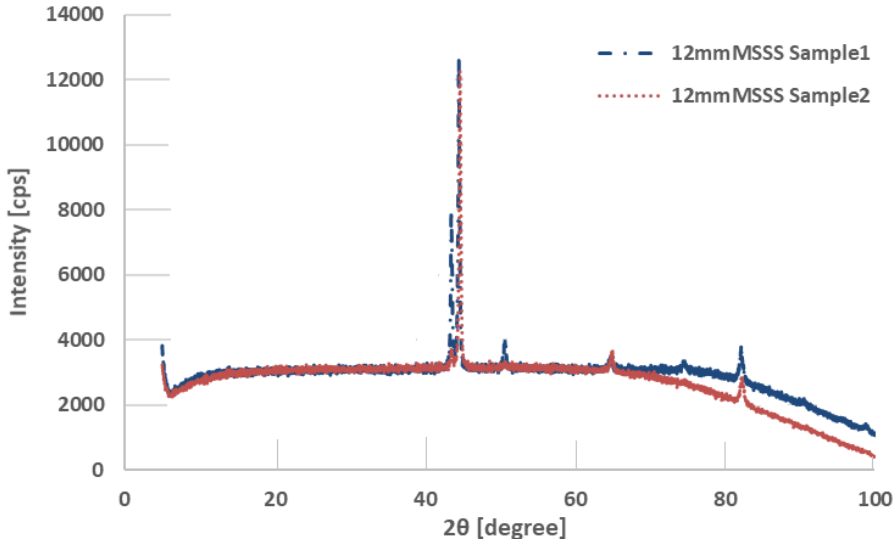

Figure 3.41 XRD Pattern for 12MSSS 1&2 revealing multiphase presence

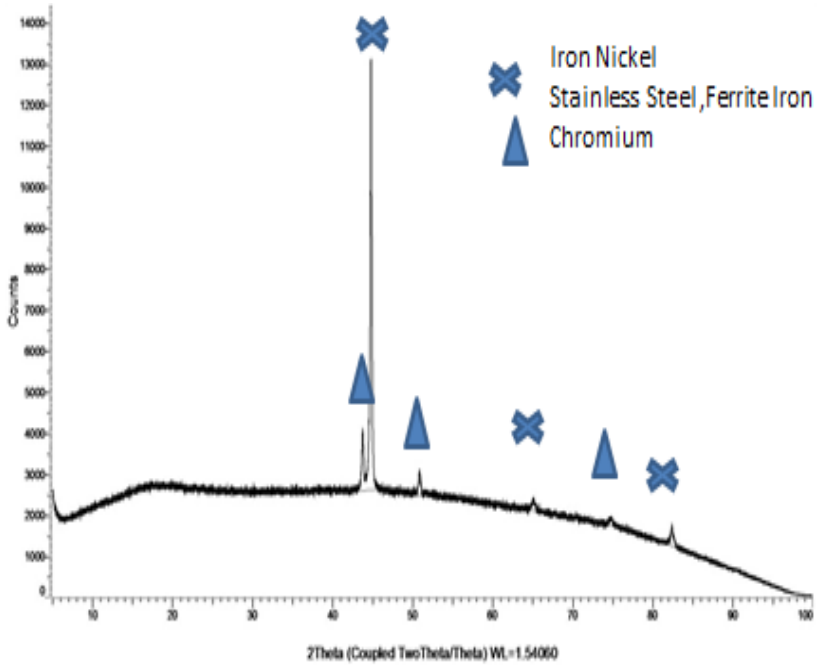

Figure 3.42 XRD Pattern for 2MSSS1 revealing multiphase presence

The highest peaks displayed in the spectra in Figure 3.42, which consequently find relevance in this 2mm Stainless steel, and mild steel weld are iron manganese and iron nickel as seen in Table 3.13. The second crystals measured correspond to the second peak highest peak on the spectra.

The highest peaks displayed in the spectra, which consequently find relevance in this 12mm Stainless steel and mild steel weld are iron nickel and manganese silicide, followed by stainless steel ferrite iron chromium. Peak occurring at 45 (2θ) shows it is Austenite. The hardness decreases from the boundary of the transition zone. Chromium-Iron (Cr0.7 Fe0.3) phase is present in 2mm MSSS weld sample-1 and hkl values are also present for 2mm MSSS weld sample-1. Manganese-Nickel (Mn Ni3) phase is present in 2mm MSSS weld sample-1 as well as the hkl values. The highest peaks displayed in the spectra, which corresponds to one of the phases presents in this 2mm Stainless steel and mild steel weld are iron manganese nickel Silicon, Iron Silicon and Molybdenum Silicon. The phases present in this 12mm Sample 2 is the Iron phase and the lron Nickel phase

3.9.3 Discussion

The nature of the spectrum (sharp and definite peaks) obtained from the XRD analysis of the 2mm MSSS and 12mm MSSS samples reveal a crystal-like structure unlike the amorphous nature of spectrum that is depicted by a continuous wave-like peak. From the 2mm MSSS Sample 1, different phases are present such as iron manganese nickel Silicon, Iron Silicon and Molybdenum Silicon. From the 2mm Sample two the phases present are α-Ferrite and iron nickel. Likewise, from the 12mm MSSS Sample 1, different phases are present such as the Manganese Nickel Silicon, Iron Silicon and Molybdenum nickel. In the 12mm MSSS Sample 2, we clearly see different phases present such as the Manganese Nickel Silicon, Iron Silicon and Molybdenum nickel. These results confirm the distribution of elements within the different zones of the welded joints of dissimilar material; with the HAZ seen to have the elements known for anti-corrosiveness and high strength which guarantees longevity of the welded joint in service and structural integrity of the pipeline in service. This further confirms with the

results from the EDAX analyses of the parent metals - stainless steel and mild steel and the weld rods (filler metals) - A15 Copper filler wire and 304/316 which reveals the presence of these elements in their composition. Refer to Tables 3.14 and also 3.15 under EDAX.

The Peak in the XRD figure above depicts the presence of Chromium Cr which is responsible for weld failure clearly experienced previously (see figure in chapter1) and discussion under SEM section (Lakshminarayanan & Balasubramanian, 2010). From the results of the EBSD, it is obvious that there exists martensitic, ferrite and austenitic phases present in the weld samples. For the XRD analysis, the index (h, k, l) pattern was obtained, and the results displayed below. The phases present were determined and their quantity as well as the crystalline size of each phase measured. The creation of Martensite consists of a systematic displacement and array of atoms. This implies that austenite and martensite will be closely interrelated which means that martensitic alterations give rise to an array of bonds between parent and product lattices that can be reproduced repeatedly. Most times the Austenite and ferrite phases are parallel and as such the directions that are confirms and matches with these planes which are also matching.

3.9.4 Summary

The XRD pattern was used to confirm that the XRD pattern in the HAZ area is similar to that of the bulk material – parent material (stainless steel and mild steel as well as filler metals (316/304 and A15 Copper wire). The microstructure although similar, cannot be the same because of the cooling conditions.

3.10 Energy Dispersive X-ray Analysis (EDXA)

This was carried out using the 840 SEM mainly to confirm the findings on the transition of elements under SEM analysis and it was discovered that there were good agreements between the results in the SEM and in the EDXA (Lyman et al, 1990; Dwivedi, 2018; Scimeca et al, 2018). The concentration of the elements in the FM and PM which is analysed in the EDAX section, favoured the diffusion of elements in the HAZ and WZ, favouring the enrichments of the welded joints with hardness, strength and anti-corrosive properties, as shown in the mapping in Figure 3.44 and 3.45.

3.10.1 EDXA of Weld Rods – Filler Metals

The A15 Copper filler wire with a thickness of 2.95mm was cut close to the burnt tip at 20mm and likewise the 304/316 filler wire having a thickness of 1.56mm. Both were sellotaped at one end. Samples are placed inside the detector with the help of a rod and analysed.

3.10.1.1 Results

The results of the elements present in the weld rods and parent metals are displayed below. It is observed that both rods contain Mn and Mo elements. These elements are responsible for increasing the hardness in the electrode and mild steel and are depicted by the high peaks seen on the plots in the hardness test section.

3.10.1.2 The 304/316 filler wire

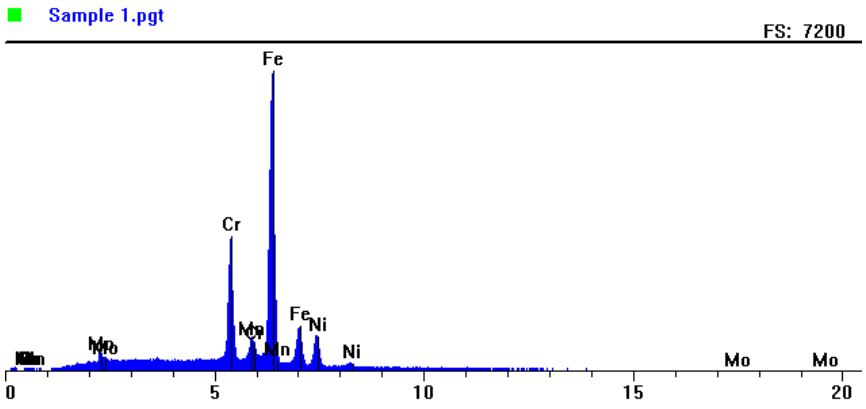

Figure 3.43 Spectrum of 304/316 filler wire NB: Iron has the highest peak followed by Chromium and Nickle

Table 3.13 Elements present in 304/316 Filler Wire

Element	Fe	Mn	Cr	Ni	Mo	Total
Wt%	66.54	1.65	18.11	9.50	4.20	100.0

Since 304/316 filler wire, is an alloy of chromium and nickel and contains high quantity of Mo to enhance the strength of the material and improve corrosion resistance, comparing the above weight percentage in Table 3.14 with the following reference value from (Matweb, 2017): 12.5% Ni, 18% Cr, and 1.8% Mn, 2.2% Mo and a high percentage of Fe, 64.3; gives a very good match of the elemental composition and characteristics.

3.10.1.3 The A15 Copper filler metal

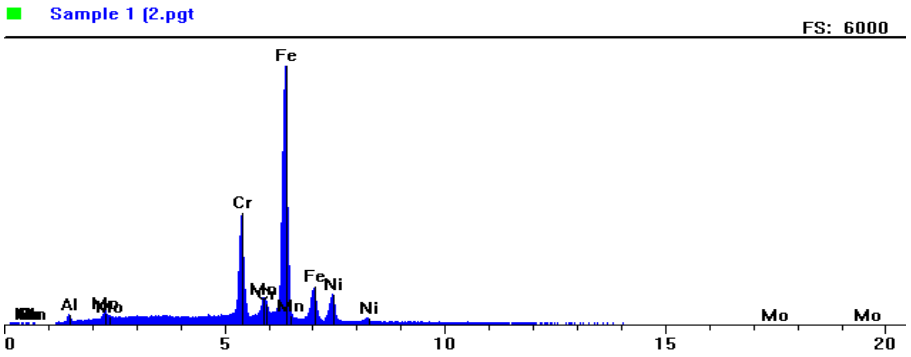

Figure 3.44 Spectrum of A15 Copper filler metal

Table 3.14 Elements present in A15 Copper Filler Metal

Element	Fe	Mn	Cr	Ni	Mo	Al	Total
Wt%	66.01	1.69	17.82	9.56	3.85	1.07	100.0

The A15 Copper filler wire comes in different sizes 1.0, 1.6 and 2.4 mm in diameters and is fundamentally a copper coated deoxidized steel rod. It has a melting point of 1450 ^{o}C. It has an ultimate tensile strength of 440 N/mm^2 and a hardness of 120 Hv. The compositions of A15 in the Table 3.15 with those provided by (Weldability, 2017) which are 0.2% Al, 0.6% Si, 0.1%C and 1.3%Mn reveals a reasonable agreement. The order of the magnitude of peaks in the above spectrum is given as Fe followed by Cr, Mn Ni and Al. It is suitable for Tungsten Inert Gas weld and for application on mild steel.

3.10.2 EDXA of Parent Material

3.10.2.1 EDXA of Stainless Steel – 2mm

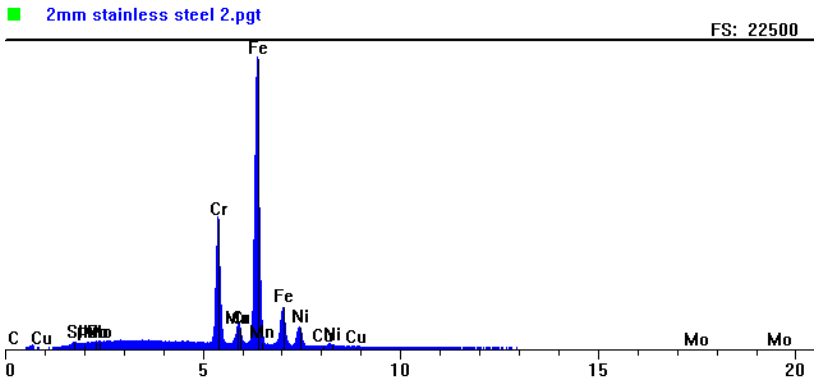

Figure 3.45 Spectrum of 2 mm Stainless Steel

Table 3.15 Elements present in 2 SS 1

Element	Cr	Fe	Cu	Mn	Ni	Mo	Si	C	P	Total
Wt%	29.68	58.15	0.14	0.52	8.30	2.77	0.36	0.04	0.04	100.0

The chemical formula of Stainless-steel 0020x grade 316 which is, Cr 10-14%, Ni 2-3%, Mo < 2%, Mn <1%, P < 0.03%, (Azom, 2017) there is a good agreement with the percentage on the stainless steel given in tables 3.16. Looking at the spectrum shows that Iron is present in high quantity followed by chromium and nickel fulfilling the 300 series of stainless steel. After that we have other element such as Mo, Si and Cu present in trace quantities.

3.10.2.2 EDXA of Stainless Steel – 12 mm

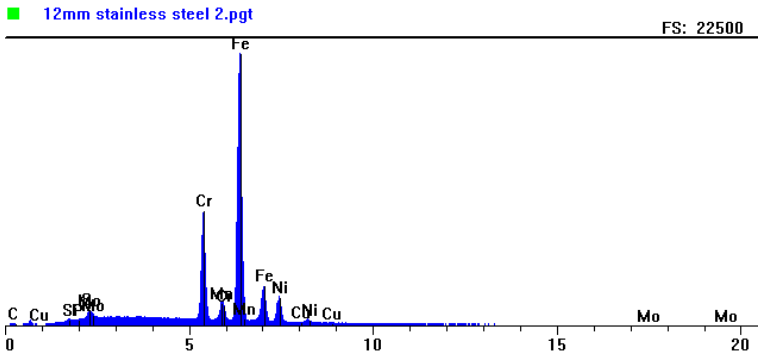

Figure 3.46 Spectrum of 12 mm Stainless Steel

Table 3.16 Elements present in 12 SS 1

Element	Cr	Fe	Cu	Mn	Ni	Mo	Si	C	P	Total
Wt%	19.81	70.64	0.05	0.41	5.31	2.46	1.29	0.02	0.01	100.0

Using the Spectrum for Stainless steel Grade 316 given by Azom as a basis for comparison, (Azom, 2017) it is obvious from the elements present in the Tables 3.17 that, the chemical formula of Stainless-steel grade 316 which is Cr 10-14%, Ni 2-3%, Mo < 2%, Mn <1%, Si < 0.045%, quite agrees with each other. Since component of Stainless steel is fundamentally Austenite and some chromium with nickel, there is high level of Iron present followed by carbon, chromium and nickel. Trace elements such as Mo, Si and Cu also exist. The 316 has got high tensile strength of 515 MPa and yield strength 205MPa.

3.10.2.3 EDXA of Mild Steel – 10 mm

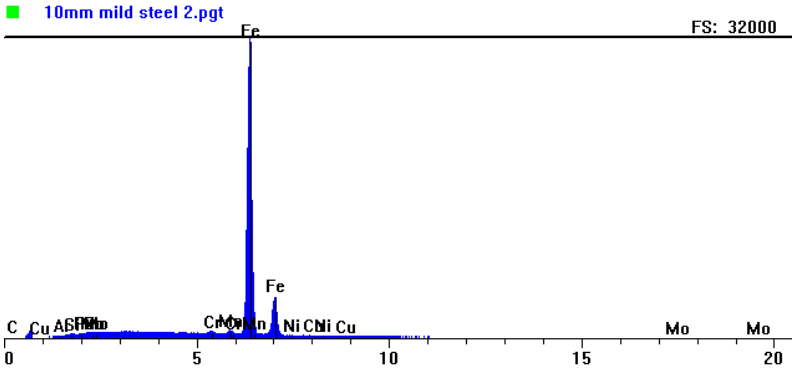

Figure 3.47 Spectrum of 10 mm Mild Steel

Table 3.17 Elements present in 10 MS 2

Element	Fe	Fe	S	Mn	Cr	Ni	Mo	C	P	Al
Wt%	32.76	66.34	0.06	0.31	0.18	0.00	0.23	0.02	0.02	0.1

3.10.3 Discussion

There are two Iron (Fe) readings on the spectrum in Figure 3.47 detected by the detector as recorded in Tables 3.18. It is possible to have more than one weight percentage of the same elements on same spectrum because it depends on the energy levels from which the elements are being excited. The presence of more than one weight percentage of elements is also dependent on the voltage and beam current used for the EDAX analysis. This because the energy of 20 kV might not be enough to excite an electron form the inner L or M shell except the outermost K shell.

Stainless steel is an alloy of chromium and nickel and contains a high quantity of Mo to enhance the strength of the material and reduce its susceptibility to corrosion. It contains 12.5% Ni, 18% Cr, and 1.8% Mn, 2.2% Mo and has a high percentage of Fe, 64.3. A comparison of the elements with Tables 3.14, 3.16 and 3.17, gives a very good match of the elemental composition and hence characteristics of the filler metal and the parents material SS and a good match is observed for the value of Fe when compared with Table 3.18 for MS (Matweb, 2017).

The composition of the filler metal alloys is influenced by corrosion resistance, weldability of the parent metal, the anodic coating standard and the minimum mechanical characteristics of the weld metal. Usually, the filler metals are matched to the base metal and the clad and are to be welded together respectively. In this experiment, the A15 Copper filler wire was matched with the mild steel, whereas the 304/316 filler wire was matched with the stainless steel for TIG and MIG Welds The filler materials for varying alloys can be obtained from BS EN 1011 Pt 4:2000. (TWI, Aluminium Alloys, 2016).

The chemical compositions of Cr4 are 0.02 P, 0.030 S, 0.40 Mn and the remaining percentage is Iron (Azom, 2017). When compared with the Table 3.18, it gives a good match. The yield strength of CR4 steel is 210 MPa and the Ultimate Tensile Strength is 350MPa (Azom, 2017).

Using the Spectrum for Stainless steel Grade 316 given by Azom as a basis for comparison, (Azom, 2017) it is obvious from the elements present in the Tables 3.14 that, the chemical formula of Stainless-steel grade 316 which is Cr 10-14%, Ni 2-3%, Mo < 2%, Mn <1%, Si < 0.045%, quite agrees with each other. Since the component of Stainless steel is fundamentally Austenite and some chromium with nickel, there is a high level of Iron present followed by carbon, chromium and nickel. Trace elements such as Mo, Si and Cu also exist. The 316 has got high tensile strength of 515 MPa and yield strength 205MPa (Azom, 2017). The measured

composition compares well with the data sheet of manufacturers and published composition of the material and literature (Lianyong et al, 2019, Ul-Hamid, 2005, Khorrami et al, 2014, Kumar & Mukherjee, 2017, Borba et al, 2016, Ren et al, 2016) and the accuracy is quite consistent.

3.11 Summary

The narrow gap welding of SS and MS using GMAW has been carried out and after the mechanical test and lab analysis had been carried out; it was observed that:

i. The trend of heat transmission via the dissimilar welded joint followed a particular trend of heat distribution, which can be explained by factors such as thermal conductivity of SS and MS, thickness of weld piece and distance away from the WA, WL, WE.

ii. High tensile strength was present at the welded joint and parent metal. The slip was observed in the stress-strain curve of the weld which was solely due to the high thermal gradient, anisotropy and the presence of martensitic transformations of the austenite present in the weld.

iii. The Charpy test revealed a fracture along the HAZ, showing the HAZ to be the weakest point of joint and quality of weld and filler metal used in the weld. This is an over matching scenario.

iv. The hardness test portrayed high hardness and subsequently a tensile strength in the HAZ compared to the parent metal.

v. The SEM revealed that there was a diffusion of elements from MS and SS, as well as the filler metals and the presence of molybdenum and manganese elements. The presence of iron from the filler metals increases the hardness of the welded joints.

vi. The EBSD brought out the different phases present in the welded joints – Austenite, Martensite and Ferrite. Of these phases, martensite was dominant.

vi. The EDAX analysis of the parent metals and filler metals further confirmed the sources of the elements required for good bonding in the welded joints and corrosion resistance.

Steels, especially austenitic have very good weldability properties. However, austenite is not stable at room temperature, hence certain alloys are required for its stability. Of these alloys, the most common is nickel, followed by carbon, nitrogen and manganese. With the addition of alloys such as chromium, nitrogen, titanium, molybdenum, columbium and nickel to stainless steel, the features of austenitic stainless steel could be enhanced, 70% as strength at high temperatures, corrosion resistance and oxidation resistance. At high temperatures, Carbon can enhance the strength of austenitic stainless steels but has the drawback of decreasing the corrosion resistance by producing a compound when reacting with chromium. Austenitic steels do not harden in the Heat affected zone primarily because they do not harden in by heat treatment. Ferritic stainless steels have some chromium present within the range of 12 to 27% and have a considerable number of alloys that produce austenite. Martensitic stainless steel has high ‘hardenability’ and when welding, they involve pre- and post-heating in the HAZ in order not to crack. The presence of filler metal in the weld zone did enhance the property of the weld as analysed in the SEM, EBSD and XRD. The choice of the filler metals: 304/316 and A15 Copper wire was appropriate for over matching characteristics and good bonding of the fusion zone as seen by the results of the Charpy test profiles and also the results of the Indentation tests. It reveals the quality of the weldment, weld and bond between the weldment which implies durability of the pipe in performance operations.

3.12 Conclusion

The study investigated the intrusion of the transition zone into the Heat affected zone and weld zone. It has been discovered that the hardness of the parent metal is less than that of the weld, which is about 30-70%. There is a high transition of elements such as Cr, Mo, Fe and carbides which increases hardness from the clad to the Heat Affected zone. A mapping of this has been carried out in Figures 3.44 and 3.45 and 3.37. There is also a transition of elements which enhances the strength of the weld joints and consequently the welded joints. The hardness of the HAZ interface was enhanced by the presence of the diffused elements. The HAZ consisted of higher concentrations of Ni, Mo and Cr, which makes it anti- corrosive, thus enhancing the attributes of the welded joints for longevity. There is also the transition of strength enhancing elements within the HAZ, as seen from the SEM results, which is further confirmed by the EDAX analysis.

Coarse austenite and an acicular martensitic/ bainitic structure – The cladding is comprised of banite, fine martensitic and austenitic dendrites structures. The HAZ is multifaceted in its structure by reason of rapid heating within a short time period and after which cooling at normal room temperature ensues for each consecutive weld pass interval. The HAZ commences from the clad / HAZ interface in the figure above. The temperature also increases with increasing depth.

The welding of 2 mm and 12 mm thick 316 stainless steel clad and 10mm carbon steel base metal have been carried out successfully WITH GMAW using A15 Copper and 304/316 filler wires. In the 2mm thick 316 stainless steel clad, the hardness value was observed to be greater than in the 12mm thick 316 stainless steel. By reason of the high quantity of the heat inputted into the weld system, the growth of the grain in the 12mm clad weld resulted in reduced impact strength values in the welded joint. In the 12mm thick 316 stainless steel clad, impact strength

was observed to be relatively stable and high compared with those in the 2mm thick 316 stainless steel. Although the 2mm weld recorded and overall distribution of high hardness, it also had very low values. By reason of the quantity of the heat inputted into the weld system, the growth of the grain in the 2mm clad weld resulted in reduced impact strength values in the welded joint. The high impact strength was seen in the 316 weld and consistently the hardness test at the Heat Affected zoned were high.

X-ray results of thermal weld experiments and mechanical testing, as well as lab analysis all show that there is a good behaviour and a match between welds of dissimilar material joints. The X-Ray diffraction patterns have been measured for 2mm MSSS weld sample and 12mm MSSS weld sample. In each case, at least 2 samples have been analysed. The X-Ray diffraction patterns analysis suggests that the HAZ area predominantly contains martensitic phase and austenitic phase. Measurement of the X-Ray diffraction patterns was measured in this research and it was found that the X-Ray Diffraction pattern of the weld HAZ matches those away from the HAZ, that is, the parent metal mild steel and stainless steel. The filler metals used at the bottom of the weld zone is A15 Copper wire filler metal and 304/316 filler wire.

NOTE: Publications based on the chapter content and published in international conferences and journals are found in Appendix 1 – first page only.

4. SIMULATION FOR THERMAL ANALYSIS

4.1 Introduction

This chapter describes the numerical procedure of acquiring the thermal analysis in a multiple pass butt-welded stainless steel and carbon steel clad pipe and plate. The geometry and the material properties of the models are defined, and results are analysed in thermal contours and graphs for two clad thicknesses in both plate and pipe models.

This research starts with thermal simulation on the same material, then covers the clad plates and pipes. This chapter also discusses the results of the finite element simulation of the transient thermal analysis in a 2D and 3D (clad plate and pipe) with respect to the experimental results. This is also compared with the results in pipes.

Chapter 4 has been written in a coherent manner with the relevant sections in chapter 4 starting with 2D and 3D domain. This is evidenced in sections 4.3. Geometry of Model followed by 4.4 Meshing and 4.8 Simulated models after which is 4.9 Results and Discussion which already follows this format.

Section 4.3 Geometry of Model commences with 4.3.1 the 2D models which encompass subsection 4.3.1 the 2D plate followed by the 3D models in subsection 4.3.2 comprising of the 3D plate in subsection 4.3.2.1, the pipe stripe in subsection 4.3.2.2 and finally the full pipe model in subsection 4.3.2.3.

Section 4.4. Meshing began with subsection 4.4.1 2D models which addressed the 2D plate model in subsection 4.4.1 followed by subsection 4.4.2 which addresses the 3D Models further split into subsection 4.4.2.1 the 3D plate and subsection 4.4.2.2 the pipe strip as well as subsection 4.4.2.3 the fully cladded pipe.

The simulated models have been discussed in section 4.8 with the 2D Model – Plate under subsection 4.8.1 followed by the 3D Model – Pipe Strip in subsection 4.8.2 and subsection 4.8.3 which is the 3D Model – Full Cladded pipe.

Section 4.9 Results and Discussion began with subsection 4.9.1 Temperature versus time plots – transient cycles in 2mm and 12mm plates followed by 4.9.2 which is the welding direction in both plates and pipes and subsection temperature distribution in 4.9.3.1 pipe strip, 4.9.3.2 Full pipe – 2mm and 4.9.3.3 full pipe 12mm

4.2 FEA Thermal Analysis

(NAFEMS, 2008) FEA thermal analysis is used to simulate the movement of heat via parts and assemblies by reason of environmental conditions and steam source, electrical generation or friction. In thermal analysis, temperature contours which determine the band of the weld region and HAZ are present.

Three basic heat transfer types exist namely conduction, convection and radiation. For heat transfer to take place, a temperature potential has to be set up whereby heat flows from a place of high temperature to another of low temperature. In this thermal analysis the types of heat flow considered are convection and radiation. In convection, the hotter fluids or liquids rise because it is less dense than the cooler fluid which sinks due to gravity – as the fluids interact together during welding. Radiation is carried out by electromagnetic radiation between the surfaces of a body and the surroundings. The Stefan-Boltzmann constant is given as $\sigma = 5.67x10^{8}W/m^{2}\text{-}K^{4.}$ The transient heat transfer requires specific heat C in kJ/kg-K and mass density in kg/m^{3} (Akin, 2009).

The method of equation solver for the stress analysis is the direct method using the solver default matrix storage (SIMULIA, 2017). The solution technique employed in this thermal

analysis is the Full Newton technique with a total of 8 iterations. The severe discontinuity iterations were propagated from the previous steps with the load variation with time ramped linearly overstep. The maximum number of increments is 10000 for each step of the analysis. An emissivity value of 0.1 per increment was used.

The factors considered for thermal analysis include penetration of the heat affected zone, thermal conductivity of each finite element mesh, and density of metal, solidus temperature and liquidus temperature as well as the latent heat capacity. The irregularity in temperature profile is also due to phase change. The temperature-dependent properties have been inputted into the inbuilt thermal profiles of the model (Yaghi et al., 2006; Deng & Murakawa, 2006; Nezamdost et al, 2016, Deng & Kiyoshima, 2010). Plots of temperature versus time and distance have been displayed in the results section.

During the welding process, the parent metal expands, compression occurs along the circumferential direction and this produces shearing and bending. This further leads to the initiation of hoop stress (in the circumferential direction) and meridian stress (in the axial direction). This further implies that the quantity of heat inputted into the model affects the geometry of the model. The design as well as the diameter of the pipe also affects the geometry. In this axisymmetric model, there are high tensile stresses in the hoop and axial directions of the inner diameter of the pipe that have resulted in the integral shrinkage of the pipe (Sinha et al, 2013).

When carrying out thermal analysis there are a list of steps and physical parameters needed, such as creating the geometry, assigning material properties, applying boundary conditions and thermal loads, meshing, creating job and analysing the results of simulation. FEA involves first modelling the geometry suitable for the challenge in question and thereafter selecting the material properties compatible for the nature of loading and boundary conditions involved – in

this case it is the convection and radiation. Meshing with the suitable element is carried out after which a job is created and submitted for analysis.

In this research, the finite element analysis of the stainless steel and the mild steel plate and pipe was carried out using ABAQUS CAE. There are two parts to the modelling. The first is the thermal modelling which involved designing and building the geometry of the model carried out under the part module. The next step is assigning material properties such as density, thermal expansivity, specific heat capacity, latent heat, solidus and liquidus temperature etc. under the Property module. The various parts created under the property were assembled under the assembly model such as the clad metal, base metal and weld metal. Heat and cool passes were created under the step module. The thermal output variables such as nodal temperature was also selected under the step module. Under the interaction module, the masses, as well as the surface film coefficient for convective and emissivity for radiative faces of each weld pass were added. Thermal loads in the form of body heat flux are applied in each heat pass and boundary conditions applied in the load module by restricting motion in y direction. Meshing is carried out under the mesh module and the job created for thermal simulation; at the end the results are analysed.

4.2.1 Consideration of Factors for Thermal Analysis

The factor considered while carrying out the modelling of the thermal analysis is the penetration of the HAZ of the weld metal into the parent metal. The thermal conductivity of each part of the Finite Element mesh equivalent to the weld passes is taken into account and prior to being positioned, the elements are assigned thermal conductivity of air, which changes to the steel value as soon as they are placed.

The density of the metal and the solidus and liquidus temperatures, as well as the specific heat capacity and latent heat capacity are also considered because, they are very vital and play a major role in determining the thermal analysis of the weld.

4.3 Geometry of Model

Considering the fact that the whole pipe (360 degrees) can be split up into smaller radii or lengths along the circumference; which if assembled together forms a complete pipe; the pipe strip can be generated as shown from the top view in Figure 4.1 below:

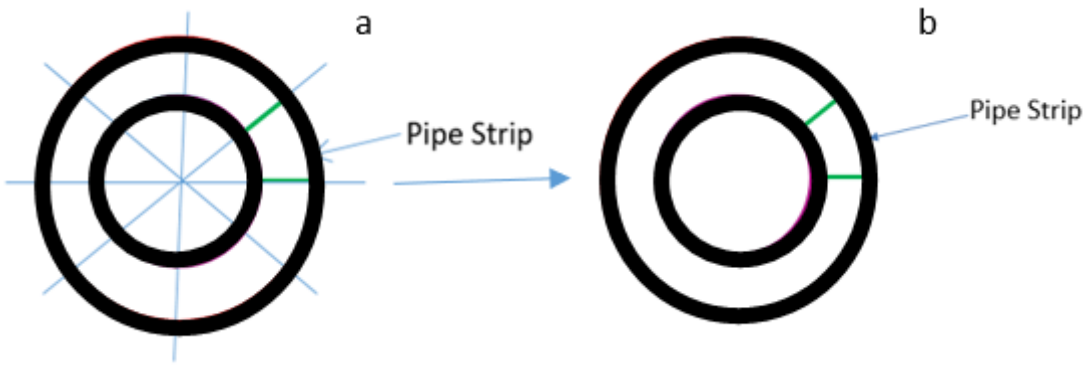

Figure 4.1 Cross-section of the top view of the circumference of a pipe split into (a) pipe strip sections. (b) pipe strip

One of these strips was closely studied and the simulation of the thermal analysis on that scale was examined and observed to confirm the same happenings as with a full pipe. Analysis and the temperature versus distance plots further confirmed this from the results under section 4.9. The full pipe model was developed after this pipe strip study/experiment was completed and the thermal analysis which was carried out on a smaller scale in the pipe strip model was carried out on full-scale with the complete pipe model. The result of the transient analysis and

temperature versus time curve from the full pipe model confirms with the finding of the thermal distribution in the pipe stripe.

The 2D Plate Model was developed to simulate the thermal analysis of a plate and to see if it conforms to that of a pipe model. This was confirmed by the outcome of the transient thermal analysis and temperature versus distance curves under section 4.9. Irrespective of the fact that it is a plate model, the results and outcomes of the plate model is in concurrence with that of the pipe. The 2D plate model was first designed and after that the 3D model was built. It was found that the thermal responses both transient and distant were confirmed true for both pipes and plates in section 4.9.

Fundamentally, pipes were welded from sheets which could be viewed as plates of infinite length and breadth as illustrated in Figure 4.2. This is in addition to the fact that the weld experiments were carried out on Clad plates.

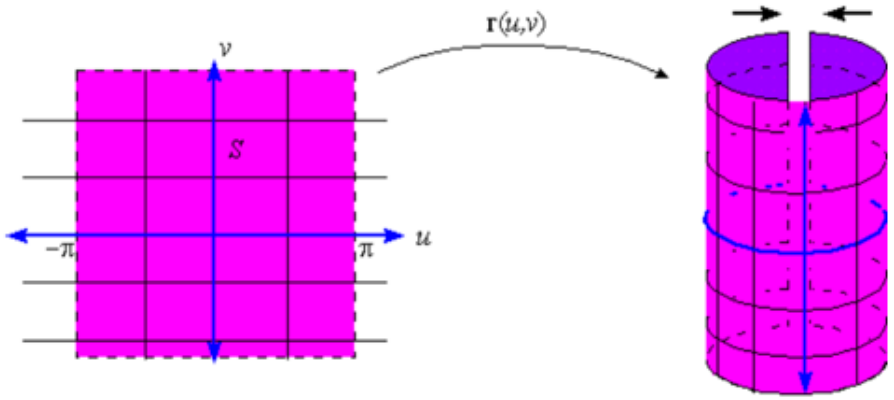

Figure 4.2 Illustrating the conversion of a Plate or Sheet into a Cylinder (Bhatia, 2014)

A cylinder and a plane as shown in Figure 4.2 are said to be isometric, meaning one can be converted into the other without altering the local distances. A plane cannot be transformed into a sphere because its dimensions of length would have to be altered in order to perfectly deform into a sphere. This means that the surface of a sphere is not Gaussian flat with respect to the plane. A Gaussian flat surface as shown on the plate in Figure 4.2 has a Gaussian curvature (as shown in the cylinder in Figure 4.2) at each point of the magnitude of zero (0).

Going by this principle, the surface of a cylinder (as shown in Figure 4.2) can be said to be a Gaussian flat plane since it can be revolved from a flat sheet or plate.

Furthermore, it implies that without stretching the plane, folding or tearing it, r (u,v) is an orthogonal parameterization of a surface (ETSU, 2014). Clad models of both plates and pipes were further developed to also confirm the above findings (scaling the dimensions) and the comparison of the experimental results and the simulated results gave a good agreement, hence verifying the results of the FEA simulation carried out.

4.3.1 2D Models

4.3.1.1 The 2D Plate

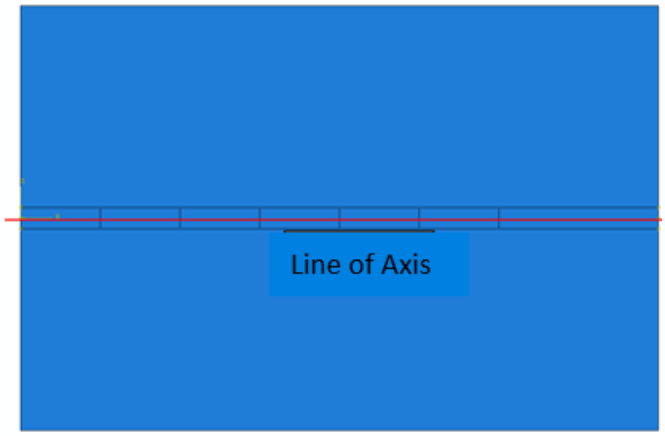

Figure 4.3 Geometry and weld line of a 2D Plate Model

Figure 4.3 above is a typical model of a 2D Plate showing the weld path across the length of a plate 30mm by 20mm and with a 1mm thick weld path**.**

4.3.2 3D Models

4.3.2.1 The 3D Plate

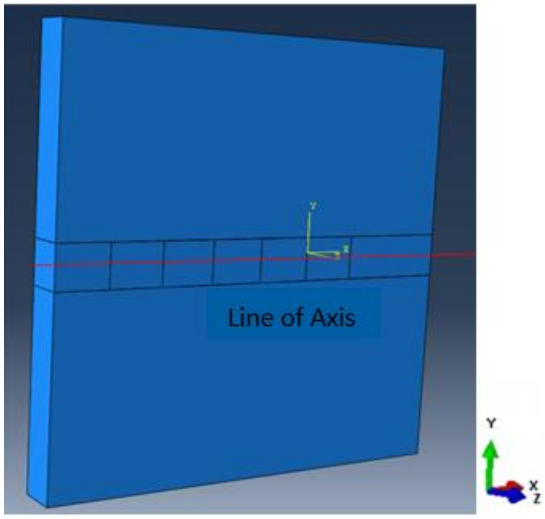

Figure 4.4 Geometry and weld line of a 3D Plate Model

Figure 4.4 is a typical model of a 3D Plate showing the weld path across the length of a plate 30mm by 20mm and with a 5 mm thick weld path**.**

4.3.2.2 The Pipe Stripe

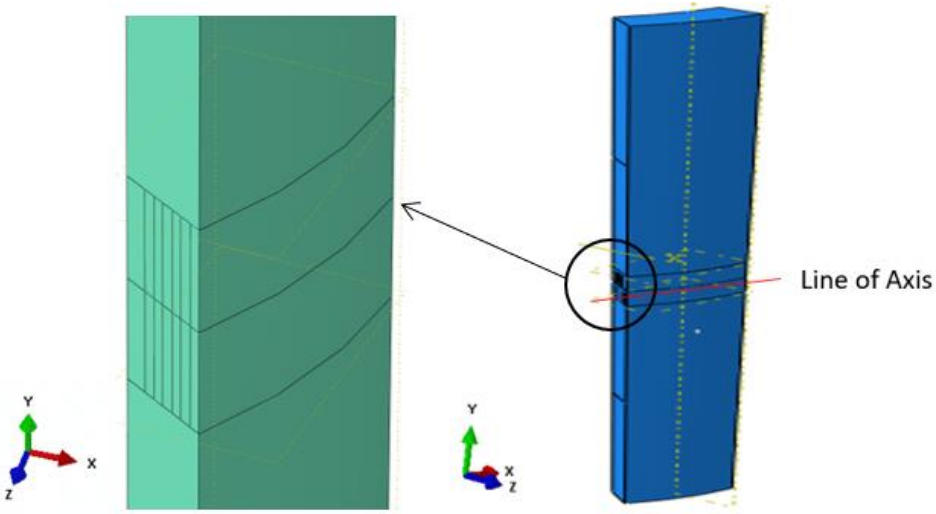

Figure 4.5 Geometry and weld line of a pipe strip. Dimensions of the pipe strip are OD 12.94, ID 10.35, thickness 5mm and height 160mm.

Figures 4.5 reveals the geometry and dimensions for the 3D pipe stripe and the weld passes in a magnified view

4.3.2.3 The Full Pipe Model

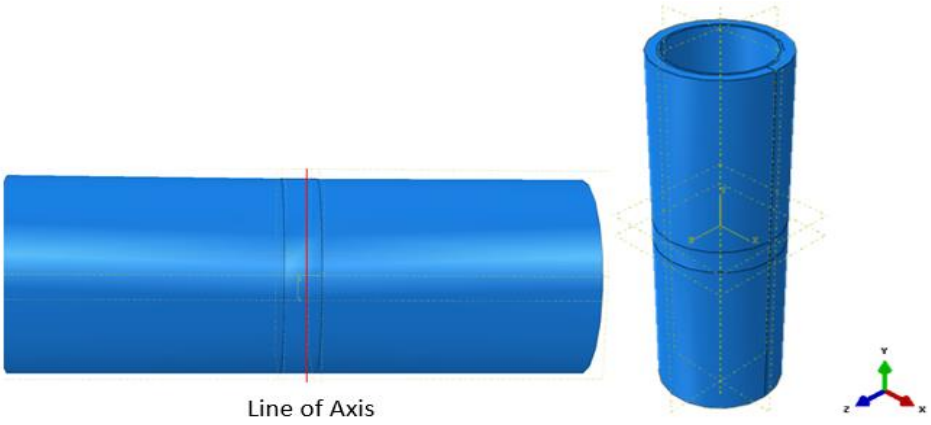

Figure 4.6 Geometry and (a) weld line of Full Pipe Model and (b) cladded section of pipe

Figures 4.6 (a) and (b) are the full pipe geometry showing the weld path across the pipe and the cladded section of pipe respectively. They each have dimensions of 160mm length, 10mm thickness for carbon steel and 2mm thickness clad, as well as 12mm thickness clad respectively.

4.4 Meshing

The Abaqus CAE has built in it, different terminologies such as library, family, geometric order and functions such as assign element types, which can be used to create and categorize meshes for different geometries. Looking at the physics of flow which indicates direction; it calls for developing meshes to track the direction of flows within an object or medium. This mesh could

be either 2D or 3D depending on the need or nature of the geometry required to meet the challenge.

4.4.1 2D Models

4.4.1.1 The 2D Plate

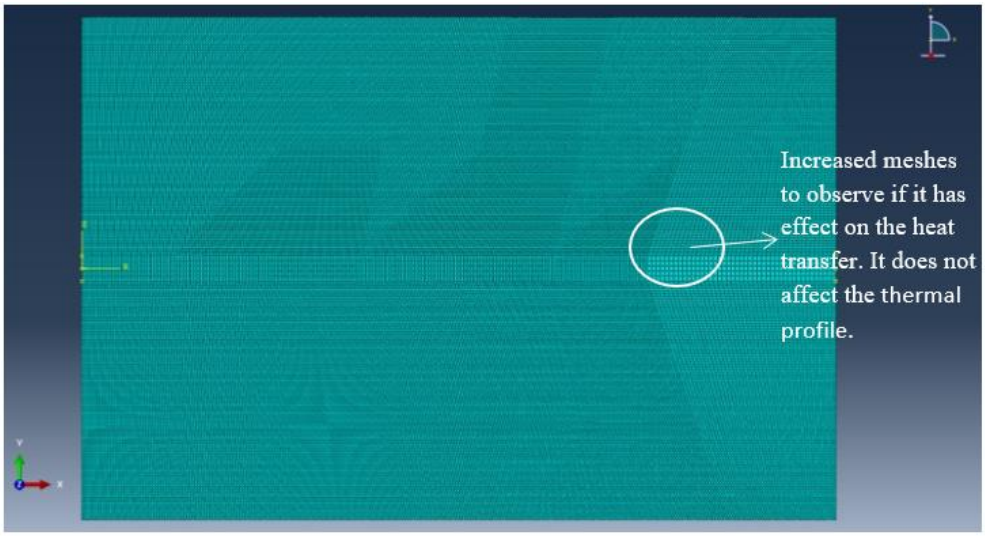

Figure 4.7 A 2D Plate showing linear quadrilateral elements of type DC2D4

A 4-node linear heat transfer quadrilateral DC2D4 was used for meshing the 2D plate in Figure 4.7 generating a total of 59,192 nodes and 58,695 elements. It can be observed that the meshes are very refined/fine towards the centre of the weld and finer on the left compared to the ones on the right; this is to examine the effect of the large meshes on the right-hand side of the plate, on the thermal simulation.

4.4.2 3D Models

4.4.2.1 The 3D Plate

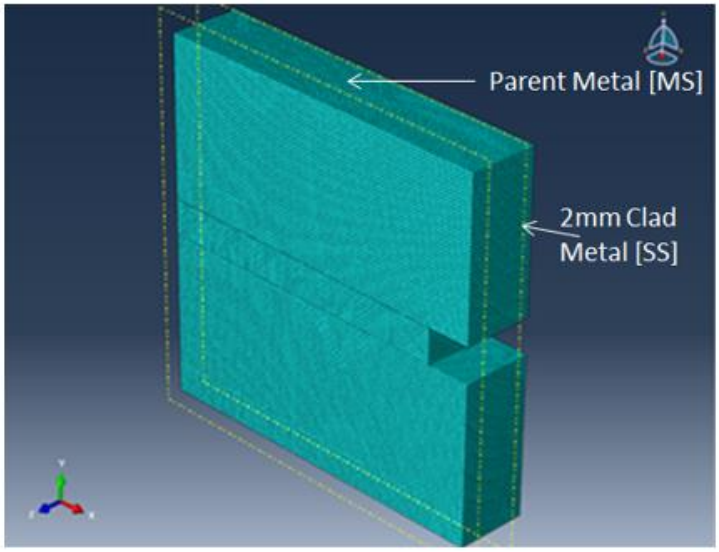

Figure 4.8 A fully clad plate showing linear brick elements of type DC3D8

A total of 217770 nodes are present in this fully cladded plate model, in Figure 4.8 with a total of 198200 linear brick elements of type DC3D8; an 8-node linear transfer brick. Family is thermal and the element library is standard.

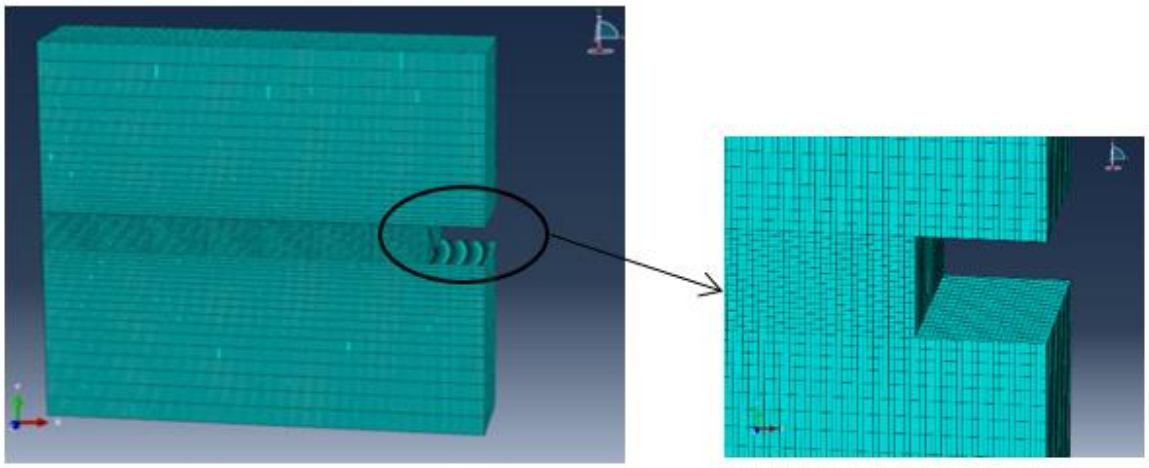

Figure 4.9 3D Plate showing an 8-Node linear heat transfer brick DC3D8

For the 3D plate shown in Figure 4.9, linear brick elements of type DC3D8 were used in meshing the plate. Linear brick elements of type DC3D8 (8 node linear heat transfer brick) were used consisting of a total of 69300 nodes and 58200 elements.

4.4.2.2 The Pipe Strip

In recent times most 3D CAD geometries are modelled using the quadratic tetrahedral elements. Hex grids are employed for both numerical and computational efficiency. Numerical in the sense that they permit defined regular spacing in the direction of flow normal to the wall without skewness (Stone et al., 2015). Mesh sensitivities were carried out and the numbers of elements were plotted against the temperature.

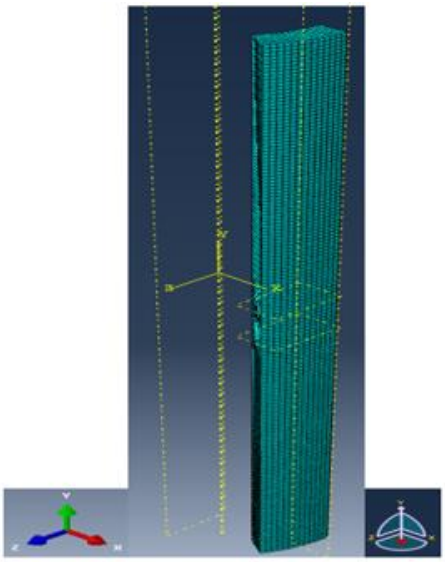

Figure 4.10 Pipe Strip showing an 8-Node linear heat transfer brick DC3D8

The family of the mesh for the thermal models in the pipe strip in Figure 4.10 is heat transfer, element library is standard, and the geometric order is linear. The 8-node linear heat transfer brick contains 18, 256 nodes and 14,742 linear brick elements of type DC3D8. Local seeds are assigned by size and where applicable, constraints are employed to either allow the number of

elements to increase or decrease. A single constraint is also applied to create a focussed profile for the mesh. This is in order to eliminate errors from the mesh profiles. Global seeds are applied in the range of 0.5 and the curvature control for both global and local seeds are 0.1. Mesh controls were also applied to the different geometries. The plate conventionally is brick whereas the technique for carrying out the meshing is structured compared with Free, Sweep or bottom up.

4.4.2.3 The Fully Cladded Pipe

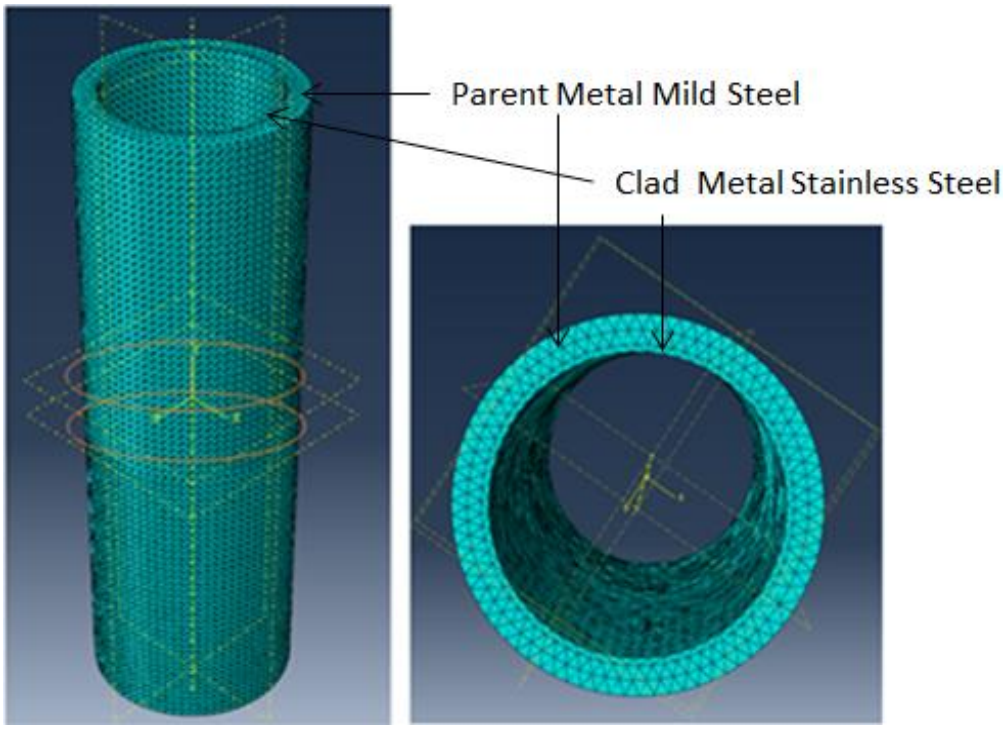

Figure 4.11 A fully clad pipe showing linear brick elements of type DC3D8

For the fully clad pipe in Figure 4.11, the total number of nodes is 208640 and the total number of elements is 180306. Abaqus use quad options and with quad, the geometry does not need to be regular or regular brick elements.

An 8-node linear heat transfer brick is generated using the brick element. The section of the meshed pipe in Figure 4.11 which corresponds to the weld is depicted by orange circles. The linear brick elements could be recommended for reduced time of computation and ease of running analysis by reason of the structured grids which make up the mesh. All elements are identical and can be easily known or predicted indirectly based on this structured array. In the long run, this implies reduced cost of running analysis for the company. Brick elements guarantee absence or minimal skewness by reason of the uniform or regular grid shape which implies reliable results; however, the hex mesh can also be unstructured depending on the way in which element indexing is executed (Stone et al., 2015).

Tetrahedral elements have greater stability at high temperatures compared to brick. With few meshing procedures, a good mesh is produced; even in complicated geometries where absolute mesh control is not feasible. The mesh attributes such as skewness, min and max angles 2x2 and 3x3 determinant, orthogonality, volume ratio and quality are resolved uniquely by each CAE software. Although it takes a longer time to run due to its lower time step, it guarantees good and reliable results (Bourdin et al., 2017). For the 3D pipe, the element for meshing is C3D10 quadratic heat transfer tetrahedron. Tet was chosen because of its very good mesh technique and can always be used in most geometry including multifaceted geometries due to their nature of grid flexibility. This makes it faster to mesh. Most FEA CAE software analyses Tet mesh with greater accuracy. It is also good for carrying out mesh convergence or refinement. In summary, the use of tetrahedral elements has high prospects (Stone et al., 2015). For the fully clad pipe, the total number of nodes is 233600, elements 157519 and the element type for cylindrical is DC3D10 – A 10 node quadratic heat transfer tetrahedron with the total number of nodes being 185029 and the total number of elements being 120926. Elements of type DC3D10 is a 10-node quadratic tetrahedron. The element type used in this mesh is Tet. The family is thermal, and the element library is standard. It has a quadratic geometric order.

4.5 Material Properties

Thermo physical properties include thermal conductivity, specific heat and density. The latent heat and expansion are also accounted for in the material properties. The material properties of the stainless-steel material for both thermal and stress analysis are plotted in a single graph according to Brickstad and Josefson shown in Figure 4.12 below (Brickstad and Josefson, 1998). The units of the parameters of thermal and stress material properties of stainless steel are shown whereas those of the finite element analysis are presented in the brackets (Yaghi et al, 2006).

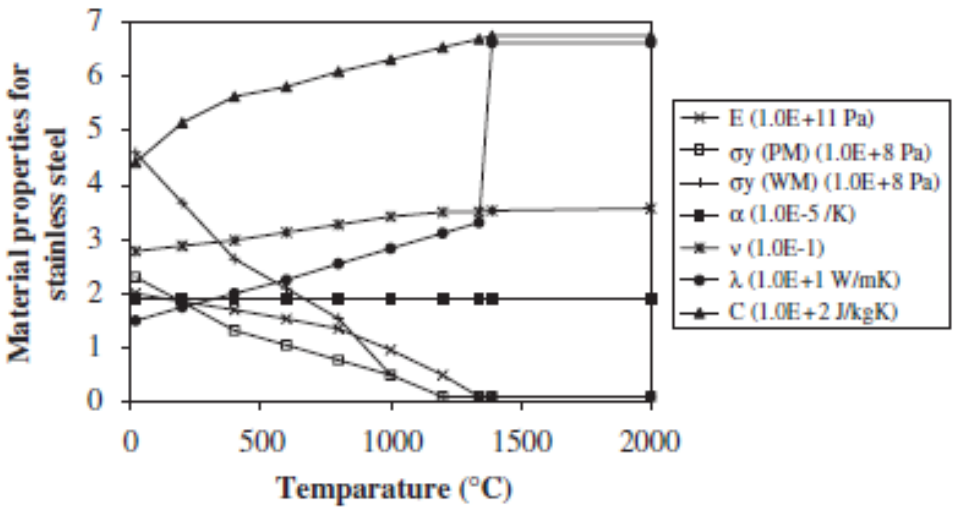

Figure 4.12 Brickstad and Josefson curve for temperature dependence material properties versus temperature (Yaghi et al., 2006).

From the above curve, the Youngs modulus E in Pa decreases with increasing temperature, whereas the thermal conductivity λ in W/mK increases with increases in temperature. The figure also shows that the heat capacity C in J/kgK also increases in temperature until it gets to the peak at a teperature of 1400^{o}C when the stainless steel melts; after which it remains constant. The phase disolution temperatures σy for the parent metal as well as the weld metal

decreases with respect to the increasing temperature. The thermal coefficient of expansion α in /K is constant. In the thermal analysis as well as stress analysis of the finite element modelling, kinematic hardening was applied. The material density is 7850kg/m^3 for carbon steel whereas stainless steel is 7970kg/m^3. The liquidus temperature employed here is 1400^{o}C for the stainless steel and the mild steel. The solidus temperature is 1375 ^{o}C. The latent heat capacity of 260kJ/kg was utilized.

The respective material properties sourced from literature, CES (Cambridge Engineering Selector) Edu Pack 2013 are outlined in Tables 4.1 – 4.3.

Tables 4.1 – 4.3 Material properties

Table 4.1 Specific Heat Capacity of X65 Carbon steel and Grade 316 stainless steel

Specific Heat [$Jkg^{-1}K^{-1}$]	Temp [^{o}C]
360.674	0
409.888	198
492.397	443
575.29	618
617.015	657
675.387	718
817.509	802
1001.83	840
1135.94	855
456.321	894
495.521	1384
570.027	1560

Table 4.2 Mass Density of Carbon Steel, Coefficient of Expansion) Latent Heat, Solidus and Liquidus Temperature of X5 and Grade 316 Stainless Steel

Properties	X65	316
Mass Density [kg/m3]	7970	7850
Expansion Coefficient [1/K]	1.30E-05	1.70E-05
Latent Heat [KJ/kg]	300000	260000
Solidus Temp [°C]	1375	1400
Liquidus Temp [°C]	1375	1400

Table 4.3 Thermal Conductivity of X65 and Grade 316 Stainless Steel

Conductivity [W/mK]		Temperature
X65	316	[°C]
36	24	0
37	23	62
38	22	208
39	19	323
40	18	508
31	17	746
28	16	861
33	15	1417
35	14	1493
39	13	1500
39	12	1523

The Abaqus FEA software has considered the thermal conductivity of the weld metal and HAZ, which are different from that of the two parent materials being welded, so that it is reflected in the thermal distribution of the FEA results. In the geometry, steps, boundary conditions and during the simulation the welded zone is clearly defined and distinct from the parent's material. After imputing the material property of the parent metal, it is intrinsically inculcated into the welded joint and zone by the Abaqus software, such that the welded joint is treated as a

combination of both parent material. The addition of filler material was modelled by de-activating and re-activating the elements that represented each pass. All passes were defined with the corresponding weld metals which were present in the model at outset, and all the elements in the weld region was deactivated before initiating the first heating step. The deposition of the weld metal was achieved by activating the elements defined for each pass, which were isolated from the previous passes.

4.6 FEA Applying Thermal Loads and BC

Within and around the FZ there are high temperatures and flux gradients, likewise the HAZ. The heat perpetuates through a distance of 10 mm on both sides of the weld line. For the butt-welding of two pipes or plates with a single V groove, the full 3D model was carried out using Abaqus CAE, boundary conditions were applied to enable the heat flow and pattern in a desired manner as to enhance the weld performance of the metals concerned. Although for the experiment, the stainless steel is only attached to the mild steel at the weld line; the stainless steel is permanently bonded or attached to the mild steel at the contact surface in the FEA model. This is because the simulation is based on perfect bonding of the two materials at the contact surface. Frictionless contact was assumed for the bonding between both surfaces in Finite Element. It should be noted here that for the lab experiment, the surfaces of both metals (stainless steel and mild steel) were grinded at the start of the experiment to ensure good contact – physically and thermally. Surface finishing of the metal surfaces using universal machines was carried out prior to spot welding the surfaces of the plates together including boundaries. Finally, G Clamps were used to hold them in place and hold them firmly within the set up; prior to welding both surfaces together.

4.6.1 Thermal Loads

The nature of the loads applied in the thermal analysis is thermal, specifically body heat flux via the heat transfer medium. The differences in average temperature are the main thermal loading parameters. Table 4.4 contains the welding process parameters.

Table 4.4 The Welding process parameters are as follows

Parameter	Minimum Value	Maximum Value
Welding Voltage [V]	230	240
Welding Current [A]	5	45
Welding Process Efficiency [%]	0.6	0.8
Welding Speed [mm/s]	0.04	0.04

4.6.1.1 Activation Processes – Birth and Rebirth of elements

In order to simulate added mass into the FE model this technical birth activate the process for the group of elements representing the added volume mass (Buhl et al, 2019, Fanous et al, 2003, Chiumenti et al, 2010). A widely technique used in simulating added mass in FE is the birth or activation process. The justification is that filler metal is added to the system, that is why the birth and activation process used by Abaqus is employed in this research. The whole purpose is to provide the capacity to add additional mass and heat into the system. All these functions are provided by Abaqus – it is an existing method ready for used and used widely by other people and it is a tested and trusted method. The activation process covers firstly, the added mass and secondly, the input of heat. Although they can be done separately but it can be done through added mass.

Activation Process of elements

Elements are added through the interaction module using the model change option during the construction of the geometry initially and then removed (deactivated) so that they become added when running the analysis at a much later stage. Steps are used to remove and include elements so that the temperature does it change considerably when running the analysis for steps that are specifically for adding and removing material.

Steps in the Structural Model

A new model – structural analysis is created from the thermal analysis using the same database, material, sections, parts, instances etc with the elements transformed into structural elements and no changes made to the mesh.

To avoid distortion of elements which can occur if the bead material is removed and also displacement of the material by removal of the bead material at the beginning of the analysis and replaced as needed during the analysis materials are at high temperatures so that the stiffness is low and the thus it will not significantly impact the analysis.

Birth and death of element

In the heat transfer model, there is material activation which takes place and also the heating and cooling from the evolving surfaces as well as the original exterior surfaces. Elements get activated at a given temperature which is the initial temperature defined which is the ambient or room temperature for the whole assembly – base material and weld material with base material being at the room temperature and weld material at the weld temperature.

Stress analysis entails uploading temperature histories and weld material will be optimized at the ultimate temperature while the base metal will be at the ambient temperature

Heating and cooling,

Heating, elements are activated at constant melt temperature which is used to create constant moving heating temperatures; whereas cooling is carried out on only active elements on free surfaces and handled internally by using Film and Radiate.

For the stress analysis,

Element activation is used to maintain the stress continuity and is identical to heat transfer whereas the temperature loading is imported from Heat Transfer loading and cut-off temperature. It also entails the temperature dependent behaviour which entails the phase transformation and phase dependent behaviour change.

4.6.2 Boundary Conditions

During simulation of a multi-pass welding thermal cycle, there are heat losses from the surface via convection and radiation. Differences in the quantity of heat inputted in each pass is accounted for and this corresponds to the total of the time taken to weld as well as the waiting time before the start of each subsequent pass. (Pathak et al, 2012) Accounting for heat loss to the surrounding implies heat loss from the surface of the metals (parent metal, weld metal and clad), via convection and radiation. Heat transfer coefficient accounts for heat loss by convection and radiation. There are two main boundary conditions considered in this analysis namely convective cooling and radiation. Frictionless contact exists for the bonding between both surfaces in Finite Element. For thermal model, all these temperatures have been applied as boundary conditions B.C. – Initial temperature, Outside temperature and Room temperature. Although the temperature dependent properties started from zero (0 ^{o}C), the outside

temperature and ambient temperature were taken to be room temperatures of the value of 20 ^{o}C.

In the analysis and simulation required for this research Abaqus is enough for the underlying physics and modelling of the problem because the weld passes have been defined using boundary conditions. (Refer to Paragraph under section 4.5 Material property).

4.6.2.1 Reflective Surfaces

The sink temperature is 20^{o}C. Heat sink simply refers to the temperature of the surrounding surfaces that helps absorb the heat away from the welded spot, hence helping in cooling down the welded spot. For the first pass, the type of surface used is film conditioning for the convection process and likewise the remaining passes. The film coefficient of 1.2E -005 was used. The sink definition is uniform. For the radiation process, the type of surface used is surface radiation for the different heat passes. The radiation type is ambient, and the emissivity distribution is uniform given to be 0.1. Ambient temperature is 20 ^{o}C.

4.6.2.2 Convection

Low order radiation boundary conditions were employed in defining convective waves (Hastrom et al., 2012). Convection is the prevailing procedure for transmission of heat from the weld sample to the immediate environs. The range of values used for this research varies from 15 to 20 Watt/m^{2} ^{o}C. Comparing the calculated thermal cycle with the experimental cycle, there, is a proper match and correlation as shown in Figures 4.24 - 4.25. Generally, natural convection was employed in this transmission of heat from the weld to the immediate environ, with the specific value of 15 used in this particular research plot (Youtsos, 2006).

4.6.2.3 Radiation

The Radiation boundary condition was designated to the open and exposed end of the weld passes, because it is the end of the weld that is exposed to the immediate environ. The temperature of the immediate environ is set to room temperature, however, it is known that the temperature difference and hence radiation between the weld passes and the immediate environ (example welder), would be greater than room temperature.

It should be noted here that the layers of the passes, the combination of the material, the weld zone which contains both stainless and mild steels have been defined in the Abaqus software.

4.7 Mesh Convergence

In order to effectively construct and build the successful thermal model of the weld, mesh sensitivities otherwise known as mesh convergence were carried out for the different models of weld. For the 2D Plate Model the following mesh convergence was obtained in Figure 4.13.

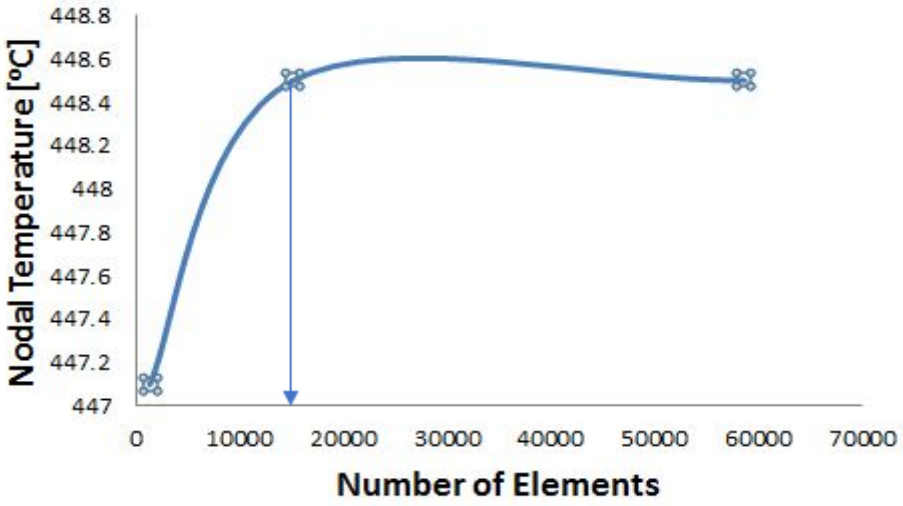

Figure 4.13 Mesh Convergence for 2D Plate

It was discovered that the first 2 rows and the very last row were more than sufficient for the convergence because of the discrepancies in the number of elements involved in the mesh convergence criteria of element size for selection. It is observed that the convergence for a nodal temperature of 448.5 first occurred at 15,150 elements. This implies that any model of the 2D Plate having a minimum of 15, 150 elements in its structural make up is suitable by the convergence standard and criteria to undertake the Convergences using a thermal analysis of the welds in plate.

4.8 Simulated Models

The thermal simulation for the different models 2D and 3D plate, pipe strip and full pipe have been discussed below under various subheadings. The weld lines have been indicated in the geometry of the model in the previous section – 4.3 'geometry', of this chapter (see Figures 4.3 to 4.6). The different colour bands for the FE results of the temperature field just show the temperature distribution, which may (as described in section 4.3) or may not correspond to the weld zone. The red-orange colouration represents the Fusion Zone, after which the yellow-green thermal contours represent the Heat Affected Zones. It should be noted here that the HAZ varies in different material welds, hence a variation in the minimum boundary. It could also extend well beyond that of a typical weld, especially due to the different weld thickness of the clad. The range of temperatures experienced by the weld zone and the Heat Affected Zones vary, as shown in Figures 4.14 through 4.23.

4.8.1 2D Model – Plate

4.8.1.1 Different Weld Steps (from left to right) at the same Time Step

Figure 4.14 below shows the thermal simulation for heat pass 1 through heat pass 7 in a full 2D Plate with different temperature contours which are seen as colour variations representing each thermal distribution shown in the temperature panel at the top left side of Figure 4.14.

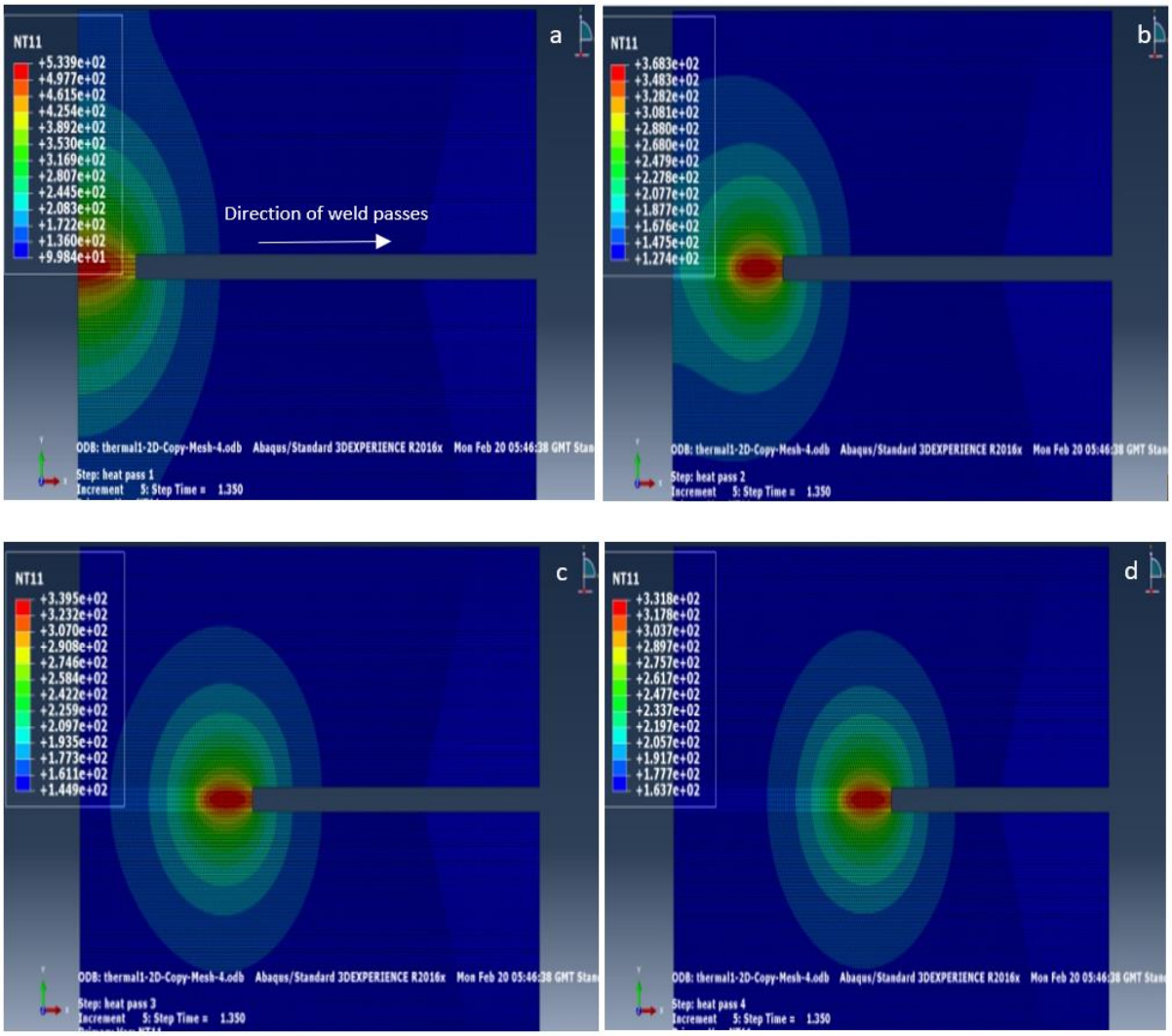

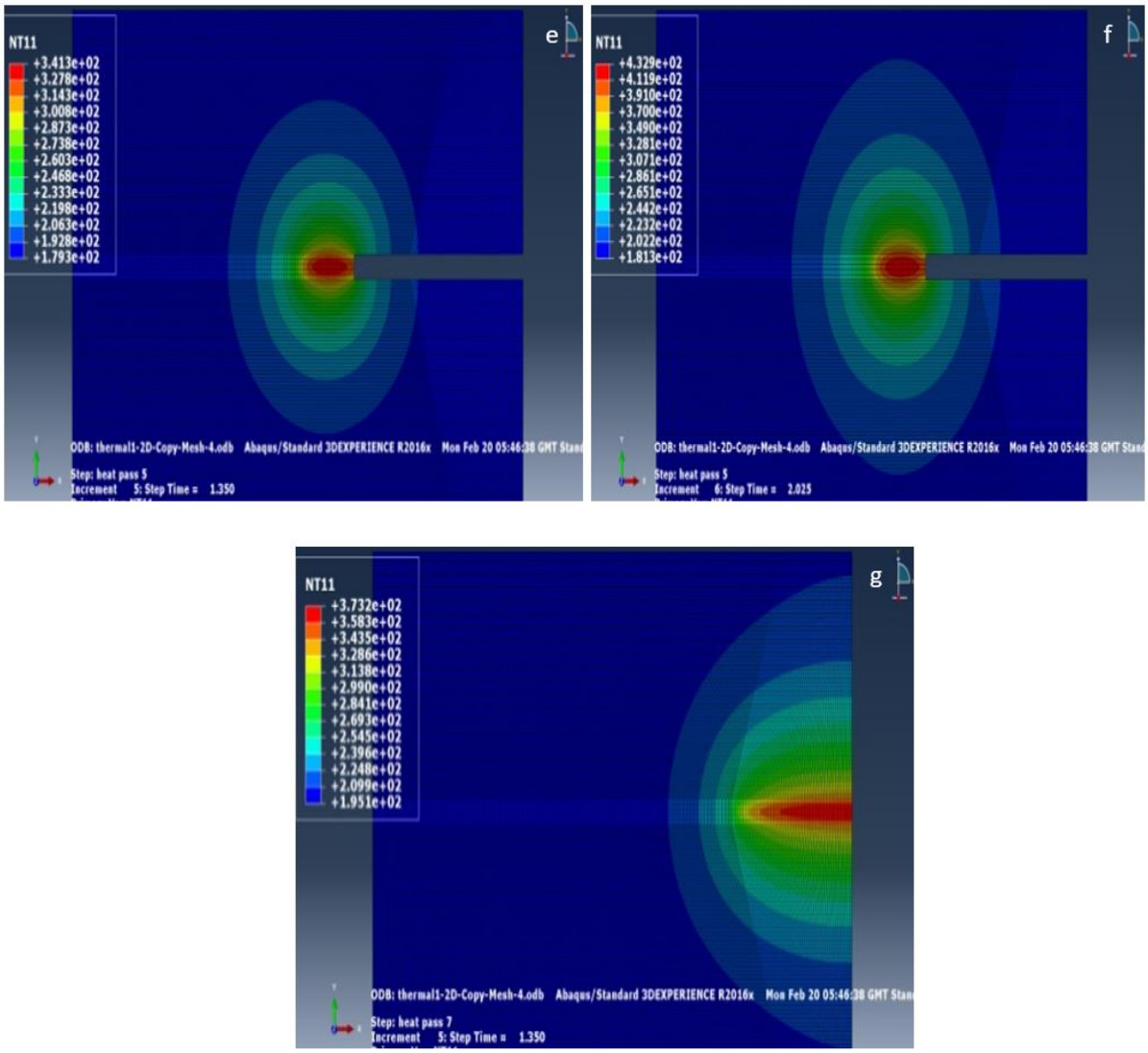

Figure 4.14 (a) heat pass 1 at time step 1.350 secs, (b) heat pass 2 at time step 1.350 secs, (c) heat pass 3 at time step 1.350 secs, (d) heat pass 4 at time step 1.350 secs, (e) heat pass 5 at time step 1.350 secs, (f) heat pass 6 at time step 1.350 secs and (g) heat pass 7 at time step 1.350 secs. Temperature profiles of a weld spot through the weld pass length.

It suffices to model a weld in 2D model using the finite element analysis (FEA) as shown in Figure 4.14 (a-g) to understand the thermal profile during the process of welding. This also has the advantage of convenience and increased speed of simulation and is referred to as Axisymmetric in an axisymmetric model. The procedure for welding entails the melting (dissolving) of the material after which it cools down for a certain period in order to solidify, thereby forming beads in the weld zone. This is the interface between the upper and lower fragments of the steel plates as shown in Figures 4.14 (a and g).

4.8.1.2 Multiple Passes Time seps in a Pass (Cooling)

The temperature contours obtained in the thermal analysis are the first set of results to be generated in the welding of finite element simulation. They depict the sections which are affected by heat as well as the sections in which melting occurs. In the following Figures 4.15 through 4.19 various temperature contours are displayed and correspond to the temperature contours for a finite element model of a 2D Plate. Different time steps for Pass 1 and Pass 3 are shown as examples. For each pass, the peak temperature is noticed halfway through the modelling.

Figure 4.15 (a) is the end of the heat pass 1 or the start of the weld cooling process for pass 1 at time zero seconds. This is immediately after the weld. Figure 4.15 (b) shows the progress of the weld heat being dissipated after 30 seconds of cooling as the heat propagation in the plate by conduction takes place. Note that there is no heat source which is removed at the beginning of the cool pass.

The cool pass is needed to represent the time period for the welding machine to return to the beginning position after completing one complete pass. The highest temperature drops over time, and at the end of the cooling time of 2 minutes, the hottest spot on the plate is not the weld spot. Graphs showing the temperature drop over time are given in the section 4.9. – Results and Discussion. This phenomenon of the heating up at the welding spot and temperature propagation is also repeated in Figures 4.18 and 4.19 for pass 3. Figure 4.18 (a) is a typical weld heat pass referring to actual welding being carried out at pass three after a time interval of 2.380 seconds into welding.

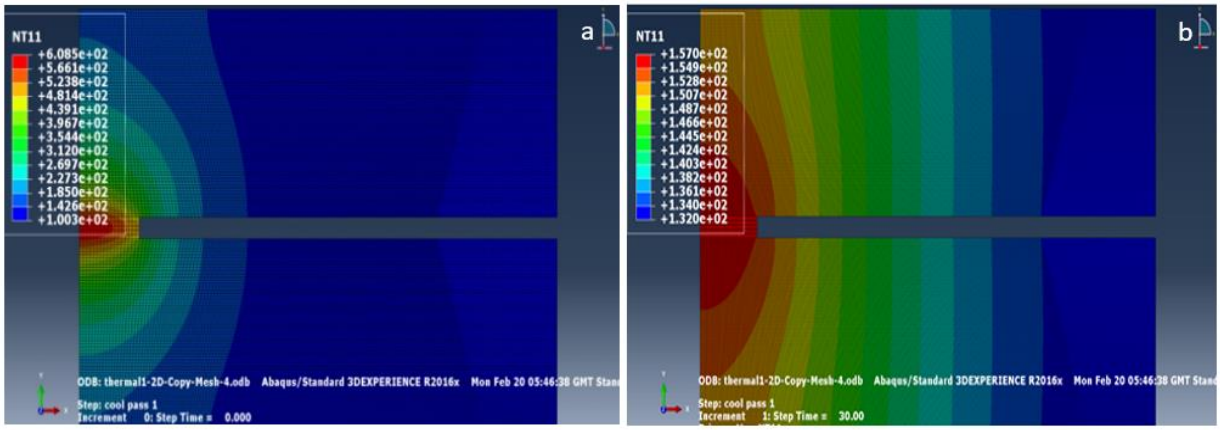

Figure 4.15 a) Step: Cool Pass 1, Increment 0, Time = 0 and b) Step: Cool Pass 1, Increment 1, Step Time = 30.00

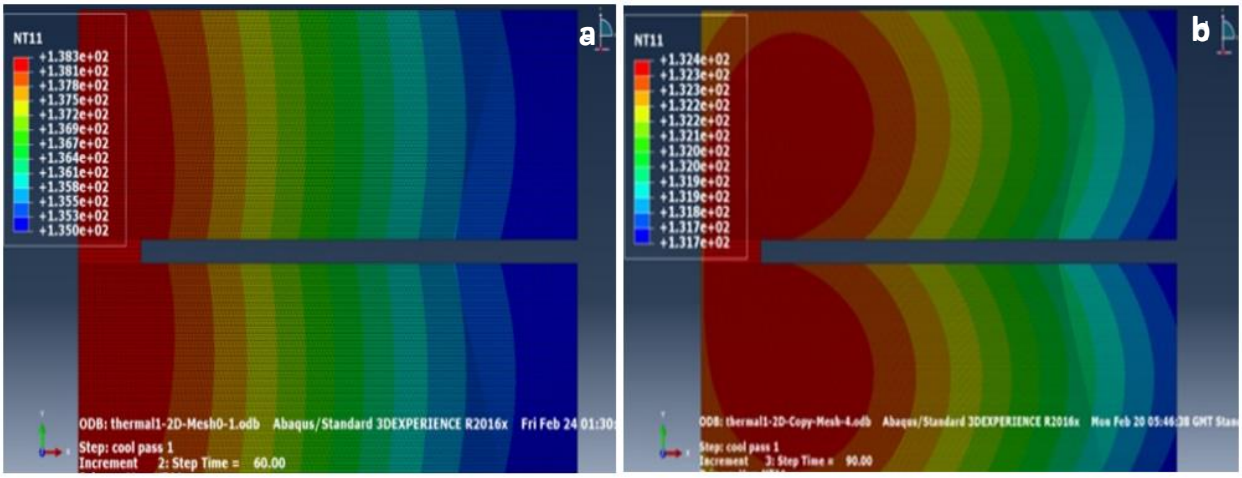

Figure 4.16 a) Step: Cool Pass 1, Increment 2, Step Time = 60.000 and b) Step: Cool Pass 1, Increment 3, Step Time = 90.000

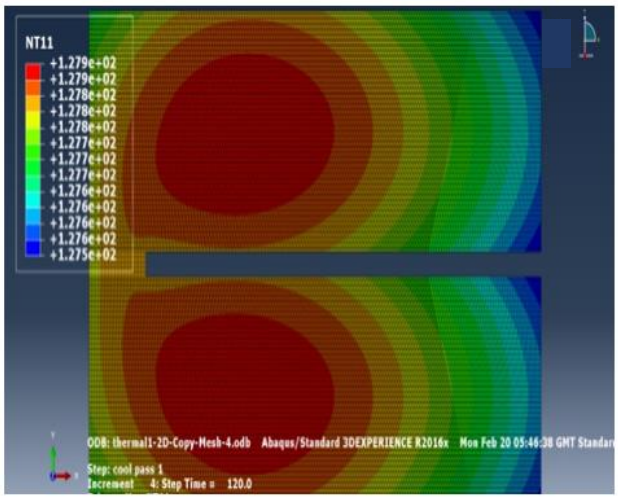

Figure 4.17 Step: Cool Pass 1, Increment 4, Step Time = 120.000 (2 minutes).

Figures 4.15 through 4.17 showing temperature profiles at different time steps, cool pass 1 during the welding process

An almost uniform temperature distribution which shows the cooling down stage.

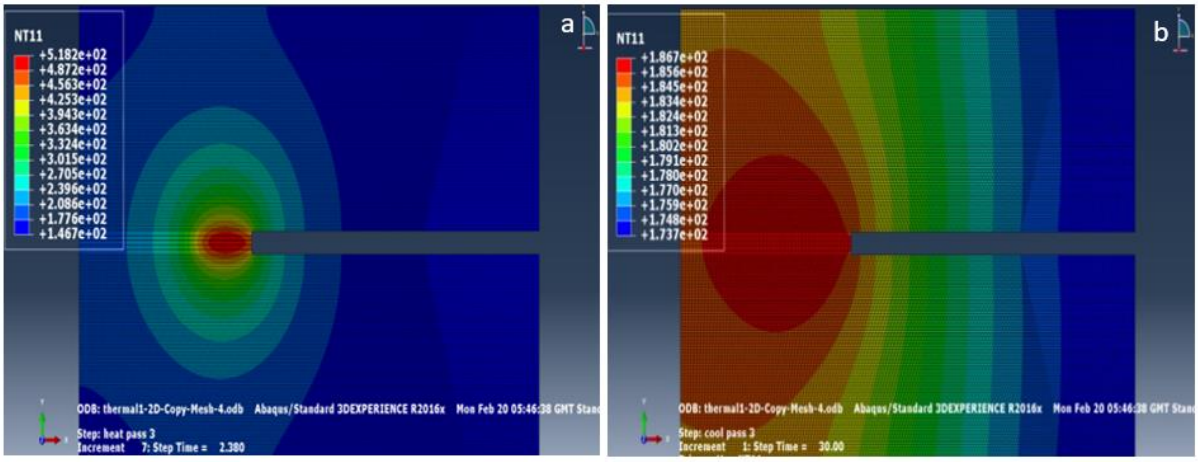

Figure 4.18 a) Step: Heat Pass 3, Increment 7, Step Time = 2.380 and b) Step: Cool Pass 3, Increment 1, Step Time = 30

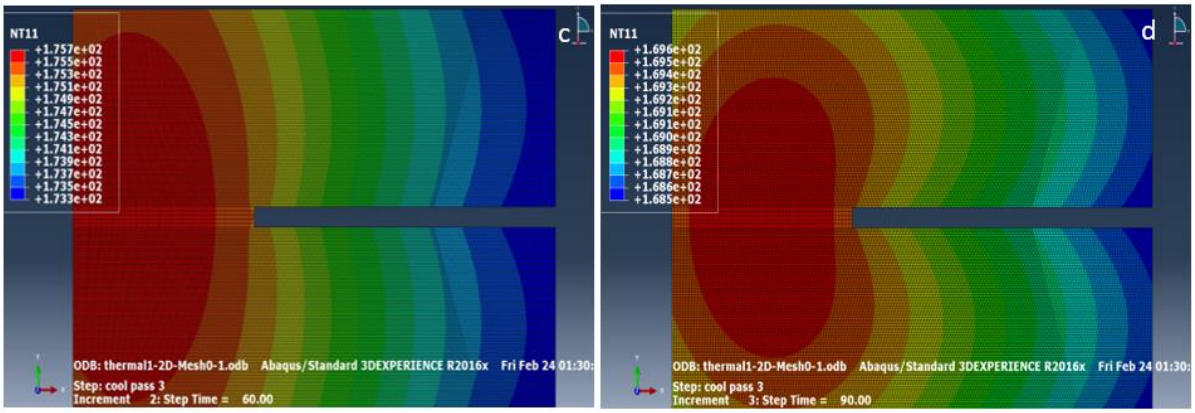

Figure 4.19 a) Step: Cool Pass 3, Increment 2, Step Time = 60.00 and b) Step: Cool Pass 3, Increment 3, Step Time = 90.00

Figures 4.18 through 4.19 Temperature profiles at different time steps of cool pass 3 during the welding process)

4.8.2 3D Model – Pipe Strip

4.8.2.1 The pipe Strip Model (Single Material)

The Pipe Strip model was the first model to be developed in this research and in accordance with the aims and objectives in chapter 1. It contains seven steps of through-the-thickness weld passes also known as sheet or strip weld passes. Each weld pass consequently possesses

different increments which are executed within different time steps for simulation of the weld passes. The different weld increments corresponding to the different time steps for weld pass one is displayed for the pipe strip model in Figure 4.20. The different colour bands represent the different weld temperatures. Colour band red to orange band represents the hottest part of the weld zone such as FZ, yellow to green stands for the intermediate temperature range whereas the blue refers to the cooling temperature such as the background. This implies that for Figure 4.20 (c), the weld zone temperature ranges from 1,162 ^{O}C to 1,375 ^{O}C, the HAZ 418 ^{O}C to 1,056 ^{O}C, while the rest of the pipe lies with the temperature range of 312 ^{O}C to 99^{O}C. In like manner, the following strip welds are deposited as shown in Figure 4.21.

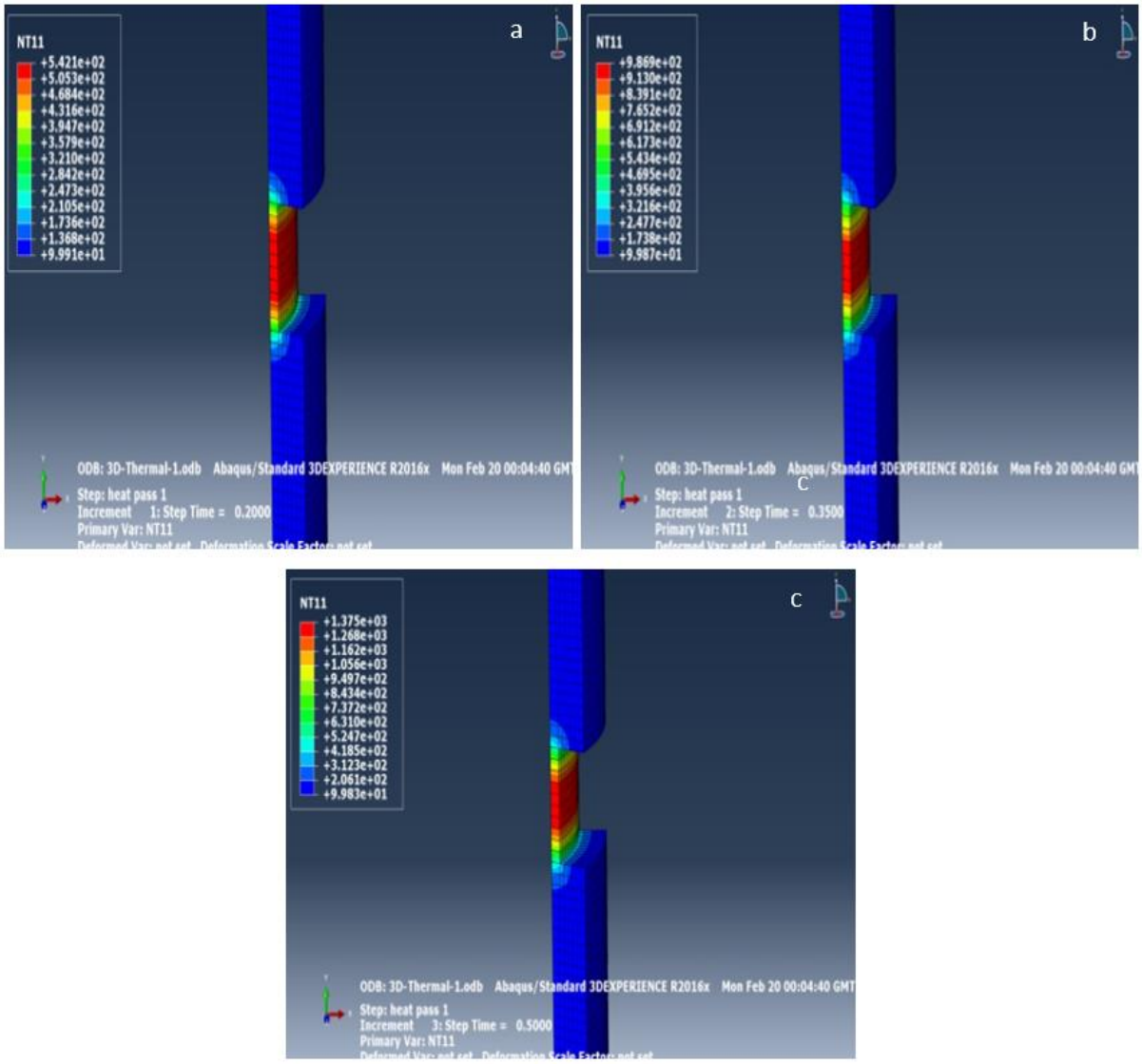

Figure 4.20 3D weld pipe strip shows the different temperature profiles for heat pass 1 at a particular time step (a) 0.2000 seconds, (b) 0.3500 seconds, (c) 0.5000 seconds

For this research, a bead is referred to as a pass. For the 2D weld models and the different thicknesses of cladding for the 3D weld models, the number of passes is seven. This is referred to as an industrial application and at the time allows weld passes in the different wall thicknesses. It is regarded as good practice to simplify weld models by representing several weld beads by a pass. For simplicity it is also assumed that the first weld bead is laid prior to the next and so on until the final weld bead (the seventh pass) is completed.

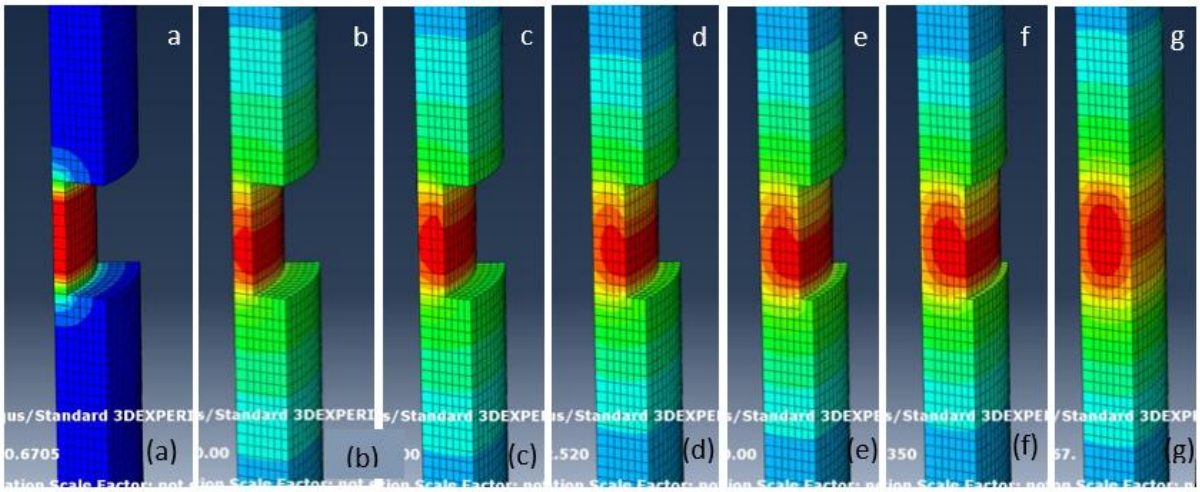

Figure 4.21 Weld profiles of (a) Pass one (b) Pass two (c) Pass three (d) Pass four (e) Pass five (f) Pass six (g) Pass Seven

The weld bead is represented in the following Figures 4.21 (a-g). These figures clearly illustrate the temperature profile of the same time step along the path line at the weld, at a constant speed. Note that the temperature distribution varies for the different weld passes irrespective of the fact that it is the same time step.

4.8.3 3D Model – Full Cladded pipe

Figure 4.22 (a-f) below shows the thermal simulation for heat pass 1 in a full 3D Pipe with different temperature contours which are seen as colour variations representing each thermal distribution shown in the temperature panel at the top left side of the figure. The red band depicts the hottest part of the weld, with a temperature of 1,391 ^{o}C, whereas the other regions indicate a lower temperature leaving the bulk of the pipe at 99 ^{o}C almost 100^{o}C.

Figure 4.23 (a and b) shows the thermal distribution for cooling step 7. It is clear to see that the overall temperature of the body is hotter than in previous weld steps as a result of temperature distribution from the weld process. The different colour bands representing the weld zone and the heat affected zones are red-orange and yellow green with blue as the background colour. These values differ for different stages of the weld and for Figure 4.22 (a) and (d); the Heat Affected Zone (HAZ) corresponds to a range of 557 to 208 and 1,089 ^{o}C to 539 ^{o}C. The method of weld deposition utilized during the welding process in the pipe is known as the added ring, whereby the weld is carried out by the deposition of a ring layer per time in the welded passes.

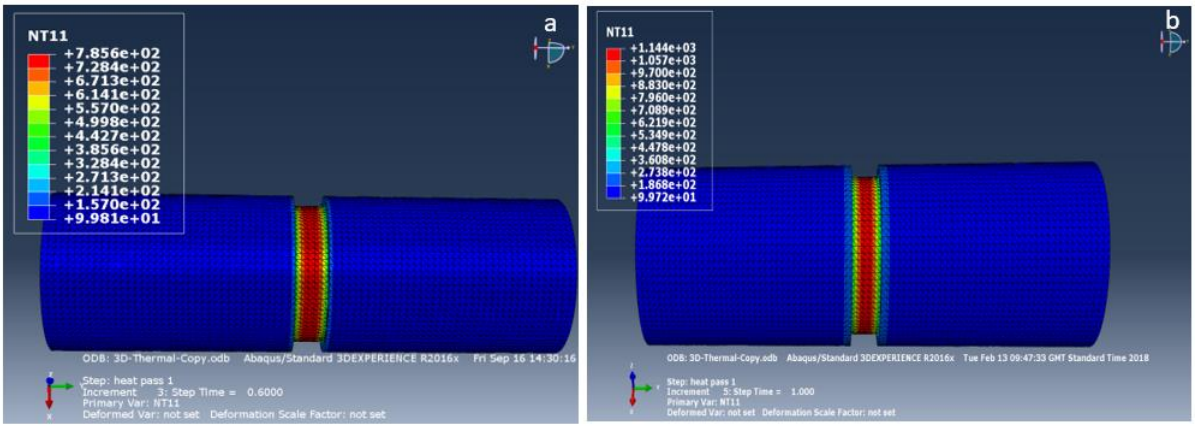

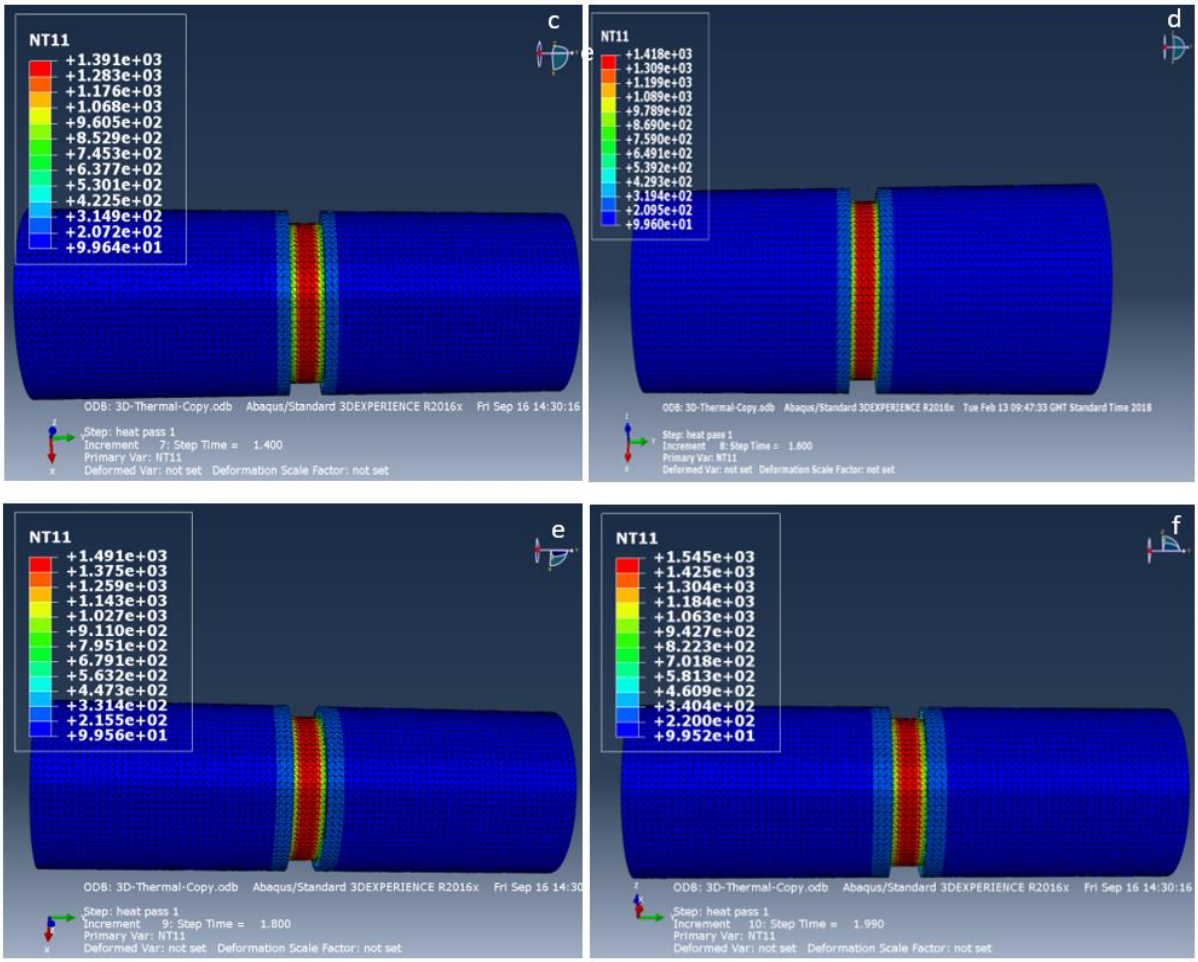

Figure 4.22 (a-f) 3D Weld Pipes showing the different Weld times for a particular weld pass – Heat Pass 1. Temperature profiles of a Ring added mass weld through the weld pass length

4.8.3.1 Cooling

Figures 4.23 (a-b) shows the cool passes for the ring added mass in the cylinder. It is important to note that the temperature range is almost the same in the cooling phase. In Figure 4.23 (a), this can be seen as 836 ^{o}C to 652 ^{o}C, with a difference of 184 ^{o}C (there is less than 200 ^{o}C difference between them). Similarly, for Figure 4.23 (b) the thermal distributions range from 363 ^{o}C to 202 ^{o}C which leaves a difference of 161 ^{o}C. Also, a value of less than 200 ^{o}C, indicates an effective cooling of the welded region. The different colour bands correspond to different temperature profiles which significantly represent the FZ, the HAZ and the rest of the pipe. In

Figures 4.23 (a) and (b), the FZ is depicted by the red-orange colour band which corresponds to 803 ^{o}C to 836 ^{o}C and 314 ^{o}C to 336 ^{o}C and are confined within the blue lines in Figure 4.23 (b); whereas the HAZ lies within the yellow to greenish blue colour band. These are the 658 ^{o}C to 716 ^{o}C, leaving the rest of the pipe at a temperature of 642 ^{o}C in Figure 4.23 (a). Likewise, further cooling occurs at 213 ^{o}C to 291 ^{o}C, leaving the pipe at 207 ^{o}C to cool down in Figure 4.23 (b)**.**

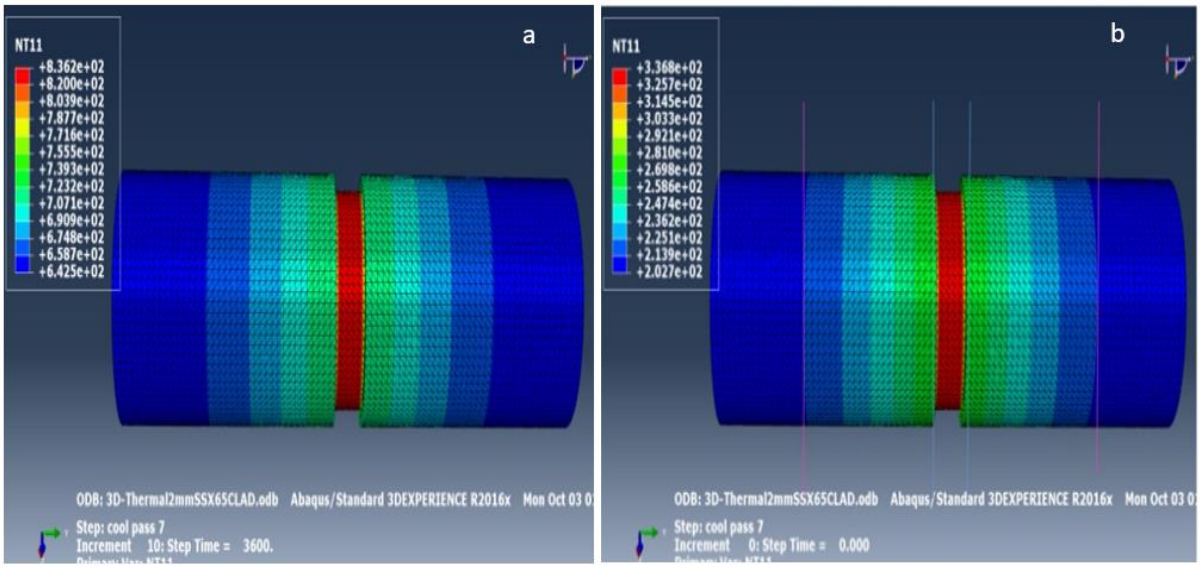

Figure 4.23 (a) complete thermal model of a fully clad pipe, cool pass 7, time step 10 and (b) complete thermal model of a fully clad pipe, cool pass 7

4.9 Results and Discussions

4.9.1 Temperature versus Time Plots – Transient Thermal Cycles

The thermal cycles shown in Figures: 4.24 and 4.25 (a-d), clearly portrays the fact that the temperature at a specific point reaches a maximum with respect to time when the weld torch

crosses a corresponding section of the weld. (Refer to Figures 3.7 (a and b) under section 3.3 Thermal Measurement in Chapter 3). The point nearest the weld line heats up to an extreme degree, whereas at the point farther away from the weld line there is a peak that occurs. The nodal spread of the temperature from the thermal analysis are fed into the input of the stress analysis. Temperature gradients which are steep in nature are seen well ahead of the heat source, this depicts the fact that the speed of the heat is faster than that of the weld torch. At the back of the heat source, the gradients show the cooling process once the peak temperature has been attained. Figures 4.24 and 4.25 (a-d) also depicts the final stage of the cooling procedure of the weldments to a uniform temperature. They also conform to literature from Dar et al (2009), Feli et al (2011) and Sinha et al (2013) Figure 2.25 (b) in chapter 2.

For the thermal analysis, the stainless steel and mild steel are the same especially since their thermal properties lie within same range. In terms of accuracy, they are still close, even though they are made up of different compositions of elements, as observed in section 3.10.2 Result of EDXA of parent materials in chapter 3.

In Table 3.3, 3.4 and 3.5 under chapter 3, the position of the thermocouples and their distance from the weld edge (WE), weld line (WL), weld start axis (WSA) and weld start (WS) have been displayed. The values of the transient and simulated temperatures and time of heat travel of the thermocouples are displayed in Tables 3.4 and 3.5. The weld start in this research is with respect to the depths of the clad and base metal since two different clad thicknesses are being considered – the 2mm clad thickness and the 12mm clad thickness. Refer to Figures 3.7 (a and b) under section 3.3 Thermal Measurement in Chapter 3.

4.9.1.1 For 2mm Clad Thickness

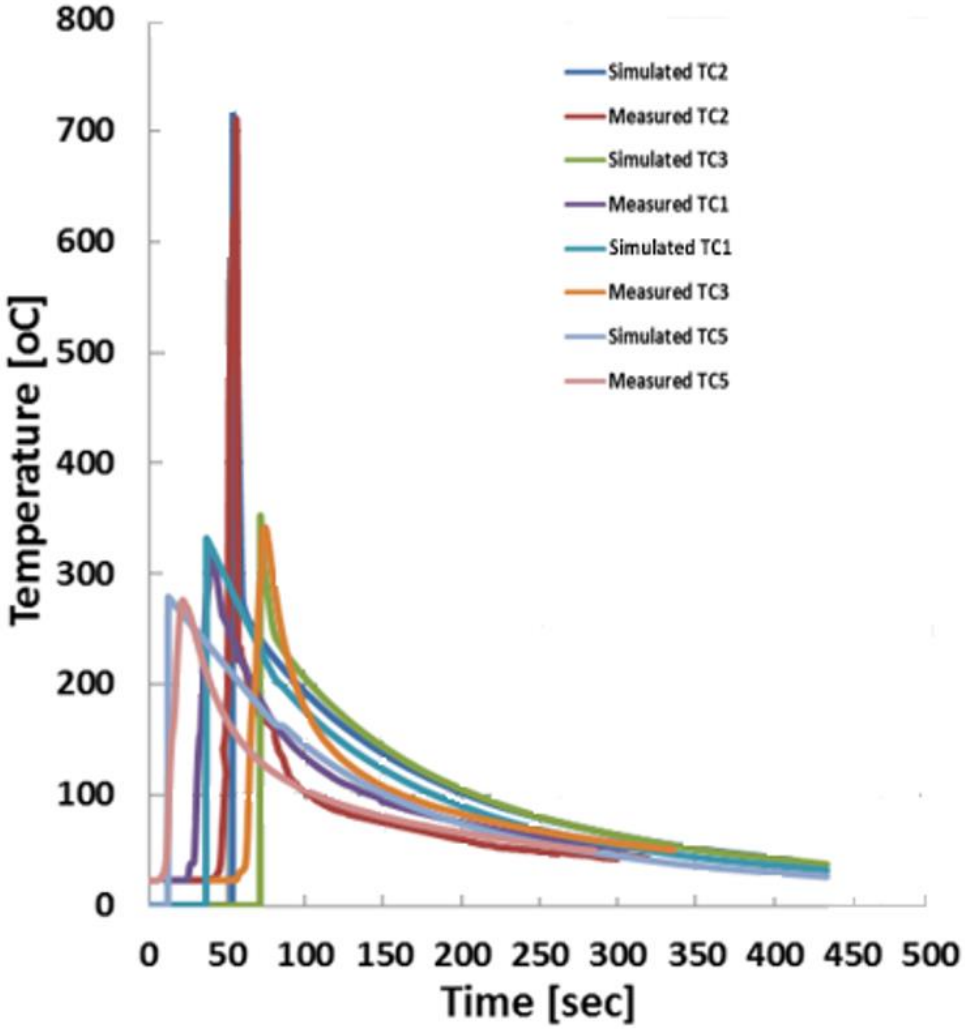

Figure 4.24 Measured and Simulated Transient Thermal Cycles for Thermocouples TC1, TC2, TC3 and TC5 at Various Points along different weld cross sections from weld start

The side-by-side evaluation of the experimental transient temperatures and the expected transient temperatures is shown in Figures 4.24 and 4.25 (a-d) below. From the results, there is a good agreement between the simulated and experimental values of the temperature change with time at the location of the thermocouples 1, 2, 3 and 5 and 1, 2, 7 and 8. In general, we can say that the results are within expectation.

In Figure 4.24, the transient curve for thermocouple 1 measured versus simulated temperature, shows that there is a good agreement between the measured readings and the simulated readings, confirming the quality of simulation carried out using the Abaqus CAE. Likewise, for thermocouple 2 in Figure 4.24, there is a good agreement between the experimental and analytical result.

The fact that the temperature varies in a parabolic form with respect to the elapsed welding pool and attains a peak value at the weld pool centroid, further proves that the quantity of heat inputted into the model affects the geometry of the model – resulting in the deformities caused. The irregularity in the temperature profile is also due to phase change. Note that the simulated curves depict isolated welding pass. This is evidenced by a peak value at the point of weld before cooling down, unlike the actual measured reading which rises slowly due to the gradual transmission of heat through the weld plate. The simulated value attains a sharp peak at the weld point because after each weld the weld temperature returns to the ambient temperature (which does not apply to the actual weld). Also, there are no thermal histories retained in order to ensure continuity from previous heat values.

From the values of the transient and simulated temperatures and time of heat travel of the thermocouples displayed in Tables 3.4 and 3.5 in chapter 3, the maximum temperature are in very good agreement, but in terms of the transient temperature, the error of about 50 ^{O}C is negligible compared to 300 ^{O}C when compared with high weld temperatures 1,200 ^{o}C to 1,500 ^{o}C, as illustrated in Figure 4.25 for TC7. The measured temperature reading commences from 20 ^{O}C unlike the simulated which commences from 0 ^{O}C. Again, 20 ^{O}C is negligible compared to 300 ^{O}C, see Figure 4.25 (d). In the cooling down phase, the measured result is faster than the simulation due to the heat conductivity of the metals; however other data can be fine-tuned in the simulation.

It has been noted in the Figure 4.24 that thermocouples TC3 and TC5 receive some thermal energy by reason of their position as displayed in Table 3.4 in chapter 3 and in the Figure 3.7 under section 3.3.1 of Chapter 3- Thermocouples. Also, in Figure 3.7 the position of the thermocouples shows that the thermal conductivity affects the temperature profiles. TC5 is placed underneath the 2 mm Clad plate stainless steel, which has a thermal conductivity of 16 [W/mK] and has access to the heat from the heat source much faster when compared to other thermocouples and as a result, TC5 has the first peak within a short period of time. TC3 which has the second highest peak has the added advantage of proximity to the weld line and being 75mm away from the heat source - which increases the contact with heat faster compared with other thermocouples. The thermocouple TC2 however, receives the highest quantity of heat compared to the others by reason of its centralised position to the heat source (50mm) and proximity to the weld line compared to other thermocouples placed close to the edges of the plates. It does not dissipate the heat built over time to the surrounding area as fast as the other thermocouples at the different ends. Rather, the heat is trapped in such a manner that allows it to slowly dissipate into the surrounding area.

4.9.1.2 For 12mm Clad Thickness

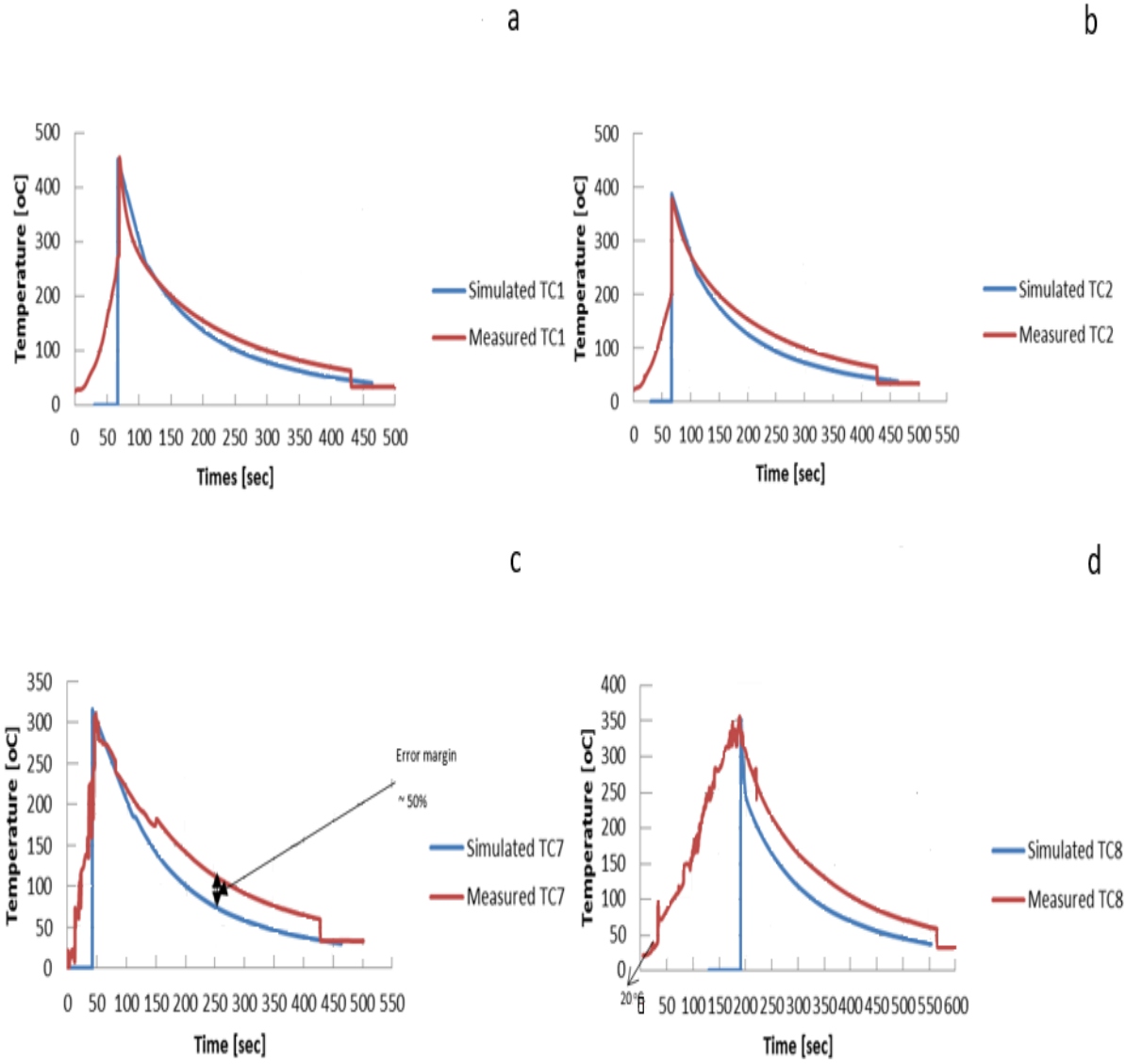

Figure 4.25 Transient curves (temperature vs time) for measured and simulated in (a) TC1, (b) TC2, (c) TC7 and (d) TC8

For the 12mm clad, the following Transient curves for the Measured versus Simulated were obtained in Figure 4.25. It is observed from Figures 4.25 (a-d) above that the thermocouples TC1 and TC2 have very high temperature ranges as a result of being situated close to the weld start positions compared to other thermocouples such as TC7 and TC8. Thermocouples TC7

and TC 8 in Figures 4.25 (c and d), are placed underneath the weld plate at a distance of 50 mm from the weld start and 13.50 mm and 26.50 mm respectively from the weld line; and as such do not receive enough heat compared to Thermocouples 1 placed 13.50 mm from the weld start (opposite TC6) and TC2 which is placed both 15mm from the weld edge and 22 mm from the heat source. It should also be noted that by reason of electric distortion there have been some unwanted signals in the temperature profiles as observed in TC7 and TC8**.**

4.9.2 Welding Direction (Nomenclature)

In order to describe the direction in of the welding carried out, the usual concept of the 90 degrees, 180 degrees, 270 degrees and 360 degrees have been used in a clockwise manner to describe the direction of the weld, as well as the 3 o'clock, 6 o'clock, 9 o'clock and 12 o'clock convention. In agreement with these previous conventions for weld direction, the concept of 45 degrees, 135 degrees, 225 and 315 degrees is hereby introduced in this research in addition to the 1:30 hours, 4:30 hours, 7:30 hours and 10:30 hours concept; all in the clockwise direction as shown in Figure 4.26.

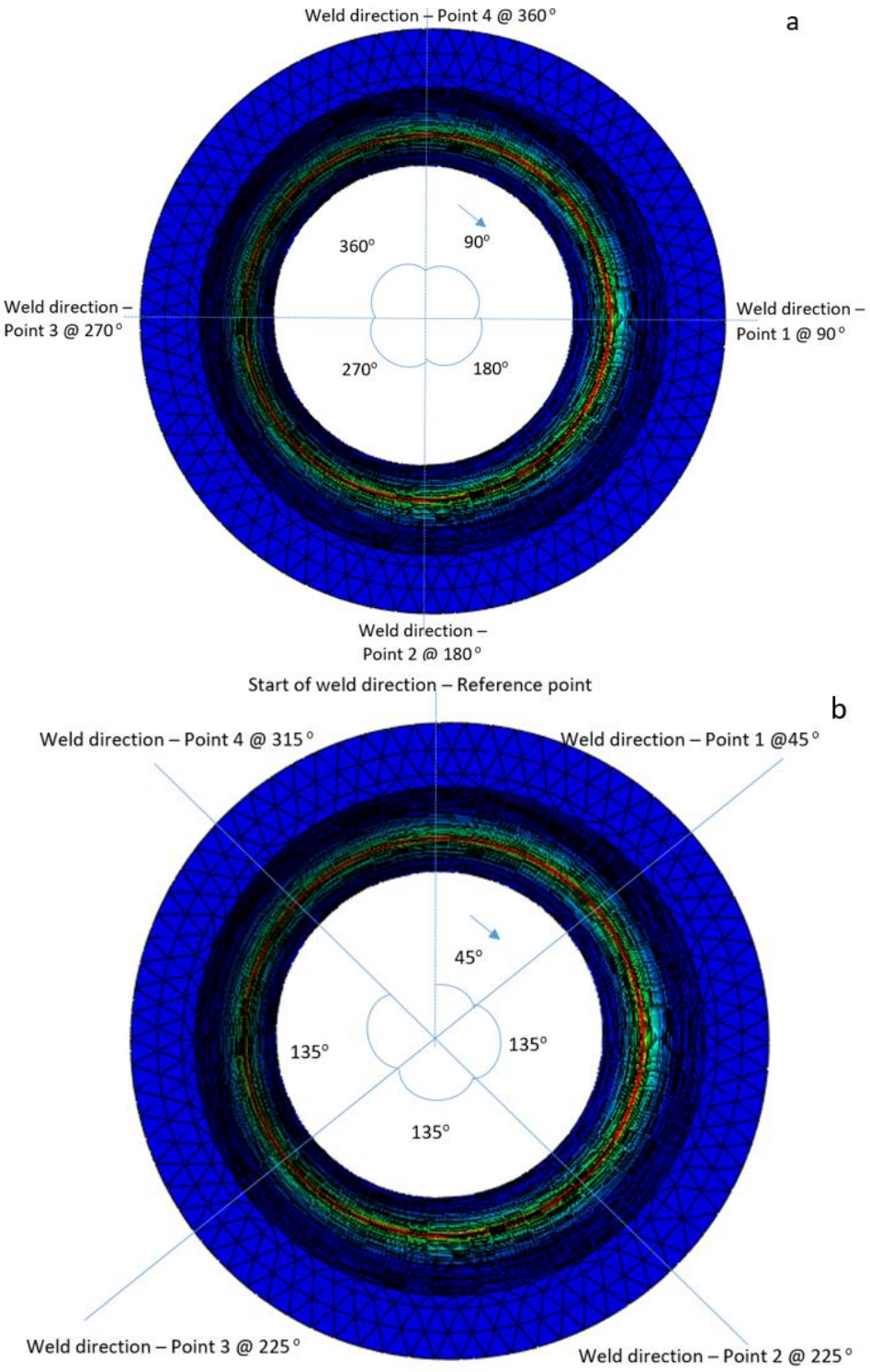

Figure 4.26 (a) A representation of the pipe rotation and nomenclature of 90, 180, 270 and 360 degrees respectively and (b) A representation of the pipe rotation and nomenclature of 45, 135, 225 and 315 degrees respectively

Presenting the 45, 135, 225 and 315-degree reference system, which is simply rotating the cross section of the pipe in Figure 4.26 (a) through an angle of 45 degrees in the clockwise direction, as illustrated in Figure 4.26 (b). It makes it convenient to view, decipher and read the weld direction especially since it is the same irrespective of the direction taken. The above theory and style of representation of a welding direction is known as 1:30 hours, 4:30 hours, 7:30 hours and 10:30 hours. A clock face is used as a temporal connotation. Recall Figure 4.2 under section 4.1.2, the geometry of model, the principle of the Gaussian flat surface having a zero Gaussian curvature at every point clearly reveals that the surface of a cylinder can be referred to as a Gaussian flat plane; revolved from a piece of paper (ETSU, 2014). Based on that, the four positions of interest on the pipe circumference can be represented onto the plate and the following output is obtained as shown in Figure 4.27.

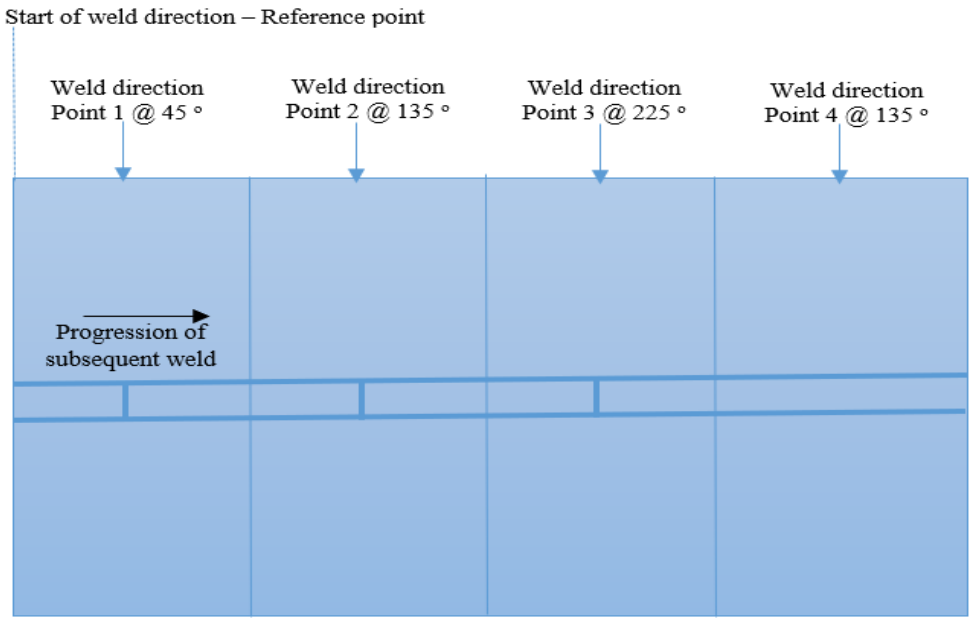

Figure 4.27 A plate representation of the pipe rotation and nomenclature of 45, 135, 225 and 315 degrees respectively. Concept and theorem explained earlier on in section 4.1.2 Geometry of models and illustrated by Figures 4.2 (a) and (b).

Figure 4.27 implies that the different weld directions can also be represented on a plane surface, as shown on the 2D plate in Figure 4.27. The same is applied to 3D Plates.

The variation of temperature with distance is displayed for 3 o'clock weld position 6 o'clock and 9 o'clock respectively in Figure 4.28 (a). For different weld angles in Figure 4.28 (b), the peak temperatures are displayed with respect to their distance from the weld line with the highest peak depicted at 60^{o} which was one of the angles used in the experimental weld.

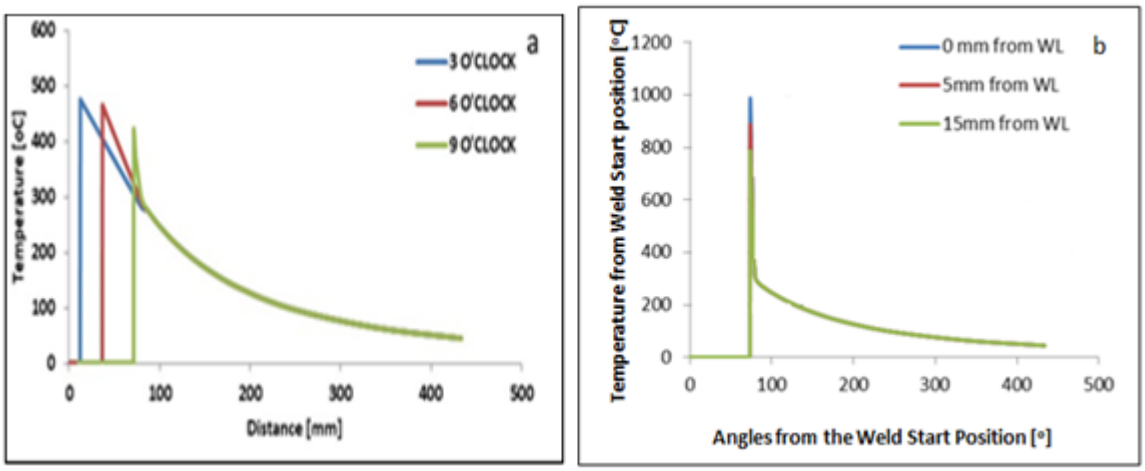

Figure 4.28 (a) Transient Thermal Cycles at 3 o'clock, 6 o'clock and 9 o'clock at different weld times (b) Transient Thermal Cycles at different weld length (distances) at 12 o'clock

4.9.3 Temperature Distribution

Figure 4.29 (a-d) shows the distribution of the axial temperature at four different time steps (3 o'clock, 6 o'clock, 9 o'clock and 12 o'clock, from the weld start to the weld progress positions. At a specific position, the temperature distribution is steep as the weld arc transverses that section (see peak of Figure 4.29 (a-d)). As the weld torches crosses the section the drop-in temperature becomes obvious from the plot, travelling at the rate of 3mm/s around a circumference of 300 x Π, it arrives at its destination after 40 seconds. The Figures 4.29 (a-d),

4.30 (a-b) and 4.31 (a-b) below also show the thermal variations for four different cross sections at differing time steps.

4.9.3.1 Pipe Strip (Single material)

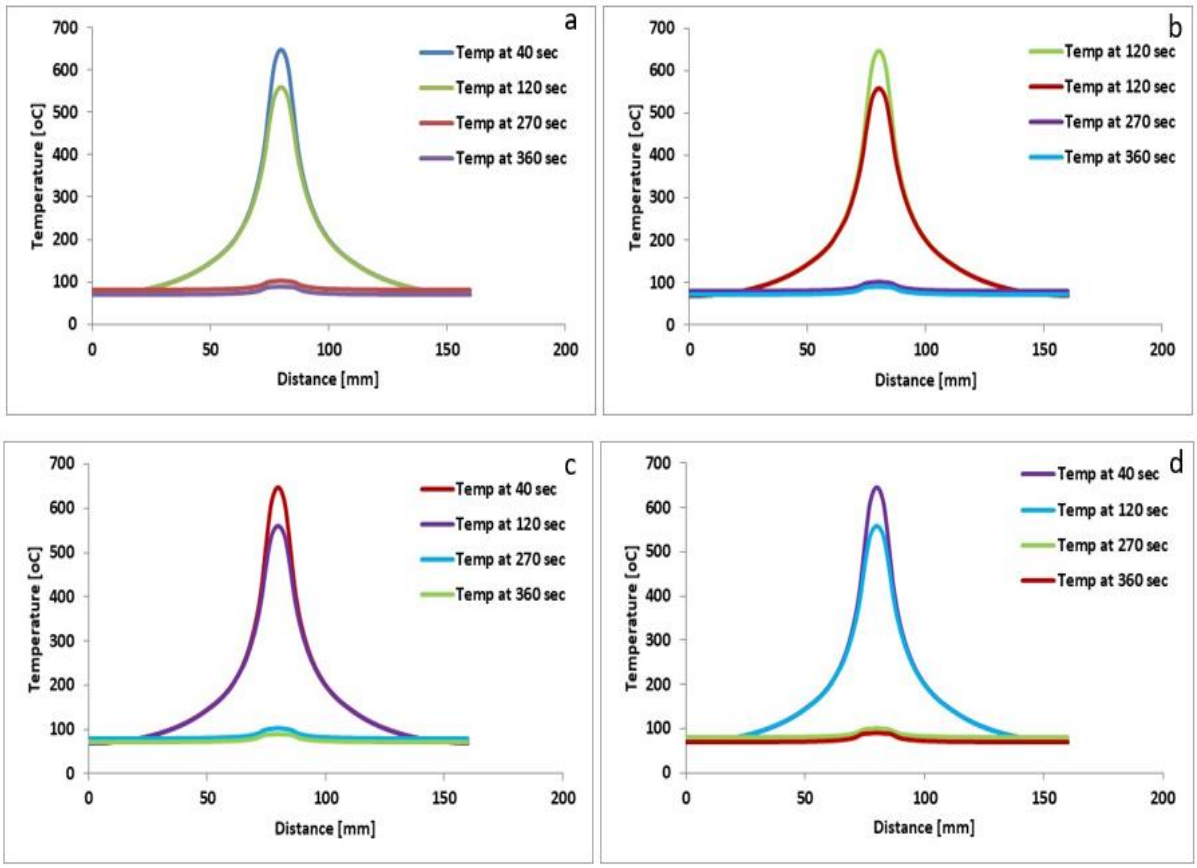

Figure 4.29 Axial Temperature distributions for four different cross sections (a) 3, (b) 6, (c) 9 and (d) 12 o'clock positions at different time steps from the weld start

No significant difference observed between nodal paths. Results are repeatable and they are in close agreement.

4.9.3.2 Full Pipe - 2mm Clad Thickness

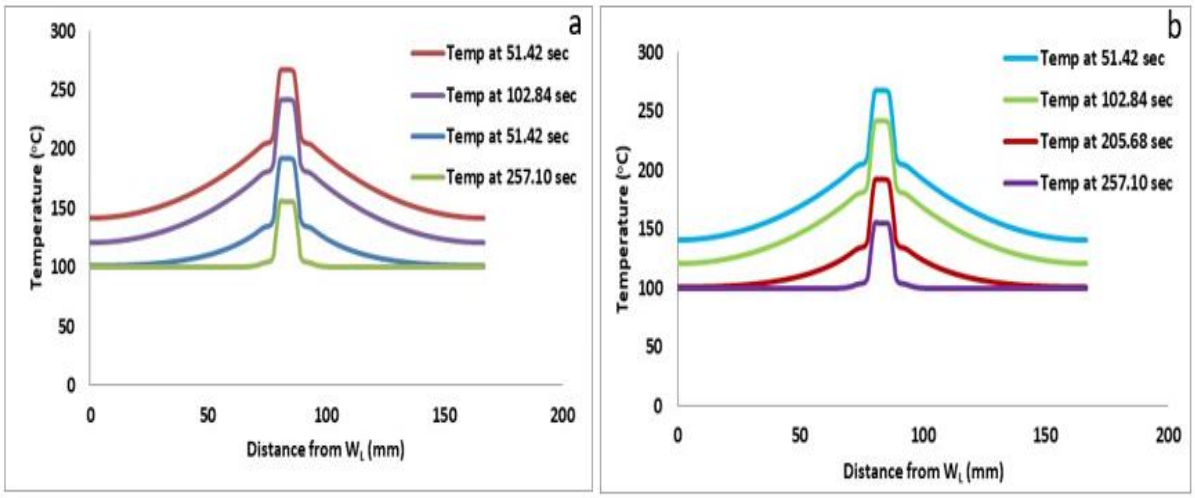

Figure 4.30 (a-b) Axial temperature distributions for 45° and 135° cross-sections at different weld times 51.42 and 102.84 seconds from the weld start in a 2mm clad

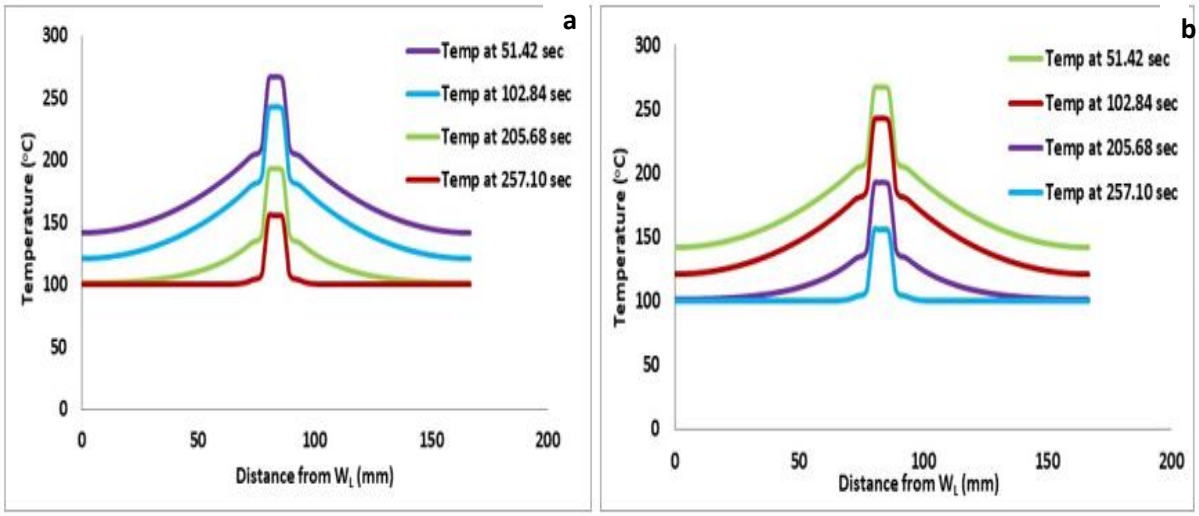

Figure 4.31 (a-b) Axial temperature distributions for 225° and 315° cross-sections at different weld times 205.68 and 257.10 seconds from the weld start in a 2mm clad

4.9.3.3 Full Pipe - 12mm Clad Thickness

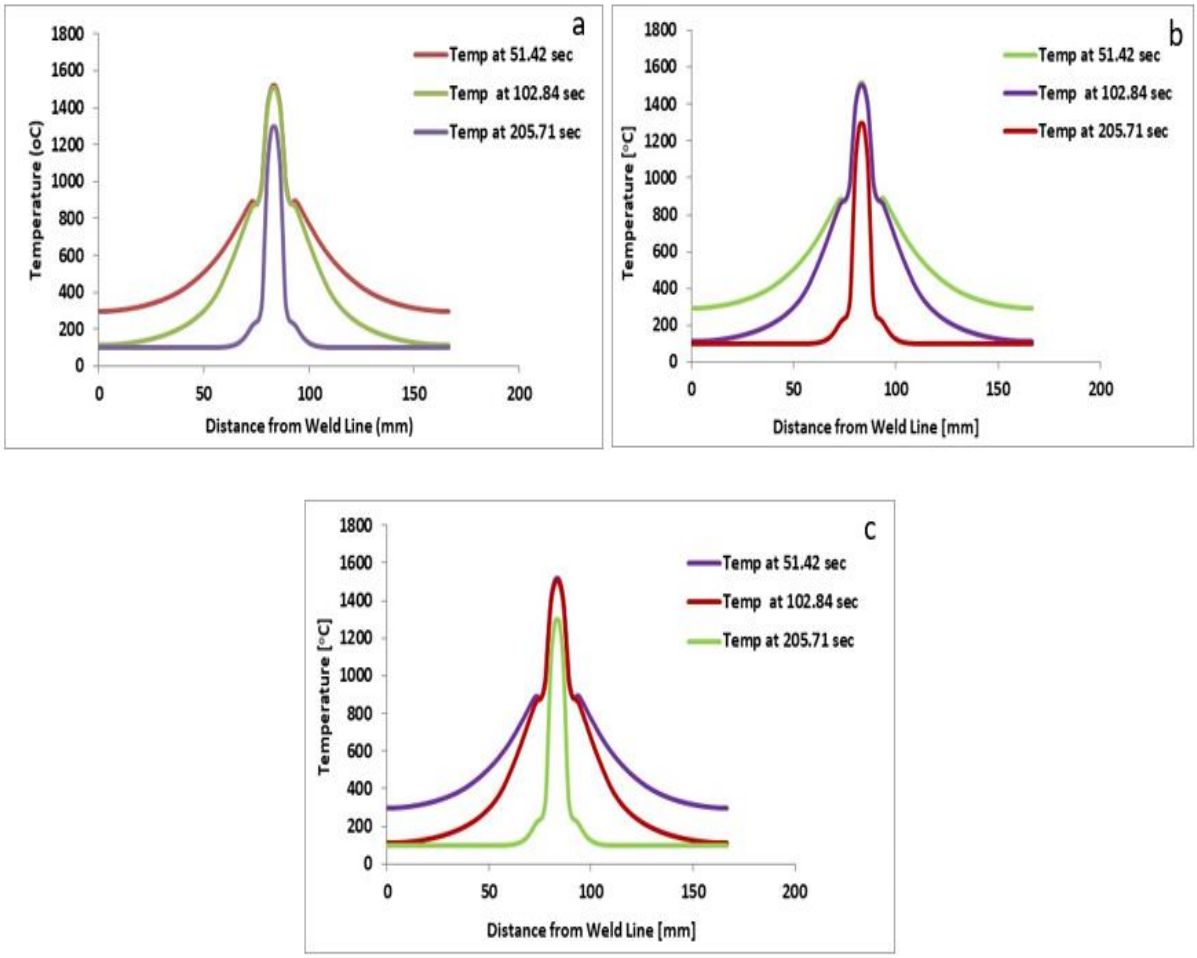

Figure 4.32 (a-c) Axial Temperature distributions for 45º, 135º and 225º Cross-sections at different weld times 51.42, 102.84 and 205.71 seconds from the weld start respectively in a 12mm Clad Pipe

From the different plots of temperature versus distance, the effect of the clad on the weld is seen as the clad effectively reducing the operating temperature thereby reducing the thermal conductivity of the welded path. The reduction in thermal conductivity enhances the effectiveness in the insulating effect of the cladding. The simulation in Figures 4.30 and 4.31 shows that the 2mm clad has lower temperature than the 12mm clad in Figure 4.32. The reason for this difference is because the 2mm clad requires only a single welding pass whereas the 12mm clad requires seven welding passes, which means more heat input, thus higher temperature. The curve from Figure 4.32 shows that the pipe performance under a high

temperature is possible with a larger clad layer compared to a smaller clad layer. Bearing in mind that temperature imparts directly on the toughness, modulus of elasticity, ultimate tensile strength and yield stress, means that increased operating temperatures will also impact upon the properties of the clad pipes.

4.10 Further Discussion

From the various plots of temperature versus distance along the path of weld propagation and direction, it has been observed that the distribution of the heat follows a unique pattern which has been displayed above in Figures 4.29 (a through d), 4.30 (a and b), 4.31(a and b) and 4.32 (a through c) whereby the different HAZ has been considered. The peaks displayed in the plot correspond to the immediate environ of the weld with the number and magnitude of the peaks increasing as the cumulative quantity of heat dispelled within the weldment, increases. Likewise, it decreases the further away one goes from the region of weld.

4.11 Summary

Based on the above findings we can draw the following conclusions:

i. Transient responses have been shown in the weld results. The experimental results match very well with the simulated results.
ii. The result of the heat input fed into the FEA analysis generates a unique set of results which has obvious effects on the thermal analysis and output.
iii. Convection is the major procedure for transmission of heat from the pipe, plate and pipe strip to the immediate environ and the maximum film coefficient value is 15Watt/m^2

^{o}C; whereas Radiation boundary conditions have minimal or no consequence on the estimated temperatures and can be overlooked.

iv. The 2D models of the pipe and plate generates meaningful and vital information regarding the mesh alignment and perfection of the finite element solution.

v. The number of load steps needed for the heating and cooling periods can be determined and have been determined by the load module and step module respectively, as seen in the FEA model in Abaqus.

vi. The 3D models of the full pipe, pipe strip and plate generate meaningful and vital information regarding the mesh alignment and perfection of the finite element solution.

4.12 Conclusion and Key Findings

For this research, the thermal analysis of girth weld in subsea pipeline has been carried out with the display of the temperature profile, consideration of the distance from the region of the weld and specifically the weldment being acknowledged. It has been observed that the measured transient heat curves match well with the simulated transient heat curves, confirming the quality of the simulation carried out. Factors such as latent heat, convection and radiative heat contribute significantly towards the regular rise and fall in temperatures profiles which is the trend observed and displayed in the peaks and valleys within the results.

From the temperature versus distance plots it is observed that for the 2 mm clad Stainless Steel and X65 weld, the thermal plots are not as high as the 12 mm clad stainless steel and X65 carbon steel clad which shows a high peak of 1500 ^{o}C. The significance of this since the melting point for stainless steel is high is that cladding with 2 mm X65 Carbon steel and Stainless steel, lowers it to a moderate value so that a good result of temperature is obtained. It should neither be too high nor too low, thus guaranteeing stability and improvement in performance of the

clad pipe and hence ensuring longevity of the service lives of pipes. The nature of the material used in the modelling (weld parameters) plays a very significant role in the temperature – the time displacement curve and being responsible for the lag observed in the transient curve for the measured data.

In the experimental data, the thermocouples detected the heat at different rates, at different times by reason of proximity and only attained peak value when the heat source was right at the same spot as the thermocouples. This clearly means that the response to the temperature was dependent on several factors, such as the nature of the material - stainless steel or mild steel, material thickness (depth, height and width), thermal conductivity of the material (stainless steel is 16 [W/mK] and mild steel is 36 [W/mK]); position from heat source (distance away from the heat source) and time of transmission (time at which the temperature reading is taken). These are all going to affect the temperature time (transient) curve being displayed in the figures.

NOTE: Publications based on the chapter content and published in international conferences and journals are found in Appendix 2 – first page only.

5. SIMULATION FOR STRESS ANALYSIS

5.1 Introduction

This chapter describes the numerical procedure of acquiring the stress analysis in a multiple pass butt welded stainless steel and carbon steel clad pipe and plate. The geometry and the material properties of the models are defined, and the results are analysed in stress distributions and graphs for two clad thicknesses in both plate and pipe models.

Butt-weld multiple passes of stainless-steel clad pipes have been simulated in a non-linear finite element analysis using the Abaqus software. The physical problem is highly nonlinear involving thermal softening (mechanical behaviour in close to welding in semi-solid states) and the interaction of dissimilar materials with different properties. As such, a nonlinear analysis becomes a necessity.

As with Physical processes which are inherently nonlinear such as stretching a plastic band and it becomes harder to pull as the deflection increase because permanent deformation is being achieved, manufacturing process like welding entails nonlinear simulation. Also, thermal variation of material properties.

The results obtained in this research are mostly nonlinear. Stress, heat transfer, graphs are nonlinear. The whole process has been done via nonlinear analysis and because nonlinear option was toggled, nonlinear information is expected from the analysis.

Through thickness variations, discrepancies of the hoop and axial stresses at the Heat Affected Zone (HAZ), and weld zone are examined at the circumferential butt welds in piping setups. There are factors that affect residual stress as well as factors arising from the weld procedures. Such factors comprise geometry of the weld joint, weld heat input parameters, wall thickness and diameter of the pipe. Tensile stresses in hoop and axial directions have been examined on

the internal pipe surface with the axisymmetric model with inbuilt shrinkage characteristics and the result was consistent in stress dimensions from measured data and FEA predicted results. An accurate and thorough assessment is needed on the associated residual stress and its effect on the structural properties of the pipeline.

3D simulations of stress in girth welded pipe sections have been carried out using the Abaqus CAE software in two steps, the first being the thermal modelling with a moving hot spot and added mass and the second being the stress or mechanical analysis. This research is fundamentally on the 3D finite element modelling of residual stresses in a stainless-steel clad girth welded x65 Carbon steel pipe; in which the modelling procedures for universal residual stress characteristic is clearly demonstrated. The different kinds of weld induced residual stress fields are hoop (meridian) and axial or longitudinal. Butt-weld geometry of the pipeline with a specification of 508mm (internal diameter), wall thickness of 50mm and API Grade of X65 carbon steel pipe clad by stainless steel grade 316; having a ring mass deposition was employed.

Through a series of the joining of both transient and non-linear analysis, thermo-mechanical process of arc welding, which is naturally multifaceted is resolved. With the aid of thermal, residual stress and deformation experiments, the validity of the thermal and stress models is verified. There is an agreeable similitude between the simulated outputs and those of other authors.

5.2 Technique of Structural Analysis

The thermal history of the various nodes from the previous thermal analysis are fed as nodal body load alongside temperature variant mechanical properties. For the part of mechanical analysis, stresses were calculated to see stress status in the materials such as the residual stress,

and to check if yielding may occur. In the simulation, Von mises stress was used together with its associated yield criteria. Stress analyses need to be carried out to find out the magnitude of stress level in the material – in particular, to see if the stress reaches the maximum yield where the failure occurs. In doing that the von mises criteria is used – that is FE analysis are carried out to find out stress distribution using the von mises stress. Von mises stress are used to check for the yielding with the three principal stresses $\boldsymbol{\sigma_1, \sigma_2}$ and $\boldsymbol{\sigma_3}$coupled with the kinematic hardening.

The displacement nodes from the previous analysis are fed in as the nodal body loading. Von misses stress is used to check the stress status and the yielding following Equation 5.1 with the three principal stresses $\boldsymbol{\sigma_1, \sigma_2}$ and $\boldsymbol{\sigma_3}$ coupled to a kinematic hardening rule:

$$\boldsymbol{\sigma_p} = \frac{1}{\sqrt{2}} [(\boldsymbol{\sigma_1} - \boldsymbol{\sigma_2})^2 + (\boldsymbol{\sigma_2} - \boldsymbol{\sigma_3})^2 + (\boldsymbol{\sigma_1} - \boldsymbol{\sigma_3})^2]^{1/2} \qquad \text{Eqn (5.1)}$$

The isotropic model suggests that if the yield surface is symmetric about the stress axes which also means that if the yield strength in tension and compression are initially the same, they remain equal as the yield surface develops with plastic strain. The kinematic hardening rule can also apply in model specific responses such as Bauschinger effect (a property of materials where stress/strain characteristics change as a result of microscopic stress distribution of material) where hardening in tension will lead to a softening in a subsequent compression. Here, the yield surface is constant in shape and size but merely translates in stress space as in Figure 5.1.

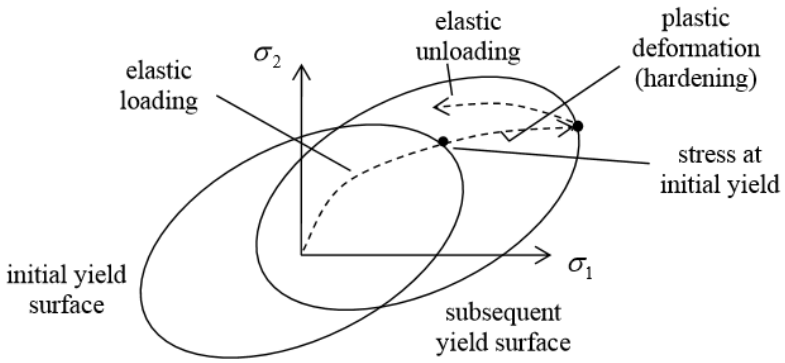

Figure 5.1 Kinematic Hardening (Kelly, 2013)

The need for the kinematic hardening has been addressed in the Abaqus software. Kinematic hardening models are employed to predict (mimic) the performance of metals exposed to cyclic loading and are therefore pressure independent plasticity models, that is, yielding of the metals is independent of the corresponding pressure stress. These models are appropriate for most metals placed under cyclic loading conditions. It is possible to employ the linear kinematic hardening model along with the Mises yield surface, however, the nonlinear isotropic/ kinematic model can only be employed with the Mises yield surface in Abaqus/Standard. Within the current model, the kinematic hardening is utilized to make sure the hardening of the material is properly addressed.

When modelling a welding process, the straining hardening effect is an important factor to be considered. Materials experience a series of repeated heating and cooling during the multi-pass welding process. This thermal cycle act as cyclic tensile and compressive loading to the material and induce stress-strain behaviour with plastic deformation hence straining hardening. In this study, a linear kinematic hardening model was employed with the consideration of Bauschinger effect which reduced elastic region (reverse yield) in a reverse loading, thereby reducing the level of residual stress.

Isotropic hardening was employed in preliminary FE models however the results were not reported in this thesis. It was found that without considering the reverse yield which is always maintained the same as the prior yield in the opposite direction, isotropic hardening model has the tendency to overestimate residual stresses. It is suggested that a combined isotropic-kinematic strain hardening model is more applicable for the actual hardening behaviour of the material. However, because of lack of material data, this hardening behaviour was not modelled.

The parameters for meshing are the same as those used when carrying out the thermal analysis, in order to facilitate convergence of the structural analysis via mapping of data and elements having similar topology. The thermal analysis enables the generation of elements as degeneration of elements (the weld-remove concept) which was inputted in the structural build-up of the model. The ambient temperature for the clad and base metals is also set in such a way that thermal strains are zero for the different thermal expansion coefficients.

The method of equation solver for the stress analysis is a direct method using the solver default matrix storage. The solution technique employed in this structural analysis is the Full Newton technique with a total of 8 iterations. The (deleted) iterations were propagated from the previous steps with the load variation time ramped linearly over each step. The maximum number of increments is 10 for each step of the analysis.

The modelling is carried out in two separate steps. First the thermal analysis was carried out and completed. Next the stress analysis was carried out with the outcome of the thermal analysis as the input of the stress analysis. In this sense the whole analysis is sequentially coupled. The stress components and invariants were utilized in the weld remove and these were also propagated with the different heat and cold passes. The plastic strain components, magnitude and logarithmic strain components were incorporated into the steps along with the

translational, rotations and velocities, as well as forces and moments. The contact stress and displacement were utilized for effective contact and nodal temperatures. The 2D model was to simplify the model and enable better understanding of the parameter before developing the 3D mode for further studies. Abaqus provides a two-stage option for thermal (Step 1) and structural (Step 2) analyses. Based on the thermal analysis, deformation or displacements of nodes are obtained. They are then used as the input to the following structure analysis, in which the corresponding stresses are obtained, generating the same deformation as in the thermal analysis. In the simulation, material properties corresponding to the temperature are needed to cater for the thermal softening effect, i.e., changes in material properties due to the temperature effect.

Different models were studied in this research and they include the 2D plate, 3D pipe strip as shown in Figure 5.2, clad pipe and clad plates (in Figure 5.3). For the pipe strip the dimension is: OD 12.94, ID 10.35, thickness 5mm and height 160mm.

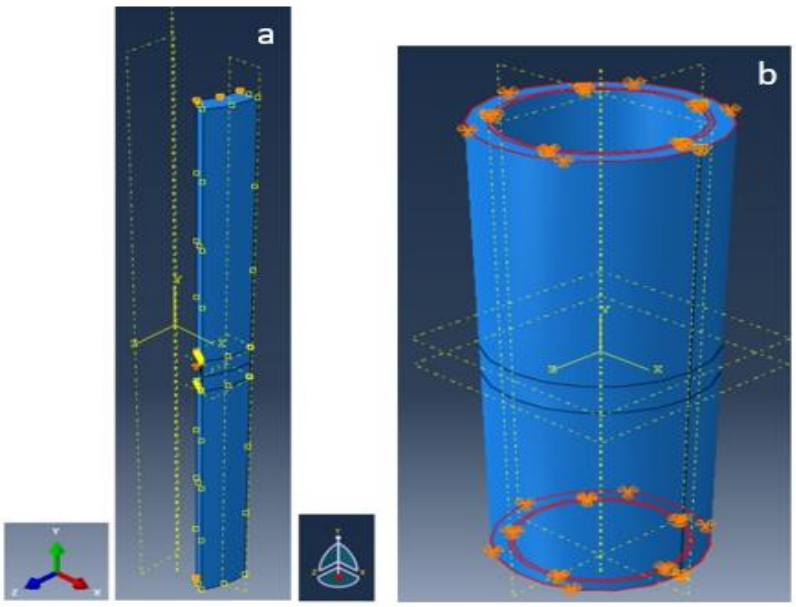

Figure 5.2 Boundary condition applied in (a) a pipe strip and (b) a full clad pipe

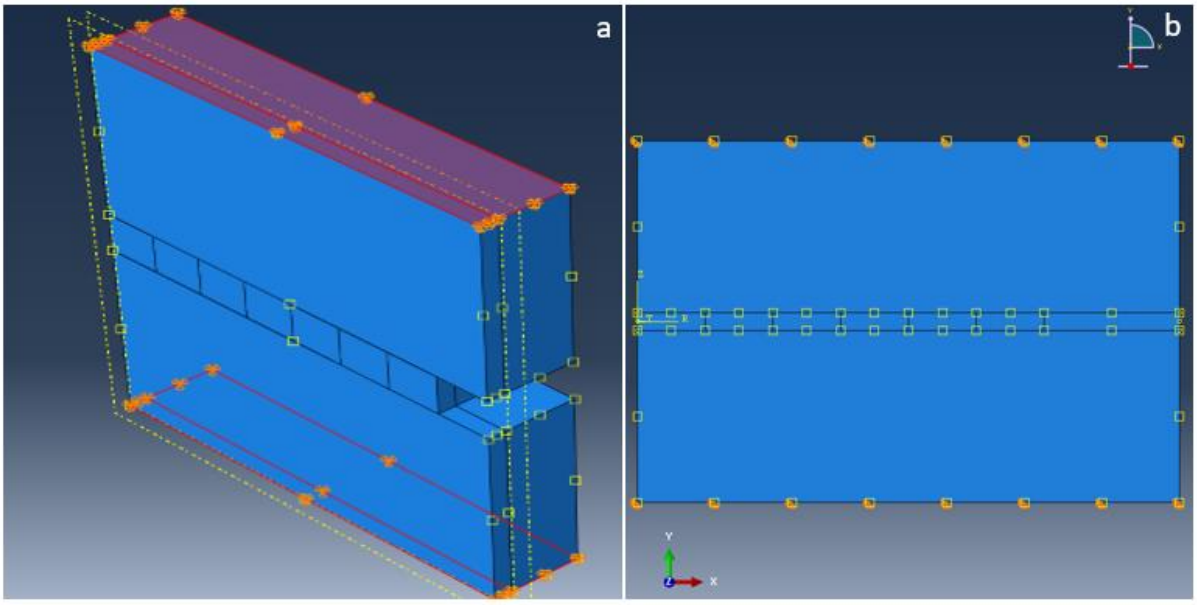

Figure 5.3 Boundary condition applied in (a) a 3D cladded plate and (b) a 2D Plate

5.3 Geometry

A modelling space of 2D and 3D were used for modelling the 2D and 3D Plate welds respectively. Deformable solid and extrusion was also utilized in creating the parts concerned. Dimensions of the 2D plate were 20mm by 30mm, whereas those of the 3D plates were 10mm by 10 mm having thicknesses of 0.4 mm and 1.6 mm.

5.4 Material Properties

Thermo-physical properties include thermal conductivity, specific heat and density; however, there are also other material properties that are fed into thermal and stress models. These include elastic – Young's Modulus, Poisson's ratio, and plastic – yield stress and plastic strain properties. The material properties used for the stainless steel and carbon steel pipes and plates are as listed below. The respective material properties were based on the data sheet provided

by material supplier starless steel as well as literature. They were also sourced from literature, CES (Cambridge Engineering Selector) Edu Pack 2013 are outlined in Tables 5.1 and 5.2 below. Since this research is part of the bigger project, the information from other part of the team was used because repeating the information was not required, however, confidence was gained in that the information was correct and was adoptable to the model in this very research. The CES Edu pack had transferred that information, so they could be relied on.

Table 5.1 Material Properties used for the SS316

	Young's Modulus [MPa]	Poisson's Ratio	Temp [^{o}C]
1	210000	0.30	20
2	190000	0.32	200
3	153000	0.34	400
4	95000	0.36	600
5	63000	0.38	900
6	11000	0.40	1200
7	7000	0.45	1500

Yield Stress [MPa]	Plastic Strain	Temp [^{o}C]
480	0.00	20
560	0.01	20
398	0.02	200
450	0.03	200
340	0.04	400
405	0.05	400
210	0.06	600
290	0.07	600
50	0.08	900
90	0.09	900
18	0.10	1200
4	0.11	1500

Table 5.2 Material Properties used for the X65 Carbon steel

	Young's Modulus [MPa]	Poisson's Ratio	Temp [^{o}C]
1	219000	0.3	20
2	154000	0.32	200
3	157000	0.34	400
4	60000	0.365	600
5	69000	0.39	900
6	12000	0.43	1200
7	6000	0.44	1500

	Yield Stress [MPa]	Plastic Strain	Temp [^{o}C]
1	460	0.00	20
2	550	0.01	20
3	388	0.02	200
4	500	0.03	200
5	335	0.04	400
6	400	0.05	400
7	206	0.06	600
8	260	0.07	600
9	31	0.08	900
10	80	0.09	900
11	15	0.10	1200
12	4	0.11	1500

Tables 5.1 and 5.2 were inputted into Abaqus standard for simulation as the material data

5.5 Applying Boundary Conditions

For the Pipe, boundary conditions were applied at the side, top and bottom of the pipes and likewise the 3D plates as seen in Figure 5.4. Displacement and rotation were restricted in the X, Y and Z directions. The distortion occurring in the model is accounted for by setting the initial strains to zero at the period of the activation of the element.

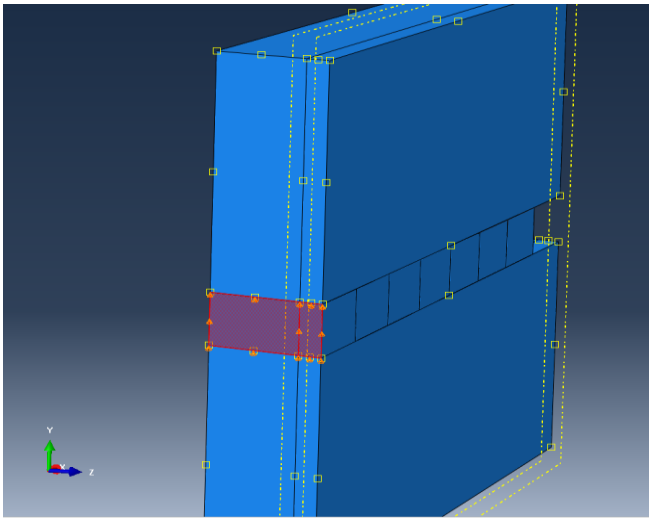

Figure 5.4 A boundary condition is applied in a clad plate. The middle of the left end of the plate and clad are constrained in the y direction. U2 = 0

Schematic of the boundary condition is seen in Figure 5.5 below:

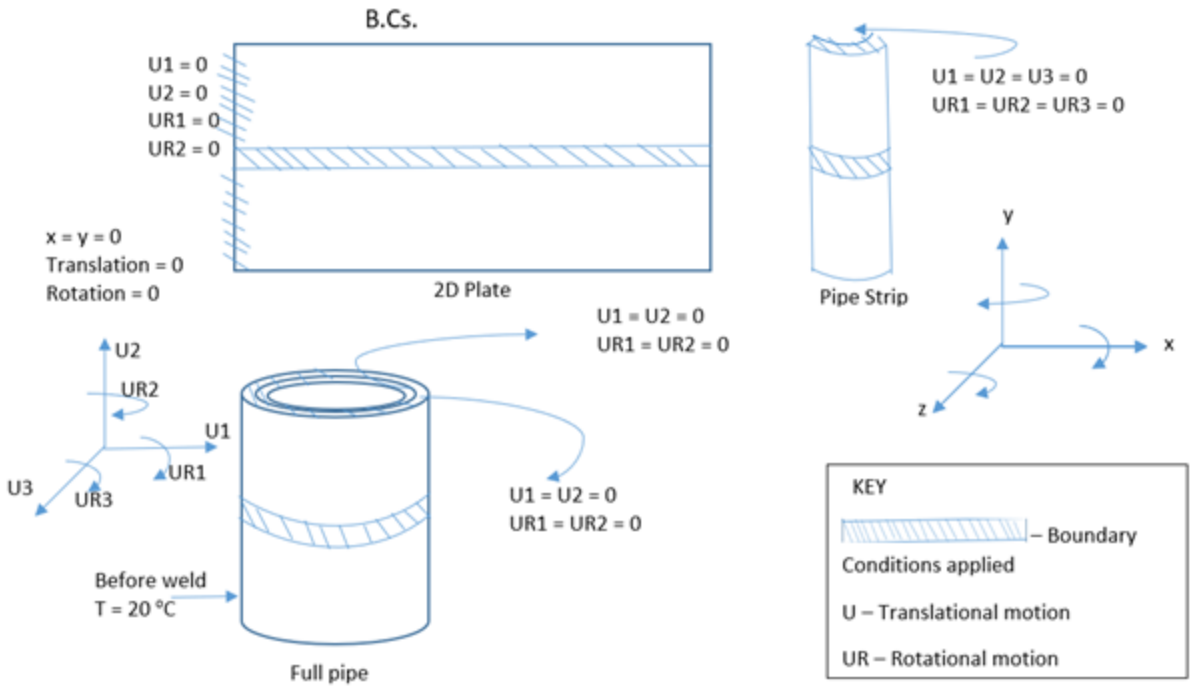

Figure 5.5 Schematic of the Boundary Condition

For the structural analysis, the boundary condition applied is at the boundaries, which denote the effect of the clamping of the cylinders in place for the welding procedure. This implied that all the nodes at the end of the pipe are fixed in the axial direction, as well as two other nodes being fixed and situated at 180 degrees from each other, also in the axial, radial and circumferential directions.

In order to obtain an accurate result, a 'Complete Newton Raphson' iterative solution technique is utilised incorporating a sparse matrix solver for both thermal and stress analysis. The reason for the choice of the Full Newton-Raphson solver is its ability to incorporate a modified material properties table alongside a stiffness matrix which reformulates after each equilibrium iteration. The typical nature of both stress and thermal models is that a huge quantity of temperature dependent data is utilized across the choice of material which changes rapidly in the course of the analysis. As such, the Newton Raphson scheme generates correct results for the analysis output compared to Initial Newton Schemes or Modified Newton Schemes. For the different weld scenarios considered in this research, the emissivity values were taken to be 0.1.

5.6 Meshing

Mesh sensitivities were carried out and 3D Stress elements were chosen from the family, and quadratic elements were used to carry out the meshing in the pipe, whereas an 8-node quadratic block was used for the Plates. The meshing parameters employed in the stress analysis is stress specific in order to speed up the mapping of the nodal data and elements having same topology to improve the convergence during structural analysis. The creation of an element occurs at the solidification temperature, whereas the melting temperature (sink) or ambient temperature is that at which the thermal strains equal zero for thermal expansion coefficients of the base

metals and filler metals. The hourglass control used in the meshing element is to enable a single point reduced integration scheme and to regulate convergence, hence preventing unnecessary locking while running the stress analysis.

Plane stress was used, and linear geometric order was used to mesh the 2D plate generating a total of 59,192 nodes and 58,695 linear quadratic elements of type CPS4R. Figure 5.6 below shows the meshing of the pipe strip using linear hexahedral elements of type C3D8R having a total number of 14742 elements and 18256 number of nodes. Family of mesh is 3D stress; the Element Library is standard and Geometric order is linear. It is an 88-node linear brick with reduced integration and hourglass control.

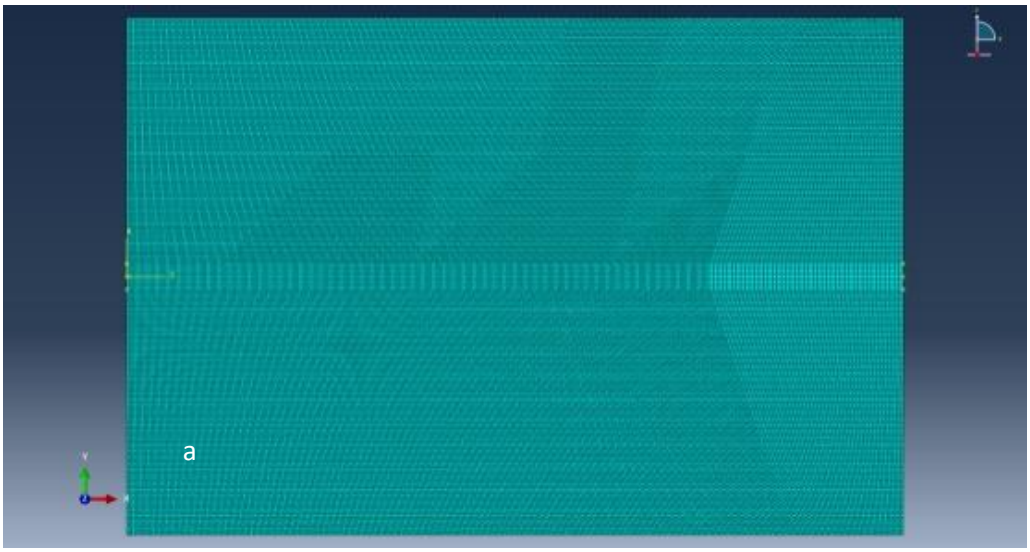

Figure 5.6 A 2D Plate showing a 4-node bilinear plane stress quadrilateral, reduced integration, hourglass control (CPS4R)

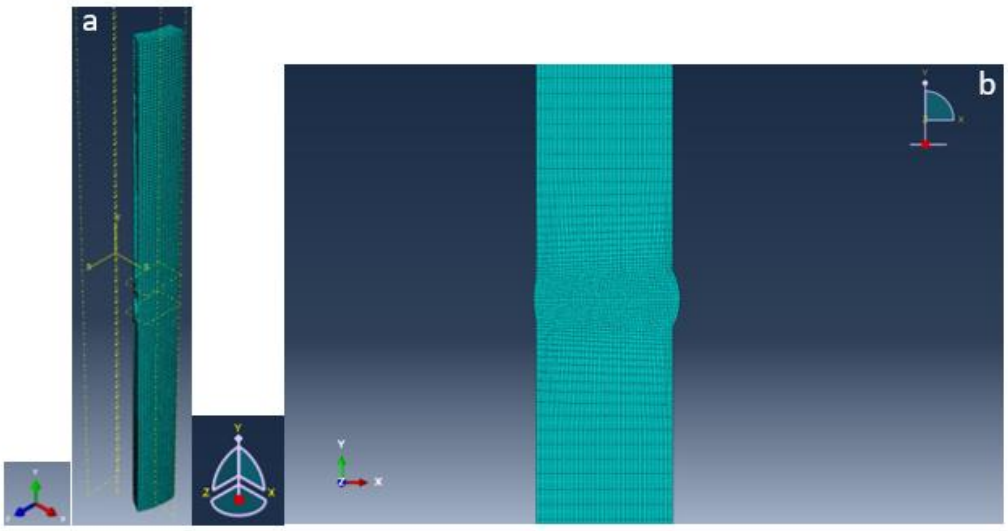

Figure 5.7 A pipe strip using linear hexahedral elements of type C3D8R (b) An Asymmetric pipe showing quadratic quadrilateral elements of type CAX8R

For the 2D axisymmetric pipe in Figure 5.7, the axisymmetric stress was used in carrying out the mesh and an 8-node biquadratic axisymmetric quadilateral of reduced integration was generated. Total number of nodes were 61, 409 and 20176 quadratic quadilateral elements of type CAX8R was generated.

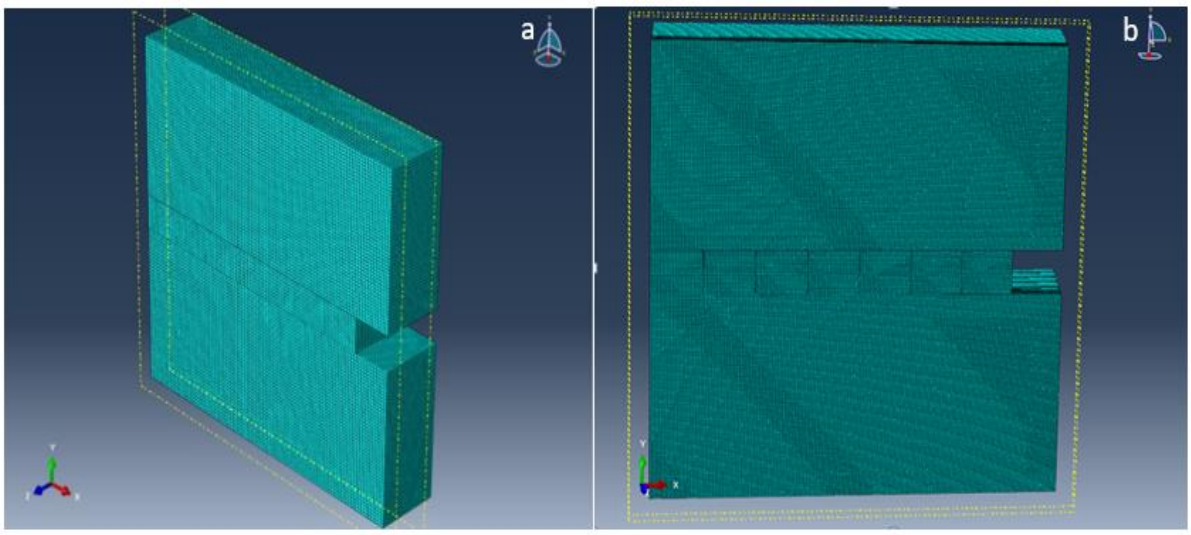

Figure 5.8 (a) A 12mm Clad Plate showing an 8-node linear brick reduced integration, hourglass control (b) A 2mm Clad Plate showing linear hexahedral elements of type C3D8R

Figures 5.8 is a meshed 3D 2mm clad plate which contains a total 600735 nodes and 561904 linear hexahedral elements of type C3D8R (An 8-node linear brick or reduced integration and hourglass control). The family is 3D Stress; element library is standard with a linear geometric order.

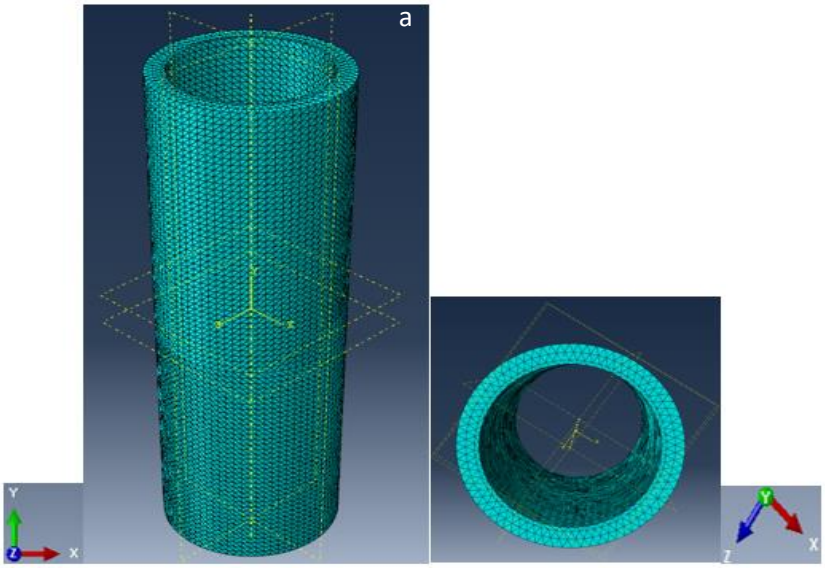

Figure 5.9 A full Clad Pipe showing quadratic tetrahedral elements of type C3D10 in (a and b)

For the fully clad pipe, as shown in Figure 5.9, the element type for cylindrical is C3D10, a 10-node quadratic tetrahedron with the total number of nodes at 222,449 and the total number of elements being 148,918. An element of type C3D10 is a 10-node quadratic tetrahedron. The element type used in this mesh is Tet. The family is 3D Stress, and the element library is standard. It has a quadratic geometric order.

The cross-sectional view of the end of the pipe in Figure 5.9 (b) clearly reveals Triangular meshes. Triangular meshes were employed because they are very good for irregular shape and random meshing. They are usually the best method to use for meshing the corners of the circular surfaces of the pipelines. Other meshing types do not give good result for corners of circles. In order to obtain good result from the corners of the cladded pipe, triangular meshing

was employed. It is also convenient to operate manually by changing the type of mesh to different type. Abaqus FEA by defaults uses triangular meshing for geometry such as circular surfaces.

5.7 Results and Discussion

5.7.1 Residual Axial Stress

Considering the residual Stress along S13 Direction (that is the x-axis) as depicted by the arrow in the FEA simulation below; the axial (longitudinal) stress across the length of the plate is shown in the graph below. This further compares to the residual stress analysis of the outer pipe carried out by Sinha and Co. in (Sinha et al, 2013)**.** Deformation refers to an alteration in the size or shape (appearance) of an object as a result of the application of energy. In this case the heat is transferred. In some other cases, the forces could be mechanical and sourced by compressive forces or pushing, torsion or bending forces and shear or even tensile forces responsible for pushing. It is also known as strain.

In the thermal analysis, heat is being applied to the body, pipes and plates resulting in mobility of grain boundaries, line and screw dislocations, point vacancies, stacking faults and twins in both crystalline and non-crystalline solids. The displacement of these defects is triggered thermally, hence hindering the rate of atomic diffusion. For deformation to occur, intermolecular forces within an object or body resist such external forces. If the forces within is great, the body assumes a new state of equilibrium and returns to its original shape. If the applied forces overcome the internal, deformation sets in.

5.7.2 Residual Axial Stress in 2D Plate

This is the stress distribution in a single plate across the weld direction at heat pass 2 in Figure 5.10. Considering the residual stress along x-axis as depicted by the coordinate arrow in Figure 5.10; the axial (longitudinal) stress across the length of the plate after second pass weld is shown in Figure 5.10. The results clearly show that the maximum residual stress occurs at weld zone where the weld meets the parent metal from both sides. Interestingly, the stress at the edges of parent plate is in tensile while in the centre of the welding zone the stress is in compression. It means the stress sign in the middle of the welding pass is negative and at the edges of the welding pass where it meets the parental plate are positive. Similar trend of stress distribution is observed in Figures 5.27 b.

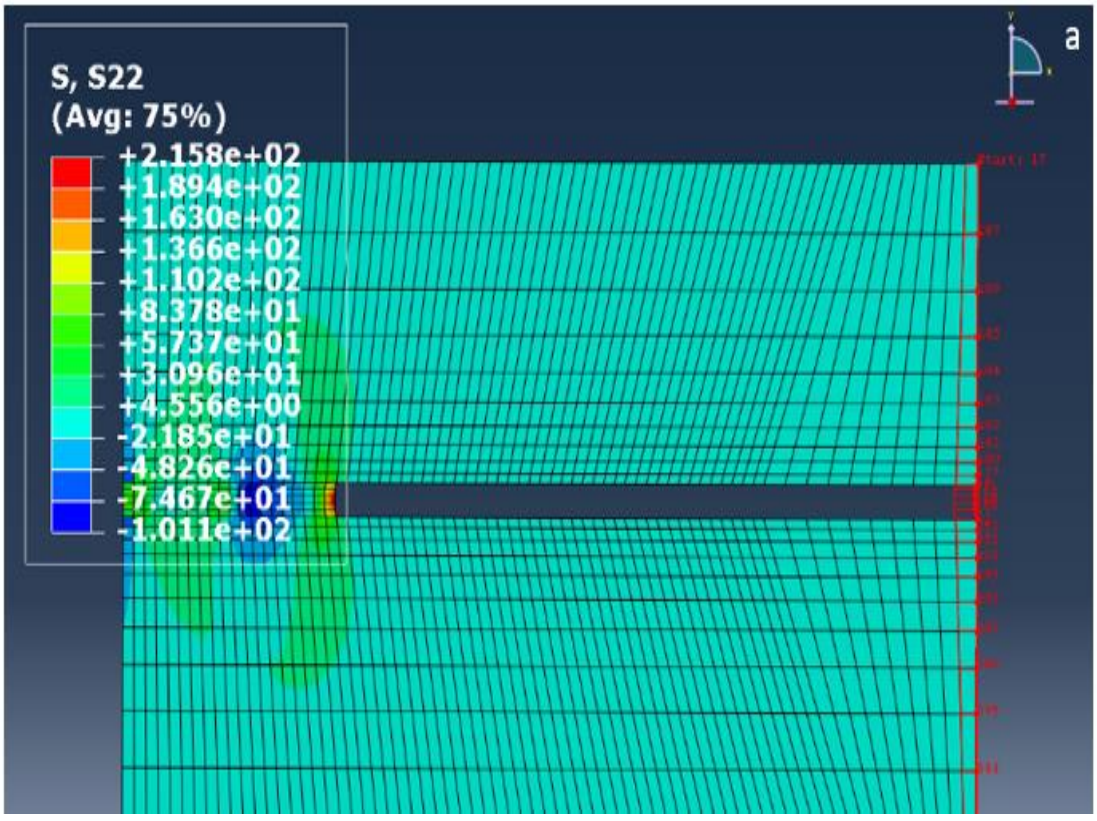

Figure 5.10 Stress distribution across the weld direction of 2D plate

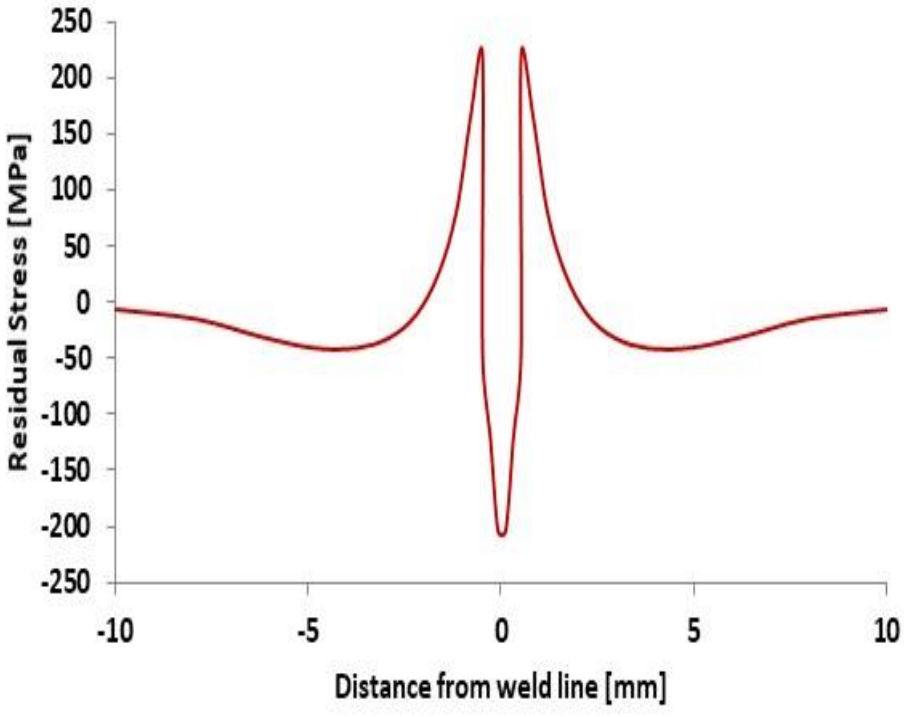

Figure 5.11 Residual stress curve of 2D plate

To validate the numerical simulation obtained in this study, a comparison made with the work carried out by (Sinha et. al., 2013) in chpater 2, is carried out. As a result of residual stress a deformation on the plate at the vicinity of the weld zone appears, of which the size or appearance of the deformation has a link with the application of energy resulted from the welding heat. It also may appear as a result of a forces (energy) generated during welding process. This force could be sourced for compressive forces or pushing, torsion or bending forces and shear or even tensile forces responsible for pushing. It causes strain on the specimen.

The reason for the stress profile in Figure 5.11 from experimental perspective is that thinner girth welded plates display more local inward deformation which is sourced from the combination of shrinkage effect on cooling of the weld metal and reduced stiffness of the thinner pipe. Deformation results in local bending inwards and hence tending towards tensile axial stresses on the surface of the plate. It is suspected that the displacement of these defects is triggered thermally, hence hindering the rate of atomic diffusion. For deformation to occur,

intermolecular forces within an object or body resist such external forces. If the forces within is great, the body assumes a new state of equilibrium and returns to its original shape. If the applied forces overcome the internal, deformation sets in or will likely take place.

Tensile stresses which are positve are seen in the 2D plate stress distribution in Figures 5.11 and also and compressive stresses in middle occur in the vicinity of the weld region, whereas farther away from it are the tensile stresses. There is no failure since the yield stress is not exceeded. Although when temperature rises, the yield stress is redueced, the value of the residual stress for the 2D plate is still within safe value.

The stress results obtained from experimental work and the simulated result have been compared in Figure 5.11 and 5.12. The simulated result has been computed with butt-welded plate done by Anderson, and Sheng and Sheng & Chen results and ultrsonic rsidual stress measurement carried out by (Javadi et al, 2012).

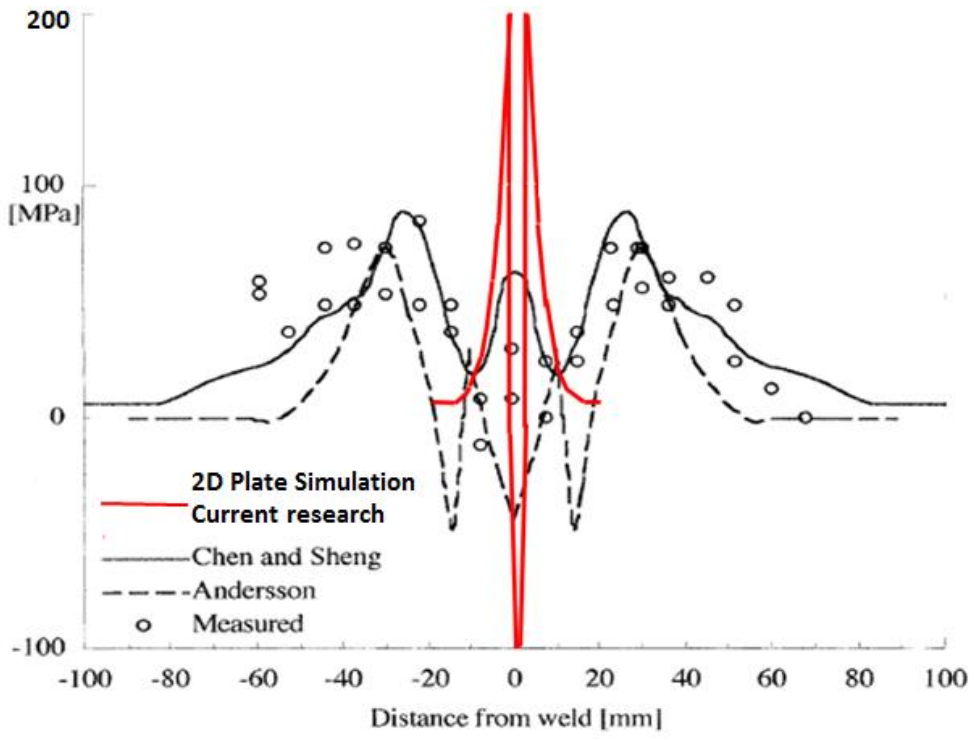

Figure 5.12 Transverse stress in a Butt-welded plate courtesy of Anderson Sheng and Chen, measured and simulated (current research) transverse stress in a plate

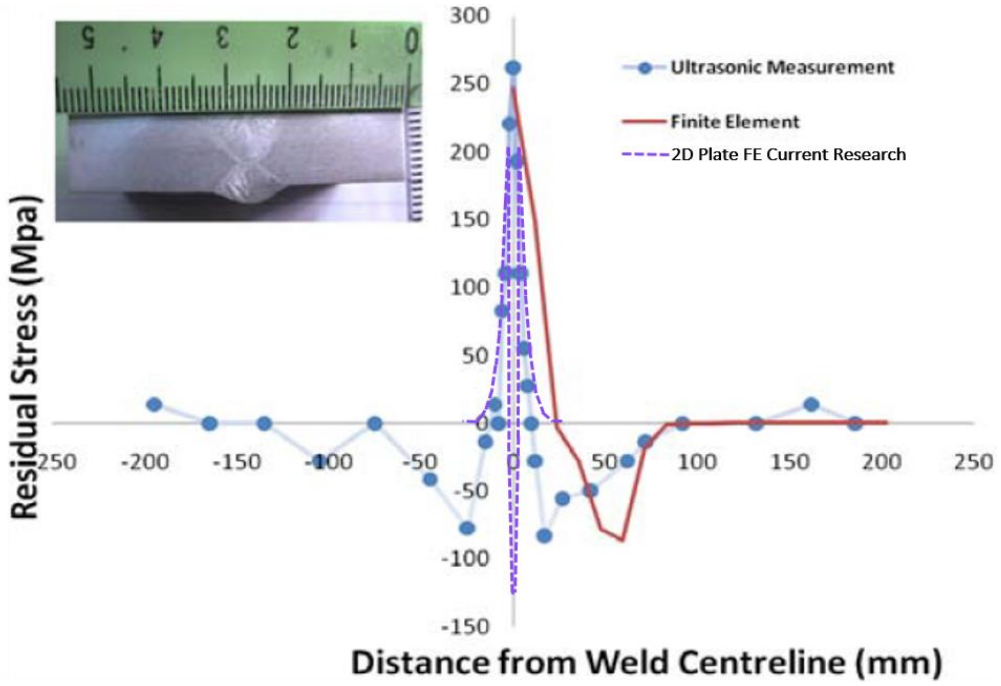

Figure 5.13 Residual stress in a Butt-welded plate courtesy of Javadi et al – Ultrasonic Measured, FE and simulated (current research) in a plate

5.7.2.1 Validating Stress in 2D Plate

In order to validate the stress models obtained from simulation, the Anderson and Sheng and Cheng model of residual stress is used as a refernce. From Anderson and Sheng and Cheng model of residual stress in a plate, the compressive stresses occur in the vicinity of the weld region whereas farther away from it are the tensile stresses. The maximum value of the tensile stress being 75 MPa and those of the compressive being 50 MPa. The straight lines are the transverse residual stresses simualted by Chen and Sheng, whereas the dotted curves represent those from Anderson's. The measured resisdual stress are those represented by tiny circles. The red-dotted line in Figure 5.11 represents the residual stress simulated in the 2D. It is shaped in distribution like that of the Anderson stress in the sense that the compressive stresses below the weld crown are shaped like a 'W' whereas the tensile stresses above the weld crown are 'M' shaped. Secondly, the value of simulated stress compared to those found by Anderson's

shows a difference. The difference in weld modelling parameters, dimension of geometry, and material property (such as yield strength, Young's Modulus) accounts for this difference in stress value. The dimesions of their plate is 100 mm in width compared to the dimension used in this research, 20 mm as depicted by the distance from weld. However, there is no failure since the yield stress of 357 MPa, is not exceeded. Although when the temperature rises, the yield stress is reduced and the value of the residual stress for the 2D plate is still within safe value.

When comparing the results of Anderson, Sheng and Cheng with the residual in Figure 5.11, it can be seen that compressive stresses occur at the vicninty of the weld, whereas at a distance farther away from the weld region, tensile stress occur. This proves the validity of the simualated results. Similar trend is observed for the Ultrasonic measured residual stress in Figure 5.12, having similar magnitude of residual stress in the range of 200 MPa when compared to 220 MPa. The difference in the width of the stress distribution is as a result of the dimension of 20mm width for the current FE research as compared to the 400 mm width employed in Javadi et al.

This and other parameters have been checked alongside the weakness of the research and that of the boundary condition of Yao Ren and those available in literature. These features have been highlighted and addressed. The reason for the inconsistencies – the width of the block used is as a result of the difference in the thickness and geometry of the models. Despite the comparison of these results, it will be proper that similar dimensions are employed in the future for ease of comparison with the exact dimensions of the model.

For some limitations, the full model of all the authors were not considered because they had different dimensions of their models. The main point and focus of the comparison made is that for the FE model, the result is similar in stress distribution, trend and magnitude in some cases.

5.7.3 Residual Stress in 3D Plate

The highest stress is observed at the HAZ. This is because when the HAZ gets cold, the weld zone is soft (molten) and can consequently readjust the stress within it, which is restricted by the already solidfied HAZ. The trend for the residual axial stresses reveals a closed analogy with past authors/ research. The high residual stress peaks observed in this research are as a result of the different material properties – mechanical properties such as high yield stresses for the base metal and weld, geometry and heat source parameters. The high yield stresses in the filler metals as discussed in Chapter 3 subsection 3.10.2 – Results, agrees with these results.

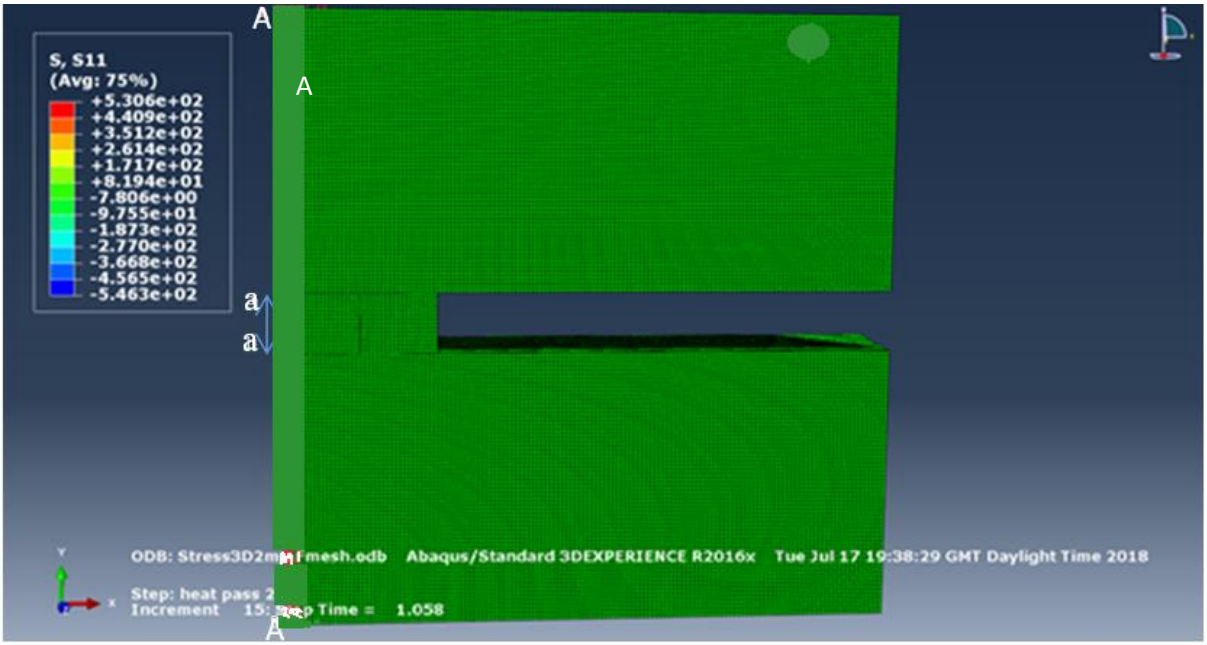

Figure 5.14 Residual Axial Stresses for 3D plate, A is edge of Plate while ‘a’ is weld zone

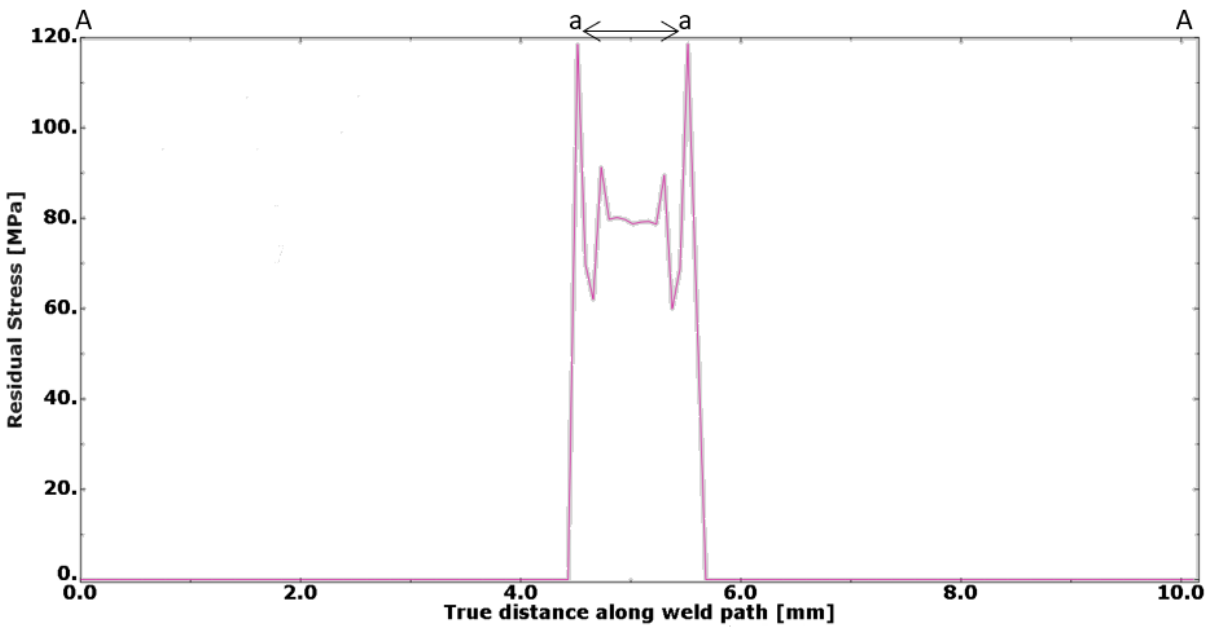

Figure 5.15 Residual Axial Stresses curve in S11 direction for 3D plate. Points A and 'a' corresponds to edge of Plate and weld zone respectively

Figure 5.15 shows the residual stress distribution in a 3D plate. The high residual stress peaks observed in this simulation are in agreement with those of the high yield stresses in the filler metals as discussed in Chapter 3 Table 3.7 under subsection 3.4.2 – Tensile Tests because the yield stress is not exceeded.

It was known from tensile and hardness tests that filler metal was overmatching parent material,

therefore, assignment of literature material properties to the weld region could be one of the reasons why the predicted residual stresses in weld region showed lower accuracy than that of parent metal. The reason for the kink observed at the sharp corner of the HAZ in Figures 5.14 – 5.16 is because the stress component parallel to the interface between two different materials is discontinuous across the interface due to the difference in the elastic and thermal properties across the interface. However, the stress component perpendicular to the interface between two different materials is continuous across the interface, and the direct strain parallel to the interface is continuous across the interface. The axial residual stress is parallel to the HAZ/weld metal interface and parent metal/HAZ interface, thus there is bound to be a stress

jump (or discontinuity) in the stress at these interfaces since the parent material, HAZ and weld metal all have different elastic and thermal properties.

A considerable effect of varying the position along the weld path is observed on the distribution of the residual stress field. The farther the position from the weld start axis, the higher the residual stress. The stress zone of influence that is the axial distance from the weld line over which the residual stress extends is a vital parameter for improved structural integrity. Smaller zone of influence is desirable in most of the engineering applications. From larger zone of influence for the residual stress is shown for the stress field on the plate surface. The zone of influence increases with increase in weld path from path 1 to path 2. For example, in the 3D Plate in Figure 5.15, an increase of 480Mpa in tensile stress fields on plate surface is observed in the weld zone and 475 MPa at the HAZ region. These higher magnitude stresses are attributed to the increased bending for larger weld path.

In addition to temperature and pressure redistribution which causes the increase in the stress distribution at the HAZ, the addition of filler material was modelled by de-activating and re-activating the elements that represented each pass. All passes were defined with the corresponding weld metals which were present in the model at outset, and all the elements in the weld region was deactivated before initiating the first heating step. The deposition of the weld metal was achieved by activating the elements defined for each pass, which were isolated from the previous passes.

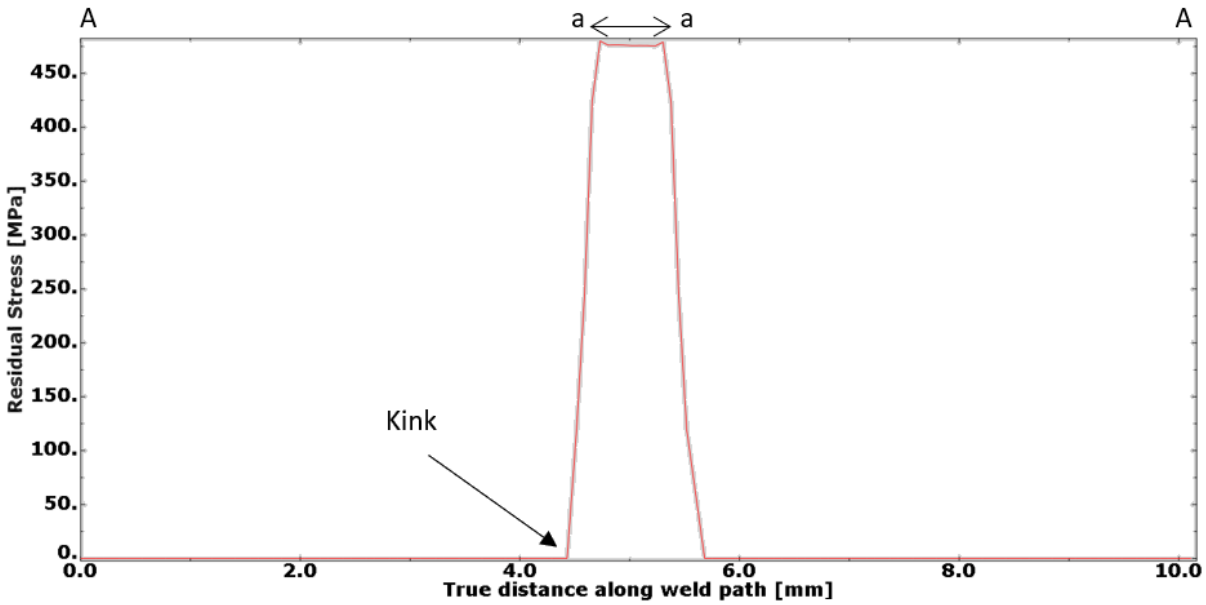

Figure 5.16 Residual Axial Stresses curve in S22 direction along the weld direction for 3D plate Points A and 'a' corresponds to edge of Plate and weld zone respectively.

The residual stress profile corresponds to the fact that compressive stresses are symmetric across the weld line and in and around the Fusion Zone and HAZ. It is of the order of 35 MPa from the curve although the simulation records a high stress of 233 MPa, which when compared with the yield stress of 357 MPa is still less within the safe margin of the stress. The reason for the kink observed at the corner of the stress distribution is due to mesh not being fine enough or because of the boundary condition being fixed, however this does not change the pattern but change the value locally.

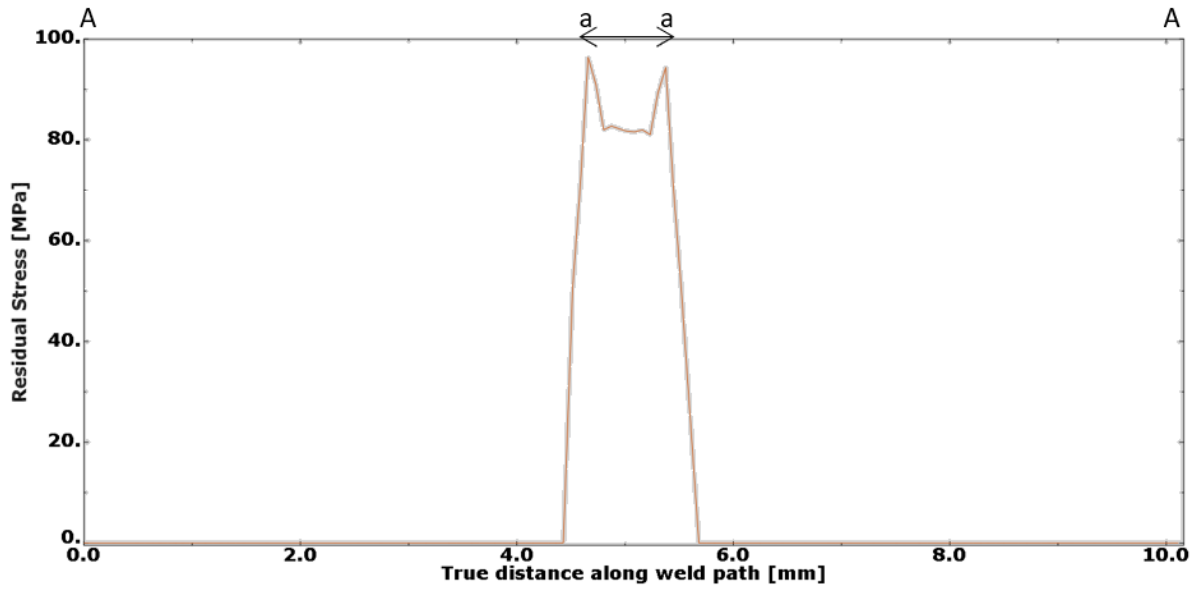

Figure 5.17 Residual Axial Stresses curve in S22 direction along the weld direction for 3D plate
Points A and 'a' corresponds to edge of Plate and weld zone respectively

From the simulated model of the 3D Plates, the residual stress value goes as high as 120 in Figure 5.15 and 450 MPa in Figure 5.16 at heat pass 1, time step 0.2969 seconds and reduces to 100 MPa at step time 0.5586 seconds in Figure 5.17. These values are reasonable when compared to the yield stress of the material coupled with the fact that the yield stress is not exceeded. The residual stress curve, however, reveals compressive stresses having negative values.

5.7.4 Residual Stress in Pipe Strip

As discussed in Chapter 1, the pipe strip model was developed and the residual stress across the length of pipe strip (axial or longitudinal stress) both internal and external surface, the residual stress distribution along the weld zone internal and external were also determined and the results displayed in Figures 5.18 – 5.23.

5.7.4.1 Residual Axial Stress Distribution on Outer surface of a Pipe Strip

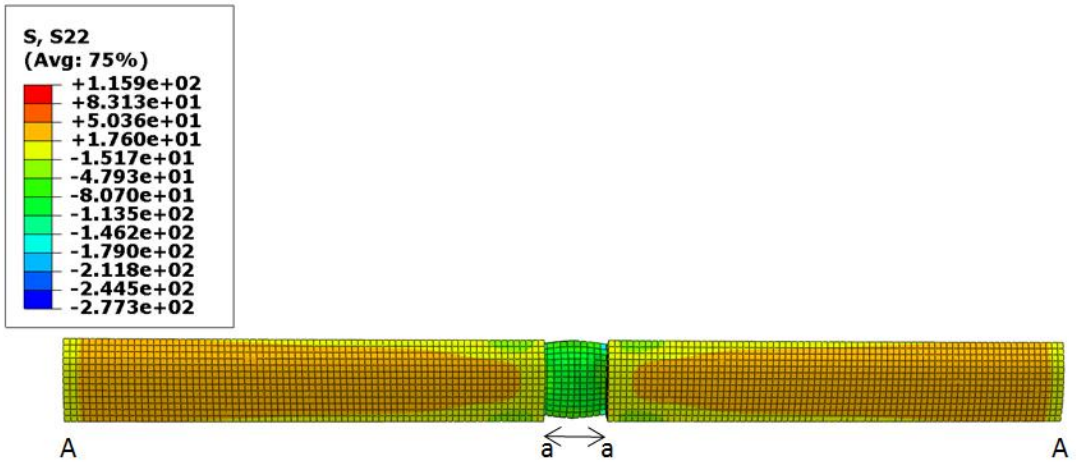

Figure 5.18 Axial stress distribution on the outer surface of pipe strip

The yield stress is 357 MPa, which is greater than the residual stress value of 115 MPa as seen in Figure 5.18. The residual stress is less than a third of the yield stress, which implies the value of the residual stress is within safe measure and not causing any material failure.

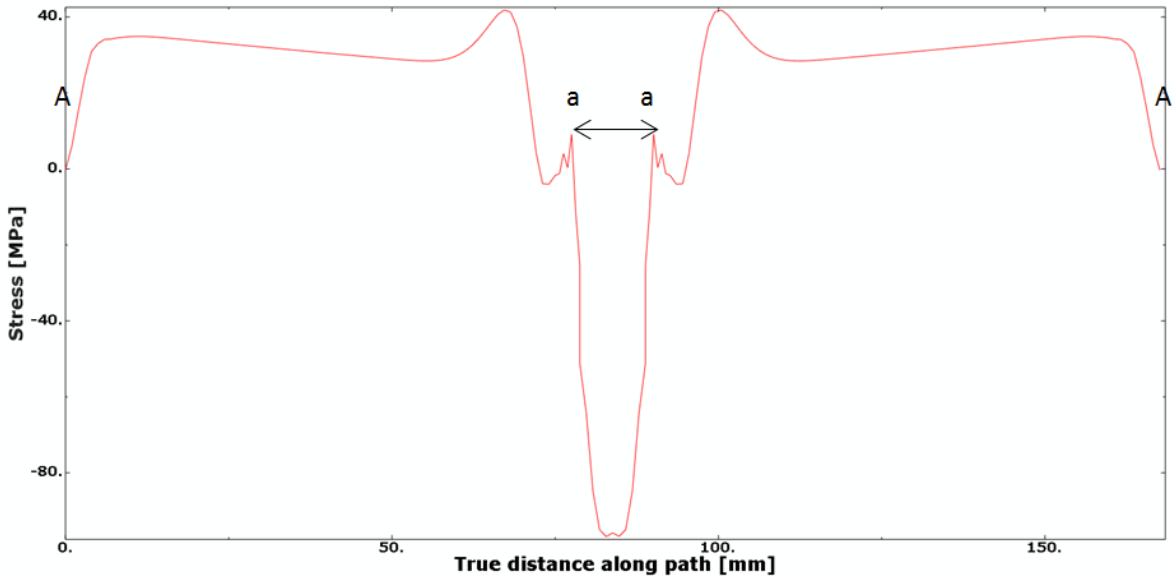

Figure 5.19 Residual Axial stress curve for the outer surface of the pipe strip

The reason for the reduction in the stress value in Figure 5.19 is as a result of the temperature and pressure redistribution across the weld zone and parent metal. Initially, the ambient temperature, is 20 ^{o}C, while the weld temperature is 1500 ^{o}C, this difference in temperature affects the stress value. From the residual stress distribution curve, at the ambient temperature, the yield stress is 357 MPa, however, as the temperature increases, the value of the yield stress decreases. This implies that at 200 ^{o}C, the value of the yield stress reduces by 20% as a result of transient heat (and not its steady state), and thus becomes 285.6 MPa. It was known from tensile and hardness tests that filler metal was overmatching parent materials, therefore assignment of literature material properties to the weld region could be one of the reasons that the predicted residual stresses in weld region showed lower accuracy than that of parent metal. Similar trend of stress distribution exists between the outer surface of the pipe strip and the outer surface of the full pipe in Figure 5.27 (b).

5.7.4.2 Residual Axial Stress Distribution on Inner surface of a Pipe Strip

FE has two contingencies: The procedure in FE entails that the initial material and weld material are defined. The software defines the HAZ automatically as evident from the FE stress distribution. In order to justify experiment; result of hardness on HAZ is higher in experiment and Hardness has a relationship with stress as seen in Equations 3.9 through 3.14 in Chapter 3. The stress passing through the HAZ has been checked and found that stress in HAZ is different. According to those formula (Equations 3.9 – 3.14), stress has direct correlation with hardness. When stress decreases hardness decreases. There is a clear agreement between what is obtained in the experiment and the FE.

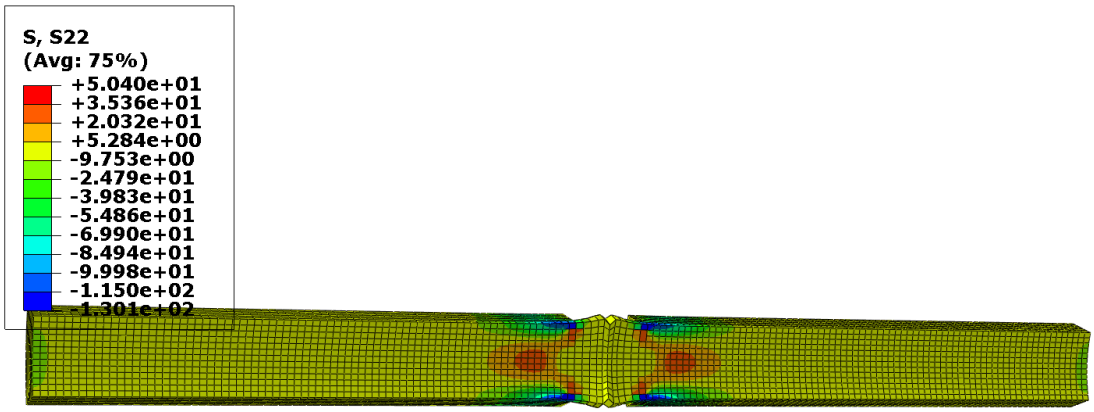

Figure 5.20 Axial stress distribution on the inner surface of pipe strip

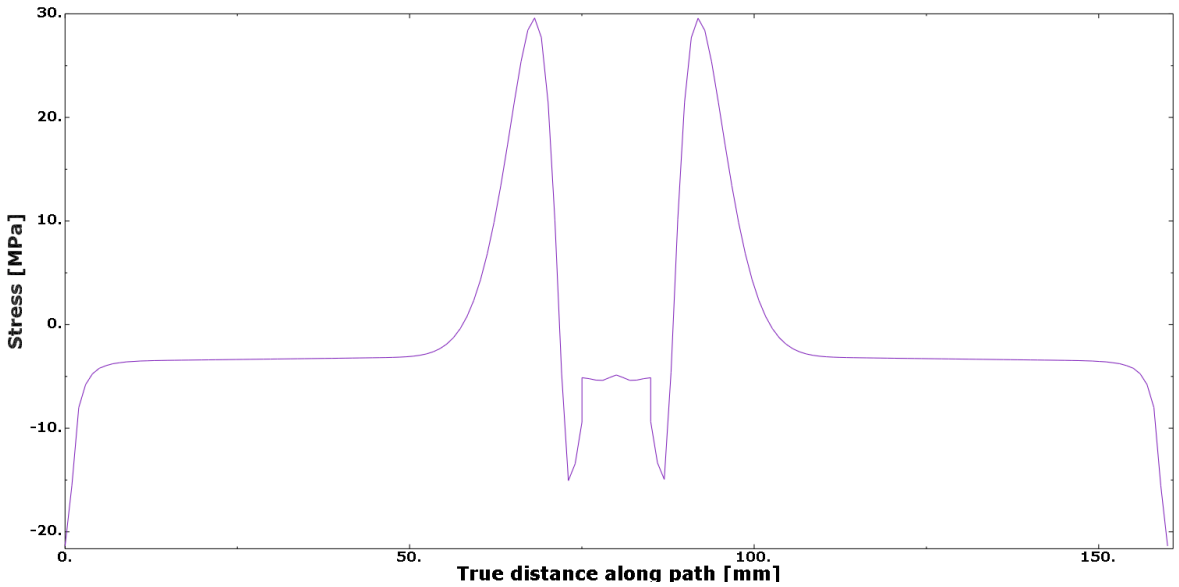

Figure 5.21 Axial stress distribution curve for the inner surface of pipe strip

Compressive stresses are symmetric across the weld line. In and around the FZ, (HAZ), stress field of great degree, are observed on the outer surface of pipe strip. Around the HAZ, there is a protuberance (hump-like) profile at the outer surface of the pipe within the region of the weld line indicating the existence of stress variation underneath the weld crown. The region of high stress exists within the Heat Affected Zone. The residual stress profile is seen in Figures 5.20 – 5.22. The maximum value of the axial residual stress field does not supersede the material yield stress. A reasonable agreement exists between the simulated values of axial stress on the

inner circumferential (surface) length of the pipe strip and the residual axial stresses on the inner surfaces of the full pipe. This can be seen in Figures 5.20, Figures 5.27 (a) and 5.28 (a), as well as findings from literature as seen in Figure 2.29 (a) and 2.33 (b) in chapter 2.

The addition of filler material was modelled by de-activating and re-activating the elements that represented each pass. All passes were defined with the corresponding weld metals which were present in the model at outset, and all the elements in the weld region was deactivated before initiating the first heating step. The deposition of the weld metal was achieved by activating the elements defined for each pass, which were isolated from the previous passes.

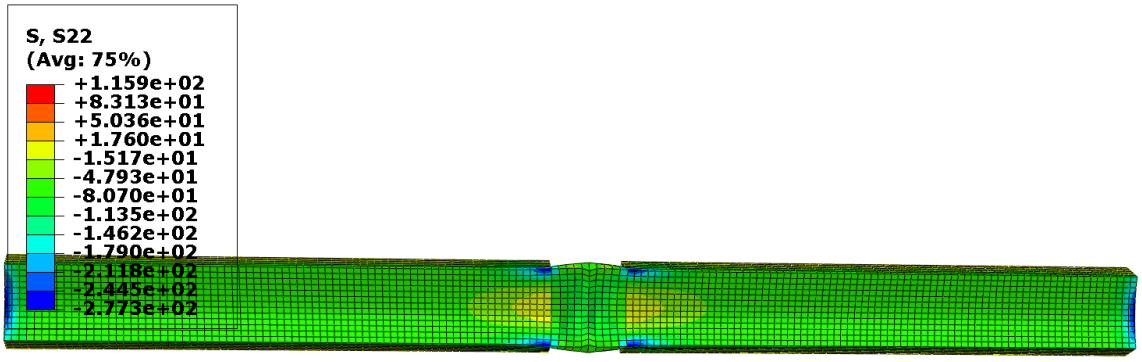

Figure 5.22 Residual stress distributions on inner surface of pipe strip

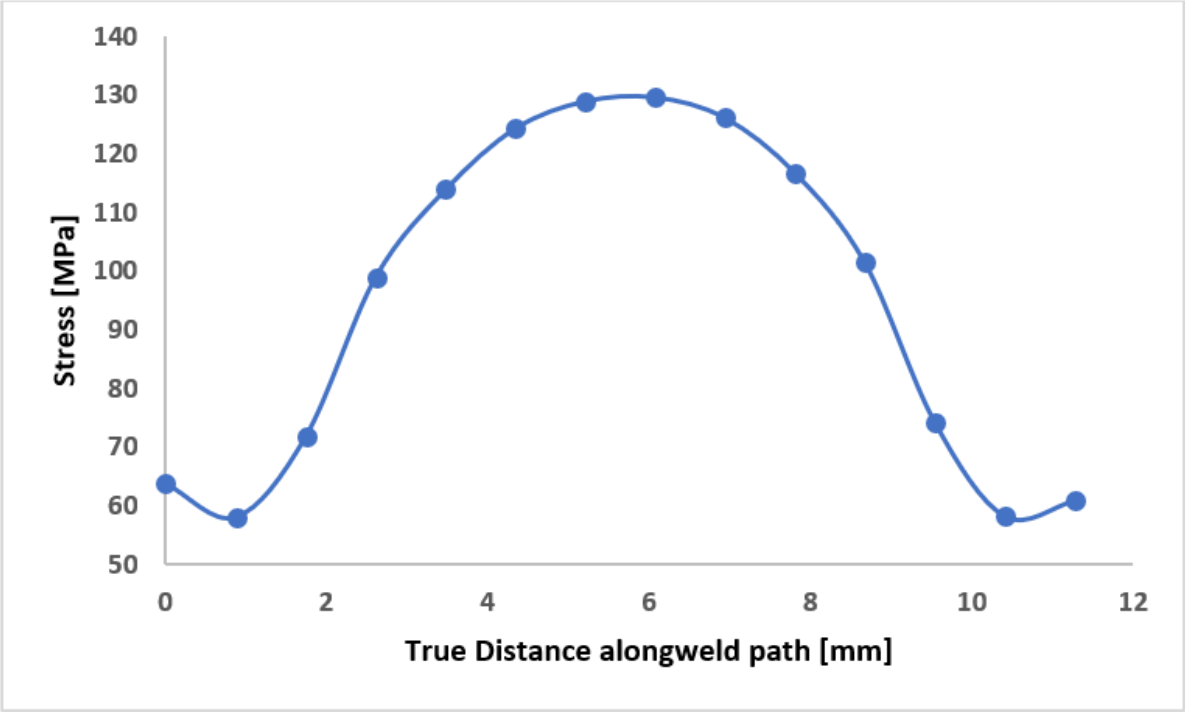

Figure 5.23 Residual (transverse) stress curve distributions on inner surface of pipe strip along weld direction

The stress distribution increases inwards from the outer circumference towards the inner circumference of the pipe strip as indicated in the Figures 5.21 and 5.23.

Careful observation of the stress distribution inside and outside of the surface of the pipe strip reveals compressive stresses are symmetric across the weld line. In and around the Fusion Zone and Heat Affected Zone, stress field of great degree, are observed on the inner surface of pipe strip. Around the HAZ, the protuberance (hump-like) profile at the outer surface of the pipe within the region of the weld line, indicates the existence of stress variation underneath the weld crown. The region of high stress exists within the HAZ. The residual stress profile is seen in Figures 5.19 – 5.22 in their self-equilibration on the graph. The maximum value of the axial residual stress field does not supersede the material yield stress. A reasonable agreement exists between the simulated values of the axial stress on the outward circumferential (surface) length of the pipe strip and the residual axial stresses of the full pipe as shown in the Figures 5.27 (b)

and 5.28 (b), as well as findings from literature, as seen in Figures 2.29 (b) and 2.33 (a) in chapter 2.

5.7.5 Residual Stress in Full Pipe

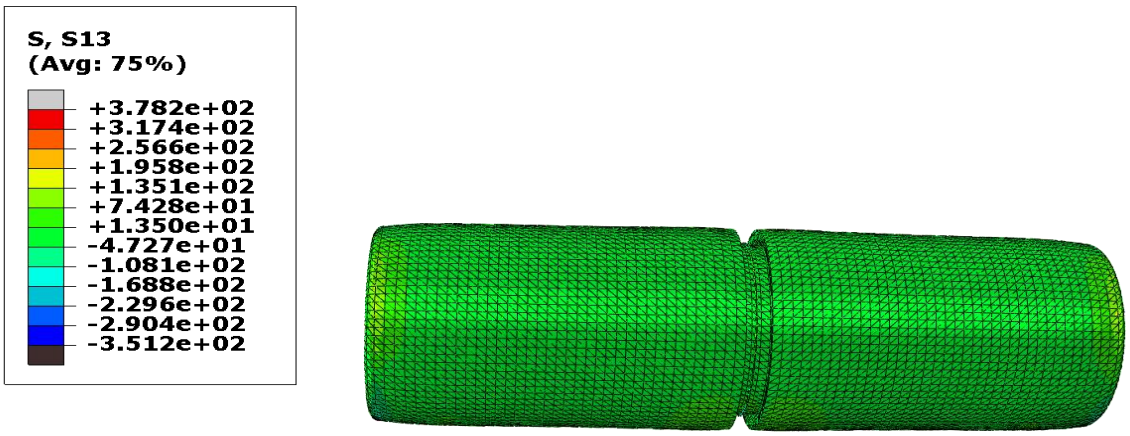

Figure 5.24 A typical FEA model showing stress in cladded pipe

5.7.5.1 Weld Direction (Nomenclature)

Figure 5.24 shows the residual axial stress in a cladded pipe. It is important to note here that the direction considered when taking the readings from the pipes are the clockwise direction with the first reading taken from an angle of 45 degrees, as illustrated in Figure 5.25 and explained earlier in section 4.10.2 of Chapter 4. Some researchers conventionally take to the 90^o, 180^o, 270^o and 360^o, also connoted as the 3 o'clock, 6 o'clock, 9 o'clock and 12 o'clock convention. This is the order in which the axial stresses were taken – 45^o, 135^o, 225^o and 315^o.

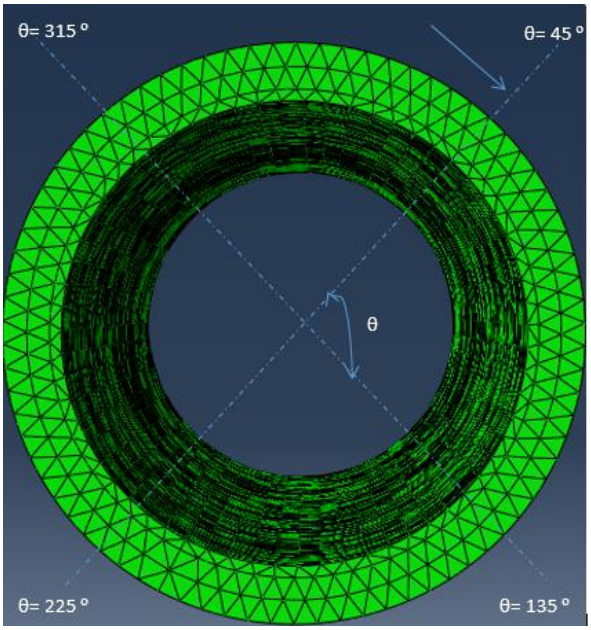

Figure 5.25 Cross section view of the pipe circumference illustrating the order of the weld direction

5.7.6 Residual Axial Stress Result for a full pipe

Residual stress differs throughout the entire length of the pipe depending on the position of the weld start and end, as well as the tack welds. From Figures 5.26 -5.27 for the residual axial stress in the cladded pipe, it is observed that close to the weld vicinity, compressive and tensile stress fields, are present in and near the section of the weld, both on the external and internal surfaces of the pipe. Furthermore, this occurrence can be credited to the varying temperature profiles without and within the surfaces of the pipe. By virtue of the thickness of the wall of the cylinder and very close to the weld line (which is represented by the vertical line), the tensile and compressive residual stress field are generated by reason of contraction occurring within the weld pipe. The residual stress curves obtained in this research is similar to that in Sinha et al (2013) in Figure 2.26 (a and b), Feli et al (2012) Figure 2.30 (a and b) and Dar et al (2009) as shown in Appendix 7 pages 338 and 339.

The differences in the values of the residual stresses are as a result of the different material properties such as yield strength for the base and filler metals, weld geometry and heat source parameters. There have been volumetric change and yield strength (as seen under tensile test curves in chapter 3 as a result of martensitic transformation which have effects on welding residual stress, by increasing the magnitude of the residual stress in the weld zone as well as changing its sign. The simulated results show the magnitude of the residual stress.

5.7.6.1 Full Pipe with 2mm Clad (2MSSS)

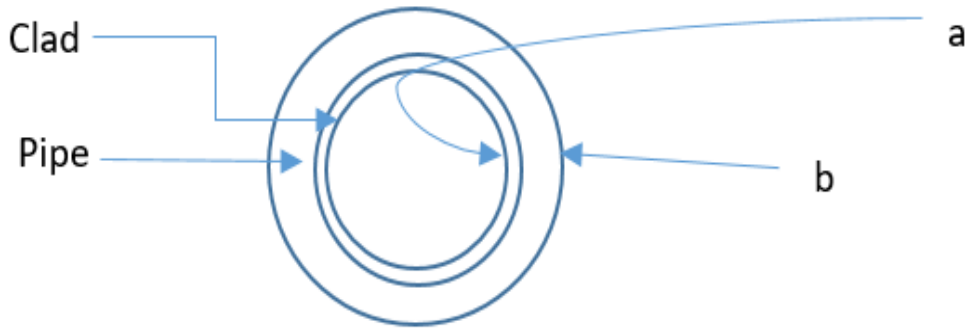

Figure 5.26 Inner and outer surfaces of the pipe – cross sectional view

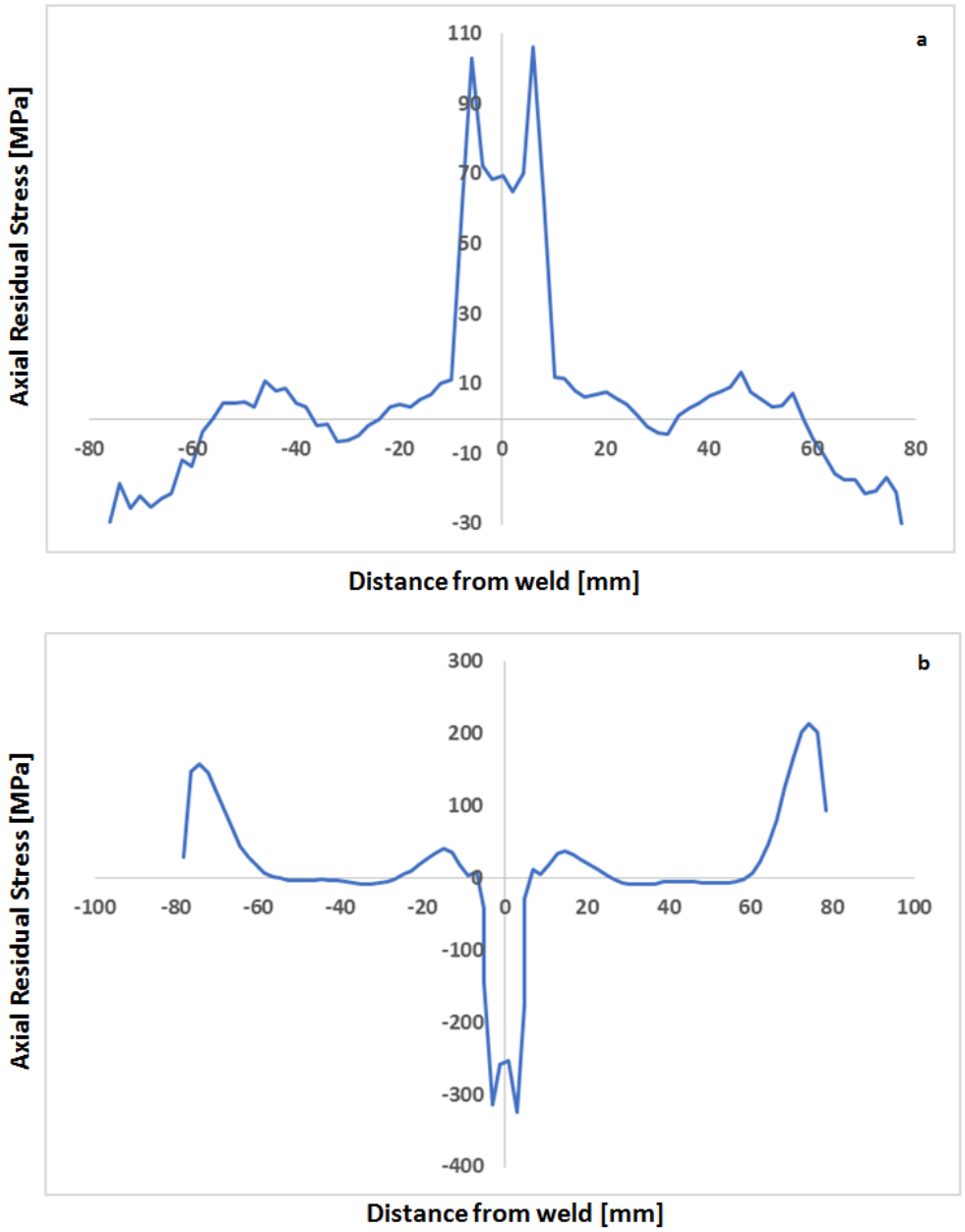

Figure 5.27 Residual axial stress curves for the (a) inner and (b) outer surfaces of the 2 mm clad Pipes

In the standard notation of stresses, positive stresses mean tension and negative stresses correspond to compression. Figure 5.25 shows the cross section of inner and outer surfaces of the pipe. It is important to note that for this simulation, tensile forces are observed on the inside of the pipe, whereas compressive stresses are observed on the outer surface of the pipe. The compressive residual axial stresses near the weld region decreases to zero (0) after 9 mm on

both sides of the weld line WL. Farther away from this point stress reversal from compressive to tensile is observed. The low magnitude tensile stresses then approach zero at 25 mm on both sides of WL in Figure 5.26 (b) a steady value of axial stress for 60 mm away from the WL can be seen in the residual stress distribution curve.

In Figure 5.26 (a) the high order of tensile stresses close to the WL decreases to a magnitude of 10 MPa at 12mm from the WL. This same tensile stress further reduces to zero magnitude 25 mm away from the WL and reverses to lower compressive residual stresses of 5MPa at 30 mm from both sides of the WL and this distribution is observed for the inner surfaces of the cylinder at different cross sections from weld start position. This distribution of stress is the trend observed for other authors referenced in this research and in the open literature such as (Jonsson & Josefson, 1988) (Deng & Murakawa, 2006) and (Rybicki et al., 1982) See Appendix 7. Comparisons with residual stresses from the literature were carried out. As the stresses in the referred articles are provided in full values and not normalised, direct comparisons were made also in full values. This also helps a practical sense with the reference to the material yield stress.

The middle region of the weld which is the HAZ reveals high tensile stresses to the order of 110 MPa on the inner surface of the pipe; whereas the end of the weld region of the pipe is held in a compressive stress of magnitude 10 MPa by reason of the tensile forces experienced from the surrounding region (weld envirion) which solidifies rapidly after weld. Compressive stresses to the magnitude of 300 MPa are observed on the outside of the pipe, while the end of the weld region of the pipe is kept in tensile stress of the order of 10 MPa. Sinha et al (2013) obtained a value of 250 MPa for the compressive stress distribution in the weld zone of their single layered pipe thickness of 2mm. There are localised stress reductions within and around the weld start/end and tract weld as observed in Figure 5.26. Further away from the weld line

and perpendicular to the weld direction, stress reversal is displayed and are not significant in the vicinity of the weld end. The weld start effect is more severe on the outer surface of the pipe compared to the inner surface of the pipe. This is potrayed in Figure 5.26 (a).

Around the HAZ, the protuberance (hump-like) profile at the outer surface of the pipe within the region of the weld line indicates the existence of stress variation underneath the weld crown. This is the region of high stress within the HAZ, and Tensile stresses are symmetric across the weld line. In and around FZ, (HAZ), the stress field to a great degree, is observed on the inner surface of the pipe. The outer pipe region of the HAZ (the compressive stresses) are symmetric across the weld line. In and around FZ, (HAZ), the stress field to a large degree, is observed on the outer surface of the pipe. The protuberance (hump-like) profile at the outer surface of the pipe (within the region of the weld line) indicates the existence of stress variation underneath the weld crown. Region of high stress exists within the HAZ.

The reason for the stress profile in Figure 5.26 (a) from experimental perspective is that thinner girth welded pipes display more local inward deformation which is sourced from the combination of shrinkage effect on cooling of the weld metal and reduced stiffness of the thinner pipe. Deformation results in local bending inwards and hence tending towards tensile axial stresses on the inner surface of the pipe.

5.7.6.2 Full pipe with 12 mm clad (12MSSS)

Tensile stresses are symmetric across the weld line. In and around FZ, (HAZ), the stress field to a great degree is observed on the surface of the pipe. For the 12 mm clad thickness, the compressive residual axial stresses near the weld region decreases to zero (0) after 10 mm on both sides of the weld line WL. Away from this point stress reversal is observed from

compressive to tensile. The tensile stresses of 140 MPa then approach zero at 30 mm on both sides of WL in Figure 5.27 (b) a fluctuation in the stress reversal is observed for the inner surfaces of the cylinder at different cross sections from weld start position up to 80 mm from the weld line on both sides of the weld. This stress reversal is known as 'creep effect', which is characteristic of the thickness of the weld section and comprise of 10m clad thickness in

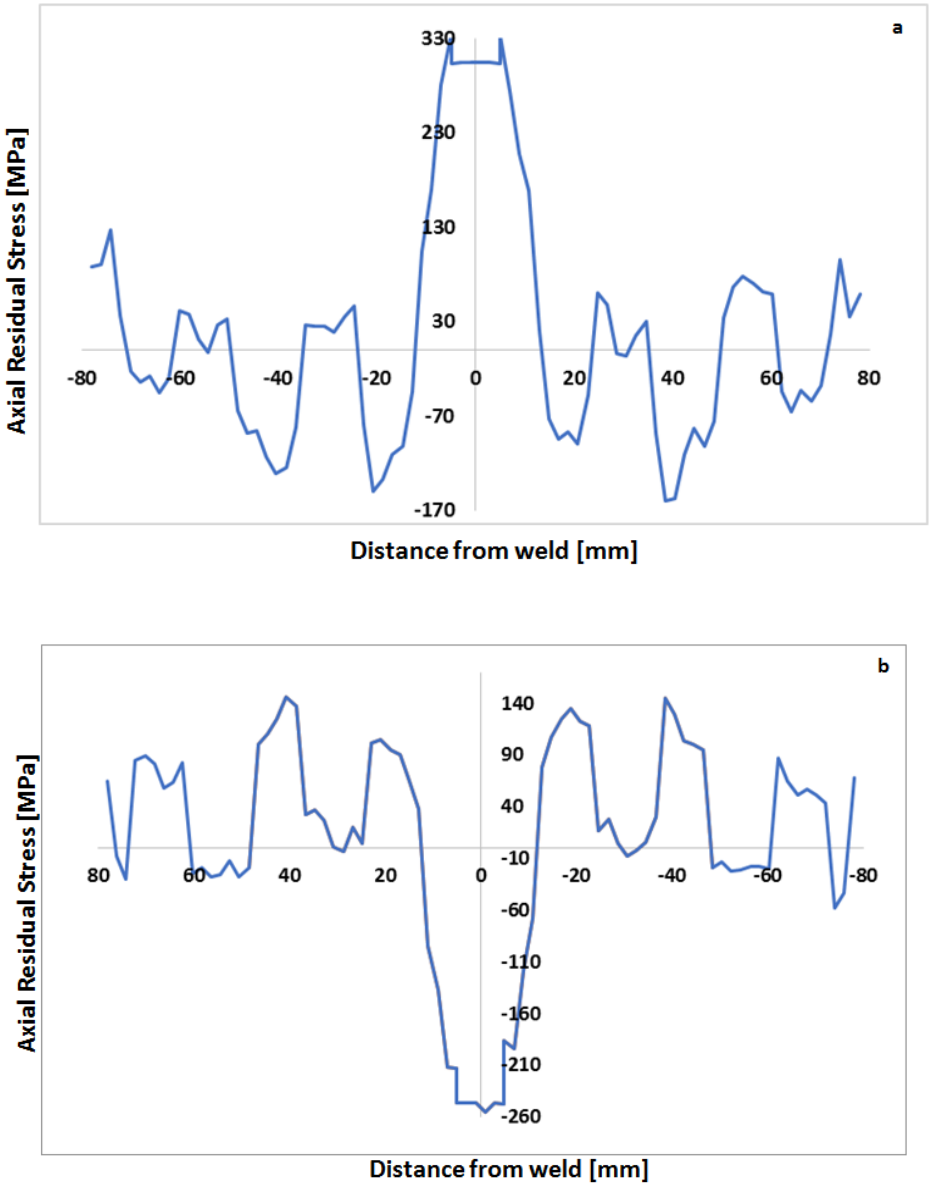

Figure 5.28 Residual Axial Stress curves on the (a) Inner and (b) Outer Surfaces of the 12 mm Clad Pipes

addition the 10 mm base metal thickness. However, there are no creep effects observed in the 2mm clad pipe although low magnitude tensile stresses of the order of 5MPa are observed. Creep is beyond the scope of this research and will be considered in future studies.

In Figure 5.27 (a) the high order of tensile stresses (330 MPa) close to the WL decreases to approximately 0 MPa at 12 mm from the WL on both sides of the weld line. This same tensile stress further reduces to a magnitude of 150 MPa at 20 mm away from the WL and reverses to lower compressive residual stresses at 25 mm from both sides of the WL and this distribution and stress reversal is observed for the inner surfaces of the cylinder at different cross sections from weld start position. This distribution of stress and stress reversal is referred to as 'Creep effect' and is as a result of the thickness of the cladded pipe walls. This further proves the relationship between pipe thickness of dissimilar material weld and residual stresses on both inner and outer surfaces of pipe and can also be confirmed from (Rybicki et al., 1982) who deduced that a relationship exists between residual stress and pipe wall thickness for only the interior of the pipe at higher thicknesses.

Thickness of the dissimilar material cladded pipe is one of the geometric parameters (such as diameter and thickness of piping connection being welded and geometry of weld grove preparation) that affect the residual stress magnitude and distribution. Since there are inherent complexities in welding processes the factors that affect the final residual stress are either categorised under geometry or press parameters. Thermal conductivity also plays a role here because the clad and base metals referred to are solids. Unlike the thermal conductivity of gases which increases with temperature as explained from kinetic theory of gases and the thermal conductivity of liquids which decreases with increasing temperature because the liquids expand and molecules move apart; the thermal conductivity of solids is such that by reason of lattice

distortions, higher temperatures make it difficult for the electrons to flow hence thermal conductivity of metals decreases.

Unlike (Rybicki et al., 1982) who experienced the greatest axial stresses in the thinner wall thicknesses compared to the larger wall thickness because axial residual stresses tend to be more compressive as pipe thicknesses increased, however in this research residual axial stresses are higher in the thicker clad thicknesses. The reason being that the greater the thickness of the clad metal, the more the plastic strain and hence the deformation increases (inducing greater residual stresses on the structure) - in order to balance out (relax) some of the residual stress strain (Jiang et al., 2011).

Throughout the length of the 12 mm clad pipes, there are highly fluctuating stress patterns transverse to weld direction that is in the axial direction. There are localised stress reductions within and around the weld start/end and tract weld as observed in Figures 5.27 (a) and (b). Further away from the weld line and perpendicular to the weld direction, stress reversal is displayed along the margin. Compared to the 2 mm clad thickness, it is observed that the thickness of the pipe wall significantly affects the residual stress distribution in a butt-welded pipe.

This oscillatory effect is due to the relatively coarse mesh pattern of the 3D pipe model. The reason the coarse model was chosen was to limit to excessive computational load. The reason for the oscillation of results in residual stresses is because from the simulation, the results from the elements and nodes and are not exactly the same – as a result of the nature of finite element. The noise and oscillation can be filtered; however, the oscillation has not been out of range in the analysis.

The oscillatory values are numerical noises because the element mesh is not optimised, which may require further improvements such as the need for further refinement a coarse mesh; or

contacts between the pipes. Looking at the highest residual stress value, it goes reasonably with the experiments. The highest stress is the most significant. The highest positive stress location is the point of crack initiation. Highest stress value is correct, and the main target is to find out where the crack may appear, and this is informed from the highest point of stress.

Also keenly observing Figures 5.26 and 5.27, it can be seen that increasing the clad thickness and hence the effective wall thickness of the pipe increase the residual stresses unlike the finding obtained from (Rybicki et al, 1982). Increasing the clad thickness and subsequently the pipe wall thickness enlarges the zone of influence of the residual stresses farther away from the weld centre line. Deformation is due to Weld metal shrinkage and stiffness of local pipes precludes localized bending deformations, there are creep effects observed for larger clad thicknesses.

In the vicinity of the weld zone and the HAZ, the protuberance (hump-like) profile at the outer surface of the pipe within the region of the weld line indicates the existence of stress variation underneath the weld crown. Region of high stress exists within the HAZ. The compressive stresses are symmetric across the weld line. In and around the FZ, (HAZ), the stress field of great degree, are observed on the outer surface of pipe.

5.7.7 Validation of Axial Stresses in 2MSSS and 12MSSS

From Figure 5.29 the results of the axial, radial and hoop stresses of the Neutron diffraction were plotted against the distance from the weld central for the inner surface of the pipe. The internal stresses are tensile and there are perturbations observed under the weld crown. The maximum value of the radial stress is 200 MPa while the axial stress is 250 MPa. The hoop stress is 500 MPa. In Figure 5.29, the ND measured stresses are also plotted against the axial

stress of the 2MSSS (2 mm clad weld of dissimilar material joint) and it is observed that the value of the axial stress for the 2MSSS which is 110 MPa, is closer to that of the ND

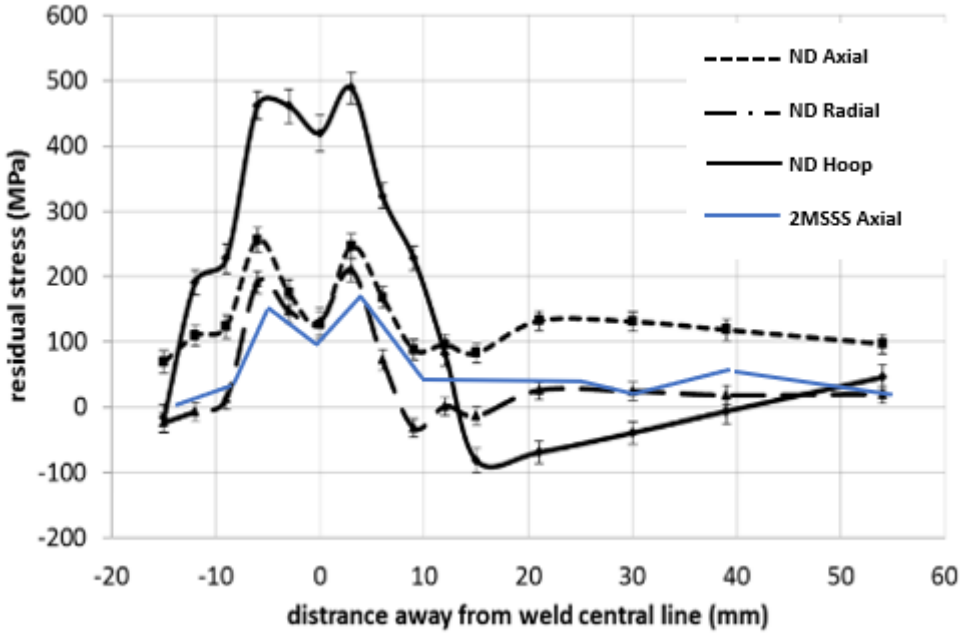

Figure 5.29 2MSSS residual axial stresses (this research) versus ND measured (Ren, 2008)

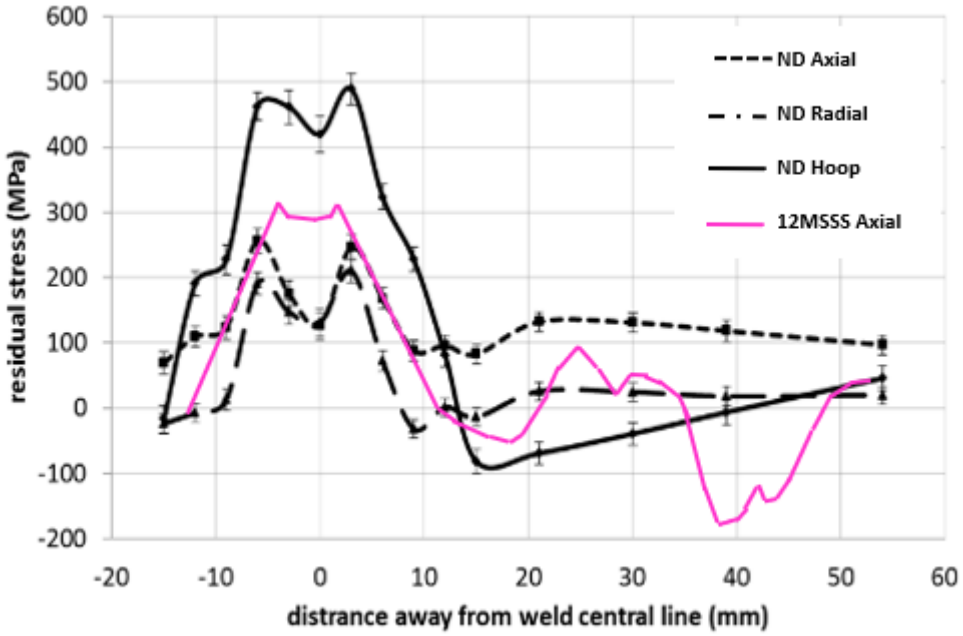

Figure 5.30 12MSSS residual axial stresses (this research) versus ND measured (Ren, 2008)

measured radial stress with a difference of 90 MPa and also comparable to the ND measured residual axial stress, with a difference of 140 MPa. In Figure 5.30, the residual axial stress in the interior of the 12MSSS (12 mm clad weld of a dissimilar material joint) 330 MPa, is comparable to the ND measured axial stress of the pipe subsurface 250 MPa with a difference of 80 MPa, hence validating the residual stress models. Both axial residual stresses of the 2MSSS and 12MSSS are compared to each other in Figures 5.29 and 5.30 and it is observed that inside the pipe surface the stresses are tensile, and the protuberance effect is observed under the weld crown. It is important to note that the yield stress is not exceeded, which means it is operating within a safe value. Other measured stresses were used to validate the simulated results obtained in this research (refer to Appendix for more details). The discussion and result of the hoop stress, radial and axial shrinkages are in the Appendix.

As explained in subsection 5.6.2.1, validating stresses in 2D plate on pages 260-261, the reason for the inconsistencies – the width of the block used is as results of the difference in the thickness and geometry of the models and the full model of all the authors were not considered because they had different dimensions of their models. The focus of the comparison made is that the result is similar in stress distribution for the FE model both in trend and magnitude in most cases. There are more validations of the residual stress distributions in the 2mm and 12 mm clad thicknesses in Appendix 7 using experimental results from open literature.

5.8 Summary and Conclusion

Different models have been developed and their residual stresses – axial and transverse have been determined. Comparisons between measured and simulated residual stresses show that to a reasonable extent there is a good agreement between measured and simulated and even literature where applicable. The 3D pipe strip model was also examined, and an interesting

trend of stress distribution was discovered. In the pipe, several reasons are responsible for the differences between the predicted and simulated, such as the estimation and errors in the measuring techniques. This will generate errors in the magnitude of the measured residual stresses.

5.8.1 From the results of the 3D stresses, the following can be deduced:

The residual stresses increase from inside the pipe strip towards the outer circumference and on the surface of the pipe strip, the residual axial (longitudinal) stress distribution increases from left to right. Through-the-thickness of a Pipe Strip – residual axial stress distribution from the right to the left outer surface of a pipe strip shows that it increases in that order. Residual axial (transverse) stress distribution from the outer circumference and top of the pipe strip increases inwards to the inner circumference and the top of a pipe strip increases in that order.

5.8.2 Results conform to stress distributions on the outside surface of the pipe.

From the results of the axial stresses the following can be deduced:

1. There exists a relationship between the pipe wall thickness of the dissimilar material weld and the residual stresses not only on the interior of the pipe but also on the external as observed from the ‘creep effect of the 12 mm clad thickness pipe when compared with the 2 mm clad thickness – effect of geometric parameter on stress.
2. By reason of the symmetry across the weld line $W_{L,}$ the axial stresses are symmetric in nature, that is compressive stresses which are high in magnitude are observed outside the pipe surfaces while tensile stresses are seen inside the pipe surfaces.

3. The circumferential position of the weld bead does not determine or affect the axial stresses. This is seen from the distribution of the axial stresses inside and outside – the pipe being similar in magnitude and distribution.
4. A protuberance (hump-like shape) is seen at the exterior surface of the pipe close to the weld line, which signifies the distribution of the stress variation under the weld crown.

5.8.3 From the results of the Transverse stresses the following can be deduced:

1. Transverse stresses are symmetric in nature as a result of the weld line symmetry
2. Higher values of tensile stresses are observed close to the fusion zone, whereas compressive stresses are seen both on the exterior and interior of the pipe away from the Heat Affected Zone (HAZ)
3. The circumferential position of the weld bead from the start of the weld to the finish directly affects the Hoop stresses and determines their distribution. In conclusion, volumetric change and yield strength which occurred under the tensile test curves as a result of martensitic transformation clearly has an effect on the welding residual stress, by increasing the magnitude of the residual stress in the weld zone, as well as changing its sign.

With the aid of residual stress and deformation experiments, the validity of the stress models is verified. There is an agreeable similitude between the simulated outputs and those of other authors – Refer to Appendix 7 for more comparison between the simulated results in this research and other experimental results.

NOTE: Publications based on the chapter content and published in international conferences and journals are found in Appendix 3 – first page only.

6 DISCUSSIONS AND CONCLUSIONS

6.1 Discussions

In this research, the experimental welding of dissimilar metals and the cladding of carbon steel and stainless steel has been carried out. The underlying principle behind the weld research is the Gaussian transformation theorem, which implies “A Gaussian flat surface has a Gaussian curvature at each and every point of the magnitude of zero”, which further showed that the thermal distributions on the surface of a cylinder can also be appreciated by studying the thermal distribution on the surface of welded plates.

The experimental findings were used to validate the 2D axisymmetric weld model, the 2D plate models, the 3D pipe strip model, the 3D clad pipe and plate models. The next stage was to examine the microstructures with the aid of laboratory examinations, in order to discover the trend of occurrences by reason of the applied thermal stresses, as well as to uncover the weakest point of a burst, which was discovered with the help of mechanical tests carried out in the laboratory.

The objectives are ground in the principle that weld thermal sources induce thermal stresses onto the weld metals (and materials), which in turn undergo residual stress transformations. Although the temperature has a first order effect on the microstructure, strain, stress, and formation of defects; the volumetric change and yield strength which are a result of the martensitic transformations, also have effects on the residual welding stress, increasing the magnitude of the stress in the welded zone. The presence of martensite in the welded zone further verified that, because there were recurrences of reheating taking place throughout the thick 12mm clad section of the weld, as well as changing its sign. The use of Finite Element Analysis to analyse these transient temperature changes and residual stress formation in the clad weld is fast gaining attention as a means of effective simulation. The use of thermocouples

in the monitoring of the variation of heat transmission within the weld metal is an avenue in the understanding of the heat distribution during the welding process.

A great deal of effort and thought has been put into designing the weld simulation technique and passes suitable to each weld model and also in carrying out of the weld experiment, mechanical tests and laboratory examinations as explained in the methodologies employed; a reasonable amount of success was attained. The key findings which define this research are in accordance with the objectives stated in chapter 1.

6.2 Findings

6.2.1 Thermal Profile for weld

The weld experiment using high temperature thermocouples revealed that the transmission of heat via the weld block is based on several factors such as thermal conductivity, time of transmission, nature of material, thickness and length of weld and clad metal (2mm and 12mm), nature of the material and distance from WE, WL, WA, and WS. The weld parameters, such as the distance of the thermocouples from the weld start (WS), weld start axis (WSA), weld line (WL) and weld edge (WE) positions, as well as the time taken to attain the peak transient temperature values, were recorded and the transient curves generated. In the 2mm clad weld, the thermocouple TC2 had the highest peak with a distance of 50mm from the weld start position (WS) and 10mm from the weld edge (WE) position. It had the slowest rate of heat loss by reason of its centralised position (being surrounded by other thermocouples) and not being located at the edge for speedy cooling. The first temperature peak, however, was observed in thermocouple TC7 located underneath on the 2mm clad plate at 50 mm from the weld start position. It was therefore resolved that by virtue of the small thickness of 2mm of the stainless-steel plate, in addition to the thermal conductivity of stainless steel which is 16[W/mK], the

speedy peak depicted in thermocouple TC5 was facilitated, compared with other thermocouples TC1 and TC3, which had closer proximity to the heat source weld start positions. In the 12mm clad, the highest peak is seen in thermocouple TC1 for its closest proximity of 13.5mm to the heat source and weld start position; however, the first temperature peak was detected in thermocouple TC7 which is located underneath the bottom plate and had the advantage of thermal conductivity 16 [W/mK] and a thickness of 12mm stainless steel, which facilitated the speed and rate of heat transmission. Comparing the number of high peaks obtained in the 2mm clad MSSS weld and the 12mm clad MSSS weld, it was observed that the 2mm clad MSSS weld had the highest peak in thermocouple TC2 (708.8 ^{o}C) followed by 339.8 ^{o}C and 320 ^{o}C, whereas the 12mm clad MSSS had high peaks ranging from 453.15 ^{o}C, 376.93 ^{o}C and 353.13 ^{o}C. Refer to Figures 3.8 (a and b), as well as Figures 4.23, 4.25 (a – d) and 4.27 (a – d).

6.2.2 Experimental

Mechanical properties of the welding – UTS of weld joint is high compared with those of parent metals showing the quality of the weld. The Charpy test samples fractured at the Heat affected zone (HAZ) depicting the quality of filler material and the weakest point of burst is HAZ due to fusion.

The hardness test shows that hardness is higher in the weld zone – more in the HAZ than the PM. This is an overmatching approach adopted for filler metal. It also means good bonding between dissimilar metal and therefore HAZ will provide a lasting effect for the pipe against corrosion.

Microstructural Observation using SEM on PM and Weld to confirm the type of phases they have present within the microstructure and structure, as well as the distribution of the elements located within the welded joints and hardness profile.

SEM – The different sections of the dissimilar welded joints were identified according to their elemental contents which came about by diffusion and transfer of elements in the course of welding and reheating of the thick weld sections. Consequently, mapping of the elements across the welded joint was created as shown in Figures 3.45 (a – c). In the HAZ the key elements that make for hardness, strength and corrosion resistance were present as well as in other parts of the weld joint microstructure. The presence of Iron was also vital in enhancing the strength of the dissimilar materials welded joints as observed in the diffusion and transfer of elements across parent metals (PM), clad metal (CL), FM and HAZ as well as transitions zones of the dissimilar welded joints. The Results of EDAX further confirmed this. Nickel and manganese in steel decreases the eutectoid temperature – lowering kinetic barriers, whereas Tungsten raises kinetic barriers. Manganese also increases the hardness in steel. The stainless-steel part of the microstructure also revealed acicular ferrites within the transition zone next to the welded metal; this was formed from the high cooling rate in the melting metal surface or material boundaries. The acicular ferrites are formed starting from the grain boundaries e.g. Plate martensite, widmannstetter ferrite, lath martensite and grain boundary ferrite.

EBSD – (Electron Back Scattering Diffraction) – Decrease in hardness from the line of the transition zone from both indentation test and micrographs. Mo and Mn minerals in weld rods decreases hardness when blended with carbon steel forming rapid cooling fine and small size grain structures.

From the tensile test, a number of factors such as temperature, strain rate (by reason of continuous loading) and anisotropy affect the shape of the stress- strain curves. Although the

profile and characteristics of the first weld sample under stress is similar to the behaviour of the parent metals pre UTS, it behaved differently from those of the parent materials – (mild steel and stainless steel) in the post UTS stage – by reason of slip occurring after the UTS. From EBSD (Bhadeshia, 2001), the formation of Martensite causes the movement of atoms connecting the Austenite and Martensite, as well as ferrite. This martensitic transformation occurs as a result of deformations of the parent metal into another product due to one-line invariant strain. The reason for the deformation of the stress-strain and force-displacement curves has been established as slip dislocation through a crystal lattice which generates shear leading to alterations in shape. The bulk deformation and yield strength, by reason of martensitic transformation, have affected the weld residual stress, thereby increasing the volume of residual stress in the welded metal and altering its direction.

There appears to be good bonding between the dissimilar material weld joint from optical observations. Hardness is high along the welded zone and especially in the HAZ. This was observed under section on Hardness test in Chapter 3. The material strength is high in both parent materials (of the order of 413 MPa for the 2 mm SS, 585 MPa for the12mm SS and 357 MPa for the 10 mm MS) generating a very high yield strength (of 570 and 725 MPa) and ultimate tensile strength (of 700 MPa and 759 MPa) in the weld. The over matching approach is adopted for the filler metal from the test of the hardness profiles, which clearly shows that the strength of the weld is high in the weld zone and especially in the HAZ compared to the parent metals. This is also true of the tensile test equivalence across the different hardness profile of the welded joints. It also confirms the findings that the tensile strength of the welded zone is higher than that for the parent material, especially in the HAZ, further confirming the overmatching of the filler material thus showing good bonding between the dissimilar materials. A linear relationship exists between the yield stress and the hardness of the weld samples, which further confirms that both 2mm and 12mm stainless steel-clad hardness

increase with decreases in temperature and applied load. The charpy test shows that the weakest point is in the HAZ because the dynamic failure and hence the impact failure occurred at the HAZ, and not in the FZ. Hardness could lead to brittle nature which could eventually lead to failure. The result of the charpy impact test also shows the quality of the filler material with respect to the good bonding of the fusion zone.

The study investigated the intrusion of the transition zone into the HAZ and weld zone, revealing that the hardness of the parent metal is less than that of the welded zone, which is about 40-70%. The transition of hardness from the clad to the HAZ is even. Diffused elements aided hardness of the HAZ interface. The HAZ consist of coarse austenite and an acicular martensitic structure. The cladding comprises of fine martensitic and austenitic dendrite structures.

Generally, the HAZ is multifaceted in its structure by reason of rapid heating within a short time period, after which cooling at normal room temperature ensues for each consecutive weld pass interval. The HAZ commences from the clad / HAZ interface. Temperatures increase with increasing depth and the effect of clad thickness on weld increased the weld zone. Clad thickness also increased the weld bead. While the increase in clad thickness meant increase in volume of fill and quantity of weldment, which also implies longer cooling time of weldment, leading to formation of coarsened grain size, the weld time on grain formation for the 2mm thick clad is smaller which means shorter cooling time and faster cooling rate, thus producing small size grains. The cooling time on grain formation results in coarse grain size generation, and this was further confirmed from the result of the charpy test which revealed that the HAZ fractured easily compared with the notch (at the fusion zone), showing it to be the weakest point of the joint and further revealing the quality of the filler metal used in the welding (A15 Cu-coated and 304/316 filler wires using GMAW) of the fusion zone – good bonding.

In the 2mm thick 361 stainless steel clad, the hardness value was observed to be greater than in the 12mm thick 361 stainless steel. Because of the high quantity of heat inputted into the weld system, the growth of the grain in the 12mm clad weld resulted in reduced impact strength values in the welded joint.

X-ray results of thermal weld experiments and mechanical testing, as well as lab analysis, all show that there is a good behaviour and match between welds of dissimilar material joints.

X-Ray diffraction patterns have been measured for the 2mm MSSS weld sample and the 12mm MSSS weld sample. At least 2 samples have been analysed in each case. The X-Ray diffraction patterns suggest that the HAZ area predominantly contains a martensitic phase and an austenitic phase. Measurement of the X-Ray diffraction patterns was carried out in this research and it was found that the X-Ray diffraction pattern of the weld HAZ matches those away from the HAZ, that is, parent metal mild steel and stainless steel. The filler metal used at the bottom of the weld zone is A15 Copper wire.

6.2.3 Thermal Analysis – Simulation

This is the creation of different models of weld passes**,** such as temperature profiles of a weld sheet through the weld pass with the thickness of a pipe strip, weld spot through the weld pass that is the length/size of 2D plates, ring added mass weld through the weld pass that is the length of a clad pipe and added mass weld through weld pass length of Narrow gap welding of thick sections of dissimilar materials joints in Abaqus FEA analysis in order to examine both temperature distribution and thermal transient flow. First of all, the modelling of each weld pass deposition technique was carried out to suit the geometry of the model, as well as to deliver the required amount of weldment within the right simulation time. These include the spot

deposition of the 2D weld plates, through-the-thickness deposition of the pipe strip, the added mass deposition of the 3D plates and the ring deposition of the 3D cladded pipes, each containing a round of seven weld passes. The heating and cooling steps were both examined.

The Gaussian transformation was employed which implies that a cylinder and plane are said to be isometric, meaning that one can be converted into the other without altering the local distances. Based on this principle, the discoveries from the weld experiments – carried out on weld plates, were applied to the simulated pipe models.

The first set of transient responses from the respective thermocouples used in the measurement of heat transmission during the weld were modelled and it was found that the results agreed well with that of the experiments, within the range of 90% to 100%. The accurate interpretation of the results depends on how well the governing physics behind the transmission of heat from the heat source through the base and clad metals to the thermocouples is understood.

It was discovered that, for part of the transient curve prior to the peak value, the simulated transient temperatures exhibited instantaneous peak values. They displayed isolated weld passes and started from zero (0 ^{o}C) because they have no histories and, as such, return back to the ambient temperature after the peak, which is not applicable in actual weld situations. The actual weld transient temperature rose slowly from 20^{o}C by reason of thermal conductivity of the mild steel (base metal) and stainless steel (clad metal) before attaining a peak value. After the peak value, there is a difference of about 50% between the measured and simulated curves. This was accounted for by the phase change. Another reason for this is that some thermocouples such as TC 2 and TC 3, which are situated in between other thermocouples and not at the edge, retain their heat and gradually dissipate it to the environment, thus retaining more heat than other thermocouples.

The distribution of heat in the thermocouples differs in the sense that, for the 2mm clad stainless-steel weld, the highest temperature peak of 708.82 ^{o}C is detected followed closely by

a temperature of 339.76 ^{o}C and 320 ^{o}C, whereas for the 12mm clad stainless steel weld, although the highest peak was not depicted, yet more values of moderately high temperatures of 453.15 ^{o}C, 376.73 ^{o}C, 353.13 ^{o}C and 306.73 ^{o}C were detected compared to the 2mm clad. This means that the temperature response is solely dependent on factors such as the nature of the material, either carbon steel or stainless steel, thermal conductivity, thickness of the material – height, width and depth, transmission time and distance (position) away from the heat source. It also goes to show that the 2mm clad is better suited for very high temperatures or functions since from the experiment it is able to tolerate high temperatures; and that for reasonably high temperatures, environments, the 12mm clad will be a formidable base for such functions or environments, because the outcome of the weld experiments clearly shows that the 12mm clad has a very good range of moderately high temperatures present in it.

Nomenclature for the thermal distribution of heat and weld direction was assigned which embraced the 45, 135, 225 and 315 degrees, also based on the Gaussian principle. This was used to display the temperature profile for the temperature-displacement curves applied to both pipe and plates. No significant difference was observed between nodal paths. Results are repeatable and are in close agreement as shown in Figures 4.29 (a and b), Figure 4.30 and Figure 5.19.

The results from the temperature versus distance curves also displayed a good agreement between the simulated results and the literature. Weld propagation follows a unique path defined by the curve, and the peaks correspond to the immediate region of the weld including the HAZ. The quantity of heat increases within the weld region and dissipates gradually away from the region of weld, bearing in mind that the temperature directly affects the yield stress, tensile strength, toughness, and modulus of elasticity of the material.

6.2.4 Stress Analysis

6.2.4.1 The Pipe Strip Model

This was built to examine the residual stress distribution and to apply it to the pipe in line with the aims and objectives mentioned in chapter one. The stress profiles, both axial and longitudinal on the inner surface, outer surface, through-the-thickness, top of pipe strip, bottom and transverse stresses were all studied, and it was discovered that the residual stress profile in a plate is similar to that of inside a pipe. However, the stress distribution on the inner and outer surfaces are similar, which is to say that since it is not enclosed like a pipe (or pressure vessel), the simulation software regards both surfaces as outer surfaces of a pipe. The stress distribution on the outer surface of the pipe strip is greater than those on the inner surface of a strip as a result of compressive forces. The inner surface of the pipe strip has compressive stresses which are symmetric across the weld line, and a stress field of reasonable magnitude compared with the other range of stresses, the yield stress of the material – which was not exceeded, is noticed on the FZ and the HAZ. Crown-like protrusions are observed above the weld region, which is caused by stress difference, thus making the HAZ a region of high stress. The stress is insignificant at the parent metal. Worthy to note is the fact that the stress does not exceed the yield limit of the material.

On the outer surface of the pipe strip, compressive stresses are also symmetric over the weld line and around the HAZ, and FZ stresses of greater dimensions are observed. Crown-like protrusion is also seen in the region of the weld line, which shows the stress profile of the HAZ and the FZ. The stresses are in self-equilibration and the material yield stress is not exceeded. Reasonable agreement exists between the residual axial stress of the pipe strip outer surface and that of the pipe surface.

It was also discovered that at the top of the pipe strip, the stress increases inwards, towards the inner circumference of the pipe, as indicated by the stress profile distribution. This is solely due to the compressive forces acting inwards from the circumference of the pipe strip; however, the value is negligible because of the edge effect.

Through-the-thickness of the pipe strip the residual axial stresses increase outward towards the outer pipe strip surface. The stress profile is also similar to that observed on the inner and outer surfaces of the pipe strip, in the sense that the weld crown indicates the presence of appreciable residual stress fields underneath it within the regions of the HAZ and the FZ. The residual stress is nominal at the parent metals.

6.2.4.2 Longitudinal and Transverse Stress within the 2D Plate

The distribution of transverse stresses within the 2D plate compared well with findings from the literature – specifically measured transverse stress, Chen and Sheng as well as Anderson, as shown in Figures 5.9 (a – c). The stress distribution in the parent metals was nominal, whereas within the HAZ and the FZ, stress profiles of high magnitude were displayed. This was observed under the weld crown, and the stress is symmetric on both sides of the weld line. The finding from the 2D plate agrees with findings from the through-the-thickness stress profile of the 3D pipe strip, and also with findings from the clad pipes. Compressive stresses are present within the vicinity of the weld arena (HAZ and FZ) and the distribution becomes tensile farther away from the region of weld (parent metals).

The results for the longitudinal stress also agreed with the findings from the literature regarding the lower section of the residual stress. Tensile stress was observed close to the weld region (HAZ and FZ), whereas nominal stress distribution was observed farther away from the weld

region (parent metal). A symmetric stress profile is seen on both sides of the weld line. This was also confirmed with results from the inner surfaces of the clad pipe.

6.2.4.3 Axial Stresses within the Clad Pipes

In the 2mm and 12mm clad pipes, it was discovered that the residual stress profiles are in their self-equilibration state. Also, because of the symmetry across the weld line $W_{L,}$ the axial stresses are symmetric in nature, that is, compressive stresses which are high in magnitude are observed outside the pipe surfaces while tensile stresses are seen inside the pipe surfaces. The circumferential position of the weld bead does not determine or affect the axial stresses. This is seen from the distribution of the axial stresses inside and outside the pipe being similar in magnitude and distribution. A protuberance (hump-like shape) is seen at the exterior surface of the pipe close to the weld line, which signifies the intensity of the stress distribution under the weld crown. These volumetric changes and yield strength which occurred under the tensile test curves as a result of martensitic transformation have direct effects on the welding residual stress, by increasing the magnitude of the residual stress in the weld zone as well as changing its sign. The simulated results demonstrate the volumetric change and the yield strength change due to the martensitic transformation effects of the welding residual stress.

From the validation of the results of the simulated axial stress and the Neutron Diffraction (ND) measured stress showing the residual axial, radial and hoop stress distributions on the inner surface of pipe, the following can be deduced:

From Figure 5.21 (a and b) the results of the axial, radial and hoop stresses of the Neutron diffraction were used to validate the axial stresses from the dissimilar welded joints of 2mm and 12 mm clad thicknesses. The result of the ND measured residual, axial and hoop stresses shows good agreement with the axial stresses of the 2 mm and 12 mm clad pipes. It is observed

that the internal stresses are tensile and there are perturbations under the weld crown. The maximum value of the radial stress is 200 MPa in Figure 5 (a), while the axial is 250 MPa and the hoop stress is 500 MPa. In Figure 5.21 (b), the ND measured stresses are plotted against the axial stress of the 2MSSS (2 mm clad weld of dissimilar material joint) and it is observed that the value of the axial stress for the 2MSSS, which is 110 MPa is closer to that of the ND measured radial stress with a difference of 90 MPa and also comparable to ND measured residual axial stress with a difference of 140 MPa. In Figure 5.21 (c), the residual axial stress in the interior of the 12MSSS (12mm mm clad weld of dissimilar material joint) at 330 MPa, is comparable with the ND measured axial stress of the pipe subsurface at 250 MPa having a similar trend of stress distribution, hence validating the residual stress models. Both axial residual stresses of the 2MSSS and 12MSSS are compared with each other in Figure 5.21 (d) and it is observed that inside the pipe surface the stresses are tensile and has the protuberance effect observed under the weld crown. It is important to note that the yield stress is not exceeded which means it is operating within a safe value.

6.2.4.4 Hoop Stresses within the Clad Pipes

Hoop stresses are symmetric in nature as a result of the weld line symmetry, and higher values of tensile stresses are observed close to the FZ, whereas compressive stresses are seen both on the exterior and interior of the pipe away from the HAZ.

Since hoop stresses are the stresses parallel to the weld bead direction, they are advanced as a result by reason of the expansion and contraction of the weld region in the radial direction during the heating and cooling occurrences in the course of the welding procedure. The distribution of the residual hoop stress for the exterior and interior surfaces of the pipe at different positions from the weld start position shows that large tensile and comprehensive

hoop stresses are present in the interior and on the exterior surfaces of the cylinder within the locality of the Weld line W_L. This also implies that the reverse is the case, which means that stress reduction and stress reversal are experienced away from the weld line, just as is the case with axial stress. This phenomenon is also confirmed by N. U. Dar et al. The disparity in the value of the hoop stress is solely due to varying weld parameters such as material properties and heat source parameters.

6.3 Conclusions

An effective weld between dissimilar metals is one in which the strength of the weld equals the weaker of the two metals being joined. This invariably means great tensile strength and ductility to prevent failure in the weld joint. This kind of desirable weld output can be achieved via several welding procedures.

The findings and relevance of the work performed in this thesis are focussed on the effects of the thermal and residual stresses on the HAZ. The HAZ is a region of the base metal and clad metal which undergoes alteration in its metallurgical properties (even though it has not melted), by high thermal energies during welding or high heat cutting. The HAZ, which has differing lengths, depths and widths also differs in areas of severity (affected by heat) and undergoes heating and cooling cycles. These changes could be metallurgical, in which case they induce stresses that subsequently reduces the strength of the material or generates nitrides within the HAZ thus affecting the weldability. The hardness of the HAZ with respect to its environment can be increased from the microstructure as well as the resistance to corrosion and/or cracking, also known as sensitization. Regulating the pre- and post-weld heat treatment conditions can enhance all these properties – high localized stresses, hardness and sensitization.

The physical attributes of the HAZ can also be altered. The extent to which the physical and metallurgical properties are altered is dependent on factors such as the filler metal, the quantity of heat inputted into the weld and the base material. The size of the HAZ is controlled by parameters such as time of exposure to heat, the welding speed and the current used in carrying out the welding.

In the residual stress analysis, there are agreements and similarities when observing the stress distributions on the graph compared with other authors validating the results of the simulation carried out in this research and also the quality of simulations carried out. Secondly, because the residual stress goes up to 110MPa in the 2mm clad pipe and 330 Mpa in the 12 mm clad pipe which implies that the yield strength of the material, 400MPa is not exceeded and there is still good agreements in the overall profile of the residual weld stress, even when compared with the stress profiles for authors who worked on same materials such as Sinha et al, Qureshi and Feli as shown in Figures 2.15 - 2.17. Indeed, it has been established that the weakest point of joint in the clad pipe weld is the HAZ, and so consideration should be given to this when designing the weld parameters and filler metals to avoid under-matching scenarios which could lead to weld failures and eventually the collapse of the entire pipe. With the aid of thermal, residual stress and deformation experiments, the validity of the thermal and stress models is verified. There is an agreeable similitude between the simulated outputs and those of other authors.

The research contained the following contributions such as:

1. Resolution of the intricacies of the heat transmission in the welded joints of dissimilar materials using the Gaussian transformation principle – which was employed and applied in order to determine the intricacies of the thermal distribution occurring during the GMAW welding process of dissimilar materials in a weld joint of a pipe. High temperature

thermocouples were positioned at strategic locations on the welded joints to accomplish this target.

2. Discovery of the different factors responsible for the unique pattern of heat distribution at the welded joints during the course of welding and the fact that these factors dictate the path through which the heat is distributed throughout the welded joint. These factors include the distance from heat source, weld line, weld axis, density, thermal conductivity and nature of material.

3. Resolving the modelling problem for multiple (seven) weld passes of thick sections of dissimilar material joints by developing different models of weld passes, such as temperature profiles of the weld sheet through the weld pass thickness of a pipe strip, weld spot through the weld pass length of 2D Plates, ring added mass weld through the weld pass length of a clad pipe and added mass weld through the weld pass length of a clad plate.

4. Resolving of the modelling problem for residual stress in (multiple) seven weld passes of thick sections of dissimilar materials joints by developing different models of residual weld stress profiles in a pipe strip, 2D plates, clad pipes and clad plates would then alleviate the stress distribution in a dissimilar material weld joint and the shrinkage effects of a pipe.

5. Representation of welding direction by employing the Gaussian transformation principle in order to enable its application on both plates and pipes.

6. Understanding of the effect of heat input on the mechanical properties and microstructures evolution of welding of dissimilar material joints, because of the continuous reheating taking place at the clad thicknesses during the welding process. The application of heat into the different clad thicknesses of the dissimilar material joint weld resulted in different rates of cooling and subsequently generated martensite in both the FZ and HAZ of GMAW, further

increasing the hardness and strengthening the FZ and HAZ of the different clad thicknesses of the dissimilar material joints.

7. Understanding the effect of solid-state phase transformation on the residual stresses of the dissimilar material joints of weld with respect to two different clad thicknesses. There were transformations from austenite to ferrite and especially the martensitic transformation of the weld microstructure altered the magnitude of the residual stress in the fusion zone and HAZ and also altered the yield strength of the FZ and HAZ, consequently producing a substantial effect on the weld microstructure and base.

6.4 Future Research

Based on the work carried out in this thesis and the discoveries made in this research, different questions have arisen and caused concerns that will be addressed in the future. Such areas of interest include the following:

6.4.1 The need to look at welding of several (more than one) layers of clad

HAZ of welds of more dissimilar materials especially for clads used in the oil and gas, petrochemical and pressure vessel, as well as the nuclear industry. In this research work, two layers of clad thicknesses were considered which were 2mm and 12mm. Nevertheless, future work should be carried out with emphasis on more than two layers of clad thicknesses - the different clad thicknesses applicable to real life situations in the industry ought to be considered. This involves 3 clad layers and 5 clad layers or more, all of or the same or of differing thickness. The ability of the thermocouples to effectively detect temperatures across the different strategic positions of these clad layers is of major concern. The nature of the

thermal responses with respect to transient temperatures of the thermocouples is a very prominent issue ranging from the temperature peaks to the cooling phases. How effective are the responses captured by the data logging device? Is the trend lost due to several clad layers or is there a good thermal response observed even for the third (3^{rd}) layer or clad, or the fifth (5^{th}) layer of clad or even the seventh (7^{th}) layer of clad? Bearing in mind that one of the novelties and major areas of concern is that this research aimed at uncovering is the dissimilar material joint, the key question would be what is the composition, feature and consequently the behaviour of the dissimilar material joint formed at the weld interfaces between several clad layers? What would the HAZ and FZ look like? Would it conform to the results obtained from two layers of clad? Or would it differ considerably and why? When subjected to mechanical testing such as tensile, charpy and hardness; would such weld interface housing the FZ and HAZ pass the test? The identification of the weakest point of the weld joint from the charpy tests would contribute to the knowledge in order that precautions could be taken in order to strengthen the bond in the affected joint. The efficacy of the filler metal in carrying out the weld across the different clad layers is also important to provide good bonding across the different profiles of the weld. Are there cases of over or under matching – should one filler metal be used across the several clad layers or different filler material? Would that address the challenge of over or under matching? What would the hardness profile look like across each of the different layers of each clad? Would the hardness be most pronounced in the HAZ, FZ or parent metal – referring to the efficiency of the weld, would it fail due to being brittle in nature and if so where? What are the different phases present in HAZ and FZ of such welded joints? At key areas such as the interface between the parent metals, what is the nature of grains formed at these interfaces and how do they affect the nature of the weld? What is the elemental reaction and diffusion in terms of chemical composition of the parent metals and the filler metal? How does that strengthen the weld?

6.4.2 The need to incorporate thicker cross sections of clad thicknesses.

Two millimetres (2mm) and twelve millimetres (12mm) clad thicknesses were considered in this research, however, for future research, it is recommended that other clad thicknesses such as 15mm and 20mm, could be considered so that a careful broader study of the thermal response of the high temperature thermocouples placed at strategic positions on these clad thicknesses could be considered pari-passu the weld plates and the mechanical tests, such as tensile tests carried out to determine the tensile strength and ultimate tensile strength of the welded-section. Hardness tests should also be carried out to determine the hardness of the HAZ, FZ and parent material in order to determine the over matching or under matching scenario presented. The Charpy test should also be carried out to further confirm the weakest point of the joint, HAZ or FZ, knowing that very hard property tends to brittleness which makes that part of the joint susceptible to failure. There is also the need to carry out thermal simulations of welding using the thicker clad sections, so as to obtain a basis of comparison of both thermally simulated results and measured results. The stress analysis also needs to be simulated using FEA models in order to verify the results of the axial stress fields.

6.4.3 Filler metal

The overmatching and under matching scenarios in a welded joint are primarily due to the type, constituent and quantity of the filler material used. In most standard labs, such as The Welding Institute (TWI) and Subsea Seven, a single choice of filler metal is used as an approach to tackling this challenge. A future work could be looking at under-matching and how the strength at the HAZ can be improved. There is also the possibility of considering different compositions of filler metals with the main aim of developing a composition with the right constituents that could better match both parent metals, so as to produce a well enhanced welded joint that could

withstand the pressures of stress both within and without the pipe as well as corrosion from the operating environment, thus ensuring long lasting pipelines.

Another suggestion would be to carry out more tests to verify the speed and efficiency of the weld with respect to its impact on the HAZ. There is the need to carry out detailed tests to capture the separate time intervals between the distinct peaks of each thermocouple.

6.4.4 Carry out more tests to verify the welds sequence and its impact on the HAZ

Different styles of weld sequence impact upon the HAZ in unique ways. In order to determine the size of the grains formed under the above conditions and its effect on the FZ and HAZ, more tests will need to be carried out. The grain size formed also impacts upon the HAZ and FZ in different ways. This will clearly reveal the impact of the weld style on the efficiency of the bond particularly at the HAZ. The most efficient style of welding could be to encourage/ to promote long lasting bonds in pie welds, thus improving the structural integrity of the weld.

6.4.5 Creep Effects in Stress Analysis

This is the challenge that occurred in the stress analysis with respect to the 12mm clad thickness. To a large extent the stress response for the FEA model of the weld was similar to that carried out both at the Subsea 7 laboratory; however, there was creep present on the axial stress. This needs to be further investigated as to why they occur only on the stress model for the 12mm thickness but not on the stress results of the 2mm thickness? Is this a clad thickness related issue? If so, it could be found for higher clad thicknesses as well as several layers of clad. It therefore calls for the need to look further into the reason for creep generation in the

thicker clad layers as a major research focus. This will help eliminate creep effects from welded structures, thus promoting stability in welded structures and durability.

Heat treatment in a clad weld in a new study and carrying out X-Ray diffraction – a method of measuring residual stresses in the different clads of dissimilar materials.

6.4.6 The need to look at Residual Stress Measurement of Dissimilar Materials using Destructive and Non-destructive Methods for more than one Layer of Clad and Multiple Samples

Due to no availability of machines and time constraint the residual stress measurement using destructive measurements such as deep hole and blank hole and non-destructive measurements like EBSD, XRD, Neutron Diffraction (ND) were not carried out – it was beyond my control. It is therefore highly recommended for future work.

The methodologies were considered (in chapter 2), however there is the need to obtain actual data by nature of scattering – more tests need to be carried out before the actual quantity value can be used.

REFERENCES

A., D. (1986). *Control of Dictortion and Residual Stresses in Girth Welded Pipes.* Massachusetts: Massachusetts Institute of Technology.

Abedrabbo, N., & Mayer, R. T. (2009). Crash response of advanced high-strength steel tubes: Experiment and model. *International Journal of Impact Engineering*, 36:1044-57. .

Abid, M. S. (2005). Finite-element simulation of tack welds in girth welding of a pipe-flange joint. *Acta Mechanica Volume 178, Issue 1–2*, pp 53–64.

Abid, M., Siddique, M., and Mufti, R. A. (2005). Prediction of Welding Distortions and Residual Stresses in a Pipe-Flang joint using the finite element technique. *Modeling Simulation in Material Science & Engineering*, 1-16.

Acar, M. O. (2017). Determination of plasticity following deformation and welding of austenitic stainless steel. *Materials Science and Engineering: A, 701*, pp. 203–213.

Acton Bright Steel. (2018, January 14). *The Metal Professionals*. Retrieved from Acton Bright Steel: www.actonbrightsteel.co.uk

Advance Steel Forum. (2016, 11 14). *Advance Steel Forum.* Retrieved from Butt Weld Symbol: https://forums.autodesk.com

Ahiale GK, O. Y.-J. (2014). Microstructure and fatigue performance of butt-welded joints in advanced high-strength steels. *Materials Science and Engineering: A.* , 597:3428.

Ahmad A.S., W. Y. (2019). Determination of the Effect of Cold Working Compression on Residual Stress Reduction in Quenched Aluminum Alloy 2219 Block. . *SV- JME. 2019;65:311–318. doi: 10.5545/sv-jme.2018.5938.*, 311-318.

Ahmad, A. S., & Wu, Y. G. (2019). Finite Element Prediction of Residual Stress and Deformation Induced by Double-Pass TIG Welding of Al 2219 Plate. *Materials 2019 12: 2251. doi: 10.3390/ma12142251*, 2251.

Akin, J. E. (2009). *Concepts of Thermal Analysis.* Retrieved Dcember 23, 2016, from FEA Thermal Concepts: https://www.clear.rice.edu/mech403/HelpFiles/FEA_thermal_concepts.pdf

Almqvist G, G. I. (1978.). Submerged arc welding. . *The Welding Institute, Cambridge.*

Analytical, P. (2016, 08 04). *Intrinsic Dissolution Rate (non-GMP)*. Retrieved from Particle Analytical: http://particle.dk/methods-analytical-laboratory/intrinsic-dissolution-rate/

Andersson, B. (1978). Thermal Stresses in Submerged Arc Welded Joint Considering Phase Transformations. *ASME Journal of Engineering Material and Technology Vol 100* , 356 - 362.

Andrews R. M., Denys R. M. Knauf G. and Zarea M. (2014) EPRG Guidelines on the Assessments of Defects in Transmission Pipeline Girth Welds – Revision 2014; European Pipeline Research Group e.V. www.eprg.net p 1- 20

Antaki, G. (2005). *Piping and Pipeline Engineering.* South Carolina, U.S.A.: Marcel Dekker Inc .

Asahi, H.; Hara, T.; Sugiyama, M.; Maruyama, N.; Terada, Y.; Tamehiro, H.; Koyama, K.; Ohkita, S.; Morimoto, H.; Tomioka, K.; Doi, N.; Murata, M.; Ayukawa, N.; Akasaki, H.; Fairchild, D.P.; Macia, M.L.; Petersen, C.W.; Koo, J.Y.; Bangaru, N.V.; Luton, M.J. (2004). Development of plate and seam welding technology for X120 linepipe. *Int J Offshore Polar Eng.*, 14:11-7.

Asahi H, Tsuru E, Hara T, Sugiyama M, Terada Y, Shinada H, et al. (2004). Pipe production technology and properties of X120 linepipe. *Int J Offshore Polar Eng.* , 14:36-41.

Asal, H. I. (2002). *Patent No. EP1231391A3.* US.

ASME, P. V. (1910, September 14). *The Procedure Handbook of Arc Welding.* Oklahoma: Lincoln Electric Company.

Azom. (2017). *Azom.* Retrieved February 25, 2017, from Azom: http://www.azom.com

B., H. (2015). *Failures in Stainless Steel Welds - Examples and Causes.* Retrieved October 03, 2016, from TWI: http://www.twi-global.com/

Bachmann, M., & Avilov, V. G. (2014). Experimental and numerical investigation of an electromagnetic weld pool support system for high power laser beam welding of austenitic stainless steel. *Journal of Materials Processing Technology*, 214:57.

Bai, Y. Q., & Bai. (2005). Use of High Strength Steel, X70. In Y. B. Bai, *Subsea Pipelines and Risers* (pp. 565 - 583). Amsterdam, Netherlands: Elsevier Inc Science Direct.

Barthoux, J. (2008, November). *Technical Papers- Focus on Nuclear Power Generation*. Retrieved August 23, 2015, from www.nuclear-exchange.com: www.nuclear-exchange.com/pdf/TP_Polysounde.pdf

Bate, S. K., Green, D. and Buttle D. (1997). *A Review of Residual Stress Distributions in welded Joints for the Defect Assessment of Offshore Structures.* Risley Culham: AEA Technology plc.

Bate, P. S. (2005). The characterization of low-angle boundaries by EBSD. *J.Microsc. vol. 220 no pt 1*, pp 36-46.

Bayley, C., & Mantei, A. (2009). Influence of weld heat input on the fracture and metallurgy of HSLA-65. *Canadian Metallurgical Quarterly*, 48:311-6.

Becker, W. T. (2002). *ASM Handbook Volume 11: Failure Analysis and Prevention.* OH, USA: ASM International.

Benyounis KY, O. A. (2005). Effect of laser welding parameters on the heat input and weld-bead profile. *Journal of Materials Processing Technology.*, 164–165:978-85.

Bernasovsky, P. (2013). CASE STUDIES OF WELDED STEEL STRUCTURE FAILURES. *Acta Metallurgica Slovaca - Conference* (pp. 159-170). Slovakia: Welding Research Institute - Industrial Institute SR, Bratislava, Slovakia.

Bhadeshia, H. K. (2001). *Materials Science & Metallurgy.* Retrieved 02 10, 2017, from Phase Transformation - Martensite: http://www.msm.cam.ac.uk/phase-trans/2002/martensite.html

Bhatia, A. (2014, September 5). *Curvature.* Retrieved December 29, 2016, from Empirical Zeal: http://www.empiricalzeal.com/tag/curvature/

Bonner NW, S. D. (1996). *Measurement of residual stresses in thick-section steel welds:.* Bristol: University of Bristol.

Bourdin, X., Trosseille, X., Petit, P.and Beillas, P. (n.d.). Comparison of Tetrahedral and Hexahedral Meshses for Organ Finite Element Modeling - An Application to Kidney Imapct. *Paper Number 07-0424*, 1-10.

Brickstad, B. and Josefson,, B.L. (1998). A parametric study of residual stresses in multipass butt-welded stainless steel pipes. *Int. J. Pressure Vessels and Piping*, Vol. 75(1) p11-25

British Energy. Assessment of the Integrity of Structures Containing Defects. Procedure R6 Revision 4. British Energy Generation Ltd; 2014

BSI, 'BS7910:2013 Guide to methods for assessing the acceptability of flaws in metallic structures,' 2013," 2013

BSI, 'BS7910:2013+A1:2015 Guide to methods for assessing the acceptability of flaws in metallic structures,' 2015," BSI Standards Limited 2016

Budden Peters J. and Sharples John K. (2015) The R6 Defect Assessment Procedure: Status and Key Recent Developments Transactions, Structural Mechanics in Reactor Technology SMiRT23, p. 1 – 10

Budden Peters J. and Sharples John K. (2017) The R6 Defect Assessment Procedure: Status and Key Recent Developments

Buhl Johannes, Israr Rameez and Bambach Markus (2019) Modeling and Convergence Analysis of Directed Energy Deposition Simulations with Hybrid Implicit / Explicit and Implicit Solutions, Journal of Machine Engineering, Vol 19 No. 3, pp 94 – 107

Busby, J. T., Hash, M. C. and Was, G. S. (2005). The Relationship between Hardness and Yield Stress in Irradiated Austenitic and Ferritic Steels. *Journal of Nuclear Materials*, Vol. 336, Issue 2-3, 267-278.

Callister W. D and Rethwisch D. G. (2011). *Materials Science and Engineering.* Asia: John Willey and Sons (Asia) Pte Ltd.

Chang, K.-H. L.-H. (2009). Finite element analysis of the residual stresses in T-joint fillet welds made of similar and dissimilar steels. *The International Journal of Advanced Manufacturing Technology*, 717-725.

Changa, P.-H. a.-L. (2004). Numerical and experimental investigations on the residual stresses of the butt-welded joints. *Computational Materials Science Volume 29, Issue 4*, pp 511-522.

Charpy Impact Test. (2016, May 25). Retrieved July 16, 16, from Charpy Impact Test: https://en.wikipedia.org/wiki/Charpy_impact_test

Chen, I. C. (1992). Modeling Welding by Surface Heating. *Journal of Engineering Material Technology* , 1-11.

Chen, Z. Y. (2012). *Some Applications of Electron Back Scattering Diffraction (EBSD) in Materials Research.* IntechOpen.

Buhl Johannes, Israr Rameez and Bambach Markus (2019) Modeling and Convergence Analysis of Directed Energy Deposition Simulations with Hybrid Implicit / Explicit and Implicit Solutions, Journal of Machine Engineering, Vol 19 No. 3, pp 94 – 107

Chung, F. H., & and Smith, D. (2000). *Industrial Applications of X-ray Diffraction.* Bosa Roca, United States: Marcel Dekker.

Chung, F. H; and Smith, D.K. (1999). *Industrial Applications of X-ray Diffraction.* Bosa Roca, United States: Taylor & Francis Inc.

Colegrove, P. I. (2013). Welding process impact on residual stress and distortion. *Science and Technology of Welding and Joining* , 717 - 725.

Conrardy, C., Huang, T. D., Harwig, D., Dong, P., Kvidahl, L., Evans, N., & Treaster, A. (2006). Practical Welding Techniques to Minimize Distortion in Lightweight Ship Structures. *Journal of Ship Production, Volume 22, Number 4*, pp. 239-247(9).

Corrosionpedia. (2016). *Girth Welds*. Retrieved March 29, 2016, from Corrosionpedia: https://www.corrosionpedia.com/definition/1951/girth-welds

CRYSTALLOGRAPHY. (2016, July 23). Retrieved August 11, 2016, from https://en.wikipedia.org/wiki/Crystallography

Cullity, B. (2001). *Elements of X-Ray Diffraction.* Massachusetts: Patience Hall.

D., R. (1946). The Theory of Moving Heat Source and its Application to Metal Trearments . *Transaction of the American Society of Mechnical Engineers* , 849-866.

Dai J., X. S. (2019). Numerical Analysis of Curing Residual Stress and Deformation in Thermosetting Composite Laminates with Comparison between Different Constitutive Models. Materials. *Materials. 2019; doi: 10.3390/ma12040572.*, 12:572.

Dar, N.U., Qureshi, E.M., and Hammouda, M.M.I. (2009). Analysis of Weld-Induced Residual Stresses and Distortions in Thin-Walled Cylinders. *Journal of Mechanical Science and Technology 23*, 1118-1131.

Das, Y. B. (2016). In situ observation of strain and phase transformation in plastically deformed 301 austenitic stainless steel, . *Materials & Design 112* , pp. 107-116.

Davies, J. R. (1994). Stainless Steel Cladding by Welding and Wed Overlays. In D. J. R., *ASM Specialty Handbook: Stainless Steels* (pp. 107-119). OH, USA: ASM International.

Davis, J. R. (2004). *Tensile Testing, 2nd Edition*, ASM International. pp. 1-13.

Dean, D. a. (2006). Prediction of welding residual stress in multi-pass butt-welded 9Cr-1Mo Steel Pipe considering phase transformation effect. *Comput. Mater. Sci.*, 209-219.

Debiccari, A. (1986). *Control of Dictortion and Residual Stresses in Girth Welded Pipes.* Massachusetts: Massachusetts Institute of Technology.

Deng D. and Murakawa,H. (2006) Numerical simulation of temperature field and residual stress in multi-pass welds in stainless steel pipe and comparison with experimental measurements, Computational Material Science, vol 37 Issue3

Deng, K., Y., G. G., & Driver, R. G. (2003). *Effect of Loading Angle on the Behaviour of Fillet Welds.* Alberta: Structural Engineering Report 251.

Deng D. & Kiyoshima K., (2010) Numerical simulation of residual stresses induced by laser beam welding in a SUS316 stainless steel pipe wit considering initial residual stress influences, Nuclear Engineeringnand Design 240; 688-696

Di Gioacchino, F. a. (2015). An experimental study of the polycrystalline plasticity of austenitic stainless steel,. *International Journal of Plasticity vol. 74* , pp. 92-109.

Dong, P. S. (2016). An IIW residual stress profile estimation scheme for girth welds in pressure vessel and piping components. *Welding in the World, Volume 60, Issue 2*, pp 283–298.

Du Toit, M. V. (2006). AN OVERVIEW OF THE HEAT-AFFECTED ZONE SENSITIZATION AND STRESS CORROSION CRACKING BEHAVIOUR OF 12% CHROMIUM TYPE 1.4003 FERRITIC STAINLESS STEEL. *IIW Doc IX-2213-06 IW Doc IX-H-640-06*, 1-15.

DuPont J, M. A. (1995). Thermal efficiency of arc welding processes. *Welding Journal-Including Welding Research Supplement.*, 74:406s.

Dwivedi, D. K. (2018). *Surface Engineering Enhancing Life of Tribological Components .* India: Springer.

Ebert, L. J. (1974). Effects of Residual Stresses upon Design Fabrication and Field Service. *Metallurgy and Materials Science*, 3-46.

Edu, C. (n.d.). *Newton Method: General Control and Variants.* Retrieved February 5, 2017, from NFEM Ch 26: http://www.colorado.edu/engineering/cas/courses.d/NFEM.d/NFEM.Ch26.d/NFEM.Ch26.Slides.d/NFEM.Ch26.Slides.pdf

EDU, M. E. (n.d.). *Guassian Curvature.* Retrieved December 29, 2016, from Math ETSU EDU: http://math.etsu.edu/multicalc/prealpha/Chap3/Chap3-8/part3.htm

Electron Backscatter Diffraction. (2016, April 20). Retrieved August 10, 2016, from https://en.wikipedia.org/wiki/Electron_backscatter_diffraction

Elmesalamy, A., Francis, J. A. and Li, L. (2014). A comparison of residual stresses in multi pass narrow gap laser welds and gas-tungsten arc welds in AISI 316L stainless steel. *International Journal of Pressure Vessels and Piping*, 113:49-59.

Elmesalamy, A., & Li, L. F. (2013). Understanding the process parameter interactions in multiple-pass ultra-narrow-gap laser welding of thick-section stainless steels. *Int J Adv Manuf Technol*, 68:1-17.

Encyclopedia. (2016). *Elasticity - Real -Life Applications*. Retrieved July 29, 2016, from Science Clarified: http://www.scienceclarified.com/everyday/Real-Life-Physics-Vol-2/Elasticity-Real-life-applications.html

Encyclopedia, B. C. (2015, April 28). *Butt Welding*. Retrieved March 29, 2016, from Wikipedia, the free encyclopedia: https://en.wikipedia.org/wiki/Butt_welding

ENCYCLOPEDIA, W. T. (2015, August 12). *Misorientation*. Retrieved August 2016, 12, from WIKIPEDIA THE FREE ENCYCLOPEDIA: https://en.wikipedia.org/wiki/Misorientation

ENCYCLOPEDIA, W. T. (2016, April 20). *Electron Backscatter Diffraction*. Retrieved August 10, 2016, from WIKIPEDIA: https://en.wikipedia.org/wiki/Electron_backscatter_diffraction

England, G. (n.d.). *Thermal Spray Coatings.* Retrieved July 15, 2016, from http://www.gordonengland.co.uk/

ESF, MSMT OP. (n.d.). *DEFORMATION OF WELD TYPES*. Retrieved Septemebr 27, 2016, from SPS-Vitkovice: http://www.sps-vitkovice.cz/texty/texty/ANT/1.%20ro%C4%8Dn%C3%ADk%2009%20-%20Deformation%20and%20types%20of%20welds%20-%20Deformace%20a%20typy%20sv%C3%A1r%C5%AF%20P.pdf

Evans, Glyn M. (1988) Effect of Molybdenum on Microstructure and properties of C-Mn all-weld metal Deposits, Joining & Materials 1 (5): 239-246

Fairchild, D. P., Macia, M. L., Bangaru, N. V and Koo, J. Y. (2004). Girth welding development for X120 linepipe. *Int J Offshore Polar Eng*, 14:18-28.

Fanous Ihab F. Z., Younan Maher Y. A., and Wifi Abdalla S. (2003) 3-D Finite Element Modeling of the Welding Process using Element Birth and Element Movement Techniques, ASME. J. Pressure Vessel Technology 125(2): 144 150

Feli, S., Aalami Aaleagha, M. E., Foroutan, M.and Borzabadi Farahani, E., (2012) Finite Element Simulation of Welding Sequences Effect on Residual Stresses in Multipass Butt-Welded Stainless Steel Pipes. ASME Journal of Pressure Vessel Technology, Transactions of the ASME (134)

Fellicia, D. M., & Sutarsis, K. B. (2017). Study of Sigma Phase in Duplex SAF 2507. *IOP Conference Series: Material Science and Engineering Volume 202 012039*.

Feng Qingshan, Sha Shengyi and Dai Lianshuang (2019) Bayesian Survival Analysis Model for Girt Weld Failure Prediction, Applied Sciences 9, 1150 p 1 – 11

Fitzpatrick, M., & Fry, A. H. (2005). *Determination of Residual Stresses by Xray Diffraction.* Measurement Good Practice Guide No. 52.

Francis, J., & Bhadeshia, H. W. (2007). Welding residual stresses in ferritic power plant steels. *Materials Science and Technology*, 23:1009-20.

Francis, J., & Turski, M. W. (2009). Measured residual stress distributions for low and high heat input single weld beads deposited on to SA508 steel. *Materials Science and Technology*, 25:325-34.

Frenk A., Vandyoussefi, M. Wagniere, J. -D. Kurz, W. Zryd A. (1997). Analysis of the Laser Cladding Process for Stellar Steel. *METALLURGICAL AND MATERIALS TRANSACTIONS B*, vol 28, Issue 3 pp 501-508.

Friedman, E. (1975). Thermo-Mechanical Analysis of the Welding Process using the Finite Element Method. *ASME Journal of Pressure Vessel Technology*, 206-213.

Frith, R., & Stone, M. (2015). Weld Efficiency Factors Revisited. *Procedia Engineering Volume 130 (2015) 434 – 44*, pp 434 - 445.

Frost P. A. (2009) Assessment Techniques Using R6 Procedure – Further Investigation of Limit Load Approach for Pipe Branch Components Frazer – Nash Consultancy Limited Surrey UK, p 1 – 18.

Fuerschbach, P. (1996). Measurement and prediction of energy transfer efficiency in laser beam welding. *Welding journal.*, 75.

Gao L, S. H. (2009). Load-carrying capacity of high-strength steel boxsections I: Stub columns. *Journal of Constructional Steel Research.*, 65:918-24.

Gianetto J, G. G. (2012). Microstructure and properties of high strength steel weld metals. *2012 9th International Pipeline Conference: American Society of Mechanical Engineers;*, p. 515-26.

Giri, A., & Sharma, K. M. (2014). Minimizing the Residual Shrinkage in Austenitic Stainless Steel Pipe Joints through Narrow Groove Welding. *First International Conference on Structural Integrity (ICONS-2014)* (pp. 299 - 305). Kalpakkam, India: Bhabha Atomic Research Centre, Trombay, Mumbai 400085, India .

Goldak J. Chakravarti A. and Bibby, M. (1984). A New Finite Element Model for Heat Sources. *Metallurgical and Materials Transactions B*, 299-305.

Goldak, J. A. (2005). *Computational Welding Mechanics .* New York: Springer.

Goldak, J. Z. (1996). Thermal Stress Analysis of Welds from Melting Point to Room Temperature. *JWRI*, 185-189.

Goldstein, J. N. (2018). *Scanning Electron Microscopy and X-Ray Microanalysis.* Springer.

Pipeline and Hazardous Materials Safety Administration (2010) United State Department of Transportation, Federal Register Vol 75, No. 56 March 24, 2010 www.govinfo.gov

Groover, M. P. (2010). *Fundamentals of Modern Manufacturing ,Materials ,Processes ,and Systems.* USA: John Wiley & Sons Inc.

Gusev, M. N.; Maksimkin, O. P.; Tivanova, O. V.; Silnaygina, N. S. and Garner, F. a. . (2006). Correlation of Yield Stress and Microhardness in 08Cr16Ni11Mo3 Stainless Steel Irradiated to High Dose in the BN-350 Fast Reactor . *Journal of Nuclear Materials*, 258-262.

Habbitt, H. D. (1973). A Numerical Thermo-Mechanical Model for the Welding and Subsequent Loading of Fabricated Structure. *Journal of Computers and Structures*, 1145-1174.

Hagstrom, & T. Becache, E. G. (2012). Complete Radiation Boundary Conditions for Convective Waves. *Commun Comput Phys*, 610-628.

Hadley Isabel (2013) BS7910:2013 in brief International Journal of Pressure Vessels and Piping 165, pp 263 – 269

Harrison PL, F. R. (1989). Application of continuous cooling transformation diagrams for welding of steels. *International Materials Reviews.*, 34:35-51.

Hashemi SH, M. D. (2012). Characterisation of weldment hardness, impact energy and microstructure in API X65 steel. *International Journal of Pressure Vessels and Piping.*, 98:8-15.

Hassan, H. (2010, October 18). *Welding and Its Classification*. Retrieved from Mechanical Engineering: http://engineeringhut.blogspot.com

He, L., & Zhao, H. N. (2018). Understanding the effect of oxygen on weld pool and keyhole in laser beam welding. *Journal of Laser Applications, https://doi.org/10.2351/1.5017703*.

HF, B. (1958). The propagation of cracks and the energy of elastic deformation. *Trans ASME*, 80:1225–30.

Hicks, J. (1999). *Welded Joint design.* Cambridge : Abington Publishing.

Hicks, J. (1999). *Welded Joint Design.* Cambridge: Woodhead Publishing Limited and TWI.

Holmes, B. (2015). *Failures in Stainless Steel Welds - Examples and Causes.* Retrieved October 03, 2016, from TWI: http://www.twi-global.com/

Hornbach, D., & Prevéy, P. (2002). The effect of prior cold work on tensile residual stress development in nuclear weldments. *Journal of Pressure Vessel Technology*, 124:359-65.

Hossain, S. (2018, April 1). *Residual Stresses within Engineering Component*. Retrieved from University of Bristol: www.bristol.ac.uk

Hosseinzadeh, F. (2009). *Residual stresses in shrink fits and quenched components:.* Bristol: University of Bristol.

Hosseinzadeh, F. M. (2011). Application of Deep Hole Drilling to the Measurement and Analysis of Residual Stresses in Steel Shrink-Fitted Assemblies . *Strain*, 47:412-26.

Hsieh, C.-C., & Wu, W. (2012). Overview of Intermetallic Sigma (σ) Phase Precipitation in Stainless Steels. *Hindawi International Scholarly Research Notices ISRN Metallurgy Volume 2012 ID 732471*, 16.

Hwang, B. Kim, Y. Lee, S. Kim, Y. Kim, N. Yoo, J. (2005). Effective grain size and charpy impact properties of high-toughness X70 pipeline steels. *Metall and Mat Trans A.*, vol 36: pp 2107-2114.

Ikeagu, S. R. (2007). *Evaluating the Effects of Different Welding Processes on the Distortion of 4mm Thick DH36 Ship Panels.* Cranefield : M. Sc. Thesis, School of Applied Sciences, Cranefield University.

Inspectioneering. (2016, June 21). *Heat Affected Zone (HAZ)*. Retrieved October 03, 2016, from Inspectioneering : https://inspectioneering.com/tag/heat+affected+zone

Institute, T. W. (2015). *TWI Technical Knowledge*. Retrieved August 23, 2015, from The Welding Institue: http://www.twi-global.com/technical-knowledge/faqs/process-faqs/faq-what-is-narrow-gap-welding/

Ispatguru. (2016). *Heat Affected Zone and Weld Metal Properties in Welding of Steels.* Retrieved from Ispatguru.com: http://ispatguru.com

James, F. (2000). *The Procedure Handbook of Arc Welding, 14th edition. .* Cleveland, USA: Lincoln Arc Welding Foundation .

James, M., & Mahoney, M. W. (June, 1999). Residual stress measurements in friction stir welded aluminum alloys. *Proceedings of the 1st International Symposium on Friction Stir Welding.* CA: Thousand Oaks.

Jang, Y.,C.; Hong, J., k.; Park, J., H.; Kim, D., W. and Lee, Y. (2008, August 12). Effects of notch position of the Charpy Impact Specimen on the Failure Behaviour in Heat Affected Zone. *Journal of Materials Processing Technology*, 419-424. Retrieved August 2016, 12, from WIKIPEDIA THE FREE ENCYCLOPEDIA: https://en.wikipedia.org/wiki/Misorientation

Javadi, Yashar (2015) Investigation of Clamping Effect on the Welding Residual Stress and Deformation of Monel Plates by Using the Ultrasonic Stress Measurement and Finite Element Method. ASME Journal of Pressure Vessel Technology, Transactions of the ASME; 137(1)

Javadi, Y., Raeisi M. H., Pirzaman H. S., (2013) Using Welding Simulation and Ultrasonic Method to Evaluate Residual Stress in Stainless Welded Plates. ASME Biennial Conference on Engineering Systems Design and Analysis ESDA 2012, 1;PP 43-50

Jiang Hai-toa, Yan Xiao-qian, Liu Ji-xiong, Duan Xiao-ge (2013). Effect of Heat Treatment on Microstructure and Mechnaical Property of Ti-steel Explosive-Rolling Clad Plate. *Sience Direct, 697-704.*, Pp 697-704.

Jiang Wenchun, Yang B., Gong J. M. and Tu S. T. (2011). Effect of Clad and Base Metal Thickness on Residual Stress in Repair Weld of a Stainless Steel CladnPlate. Journal of Pressure Vessel Technology ASME Vol 133, 061401 pp 1-9.

Jonsson, M. & Josefson, B. L. (1988) Experimentally determined transient and residual stresses in the butt-welded pipes, Journal of Strain Analysis, vol 23 Issue 1 pp 25-31

Kah, Paul; Martikainen, Madan Shrestha Jukka (2014). Trends in Joining Dissimilar Metals by Welding. *Applied Mechanics and Materials*, vol 440, pp 269-276.

Karimzadeh, F. S. (2005). Effect of Mircroplasma Arc Welding Process parameters on Grain Growth Porosity Distribution of Thin Sheet Ti6A14V Alloy Weldment *Materials and Manufacturing Processes*, pp 205 - 219.

Kartal, M., & Liljedahl, C. G. (2008). Determination of the profile of the complete residual stress tensor in a VPPA weld using the multi-axial contour method. *Acta Materialia vol 56*, 4417-4428.

Kathleen, M. (1983). Metals handbook: Welding, brazing, and soldering:. *American Society for Metals;*.

Keehan E, Karlsson L, Andren H, Bhadeshia H. Influence of C, Mn and Ni contents on microstructure and properties of strong steel weld metals, part II. Impact toughness gain from manganese reductions. https://www.researchgate.net/publication/267798436

Keehan E, Karlsson L, Andren H-O, Bhadeshia H. K. D. H. Influence of carbon, Manganese and nickel microstructure and properties of strong steel weld metals, Part 3- Increased strength resulting from carbon additions. Science and technology of welding & Joining. 2006; 11:19-24 .

Kelkar, G. P. (2019, 05 27). *Weld Cracks.* Retrieved from WJM Technologies: www.welding-consultant.com

Kellar E. J. C. and Smith F. . (2005, April). *Comeld - A New approach to damage control for composite to metal joints*. Retrieved September 03, 2016, from The Welding Institute TWI: http://www.twi-global.com/technical-knowledge/published-papers/comeld-a-new-approach-to-damage-control-for-composite-to-metal-joints-april-2005/

Kelly. (2019, November 20). Retrieved from University of Auckland: SolidMechanicsBooks/Part_II/08_Plasticity/08_Plasticity_06_Hardening *Plasticity Hardening Solid mechanics part II Section 8.6 pp 301 – 314 .*

Khurshid M, B. Z. (2012). Ultimate strength and failure modes for fillet welds in high strength steels. *Materials & Design.*, 40:36-42.

Kiran, D., & Basu, B. D. (2012). Influence of process variables on weld bead quality in two wire tandem submerged arc welding of HSLA steel. *Journal of Materials Processing Technology*, 212:2041-50.

Kitada T, Y. T. (2002). New technologies of steel bridges in Japan. . *Journal of Constructional Steel Research.*, 58:21-70.

Kolhe KP, D. C. (2008). Prediction of microstructure and mechanical properties of multipass SAW. *Journal of Materials Processing Technology.*, 197:241-9.

Koo, J. Y., Luton, M. J., Bangaru, N. V., Petkovic, R. A., Fairchild, D. P.,Petersen, C. W., Asahi, H., Terada Y., Suggiyama, M., Tamehiro, H., Komizo, Y., Okaguchi, S., Hamada, M., Yamamoto, A. and Takeuchi, I. (2004). Metallurgical design of ultra high-strength steels for gas pipelines. *Int J Offshore Polar Eng.* , 14:2-10.

Kovacevic, R. (2012). *Weld Processes.* Welding Processes. Retrieved from http://www.intechopen.com/books/welding-processes

Krawitz, A., & Winholtz, R. (1994). Use of position-dependent stress-free standards for diffraction stress measurements. *Materials Science and Engineering: A.*, 185:12330.

Krishna, M. Z. (2014, November 26). *Tensile Testing on Pipes.* Retrieved February 14, 2017, from ResearchGate: https://www.researchgate.net/post/Is_it_possible_to_do_tensile_testing_on_pipes

Kursun T. (2011). Effect of the GMAW and the GMAW-P Welding Processes on the Microstructure, Hardness, Tensile and Impact Strength of AISI 1030 Steel Joints fabricated by ASP316L Austenitic Stainless Steel Filler Metal. *Archives of Metallurgy and Materials*, 56:955-963.

Lakshminarayanan, A. K. and Balasubramanian, V. (2010). An Assesment of Microstructure Hardness Tensile and Impact Strenght of Friction Stir Welded Ferritic Satainless Steel Joints. *Materials and Design 31*, 4592-4600.

Lampman, S. (2001). *Weld Integrity and Performance.* Ohio: ASM International.

Lan L, Q. C. (2012). Analysis of microstructural variation and mechanical behaviors in submerged arc welded joint of high strength low carbon bainitic steel. *Materials Science and Engineering: A.*, 558:592-601.

Lancaster, J. F. (1992). *Handbook of Structural Welding: Processes, Materials and Methods Used in the Welding of Major Structures, Pipelines and Process Plant.* Cambridge UK: Woodhead Publishing Limited with TWI.

Lau, T. W. (1985). FIRST REPORT OF HAZ STUDY. *Proceedings of the International Conference on Welding for Challenging Environments* (pp. 167 - 180). Toronto, Ontario, Canada, 15–17: Elsevier Ltd.

Lawrence, B. L. (2004). *Metallography and Microstructures of Carbon and Low-Alloy Steels.* ASM Handbook Volume 9, Metallography and Microstructures (ASM International.

Lee, C. H. and Chang, K. H. (2008). Three Dimensional finite Element Simulation of Residual Stresses in Circumferential Welds of Steel Pipe Including Pipe Diameter Effects. *Journal of Material Science and Engineeirng A*, 210-218.

LEE, K. H. (2014). EFFECTS OF TEMPERING AND PWHT ON MICROSTRUCTURES AND MECHANICAL PROPERTIES OF SA508 GR.4N STEEL. *NUCLEAR ENGINEERING AND TECHNOLOGY, VOL.46 NO.3* , pp 413 - 422.

Leggatt, R. H. (2008). Residual stresses in welded structures. *International Journal of Pressure Vessels and Piping Volume 85, Issue 3*, Pages 144-151.

Leggatt, R. H. (2008). Residual stresses in welded structures. *International Journal of Pressure Vessels and Piping*, pp 144 -151.

Li, R., & Wang, T. W. (2014). A study of narrow gap laser welding for thick plates using the multi-layer and multi-pass method. *Optics & Laser Technology*, 64:172-83.

Lindgre, L.-E. (2006). FINITE ELEMENT MODELING AND SIMULATION OF WELDING. PART 3: EFFICIENCY AND INTEGRATION. *Journal of Thermal Stresses*, Pg 15.

Lindgren. (2001). Finite Element Modeling and Simulation. Part 2: Improved Material Modeling. *Journal of Thermal Stresses*, 195-231.

Lindgren, L. E. (2001). Finite Element Modeling and Simulation. Part 1: Increased Complexity. *Journal of Thermal Stresses Vol 24*, 141-192.

Long, H. G. (2009). Prediction of welding distortion in butt joint of thin plates. *Materials & Design Volume 30, Issue 10*, pp 4126 -4135.

Lu, B. T. (2005). Pitting and stress corrosion cracking behavior in welded austenitic stainless steel. *Electrochimica Acta, Vol 50, Issue 6*, 1391-1403.

Lu, J. (1996). *Handbook of measurement of residual stresses:.* Fairmont Press.

Lu, Z. S. (2011). Characterization of microstructure and local deformation in 316NG weld heat-affected zone and stress corrosion cracking in high temperature water. *Corrosion Science*, 1916 - 1932.

Lucas, B. V. (2016). *Distortion - Types and Causes*. Retrieved September 27, 2016, from TWI: http://www.twi-global.com/technical-knowledge/job-knowledge/distortion-types-and-causes-033/

Lyman, C. I.-R. (1990). *Scanning Electron Microscopy, X-Ray Microanalysis and Analytical Electron Microscopy.* Newyork: Plenum Press.

Esmailian M (2010). The Effect of Cooling Rate and Austenite Grain Size on the Austenite to Ferrite Transformation Temperature and Different Ferrite Transformation Temperature and Different Ferrite Morphologies in Mcroalloyed Steels. *Iranian Journal of Material Science & Engineering* ,vol 7, No 1, pp7-14.

Mahmoudi, A., & Hossain, S. T. (2009). A new procedure to measure near yield residual stresses using the deep hole drilling technique. *Experimental Mechanics*, 49:595-604.

Malik, A. M., Qureshi, E. M. and Dar, N. U. (2008). Analaysis of Arc Welded ThinWalled Cylinders to Investigate the Effects of Welding Process Parameters on Residual Stresses. *Material Science Forum*, 763-768.

Masubuchi, K. (1980). *Analysis of Welded Structures.* Pergamon Press.

Materia, T. (2006, August). *Welding of Dissimilar Metals.* Retrieved October 04, 2016, from Total Materia: http://www.totalmateria.com

Material Grades. (2017). Retrieved February 25, 2017, from Material Grades: http://www.materialgrades.com

Math ETSU EDU. (n.d.). Retrieved December 29, 2016, from Guassian Curvature: http://math.etsu.edu/multicalc/prealpha/Chap3/Chap3-8/part3.htm

Matweb. (2017). *Matweb.* Retrieved February 25, 2016, from Matweb: http://www.matweb.com

MB, P. (2001). Cross-sectional mapping of residual stresses by measuring the surface contour after a cut. *Journal of Engineering Materials and Technology*, 123:162-8.

McDill, J. M. (1995). A Non-Conforming Eight to 26-Node Hexahedron for Three Dimensional Thermal-Elasto-Plastic Finite Element Analysis. *Journal of Computers and Structures*, 183-189.

McDill, J. M. (1999). An 8-to-16 Node Solid Graded Shell Elements for Far-Field Applications in 3-D Thermal Mechnical FEA. *12th International Conference on Mathematical and Computer Modeling and Scientifc Conputing*.

Menon, H. (2017, September 27). *Heat Affected Zone.* Retrieved from Heat Thermodynamics: https://www.quora.com

Milella, P. P. (2013). *Hydrogen Embrittlement and Sensitization Cracking. In: Fatigue and Corrosion in Metals.* Milano: Springer.

Miller, R. (2013, March 15). *Why Pipes Matters - Importance of Clad Pipe in the Oil and Gas Industry.* Retrieved December 21, 2016, from Breaking Energy: http://breakingenergy.com/2013/03/15/why-pipes-matter-the-importance-of-clad-pipe-in-the-oil-and-gas/

Milne I., R. Ainsworth, A. Dowling, and A. Stewart (1988), "Assessment of the integrity of structures containing defects," Int. J. Press. Vessel. Pip., vol. 32, no. 1–4, pp. 3–104,

Mingsan Xua, J. L. (2015). Influence of powders and process parameters on bonding shear strength and micro hardness in laser cladding remanufacturing . *Elsevier Procedia CIRP Vol 29*, 804 – 809 .

Minnick William, H. (1992). *Gas Tungsten Arc Welding Handbook.* USA: Goodheart-Willcox Co Inc.

Misorientation. (2015, August 12). Retrieved August 2016, 12, from https://en.wikipedia.org/wiki/Misorientation

Mithilesh, P. V. (2013). Investigations on Dissimilar Weldments of Inconel 625 and AISI 304. *MRS Singapore - ICMAT Symposia Proceedings* (pp. 66-70). Vellore India: Elsievier Ltd.

Moeinifar, S., & Kokabi, A. H. (2011). Role of tandem submerged arc welding thermal cycles on properties of the heat affected zone in X80 microalloyed pipe line steel. *Journal of Materials Processing Technology*, 211:368-75.

Mohandas T, M. R. (1997). A comparison of continuous and pulse current gas tungsten arc welds of an ultra high strength steel. *Journal of Materials Processing Technology.*, 69:222-6.

Mourada, A.-H. I. (2012). Gas tungsten arc and laser beam welding processes effects on duplex stainless steel 2205 properties. *Materials Science and Engineering: A*, pp 105 - 113.

Muhammad, E. (2008). *Analysis of Residual Stresses and Distortions in Circumferentially Welded Thin-Walled Cylinders.* Parkistan: National University of Science and Technology, Parkistan.

Murti, V. S. R., Srinivas, P. D., Banadeki, G. H.D. and Raju, K. S. (1993). Effect of heat input on the metallurgical properties of HSLA steel in multi-pass MIG welding. *Journal of Materials Processing Technology.*, 37:723-9.

Murugan, S., Rai, S. K., Kumar, P. V., Jaykumar, T., Raj, B. and Bose, M.S.C. (2001). Temperature distribution and residual stresses due to multipass welding in type 304 stainless steel and low carbon steel weld pads. *International Journal of Pressure Vessels and Piping*, 78:307-17.

MWC. (2016). *Gas Metal Arc Welding*. Retrieved from MeWelding: http://mewelding.com

N.H., B. (2016). *Metallurgy of Cast Iron & Steels.* Retrieved February 15, 2017, from Steel.

Naeem Ullah Dar, Ejaz M. Qureshi and M.M.I. Hammouda. (2009). Analysis of Wled-Induced Residual Stresses and Distortions in Thin-Walled Cylinders. *Journal of Mechanical Science and Technology*, 1118-1131.

NAFEMS. (2008, July 30). *Introduction to Finite Element Analysis.* Retrieved December 23, 2016, from NAFEMS.Org: https://www.nafems.org

Newswatch, A. i. (2006). *http://www.africansinamericanewswatch.com.* Retrieved October 23, 2016, from http://www.africansinamericanewswatch.com/a/p/photonew/photo020.html: www.brunel.ac.uk

Nezamdost, M. R., Nekouie Esfahani, M. R., Hashemi, S. H. and Mirbozorgi, S. A. (2016), Internation J Advance Manufacturing Technology, 87:615-624

Norwegian, G. (2012, July 20). *DEFORMATION AND TYPES OF WELD.* Retrieved Septemebr 27, 2016, from SPS-Vitkovice: http://www.sps-vitkovice.cz

Ogawa, K., & Osuki, T. (2019). Effects of Alloying Elements on Sigma Phase Precipitation in Duplex Stainless Steel (1) - Modelling of Effects of Chrovmium, Molybdenum and Tungsten on Sigma Phase Growth Rate in Super Duplex Stainless Steel -. *ISIJ International, Volume 59 Issue 1*, pp 122 - 128.

Olabi, A. G. (1996). Stress relief procedures for low carbon steel (1020) welded components. *Journal of Materials Processing Technology Volume 56, Issues 1–4*, pp 552-562.

Pagliaro, P., & Prime, M. C. (2009). Known residual stress specimens using opposed indentation. *Journal of Engineering Materials and Technology*, 131:031002.

Pande, C., & Imam, M. (2007). Nucleation and growth kinetics in high strength low carbon ferrous alloys. *Materials Science and Engineering: A*, 457:69-76.

Pathak, C.S.; Navale, L., G.; Sahasrabudhe, A. d. and Rathod, M. J. (2012). Analysis of Thermal Cycle during Multipass Arc Welding. *Welding Journal*, 149-154.

Pavlina, V. T. and Van Tyne C. J. (2008). Correlation of Yield Strength and Tensile Strength with Hardness for Steels. *Journal of Materials Engineering and Performance*, 888-893.

Pecharsky, .. K., & and Zavalij, P. (2003). *Fundamentals of Powder Diffraction and Structural Characterization of Materials.* New York: Kluwer Academic, Springer.

Pecharsky, K., & Zavalij, P. (2009). *Fundamentals of Powder Diffraction and Structural Characterization of Materials.* New York: Springer.

Piccini J and Svoboda H. (2012). Effect of the plasma arc welding procedure on mechanical properties of DP700 steel. *Procedia Materials Science.*, 1:50-7.

Poorhaydari K, P. B. (2006). Transformation twins in the weld HAZ of a low-carbon high-strength microalloyed steel. *Materials Science and Engineering: A.* , 435–436:371-82.

Prime MB. (2001). Cross-sectional mapping of residual stresses by measuring the surface contour after a cut. *Journal of Engineering Materials and Technology*, 123:162-8.

Prime, M. (2010). Plasticity effects in incremental slitting measurement of residual stresses. *Engineering Fracture Mechanics*, 77:1552-66.

Qiang X, B. F. (2012). Post-fire mechanical properties of high strength structural steels S460 and S690. *Engineering Structures.* , 35:1-10.

Qureshi, M. E. (2008). *Analysis of Residual Stresses and Distortion in Circumferentially Welded Thin-Waleed Cylinders.* Pakistan: Department of Mechanical Engineering, College of Electrical and Mechanical Engineering .

Radaj, D. (1992). *Heat Effects of Welding: Temperature Field, Residual Stress, Distortion.* New York: Springer- Verlag.

Radaj, D. (1992). Heat effects of welding; temperature field, residual stresses, distortion. *Berlin: Springer-Verlag;*.

Rajan, K. (2016, April 06). Nuclear Reactor Technology. *NPTEL - Chemical Engineering - Nuclear Reactor Technology*, pp. 1-5. Retrieved from nptel.ac.in

Rammerstorfer, F. G.-J. (1992). The Influence of Welding Stresses and Distortions on the Stability of Shells of Revolution. *Mechanical Effects of Welding*, pp 239-259.

Randle, V. (2003). *B0798 Microtexture Determination and its Applications (Matsci).* Swansea: Casemate Academic.

Rao, K. S. (2004). PITTING CORROSION OF HEAT-TREATABLE ALUMINIUM ALLOYS AND WELDS: A REVEIW. *Trans. Indian Inst. Met. Vol.57, No. 6*, pp. 593 - 610.

Ravi Shankar A, G. G. (2009). Effect of heat input on microstructural changes and corrosion behavior of commercially pure titanium welds in nitric acid medium. *J of Materi Eng and Perform.* , 18:1116-23.

Ravichandran, G. R. (1996). Analysis of Temperature Distribution during Circumferential Welding of Cylindrical and Spherical Components using the Finite Element Method. *Journal of Computer and Structures*, 225-255.

Ren, Y. P. (2016). Challenges of measuring residual stresses in large girth welded pipe spools by neutron diffraction. *Materials Research Forum*, pp. 575 - 580.

Ren, Y., & Paradowska, A. W. (2018). Residual Stress State of X65 Pipeline Girth Welds before and after Local and Furnace Post Weld Heat Treatment. *Journal of Pressure Vessel Technology*, 1-43.

Ren, Y. (2018). *Investigation of Residual Stresses in X65 Narrow-Gap Pipe Girth Welds.* London: Brunel University London.

Rosenthal, D. (1946). The Theory of Moving Heat Source and its Application to Metal Trearments. *Transaction of the American Society of Mechnical Engineers*, 849-866.

Rossiniab, N. S. (2012). Methods of measuring residual stresses in components. *Materials & Design Volume 35*, pp 572-588.

Runnemalm, H. a. (2000). Three-Dimensional Welding Analysis using an Adaptive Mesh Scheme. *Computer Methods in Applied Mechanics and Engineering*, 515-523.

Rybicki, E. F., Schmueser, D. W., Stonesifer, R. W., & Groom, J. J. (1978). A Finite Element Model for Residual Stresses and Deflections in Girth-Butt Welded Pipes. *J. Pressure Vessel Technol*, 256-262.

Rybicki, E. F. McGuire, P. A. Merrick E and Wert J. (1982) The effect of Pipe thickness on residual stresses due to girth welds. ASME Journal of Pres-sure Vessel Technology, vol 104 pp 204-209

Saadeldin, R., Hu, Y. and Henni, A. . (2015). Numerical Analysis of Buried Pipes under Field Geo-Environmental Conditions . *International Journal of geo-Engineering*, 1-22.

Sabapathy P. N., Wahab, M.A., Painter, M. J. (2001). Numerical Models of In Service Welding of Gas Pipeline. *Journal of Materials Processing Technology*, 118:14-21.

Safety, C. C. (2016, 07 29). *OSH Answers Fact Sheets*. Retrieved 08 03, 2016, from Canadian Centre for Occupational Health and Safety: https://www.ccohs.ca/oshanswers/safety_haz/welding/fumes.html

Savage, W. F., & Nippes, E. F. (1978). Liquid-Metal Embrittlement of the Heat-Affected Zone by Copper Contamination. *Welding Research Supplement*, pp 237 - 245.

Scervini, M. (2009, August 31). *Thermoucouples.* Retrieved February 24, 2017, from University of Cambridge: //www.msm.cam.ac.uk/utc/thermocouple

Schwartz, A. J. (2009). *Electron Backscatter Diffraction in Materials Science.* USA: Springer.

Scimeca, M. B. (2018). Energy Dispersive R-ray (EDX) Microanalysis: A Powerful tool in Biomedical Research and Diagnosis. *European Journal of Histochemistry Vol 62*, pp 2018 - 2841.

Shen S, O. I. (2012). Effect of heat input on weld bead geometry of submerged arc welded ASTM A709 Grade 50 steel joints. *Journal of Materials Processing Technology.*, 212:286-94.

Sheng, Y. C. (1992). RESIDUAL STRESS IN WELDMENT . *Journal of Thermal Stresses*, 53-69.

Shi G, J. X.-M. (2014). Experimental study on column buckling of 420 MPa high strength steel welded circular tubes. . *Journal of Constructional Steel Research.*, 100:71-81.

Shi Y, C. D. (2004). HAZ microstructure simulation in welding of a ultra fine grain steel. *Computational Materials Science.*, 31:379-88.

Shi, & G, S. Y. (2008). Engineering application of ultra-high strength steel structures. *Progress in Steel Building Structures*, 10:32-8.

Shin SY, H. B. (2007). Correlation of microstructure and charpy impact properties in API X70 and X80 line-pipe steels. *Materials Science and Engineering: A.* , 458:281-9.

Shin, Y. T. (2012). Effects of Heat Input on Pitting Corrosion in Super Duplex Stainless Steel Weld Metals. *Met. Mater. Int., Vol. 18, No. 6*, pp 1037 - 1040.

Siltanen J, T. S. (2015). Laser and laser gas-metal-arc hybrid welding of 960 MPa direct-quenched structural steel in a butt joint configuration. *Journal of Laser Applications.*, 27:S29007.

SIMULIA, A. (2017, February 5). *Nonlinear Solution Methods in Abaqus/Standard.* Retrieved from Abaqus doc Ucalgary: http://abaqusdoc.ucalgary.ca

SIMULIA, A. 6. (n.d.). *Nonlinear Solution Methods in Abaqus/Standard.* Retrieved February 5, 2017, from Abaqus doc Ucalgary: http://abaqusdoc.ucalgary.ca/books/stm/default.htm?startat=ch02s02ath14.html

Sinha, P. K., Islam, R., & Prasad, C. a. (2013). Analysis of Residual Stresses and Distortions in Girth-Welded Carbon Steel Pipe. *International Journal of Recent Technology and Engineering (IJRTE)*, 2277-3878.

Smith. (2012). *Engineering with Clad Steel.* Nicckel Institute Technical.

Smith D & Bonner N. (1994). *Measurement of residual stresses in a thick section steel weld.* Birmingham: Engineering integrity assessment Engineering Materials Advisory Services Chamelon Press.

Smith, D., & Bouchard, P. G. (2000). Measurement and prediction of residual stresses in thick-section steel welds. *The Journal of Strain Analysis for Engineering Design*, 35:287-305.

Smith, L. M. (1992). Clad Steel: An Engineering Option. *Offshore Technology*, 1-14.

Soul, F., & Hamdy, N. (2012, November 21). *Numerical Simulation of Residual Stress and Strain Behaviour Afer Temperature Modification.* Retrieved September 27, 2016, from INTECH Open Sciecne Open Minds: http://cdn.intechopen.com/pdfs-wm/40995.pdf

Steel, P. (2016, April 1). *pearlitesteel.com*. Retrieved July 7, 2016, from Difference between Stainless Steel and Mild Steel: http://pearlitesteel.com/difference-between-stainless-steel-and-mild-steel/

Stone, & C. P. Omnes, P. R.-S. (2015, February 20). *Research Gate*. Retrieved September 12, 2016, from www.researchgate.net: https://www.researchgate.net

Sun, D. S.; Liu, Q.; Brandt, M.; Janardhana, M. and Clark, G. (2012). Microstructure and Mechanical Properties of Laser Cladding Repair of AISI 4340 Steel. *International Congress of the Aeronautical Sciences*, 1-9.

Swap, S. (n.d.). *Electron Backscatter Diffraction (EBSD).* Retrieved August 10, 2016, from Geochemical Instrumentation and Analysis: http://serc.carleton.edu/research_education/geochemsheets/ebsd.html

Swap, S. (n.d.). *Electron Backscatter Diffraction (EBSD)*. Retrieved August 12, 2016, from Integrating Research and Education: http://serc.carleton.edu/research_education/geochemsheets/ebsd.html

TANIGUCHI, S. a. (2015). *Refinement Mechanism of Heat-Affected Zone Microstructures on TiO Steels.* Amagasaki City, Hyogo : NIPPON STEEL & SUMITOMO METAL TECHNICAL REPORT No. 110 SEPTEMBER 2015.

Tapany, U. (2007, May-August). *Suranaree University of Technology.* Retrieved 09 26, 2016, from Tension Test: eng.sut.ac.th/metal/images/stories/pdf/08_Tension_test

Technologies, S. a. (2012, 06 01). *Iron-Carbon Phase Diagram*. Retrieved 07 09, 2016, from SubsTech: http://www.substech.com/dokuwiki/doku.php?id=iron-carbon_phase_diagram

Technology, T. U. (2007, september - December). *Weld Microstructure.* Retrieved August 14, 2016, from www.eng.sut.ac.th: http://eng.sut.ac.th/metal/images/stories/pdf/04_Weld%20microstructure01.pdf

Teng, T.-L. F.-P.-H.-C. (2001). Analysis of residual stresses and distortions in T-joint fillet welds. *International Journal of Pressure Vessels and Piping*, pp 523 - 538.

Terashima, S., & Bhadeshia, H. K. (2006). Changes in toughness at low oxygen concentrations in steel weld metals. *Science and Tehcnology of Welding and Joining Volume 11, 2006 - Issue 5*, pp 509-516.

Testing, A. S. (2005). *Hardness Conversion Tables for Metals Relationship Among Brinell Hardness, Vickers Hardness, Rockwell Hardness, Superficial Hardness, Knoop Hardness and Scleroscope Hardness.* West Conshohocken, Pennsylvania, USA: Annual Book of ASTM Standards, vol. 3.01. American Society for Testing and Materials.

Thermodynamics, C. (2011). *Calculation of Phase dIADRAMS USING THE calphad mETHOD*. Retrieved 07 09, 2016, from http://www.calphad.com/iron-carbon.html

TIP TIG, U. (2019, August 18). *The Evolution of TIG*. Retrieved from Inconnel Welding Applications: http://tiptigusa.com

Traore, Y., & Bouchard, P. F. (2011). A novel cutting strategy for reducing plasticity induced errors in residual stress measurements made with the contour method. *ASME 2011 Pressure Vessels and Piping Conference:* (pp. pp1201 -12). American Society of Mechanical Enginneers.

TWI. (2004, May-June). *Mechnical Testing Part - Tensile Testing Part II.* Retrieved February 14, 2017, from TWI: http://www.twi-global.com

TWI. (2007). *Cladding.* Retrieved December 21, 2016, from TWI- Capabilities: http://www.twi-global.com/capabilities/materials-and-corrosion-management/surface-engineering-and-advanced-coatings/cladding/

TWI. (2011). Assessment of Flaws in Pipe Girth Welds. *CBMM-TMS International Conference on Welding of High Strength Pipeline Steels* (pp. 1-6). Brazil: TWI Ltd. Retrieved from TWI.

TWI. (2016). Retrieved August 6, 2016, from http://www.twi-global.com/technical-knowledge/faqs/material-faqs/faq-what-is-the-difference-between-heat-input-and-arc-energy/

TWI. (2016). *Aluminium Alloys*. Retrieved August 6, 2016, from TWI GROUP Websites: http://www.twi-global.com/technical-knowledge/job-knowledge/weldability-of-materials-aluminium-alloys-021/

TWI. (2016, January 5). *Cladding.* Retrieved December 21, 2016, from TWI- Capabilities: http://www.twi-global.com

TWI. (2016). *What are the Factors Affecting Distortion*. Retrieved July 6, 2016, from TWI GROUP WEBSITES: http://www.twi-global.com/technical-knowledge/faqs/process-faqs/faq-what-are-the-factors-affecting-distortion/

TWI. (2016). *What is the relationship between Hardness, Microstructure and Toughness in Steel Heat Affected Zones?* Retrieved 8 6, 2016, from TWI Group Websites: http://www.twi-global.com/technical-knowledge/faqs/material-faqs/faq-what-is-the-relationship-between-hardness-microstructure-and-toughness-in-steel-heat-affected-zones/

TWI. (2019, 09 14). *Design Part 3.* Retrieved from TWI: https://www.twi-global.com

Ueda, Y. a. (1971). Analaysis of Thermal-Elastic Stress and Strain during Welding by Finite Element Method . *JWRI*.

Ueda, Y. F. (1986). New Measuring Method of Axis-symmetric Three-Dimensional Residual Stresses Using Inherent Strains as Parameters. *Journal of Engineering Materials and Technololgy*, 108: 328-334.

Vaidyanathan, S., Todato, A. F. and Finnie, I. (1973). Residual Stress Due to Circunferential Welds. *Journal of Engineering Material and Technology* , 95: 233-237.

Vida-Simiti, I. J. (2004). *Applications of Scanning Eletron Microscopy (SEM) in Nanotechnology and Nanoscience.* Romania: Technical University of Cluj-Napoca.

Vladimir, K. (2014, 03 07). *Process integrated chracterization using X-ray Diffraction Method - Laserprocessing.* Retrieved from Institute of Applied Materials: https://www.iam.kit.edu/wk/english/307.php http://www.iam.kit.edu/

Wang, W. (2016, February 11). *Weld failure Analysis* . Retrieved October 03, 2016, from EWI We Manufacture Innovation: https://ewi.org/eto/wp-content/uploads/2016/01/Weld-Failure-Analysis-Wang.pdf

Wang Yong -Yi and Liu Ming (2004) A Comprehensive Update in the Evaluation of Pipeline Weld Defects U.S. DOT Agreement No. DTRS56-03-T-0008, PRCI Contact No. PR-276-04503. P 1 – 78

Weldability. (2017). *Weldability.* Retrieved February 25, 2017, from Weldability: www.weldability-sif.com

Wiesner C. S., Maddox S. J., Xu W., Webster G. A., Burdekin F. M., Andrews R. M. and Harrison J. D. (2000), Engineering Critical Analyses to BS 7910 – The UK Guide on methods for assessing the acceptability of flaws in metallic structures IJPVP 77, 883 – 893

Withers P. J. and Bhadeshia H. K. D. H. (2001). Residual stress Part 2 – Nature and origins. *Materials Science and Technology*, 17:366-75.

Withers P. J. (2007) Residual Stress and Its Role in Failure, Report on Progress in Physics, IOP Publishing Ltd. 70: 2211 - 64

Withers P. J. & Bhadeshia H. K. D. H. (2001). Residual stress. Part 1–Measurement techniques. *Materials Science and Technology*, 17:355-65.

Wolfgang, Schulz, K., & Josef, W. K. (August 24, 1999). *Patent No. 5,940,951.* USA.

Xi, L., Banu, M., Hu, S.J., Cai, W. and Abell, J. (2016). Performance Prediction for Ultrasonically Welded Dissimilar Materials Joints. *Journal of Manufacturing Science and Engineering*, 1 to 13.

Xiangyang, L. (2002). *Influence of Resisdual Stress on Fatigue Failure of Welded Joints.* North Carolina: PhD Thesis, North Carolina State University.

Xu, Z. (2014). *Finite Element Modelling of Residual Stress of Welding (M.Sc.Thesis).* London: Brunel University London.

Yaghi, A. B. (2004). *State of the Review-Welding Simulation using Finite Element Methods,.* Nottingham: The University of Nottingham.

Yaghi, A.; Hyde, T. H.; Becker, A. A.; Sun, W. and Williams J. A. (2006). Residual Stress Simulation in Thin and Thick-Walled Stainless Steel Pipe Welds including Pipe Diameter Effects. *International Journal of Pressure Vessels and Piping*, 864-874.

Yan W, Z. L.-y. (2009). Change of tensile behavior of a highstrength low-alloy steel with tempering temperature. . *Materials Science and Engineering: A*, 517:369-74.

Yang H, Z. Y. (2008). An experimental investigation on critical specimen sizes of high strength steels DP600 in resistance spot welding. *Materials & Design*, 29:1679-84.

Yousefieh, M. S. (2011). Optimization of the pulsed current gas tungsten arc welding (PCGTAW) parameters for corrosion resistance of super duplex stainless steel (UNS S32760) welds using the Taguchi method. *Journal of Alloys and Compounds*, pp 782 - 788.

Youtsos, A. G. (2006). *Residual Stress and Its Effect on Fatigue and Fracture.* Greece: Springer.

Youtsos, A. G. (2006). *Residual Stress and Its Effects on Fatigue and Fracture.* Dordrecht, The Netherlands: Springer.

Yupiter H.P., M. A. (2013). Welding distortion analysis of multipass joint combination with different sequences using 3D FEM and experiment. *Int. J. Press. Vessel. Pip.*, 111–112:89–98.

Zhang C, S. X. (2012). Effect of microstructure on mechanical properties in weld-repaired high strength low alloy steel. *Materials & Design.*, 36:233-42.

Zhang, C., & Lu, P. H. (2012). Effect of buffer layer and notch location on fatigue behavior in welded high-strength low-alloy. *Journal of Materials Processing Technology*, 212:2091-101.

Zhao, W. Wang, W. Chen, S. Qu, J. A. (2011;). Effect of simulated welding thermal cycle on microstructure and mechanical properties of X90 pipeline steel. . *Materials Science and Engineering:*, 528:7417-22.

Zhao, M.-C., & Shan, Y.-Y. X. (2002). Investigation on the H2S-resistant behaviors of acicular ferrite and ultrafine ferrite. *Materials Letters*, 57:141-5.

APPENDIX 1- Publications based on work presented in Chapter 3

Proceedings of the ASME 2017 Pressure Vessels and Piping Conference
PVP2017
July 16-20, 2017, Waikoloa, Hawaii, USA

PVP2017-66272

THERMAL ANALYSIS OF GIRTH WELDED JOINTS OF DISSIMILAR METALS IN PIPES WITH VARYING CLAD THICKNESSES

Bridget Kogo
Brunel University London
London, Middlesex, United Kingdom

Bin Wang
Brunel University London
London, Middlesex, United Kingdom

Luiz Wrobel
Brunel University London
London, Middlesex, United Kingdom

Mahmoud Chizari
Brunel University London
London, Middlesex, United Kingdom

ABSTRACT

Thermal analyses of girth welded joints of clads have been carried out using 2D and 3D finite element analysis (FEA) by using the engineering software Abaqus v.2016 (Dassault Systèmes). Transient temperature curves have been generated for different cladding thicknesses (of stainless steel and mild steel). The welding of the two dissimilar materials has been carried out in-house with the aid of a Tungsten Arc weld with dynamic measurement of the temperature profile in the vicinity areas of the welding track using high temperature thermocouples. Comparison of the measured temperature versus the simulation results shows close agreement.

INTRODUCTION

Welding is a joining technology used in the process of fabrication and manufacturing of offshore pipelines before laying them on the sea floor and prior to use in deep offshore operations. Up until now welding, particularly in cylindrical objects (most especially pipelines), has remained a source of concern due to its complexity.

The novelty of this paper is that we address the welding of two dissimilar materials. The demand for reliable, long-lasting and safe engineering facilities, mode of operation and working environment is high in every industrial application. This spurs the need for joining dissimilar metals with the main aim of achieving enhanced and improved components with better mechanical and thermal properties, light weight and outstanding performance, as well as prolonged in-service life [1]. An effective weld between dissimilar metals is one in which the strength of the weld equals the weaker of the two metals being joined. This invariably means great tensile strength and ductility to prevent failure in the weld joint [2]. The welding of two dissimilar materials (mild steel and stainless steel, MSSS) with varying clad thicknesses was carried out in- house with dynamic measurements of the temperature profile in the vicinity areas of the welding track using high temperature thermocouples, in order to obtain the transient thermal responses so as to enable a deeper understanding of the thermal loading associated with the welding of two dissimilar metals, hence advancing the performance of pipelines in service.

Another contribution of this research is the cladding layer (double layer) as compared with a single layer of pipe welds, which is the predominant manner of welding in pipeline industries. High corrosion resistant materials such as stainless steel possess good strength and are tough in nature; however, there are corrosion-resistant materials such as gold and glass which cannot be used for every structure due to their low strength and high cost. Cladding provides corrosion resistance. The use of a clad layer on a base metal helps reducing the cost, enhancing manufacturing outcome [3].

The thickness of a clad layer usually varies from 2mm to 20mm and finds use in different weld techniques such as Gas Metal Arc Welding (GMAW), Manual Metal Arc Welding (MMAW), Submerged Arc Welding (SAW), Flux Cored Arc Welding (FCAW), Laser Deposition and Gas Tungsten Arc Welding (GTAW) [3]. The clad, which in this case is a stainless steel layer in the interior of the pipe, provides the required resistance to abrasion, corrosion and oxidation whereas carbon steel, which is the base metal of the outer pipe layer, supplies the strength, increases the thermal conductivity of the overall structure as well as its fabricability.

It is of great importance to guarantee the integrity of the Heat Affected Zone (HAZ) and the clad metal while concurrently ensuring the material properties of the base metal. Invariably, the

SpringerLink

The World Congress on Engineering
WCE 2017: Transactions on Engineering Technologies pp 389-403 | Cite as

Residual Stress Simulations of Girth Welding in Subsea Pipelines

Authors | Authors and affiliations

Bridget Kogo, Bin Wang, Luiz Wrobel, Mahmoud Chizari

Conference paper
First Online: 18 August 2018

Abstract

Simulation of the welding of two dissimilar materials, stainless steel and mild steel, has been carried out using finite element together with experiments to validate the method and better understand the transient temperature profiles and the stress distribution in a cladded pipe. The results clearly show that the temperature distribution in the modelled pipe is a function of the thermal conductivity of each weld metal as well as the distance away from the heat source. The outcome of the study has been compared with previous findings.

Keywords

Dissimilar material joint | FEA | Girth weld | Residual stress | Subsea pipelines | Transient temperature response

Notes

Acknowledgements

The authors want to express their gratitude to IAENG and WCE for the great privilege of being awarded Best Student Paper Publication at the WCE 2017 Conference and for the opportunity to publish this paper as an IAENG publication.

The authors want to express their gratitude to Brunel University London for the facilities provided and conducive research environment.

The first author also thanks The Petroleum Technology Development Fund (PTDF) for their funding and support through which this research has been made possible.

Residual Stress Simulations of Girth Welding in Subsea Pipelines

Bridget Kogo, Bin Wang, Luiz Wrobel and Mahmoud Chizari

Abstract Simulation of the welding of two dissimilar materials, stainless steel and mild steel, has been carried out using finite element together with experiments to validate the method and better understand the transient temperature profiles and the stress distribution in a cladded pipe. The results clearly show that the temperature distribution in the modelled pipe is a function of the thermal conductivity of each weld metal as well as the distance away from the heat source. The outcome of the study has been compared with previous findings.

Keywords Dissimilar material joint · FEA · Girth weld · Residual stress
Subsea pipelines · Transient temperature response

1 Introduction

Welding of cylindrical objects is complex and poses a source of concern in the manufacturing processes. There are several benefits of welding as a joining technology which includes cost effectiveness, flexibility in design, enhanced structural integrity, and composite weight reduction. However, thermal stresses are usually initiated on the weld and the base metal [1–5]. Poorly welded joints result in leakages, pipe

B. Kogo (✉) · B. Wang · L. Wrobel · M. Chizari
Mechanical, Aerospace and Civil Engineering Department, College of Engineering, Design and Physical Sciences, Brunel University London, Uxbridge UB8 3PH, UK
e-mail: biddyagada@yahoo.com

B. Wang
e-mail: Bin.Wang@brunel.ac.uk

L. Wrobel
e-mail: Luiz.Wrobel@brunel.ac.uk

M. Chizari
e-mail: mahmoudchizari@yahoo.com

M. Chizari
School of Mechanical Engineering, Sharif University of Technology, Tehran, Iran

S.-I. Ao et al. (eds.), *Transactions on Engineering Technologies*,
https://doi.org/10.1007/978-981-13-0746-1_30

459098_1_En_30_Chapter ☑ TYPESET ☐ DISK ☐ LE ☑ CP Disp.:7/6/2018 Pages: 16 Layout: T1-Standard

Microstructural Analysis of a Girth Welded Subsea Pipe

Bridget E. Kogo, Bin Wang, Luiz C. Wrobel and Mahmoud Chizari, *Member IAENG*

***Abstract*—This research focuses on simulation of the dissimilar materials' welding, stainless steel and mild steel, using finite element and experiment to enhance the method and better understand the transient temperature profiles and the stress distribution in a cladded pipe. The microstructural come as fenestrated and the computer results show that the temperature distribution in the modelled pipe is a function of the thermal conductivity of each weld metal as well as the distance away from the heat source.**

***Index Terms*—Transient temperature response, dissimilar material joint, girth weld, microstructure**

I. Introduction

It is known that the welding of cylindrical objects is complex and poses a source of concern in manufacturing processes. There are several benefits of welding as a joining technology which includes cost effectiveness, flexibility in design, enhanced structural integrity, and composite weight reduction. However, thermal stresses are usually initiated on the weld and the base metal [1-4]. Poorly welded joints result in leakages, pipe failures and bursts, which lead to possible environmental hazards, loss of lives and properties. Welding of dissimilar materials is carried out in-house using Gas Metal Arc Weld (GMAW), and a finite element analysis (FEA) on pipe models having different clad thicknesses of 2mm and 12mm, respectively, and the temperature versus distance profile obtained. The 12mm cladded pipe results are discussed in this paper [3].

The process of carrying out welding using an arc weld entails melting down the base metal and, in this research, it also involves melting down the clad metal. In the course of carrying out the welding, filler metals are also melted such that the solution formed by heating up all these materials and holding them at that range of temperature long enough permits the diffusion of constituents into the molten solution; this is followed by cooling down rapidly in order to maintain these constituents within the solution. The result of this procedure generates a metallurgical structure positioning in-situ the material which supplies superior tensile strength. The bulk of the material immediately after the fusion zone (FZ), which has its characteristics altered by the weld, is termed Heat Affected Zone (HAZ). The volume of material within the HAZ undergoes considerable change which could be advantageous to the weld joint, but in some circumstances, might not be beneficial. The aim of this paper it to closely look at welding of dissimilar materials and compare the results with the computer modelling of different cladding thickness.

Manuscript received Feb 15, 2017; revised January 17, 2018. This work is extended and revised version of previous publication in WCE2017 as referenced in [3].

Bridget E. Kogo (corresponding author) is with Mechanical, Aerospace and Civil Engineering Department, College of Engineering, Design and Physical Sciences, Brunel University London, UK (e-mail: biddyagada@yahoo.com)

Bin Wang is with Mechanical, Aerospace and Civil Engineering Department, College of Engineering, Design and Physical Sciences, Brunel University London, UK (e-mail: bin.wang@brunel.ac.uk)

Luiz C. Wrobel is with Mechanical, Aerospace and Civil Engineering Department, College of Engineering, Design and Physical Sciences, Brunel University London, UK (e-mail: luiz.wrobel@brunel.ac.uk)

Mahmoud Chizari is with the School of Mechanical Engineering, Sharif University of Technology in Tehran. He is also with Mechanical, Aerospace and Civil Engineering Department, College of Engineering, Design and Physical Sciences, Brunel University London, Uxbridge, UB8 3PH, UK (e-mail: mahmoudchizari@yahoo.com)

II. Tensile Testing

Several factors such as temperature, strain rate and anisotropy affect the shape of the stress- strain curves. The parent metals have different elongation characteristics, and each exhibit this at different rates because of the applied stress under which it is stretched. Similarly, the behaviour of the weld metal under the displacement curve is also due to slip, which is caused by the elongation and failure of the different metals (mild steel and stainless steel) present within the weld samples, since they each have their original ultimate tensile stress (UTS). The volumetric change and yield strength in Figure 1 as a result of martensitic transformation have influences on the welding residual stresses, increasing the magnitude of the residual stress in the weld zone as well as changing its sign.

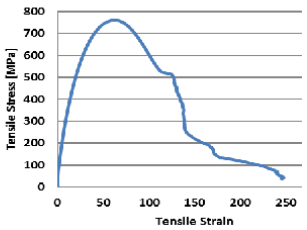

Fig. 1. Stress-strain curve of 12mm cladded pipe

III. Electron Microscopy Examination

A. Sample Preparation

1. Two different samples of weld were cut from the main weld. The samples each of the parent material: 12mm stainless steel and 10mm mild steel were cut into dimensions: 40mm x 20mm and 20mm.

2. The parent material samples were formed into a mould using 5 spoonsful or 2.5 spoonful of Bakelite S and

International Journal of Offshore and Polar Engineering (ISSN 1053-5381)
http://www.isope.org/publications/publications.htm

Vol. 28, No. 4, December 2018, pp. 380–386; https://doi.org/10.17736/ijope.2018.oa22

Experimental and Numerical Simulation of Girth Welded Joints of Dissimilar Metals in Clad Pipes

Bridget Kogo*, Bin Wang and Luiz C. Wrobel
Department of Mechanical, Aerospace and Civil Engineering, Brunel University
London, Uxbridge, Middlesex, United Kingdom

Mahmoud Chizari
School of Mechanical Engineering, Sharif University of Technology
Tehran, Iran

The welding of two dissimilar materials was carried out in-house with the aid of a tungsten arc weld having dynamic measurement of temperature profiles in the vicinity areas of the welding track using high-temperature thermocouples. A previous comparison of the simulated and measured transient temperatures versus finite element simulation is shown. Stress analyses of the pipe were carried out using finite element analysis (FEA) simulations with two different clad thicknesses. Results of thermal analysis show a close match, and laboratory tests reveal occurrences at the welded joints, the fusion zone and the heat-affected zone (HAZ); the result of stress analysis also shows good agreement when validated with neutron diffraction experimental results.

INTRODUCTION

In joining technology, welding is one of the vital techniques used to make continuous pipelines in industry. The thermal and mechanical loading in the process has a profound impact on the integrity of the pipeline over its service life. An accurate and thorough assessment is needed on the associated residual stress and its effect on the structural properties of the pipeline.

One of the novelties of this research is the understanding of the welded joints' temperature responses, as demonstrated by positioning high-temperature thermocouples at strategic points on the welded joints to capture the transient temperature response at different points. It is not enough to assume that the distribution of heat through the weld metal will depend on the distance from the thermocouples to the heat source only; the temperature profile must actually be studied to uncover any peculiar trends.

The second impact of this research is the treatment of dissimilar materials through the implementation of a cladded layer. Previous experimental works have been carried out on the welding of single-layer pipes, but very little work has been carried out on cladding. Cladding is carried out mainly for the purpose of increased strength after which other qualities such as enhanced corrosion resistance can follow. Since two metals of different chemical constituents are welded together, we study the properties of the newly formed weld joint in terms of its chemical composition, strength, corrosion resistance, etc. (Total Materia, 2006; Kah et al., 2014).

The heat-affected zone (HAZ) also has an impact as it addresses a gap in knowledge. Since welding is carried out on two dissimilar materials, there is the need to investigate what occurs in the HAZ of the welded joint because the chemical component of the HAZ is altered via high weld temperatures. There is also a need to understand the location of the weakest point of burst because if a structure is to fail, the failure begins at that point.

The thermal properties of the inner and outer surfaces of the pipe are clearly defined and described in the next section of this paper. The finite element analysis (FEA) software considers the transient temperature variations and obtains close agreement with the experiment. We note that the friction between the two layers has not been considered—we define a frictionless contact between the two layers because we consider the relative motion between the two layers to be negligible; friction, however, can be considered in future research.

The thermal analysis in cladded girth welded joints was carried out using three-dimensional (3D) finite element analysis in Abaqus. Results of the transient temperature curves have been generated for the different cladding thicknesses (stainless steel and mild steel).

Welding of the two dissimilar materials was also carried out in-house with the aid of a tungsten arc weld with dynamic measurement of temperature profile in the vicinity areas of the welding track using high-temperature thermocouples. A comparison of the measured temperature with the simulation outcome shows good agreement. Laboratory tests were also carried out to reveal the occurrences at the fusion zone (FZ) and the HAZ of the welded joints.

In the thermal model, it was observed that the distribution of heat in the HAZ was maximum at the heat source position and minimum at the start and end points, indicating that heat was trapped in the middle region, which is responsible for the fluctuations in the heat distribution in these zones (Inspectioneering, 2016). It has therefore been deduced that the heat was retained within the welding spool for approximately 10 seconds in the middle region of the weld prior to cooling. The distribution was also considered in the final output as a result of the cavities present within the model (Lampman, 2001; Goldak and Akhlaghi, 2005; Youtsos, 2006; Qureshi, 2008).

Convection is the major procedure for transmission of heat from the weld strip to the immediate environment, whereas the

*ISOPE Member.

Received February 7, 2018; updated and further revised manuscript received by the editors March 23, 2018. The original version (prior to the final updated and revised manuscript) was presented at the Twenty-seventh International Ocean and Polar Engineering Conference (ISOPE-2017), San Francisco, California, June 25–30, 2017.
KEY WORDS: Thermal analysis, dissimilar metals, girth welding, clad pipes, 3D finite element modelling, heat-affected zone, fusion zone.

Proceedings of the Twenty-seventh (2017) International Ocean and Polar Engineering Conference **www.isope.org**
San Francisco, CA, USA, June 25-30, 2017

ISBN 978-1-880653-97-5; ISSN 1098-6189

Thermal Analysis of Girth Welded Joints of Dissimilar Metals in Clad Pipes: Experimental and Numerical Analysis

Bridget Kogo, Bin Wang, Luiz Wrobel and Mahmoud Chizari
Mechanical, Aerospace and Civil Engineering, Brunel University London.
Uxbridge, Middlesex, United Kingdom

ABSTRACT

Welding of two dissimilar materials was carried out in-house with the aid of a Tungsten Arc weld with dynamic measurement of temperature profiles in the vicinity areas of the welding track using high temperature thermocouples. A comparison is shown of the measured transient temperatures versus the FEA simulations. Results showed a close match and laboratory tests revealed the occurrences at the welded joints, FZ and HAZ. Mechanical tests showed that for cladded pipes of thickness 2mm and 12mm, the weakest point of the joint is the HAZ. This is clearly supported by findings from the experimental analyses.

KEY WORDS: Thermal Analysis; Dissimilar Metals; Girth Welding; Clad Pipes; 3D Finite Element Modeling; HAZ; FZ

NOMENCLATURE

BC Boundary Condition
CES College of Engineering and Sciences
CM Clad Metal
FEA Finite Element Analysis
FZ Fusion Zone
GMAW Gas Metal Arc Weld
HAZ Heat Affected Zone
MS Mild Steel
PM Parent Metal
WA Weld Axis
WE Weld Edge
WL Weld Line
WM Weld Metal
WS Weld Start
SS Stainless Steel
TC Thermocouples

INTRODUCTION

Welding is the primary joining technology used to make continuous pipelines in industry. The thermal and mechanical loading in the process has a profound impact on the integrity of the pipeline over its service life. An accurate and thorough assessment is needed on the associated residual stress and its effect on the structural properties of the pipeline.

One of the major gaps in knowledge addressed by this research is the understanding of the temperature responses from the welded joints. This is done with the aid of thermocouples positioned at strategic points on the welded joints, in order to capture the transient temperature response at different points. It is not enough to assume that the distribution of heat through the weld metal will depend on the distance from the thermocouples to the heat source only, but to actually study the temperature profile in order to uncover any peculiar trends.

Another gap addressed here is the treatment of dissimilar materials through the implementation of a cladded layer. Previous experimental works have been carried out on the welding of single layer pipes, but very little work has been carried out on cladding. Cladding is carried out mainly for the purpose of increased strength after which other qualities like enhance corrosion resistance can follow. Since two metals of different chemical constituents are welded together, we study the properties of the newly formed weld joint in terms of its chemical composition, strength, corrosion resistance, etc. (Materia, 2006; Kah et al., 2014).

The Heat Affected Zone (HAZ) is also addressed as a gap in knowledge. Since welding is carried out on two dissimilar materials, there is the need to investigate what occurs in the HAZ of the welded joint since the chemical component of the HAZ is altered via high weld temperatures. There is also a need to understand the location of the weakest point of burst because if a structure is to fail, the failure begins at that point.

The thermal properties of the inner and outer surfaces of the pipe have been clearly defined and described in the paper. The FEA software has considered the transient temperature variations and has obtained close agreement with the experiment. It has been noted that the friction

Thermal Analysis of Cladded Pipe at a Joint Connection

Bridget KOGO [1,*], Bin WANG [1], Luiz WROBEL [1], Mahmoud CHIZARI [1]

* Corresponding author: Tel.: ++44 (0)7825222578; Email: bridget.kogo@brunel.ac.uk

1 College of Engineering, Design and Physical Sciences, Brunel University London, UK

Abstract Thermal analyses of girth welded joints of clads have been carried out using both finite element analysis and experimental simulation. Transient temperature curves have been generated for different cladding thicknesses (of stainless steel and mild steel). The welding of the two dissimilar materials has been carried out in-house with the aid of a Tungsten Arc weld with dynamic measurement of the temperature profile in the vicinity areas of the welding track using high temperature thermocouples. Comparison of the measured temperature versus the simulation results shows close agreement.

Keywords: Heat transfer, Clad Pipe, Thermal Conductivity, Numerical Modelling, Experimental Study

1. Introduction

Welding is a joining technology used in the process of fabrication and manufacturing of offshore pipelines before laying them on the sea floor and prior to use in deep offshore operations. Up until now welding, particularly in cylindrical objects (most especially pipelines), has remained a source of concern due to its complexity. The novelty of this paper is the welding of two dissimilar materials.

2. Thermal Analysis

2.1 Experimental Method The relevance of this research is that it points out the thermal effects of welding as it concerns the Heat Affected Zone, temperature profile and heat distribution. The temperature responses from the welded joint are obtained with the aid of thermocouples positioned at strategic points on the welded joints, in order to capture the transient response at these different points and with the main aim of understanding and justifying the reasons for the thermal responses. It is not enough to presume that the distribution of heat through the weld metal will depend on the closest thermocouple to the heat source only but to actually study the temperature profile and heat distribution in order to be able to account for any peculiarities discovered in the thermal distribution which occur in plates, as well as circumferentially welded pipe joints or cylinders. The factors considered for the thermal analysis include penetration of the HAZ, thermal conductivity and density of the metals, solidus and liquidus temperatures as well as the latent heat capacity [1]; [2].

Fig 1: 2mm MSSS clad showing thermocouples 1 to 4 positions;

The result of the 2mm clad in Figure 3, show the speed or rate of travel of the temperatures from the point of weld (weld line WL) to the respective thermocouples. There is a gradual cooling down period after the peak temperatures are attained. Although thermocouple 2 reaches the highest peak in view of its centralized position (10mm from the weld edge and 50mm from the weld start), and slowly dissipates the heat to the surrounding

APPENDIX 2 – Publications based on work presented in Chapter 4

Proc. of the Third Intl. Conf. Advances in Civil, Structural and Mechanical Engineering- CSM 2015

ISBN: 978-1-63248-062-0 doi: 10.15224/ 978-1-63248-062-0-56

3D SIMULATION OF STRESS IN GIRTH WELDING OF PIPELINE

Thermal Analysis of Girth Welding in Pipeline

[Bridget Kogo, Dr. Bin Wang, Dr. Mahmoud Chizari]

Abstract—**Welding is the primary joining technology used to make continuous pipelines in the industry. The thermal and mechanical loading in the process has a profound impact on the integrity of the pipeline over its service life. An accurate and thorough assessment is needed on the associated residual stress and its effect on the structural properties of the pipeline.**
3D simulations of stress in girth welded pipe sections have been carried out using the Abaqus CAE software in two steps, the first being the thermal modelling with a moving hot spot and added mass whereas the second being the stress or mechanical analysis.
In the Thermal Model, it was observed that the distribution of heat in the heat affected zone (HAZ) was maximal at the apex of the heat flux whereas minimum at the start and end points indicating that heat was trapped in the middle region which is responsible for the fluctuations in the heat distribution in these zones. Contour plots of these results further confirm same pattern of temperature distribution. This further implies that the quantity of heat inputted into the model affects the geometry of the model. The design as well as the diameter of the pipe also affected the geometry. It has therefore been deduced that the convective heat was retained within the welding spool for some length of time approximately 10 seconds in the middle region of the weld prior to cooling. The significance of the radiative heat distribution was also considered in the final result as a result of the cavities present within the model.
Due to insufficient time, the thermal analysis has been projected in this paper. The Stress analysis will follow in due course.

Keywords—Weld , Girth Weld, Heat Affected Zone (HAZ), Thermal analysis, Stress and Pipeline (key words)

Introduction

This particular model entails a two material weldment model consisting of the parent metal and the weld metal, with a Heat Affected Zone (HAZ) being considered. The specific type of solid element used in this analysis is the 20-node quadratic hexahedral elements of type DC3D20, heat transfer brick. [1]. It has been confirmed that temperature field produces thermal strain during the welding process which results in residual stress induced elastoplastic behaviour of the material in response to the transient thermal stresses. (Piekara et al).

The Stress induced from welding is one of the bases for cracking and fracture in welded pipes; which imply that the thorough understanding of this phenomenon will enable accurate prediction of the weld induced stresses and as a result aids the design of welded structures.

The quantity of heat applied to the metal defines the degree of melting and distortion welding stress. The Phase transformation from solid to liquid in the state is also accounted for during the welding process, the latent heat of fusion is used to define heat effects similar to molten metal of the weld pool.

Bridget Kogo
College of Engineering, Design and Physical Sciences/ Brunel University London
United Kingdom

Dr Bin Wang
College of Engineering, Design and Physical Sciences/ Brunel University London
United Kingdom

Dr Mahmoud Chizari
College of Engineering, Design and Physical Sciences/ Brunel University London
United Kingdom,

Factors Considered

Consideration of Factors for Thermal Analysis

The factors considered while carrying out the modelling of the thermal analysis is the penetration of the Heat Affected Zone (HAZ) of the weld metal into the parent metal. The thermal conductivity of each part of the Finite Element mesh equivalent to the weld passes is taken into account and prior to being positioned, the elements are assigned thermal conductivity of air, which changes to the steel value as soon as they are placed. [51].

The density of the metal and the solidus and liquidus temperatures as well as the specific heat capacity and latent heat capacity are also taken into consideration considering the fact that they are very vital and play major role in determining the thermal analysis of the weld.

Geometry of Model

The Welding simulation was carried out on X65 Carbon Steel Pipe having an outer diameter of 30 inches (21.98mm), and wall thickness of 50 mm. Weld mental that was modelled has same material properties as the parent material. The kind of welding utilized in this analysis is the Girth weld from the first weld bead to the seventh. Figure 1 shows the weld model and the sequence of the welds.

For Weld Model containing the passes in their order of sequence, starting from the Left to the right. The first bead otherwise known as root bead is 1.06mm in layer while subsequent beads, are 0.61mm.

The welding procedure involves the dissolving of the welding and letting to cool thereby leaving behind a solidus connecting parent metal to weld. [1].

APPENDIX 3 – Publications based on work presented in Chapter 5

Proceedings of the World Congress on Engineering 2017 Vol II
WCE 2017, July 5-7, 2017, London, U.K.

Residual Stress Simulations of Girth Welding in Subsea Pipelines

Bridget E. Kogo, Bin Wang, Luiz C. Wrobel and Mahmoud Chizari, *Member, IAENG*

***Abstract*—Numerical modelling of the welding of dissimilar materials, stainless steel and mild steel, has been carried out using Abaqus together with Gas Metal Arc Weld (GMAW) in order to provide a better understanding of the transient temperature profiles and the stress distribution in a pipe. The results clearly show that the temperature distribution in the modelled pipe is a function of the thermal conductivity of each weld metal as well as the distance away from the heat source. Results also clearly show agreement with previous findings.**

Index Terms—Transient temperature response, dissimilar material joint, FEA, girth weld

I. Introduction

WELDING of cylindrical objects is complex and poses a source of concern in manufacturing processes. There are several benefits of welding as a joining technology which includes cost effectiveness, flexibility in design, enhanced structural integrity, and composite weight reduction. However, thermal stresses are usually initiated on the weld and the base metal [1-4]. Poorly welded joints result in leakages, pipe failures and bursts, which lead to possible environmental hazards, loss of lives and properties. Welding of dissimilar materials is carried out in-house by using GMAW, and an FEA analysis was carried out on pipe models having different clad thicknesses of 2mm and 12mm, respectively, and the temperature versus distance profile obtained. The 12mm cladded pipe results are discussed in this paper.

The process of carrying out welding using an arc weld entails melting down the base metal and, in this research; it also involves melting down the clad metal. In the course of carrying out the welding, filler metals are also melted such that the solution formed by heating up all these materials and holding them at that range of temperature long enough permits the diffusion of constituents into the molten solution; this is followed by cooling down rapidly in order to maintain these constituents within the solution. The result of this procedure generates a metallurgical structure positioning in-situ the material which supplies superior tensile strength. The bulk of the material immediately after the fusion zone (FZ), which has its characteristics altered by the weld, is termed Heat Affected Zone (HAZ). Referring to Figures 5 (a) and 13, the volume of material within the HAZ undergoes considerable change which could be advantageous to the weld joint, but in some circumstances might not be beneficial.

Manuscript received Feb 15, 2017; revised April 05, 2017.

Bridget E. Kogo (corresponding author) is with Mechanical, Aerospace and Civil Engineering Department, College of Engineering, Design and Physical Sciences, Brunel University London, UK (e-mail: biddyagada@yahoo.com)

Bin Wang is with Mechanical, Aerospace and Civil Engineering Department, College of Engineering, Design and Physical Sciences, Brunel University London, UK (e-mail: bin.wang@brunel.ac.uk)

Luiz C. Wrobel is with Mechanical, Aerospace and Civil Engineering Department, College of Engineering, Design and Physical Sciences, Brunel University London, UK (e-mail: luiz.wrobel@brunel.ac.uk)

Mahmoud Chizari is with the School of Mechanical Engineering, Sharif University of Technology in Tehran. He is also with Mechanical, Aerospace and Civil Engineering Department, College of Engineering, Design and Physical Sciences, Brunel University London, Uxbridge, UB8 3PH, UK (e-mail: mahmoudchizari@yahoo.com).

II. FE Analysis

A. Numerical Analysis

The underlying theory behind weld research is based on the Gaussian transformation principle, which states that 'A Gaussian flat surface has a Gaussian curvature at each and every point of the magnitude of zero'. Going by this principle, the surface of a cylinder can be said to be a Gaussian flat plane since it can be revolved from a piece of paper. Furthermore, the implication is that this can be done without stretching the plane, folding or tearing it. The parameter *r(u,v)* is an orthogonal parameterization of a surface [5]. This is further illustrated in Figure 1.

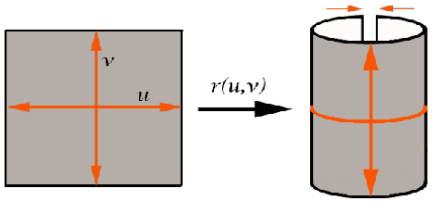

Fig. 1. Conversion of a plate of a certain dimension into a cylinder of the same dimension

This means that the thermal distributions on the surface of a cylinder can also be appreciated by studying the thermal distribution on the surface of welded plates.

For the fully cladded pipe in Figure 2, the total number of nodes in the FEA mesh is 208,640 and elements 180,306. An 8-node linear brick is generated using a hexagonal element. The section of the meshed pipe in Figure 2 which corresponds to the weld is depicted by two squares in the middle. Linear hexahedral elements are recommended for their reduced computation time and ease of running analysis due to the structured grid which makes up the mesh. All elements are identical on this structured array. Hexahedral elements guarantee minimal skewness because of their uniform grid shape; however, a hexahedral mesh can also be unstructured depending on the manner in which element indexing is executed [6].

ISBN: 978-988-14048-3-1
ISSN: 2078-0958 (Print); ISSN: 2078-0966 (Online)

Proc. of the Eighth Intl. Conf. on Advances in Civil, Structural and Mechanical Engineering - CSM 2019

ISBN: 978-1-63248-170-2 DOI :10.15224/978-1-63248-170-2-01

Authentication in Welded Clad Plate with Similar Material and Thickness

Bridget Kogo, Bin Wang, Luiz Wrobel and Mahmoud Chizari

***Abstract*— This paper continues the research previously done by authors on numerical modelling of the dissimilar welded joints with varying clad thicknesses using a commercial finite element software. The current study simulates the welding conditions of a similar clad plate with a thin thickness. The computer simulated outcome then verified with the measured data of from other researchers. A close match between the numerical models and the experimental data was found.**

Keywords*— *FEA, stress analysis, clad plates, stress authentication, similar-dissimilar material

I. Introduction

In authors previous papers [1-9] residual stress was introduced as the key advancement in the field of material joining and hybrid programming of material joining concentration technology. Among the various manufacturing methods, the welding a particular type of joining technique in dissimilar materials also poses a contributory factor in the formation of residual stresses within the metal structures. The gas metal arc welding (GMAW) method of joining dissimilar metal plates; stainless steel and mild steel; having different clad thicknesses was carried out in house. In parallel, stress profiles were obtained for the plates using a finite element (FE) modelling. The underlying theory behind this weld research is based on the Gaussian transformation principle and the consequently can be carried out without stretching the plane, folding or tearing it.

The numerical simulation of the similar welded joints with a certain thickness was carried out using Abaqus 2018 (Simulia, US). The computer model was verified using the measured data of from other researchers [3-8]. A close match found between the data obtained from the numerical simulation and those found from the experiment.

To enhance the quality of the study, the residual stress profiles obtained from current study, validated against existing ultrasonic data which was developed practically by other researchers and found close agreement between the outcome of the studies.

Bridget Kogo
Brunel University London, Uxbridge, UK

Bin Wang
Brunel University London, Uxbridge, UK

Luiz Wrobel
Brunel University London, Uxbridge, UK

Mahmoud Chizari
University of Hertfordshire, Hatfield, UK

Sharif University of technology, Tehran, Iran

For the surfaces of the plates, it was discovered that the transverse stress profile near the region of weld experienced perturbations and 'crown effects' of the stress whereas farther away towards the end of the plates, no perturbation exists, hence zero effect due to edge tack.

II. Computer simulation

A. *Specimen's geometry*

The below is a typical model of a 2D Plate showing the weld path across the length of a plate with dimension of 30mm by 20mm and thickness of 1mm. The weld axis line in the center of the plate (red line) has been highlighted in Figure 1. Seven welding stages was defined for the model to complete the welding of the plate across line of axis as shown in Figure 1.

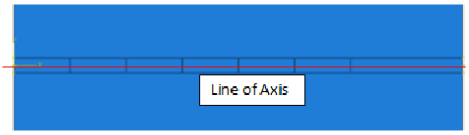

Figure 1. Weld line of a 2D plate model. Seven stage welding was defined for the model to complete the welding of the plate.

B. *FE Meshing*

A mesh convergence analysis was carried out to obtain an optimum element size and type for the model. A 2D stress elements were chosen from the element family, and quadratic elements were used to carry out the meshing in the plate, whereas an 8-node quadratic block was used for the plates. The meshing parameters employed in the stress analysis a stress specific in order to speed up the mapping of the nodal data and elements having same topology in order to improve the convergence during structural analysis. The creation of an element occurs at the solidification temperature, whereas the melting temperature (sink) or ambient temperature is that at which the thermal strains equal zero for thermal expansion coefficients of the base metals and filler metals. The hourglass control used in the meshing element is to enable a single point reduced integration scheme and to regulate convergence, hence preventing unnecessary locking while running the stress analysis in the finite element model.

ASME OMAE – International Conference on Ocean, Offshore and Artic Engineering
OMAE 2019
June 9-14, 2019, Glasgow Scotland, UK

OMAE2019-96348

ASSESSMENT OF WELD OVERLAYS IN A CLADDED PIPING SYSTEMS WITH VARIED THICKNESSES

Bridget Kogo
PhD Student of Mechanical Engineering
Brunel University London, UK

Bin Wang
Reader in Mechanical Engineering
Brunel University London, UK

Luiz Wrobel
Professor in Mechanical Engineering
Brunel University London, UK

Mahmoud Chizari
Senior Lecturer in Mechanical Engineering
University of Hertfordshire, UK

ABSTRACT

This paper continues the research previously done by authors on computer simulation of the dissimilar welded joints with varying clad thicknesses using numerical methods. For different cladding thicknesses comprising of stainless steel and mild steel, stress curves have been generated. The welding of the two dissimilar materials has been carried out in-house with the aid of a tungsten arc weld with dynamic measurement of the temperature profile in the vicinity areas of the welding track using high temperature thermocouples. Comparison of the experimentally measured stresses from literature versus the simulation results shows close agreement.

INTRODUCTION

In order to curtail these unfortunate and rather unhealthy occurrences, there is the need to examine and closely verify the integrity of the welded joints in these pressure vessels [1-3]. The current study addresses the validation of stresses within the welded joints of two dissimilar materials having differing clad thicknesses. This is in continue of the authors previous study [3-8]. The novelty in this paper is seen in addressing the welding between two dissimilar materials. It is obvious from the analysis of weld failure studied above, the demand for reliable long-lasting and very safe engineering facilities, mode of operation and working environment is on high demand in every industrial application. This spurs the need for joining dissimilar metals with the main aim of achieving enhanced and improved components with better mechanical and thermal properties (qualities), light weight and outstanding performance as well as prolonged in-service life for such facilities [2-4]. An outstanding and effective weld between dissimilar metals therefore is one in which the strength of the weld equals the weaker of the two metal being joined. This invariably means great tensile strength and ductility to prevent failure in weld joint [8,9]. The welding of two dissimilar materials; mild steel and stainless steel, (MSSS) with varying clad thicknesses was carried out in- house with dynamic measurements of the temperature profile in the vicinity areas of the welding track using high temperature thermocouples, in order to obtain the transient thermal responses so as to enable a deeper understanding of the thermal loading associated with the welding of two dissimilar metals, hence advancing the performance of pipelines in service [10,11].

Another contribution and novelty of this research is the cladded layer (double layer) as compared with single weld layer of pipe welds which is the predominant manner of welding in pipeline industries. High corrosion resistant materials such as stainless steel possess good strength and are tough in nature; there are corrosion resistant materials such as gold and glass which cannot be used for every structure by reason of their low strength and high cost. Cladding provides corrosion resistance. The use of clad layer on a base metal helps reduce the cost enhancing manufacturing outcome [11,12,13].

The thickness of a clad layer usually varies from 2mm to 20mm and finds use in different weld techniques such as gas metal arc welding (GMAW), manual metal arc welding (MMAW), submerged arc welding (SAW), flux cored arc welding (FCAW), laser deposition and gas tungsten arc welding (GTAW) [3-5].

The clad which in this case is stainless steel layer in the interior of the pipe provides the require resistance to abrasion, corrosion and oxidation, whereas the carbon steel is the base metal of the outer pipe supplies the strength, increases the thermal conductivity of the overall structure as well as the fabricability.

It is of great importance to guarantee the integrity of the heat affected zone and the clad metal while ensuring the material properties of the base metal, concurrently. Invariably, the metallurgy of the clad metal and base metal must be clearly understood [13,14].

APPENDIX 4 – More detailed Information on calculated Hoop Stress

Analysis of Residual Hoop Stress Result

Hoop stresses are the stresses parallel to the weld bead direction and these are developed as a result of the expansion and contraction of the weld region in the radial direction during the heating and cooling occurrences in the course of the welding procedure. The distribution of the residual hoop stress for the exterior and interior surfaces of the pipe at different positions from the weld start position W_L are shown in figures below. It can be seen that the large tensile and comprehensive hoop stresses are present on the interior and exterior surfaces of the cylinder within the locality of the Weld line W_L. The reverse is the case; that is stress reduction and stress reversal away from the weld line just as is the case with axial stress. This phenomenon is also confirmed by (Dar et al, 2009). The disparity in the value of the hoop stress is solely due to varying weld parameters such as material properties and heat source parameters.

2mm Clad Pipe

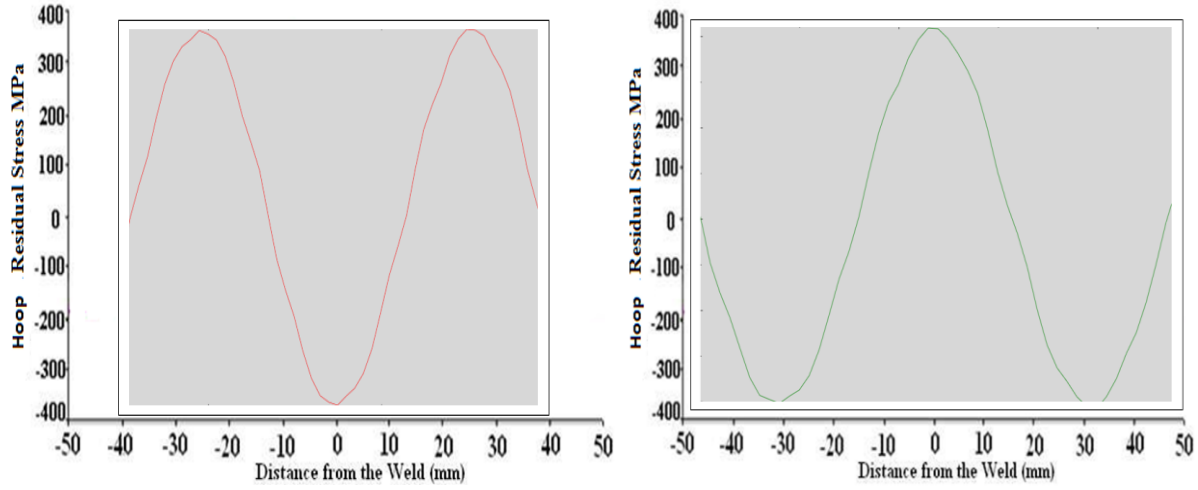

Figure 10.1 (a) Residual hoop stresses versus distance curve on the outer and (b) inner surfaces of the HAZ

Proceedings of the ASME 2020 39th International
Conference on Ocean, Offshore and Arctic Engineering
OMAE2020
August 3-7, 2020, Virtual, Online

OMAE2020-18897

CLAMPING EFFECT ON THE WELDING DEFORMATIONS IN DISSIMILAR WELDED PIPES (JOINTS) WITH VARIED THICKNESSES: AXIAL AND RADIAL SHRINKAGE

Bridget Kogo[1*], Bin Wang[1]
Department of Mechanical, Civil and Aerospace
Brunel University London, UK

Mahmoud Chizari[2]
Senior Lecturer in Mechanical Engineering
University of Hertfordshire, UK
Sharif University of Technology, Ir

ABSTRACT

This study investigates and evaluates the welding residual stresses and deformations in the dissimilar material MSSS metals in order to verify the clamping effect on the residual stresses and deformations and entails comparison with the finite element simulation, the critically reflected longitudinal ultrasonic stress measurement and the hole-drilling residual stresses in a Butt-welded plate courtesy of Javadi et al [1]. The angular shrinkage measurement and vertical displacement were used to achieve this objective. The outcome of the study proved that the measurement of residual stress using protractor is an effective way of differentiating the influence of clamps on the longitudinal stresses.

Keywords: welding deformation, clamping, dissimilar material, axial and radial shrinkage and residual stress

NOMENCLATURE

$\partial\Omega$	domain
H	enthalpy
k	thermal conductivity
n	outward normal domain vector
Q	internal heat source
q	density of the heat flux
T	temperature
T_P	prescribed temperature
t	time
AISI	American International Standard
ASTM	American Society of Testing Materials
CAE	Computer Aided Design
CMM	Coordinate Measuring Machine
DC2D4	2d Linear Heat Transfer Quadrilateral
FEA	Finite element analysis
LCR	Criticaly Reflected Longitudinal
MPa	Mega Pascal
MSSS	Mild Steel Stainless Steels
HAZ	Heat Affected Zone
TIG	Tungsten Inert Gas

INTRODUCTION

In the current study Butt welding of two dissimilar materials; stainless steel of grade AISI 316 and mild steel of grade CR4 was carried out with the aid of the tungsten inert gas welding process (TIG) at a voltage of 240volts using metal filler elements of A15 copper wire and 304/316 SS filler metals for the carbon steel and stainless steel sections of the weld, at the Brunel University's laboratory.

Different thicknesses (2mm and 12mm) of stainless steel clad in the dissimilar material clad joints has been investigated and examined and the dissimilar interface region in adjacent clads investigated to study the shrinkage occurring in the dissimilar welded joint.

* Contact author: Bridget Kogo, Department of Mechanical Aerospace and Civil Engineering, Brunel University London. biddyagada@yahoo.com

Proceedings of the ASME 2020
Pressure Vessels & Piping Conference
PVP2020
July 20-24, 2020, Virtual, Online

PVP2020-21694

VERIFICATION OF STRESS MODEL IN DISSIMILAR MATERIALS OF VARYING CLADDED PIPES USING A SIMILAR CLADDED PLATE MODEL

Bridget Kogo[1•], **Bin Wang** [1]
School of Engineering and Physical Sciences
Department of Mechanical, Civil and Aerospace
Brunel University London, UK

Mahmoud Chizari [2+]
[2] Department of Engineering
University of Hertfordshire, UK
[+] Sharif University of Technology, Iran

Luiz Wrobel [3§]
[3] Department of Mechanical, Civil and Aerospace
Brunel University London, UK
[§] PUC-Rio, Rio de Janeiro, Brazil

ABSTRACT

This paper continues previous research performed by the authors on the modelling of dissimilar welded joints with varying clad thicknesses. This study aims to validate the use of a clad plate model as a replacement to the previous clad pipe model. To fulfill the hypothesis of the study, possible deformation or angular shrinkages occurring at weld joints have been simulated using a commercial finite element software. In parallel, angular shrinkages have been validated using the experimental data with the underlying concept of Gaussian transformation of plates into pipes. The welding of the two dissimilar materials has been carried out in-house with the aid of a Tungsten Arc weld with dynamic measurement of the temperature profile in the vicinity areas of the welding track using high temperature thermocouples. It was discovered that for each deformation angle of 11.5°, 22.75°, 40° and 45°, there exists shrinkage of the order of 0.01mm. Transient temperature curves have been generated for different cladding thicknesses (of stainless steel and mild steel). Comparison of the measured data versus the simulation results shows close agreement.

Keywords: welding deformation, dissimilar material, cladded plate model, cladded pipes and Finite Element Analysis.

NOMENCLATURE

CAE	Computer Aided Design
CMM	Coordinate Measuring Machine
C3D10	10-node quadratic tetrahedron
FEA	Finite Element Analysis
FEM	Finite Element Model
FZ	Fusion Zone
GMAW	Gas Metal Arc
HAZ	Heat Affected Zone
MPa	Mega Pascal
MSSS	Mild Steel Stainless Steels
PM	Parent Metal
TIG	Tungsten Inert Gas

INTRODUCTION

In previous studies, the weld integrity of clad pipes was discussed by current authors and others [1-7]. Previous researches aimed to address the residual stresses present in the welding of two dissimilar materials and explains the reasons for the stress distributions observed in two clad thicknesses of the welded metals [8-13].

Certain shrinkage can be observed in Butt welds and although this could be substantial in thin walled stainless steel pipes, the main reason is related to the thermal expansion coefficient. The shrinkage of stainless steel can be approximately one and half times that of carbon steel. Localized residual stresses in excess of the yield strength are produced during solidification of the metal in the weld and in the heat affected zone, causing redistribution of stresses. While strain values of 1.4% and 3.4% were observed for larger and smaller pipes in the

[•] Contact author: Bridget Kogo, Department of Mechanical Aerospace and Civil Engineering, Brunel University London. biddyagada@yahoo.com

APPENDIX 5 – More detailed Information on calculated Shrinkage

Radial shrinkage and Axial Shrinkage

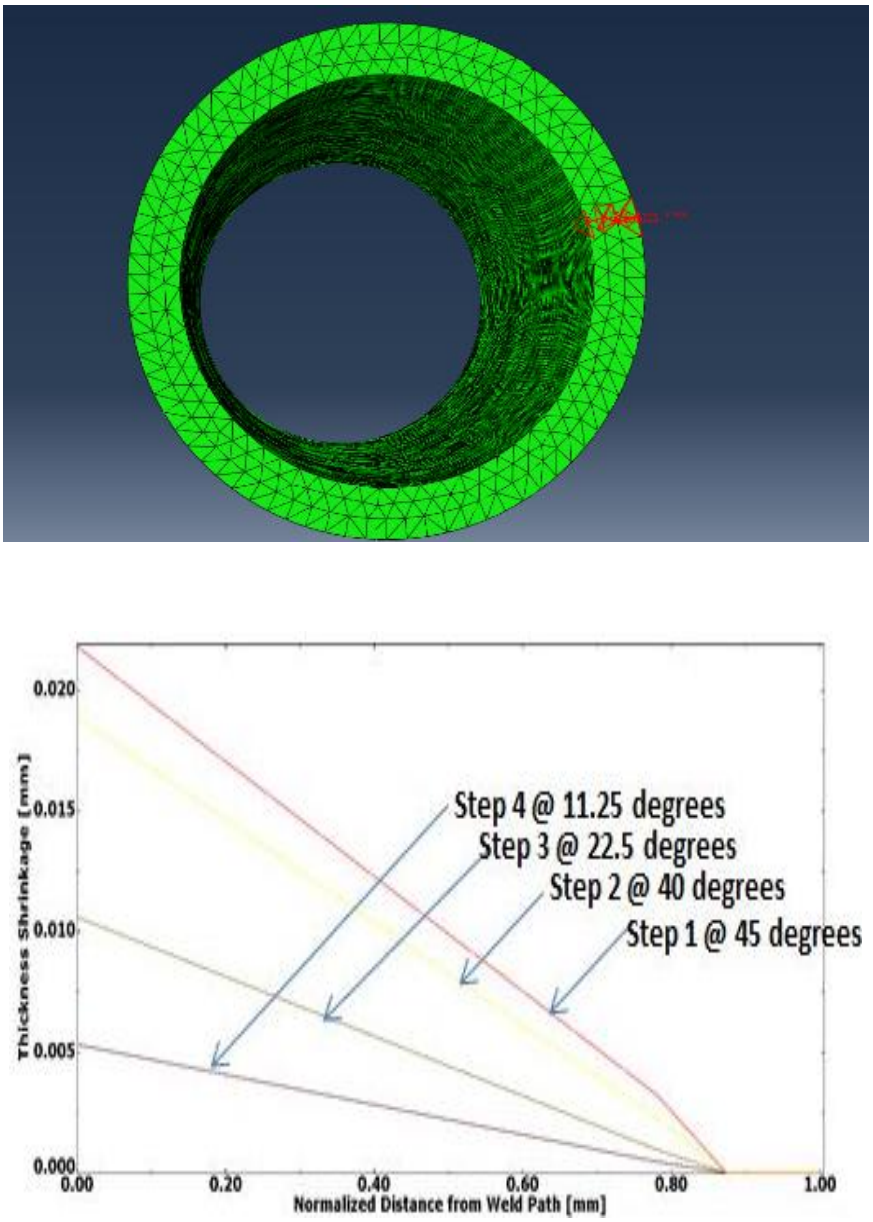

Fig 11.1 (a) Pipe model showing nodal readings for radial shrinkage (b) Radial shrinkage versus normalized distance curve on outer surface of 12 mm clad pipe end

When the weldment cools down, there is usually an axial inclination of the constraint free end of the pipe taking place. The thickness of the pipe is considered for the radial shrinkage and measured for four different increments, so that the shrinkage in thickness could be appreciated

as shown in Figure 11.1. At a tilt angle of 45 degrees, the radial shrinkage is 0.022 mm, and similarly at at an angle of 27.5 degrees, the radial shrinkage is 0.010 mm.

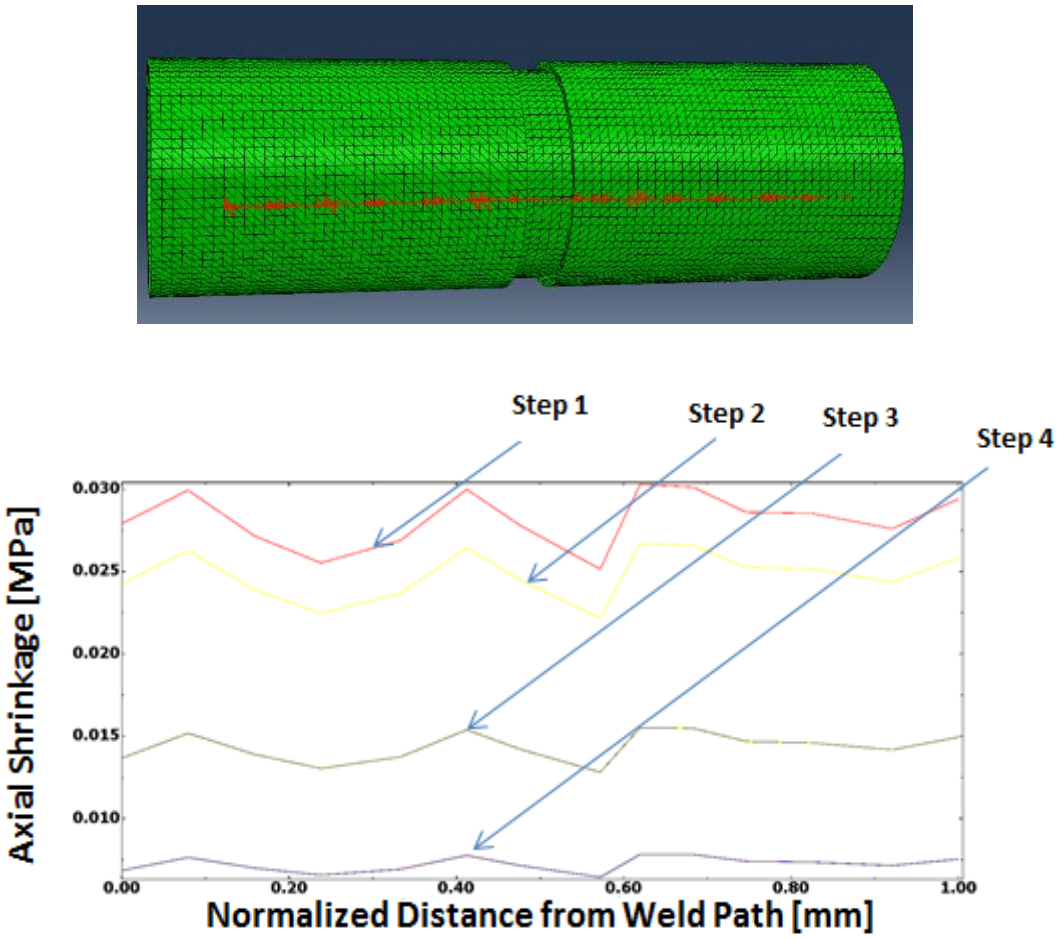

Fig. 11.2 (a) Pipe model showing nodal points for axial shrinkage (b) axial shrinkage versus normalized distance curve on outer surface of HAZ of the 12 mm clad pipe

For four different increments of the axial lenght, the shrinkage is measured and plotted against the normalized distance from the weld path as dhown in Figure 11.2. The axial shrinkage at lower increments is slightly different from those at higher increments, because there are high thermal gradients experienced during butt welding leading to residual stress and discrepancy in hardness, hence a creep effect is observed at higher increments.

APPENDIX 6 – Additional Comparison with Published Experimental Work

Neutron Diffraction (ND) Measured Stress Curve

Being part of a team involved in carryng out Narrow Gap Weld experiment and measurement at subsea 7 standard laboratory in Glassgow, the ND measured stress was carried out and here is the curve obtained from the weld measuremnt. The Residual, Axial and Hoop stress measurement are displayed below. Residual Axial Stress on the inside of the pipe with outer diameter of 14 inch, wall thickness of 19.05 mm and a length of 750 mm. A typical ND Measured Stress showing the stress distributions is shown in the Figure 12.1.

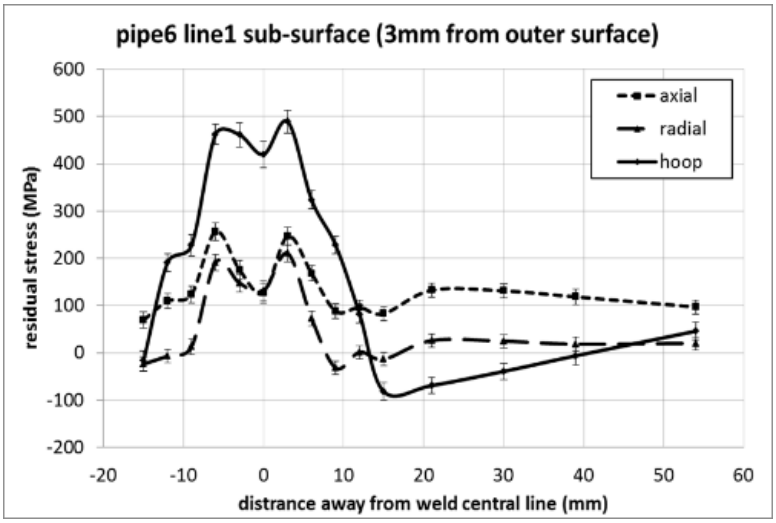

Figure 12.1 A typical Neutron Diffraction (ND) Measured Stress showign the residual axial, radial and hoop stress distributions on the inner surface of pipe (Ren, 2018)

Observations:

Close to the region of weld comprehensive axial, radial and hoop stresses can be observed but farther away from the weld region, tensile stresses become the trend.

From the results of the simulated axial stress and the typical ND measured stress showing the residual axial, radial and hoop stress distributions on the inner surface of pipe the following can be deduced:

1. Close to the region of weld comprehensive axial, radial and hoop stresses can be observed but farther away from the weld region, tensile stresses become the trend. These findings comply with the welding procedure as discussed in chapter one under section 2.3.1 Weld Induced Residual Stresses and Distortions under Chapter 2.
2. Also, by reason of the symmetry across the weld line $W_{L,}$ the axial, radial and hoop stresses are symmetric in nature
3. The result of the ND measured stress experiment at the Subsea 7 standard laboratory, further confirms the validity of the simulation carried out in this research.

APPENDIX 7 – Additional Information on Simulated Results with Experimental Data in Open Literature

Residual stresss validity of 12 mm and 2mm cladded pipe – Internal surface with (Feli et al., 2012)

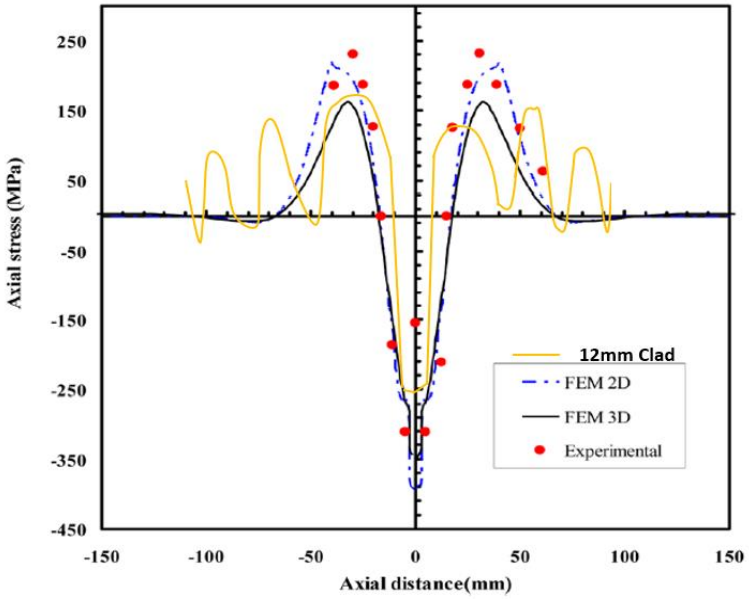

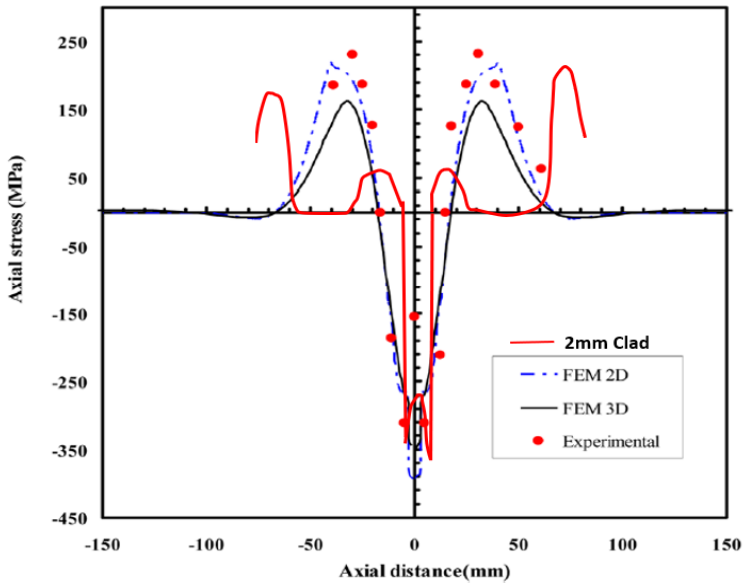

12 mm and 2mm cladded pipe – External surface. Residual stress validated by (Feli et al., 2012)

Residual stress validity of 12 mm and 2 mm cladded pipe – Internal surface by (Feli et al., 2012)

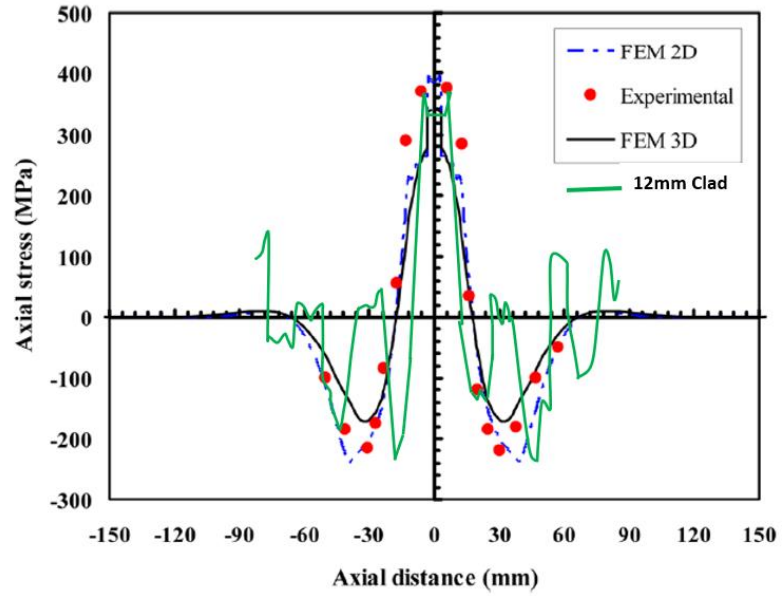

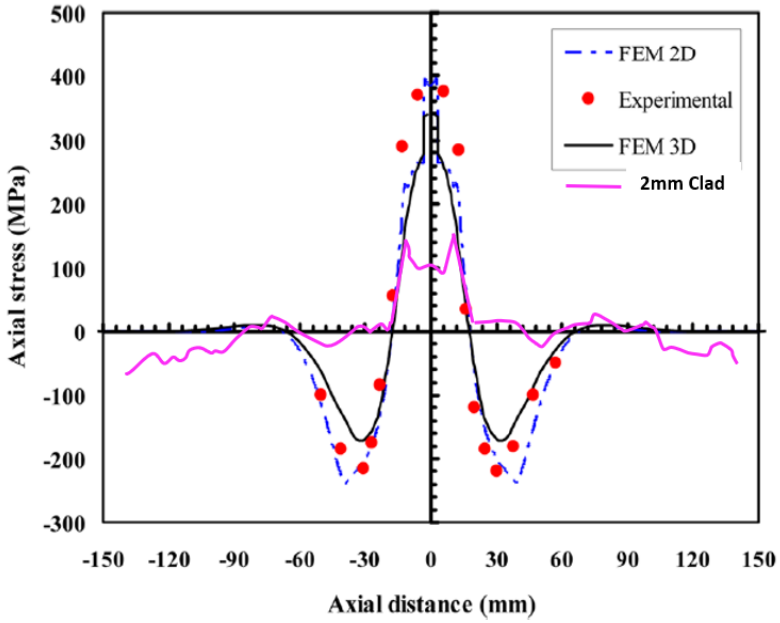

12 mm and 2mm cladded pipe – Internal surface. Residual stress validated with (Feli et al., 2012)

Residual stress validity of 12 mm and 2 mm cladded pipe – External surface with (Sinha et al., 2013)

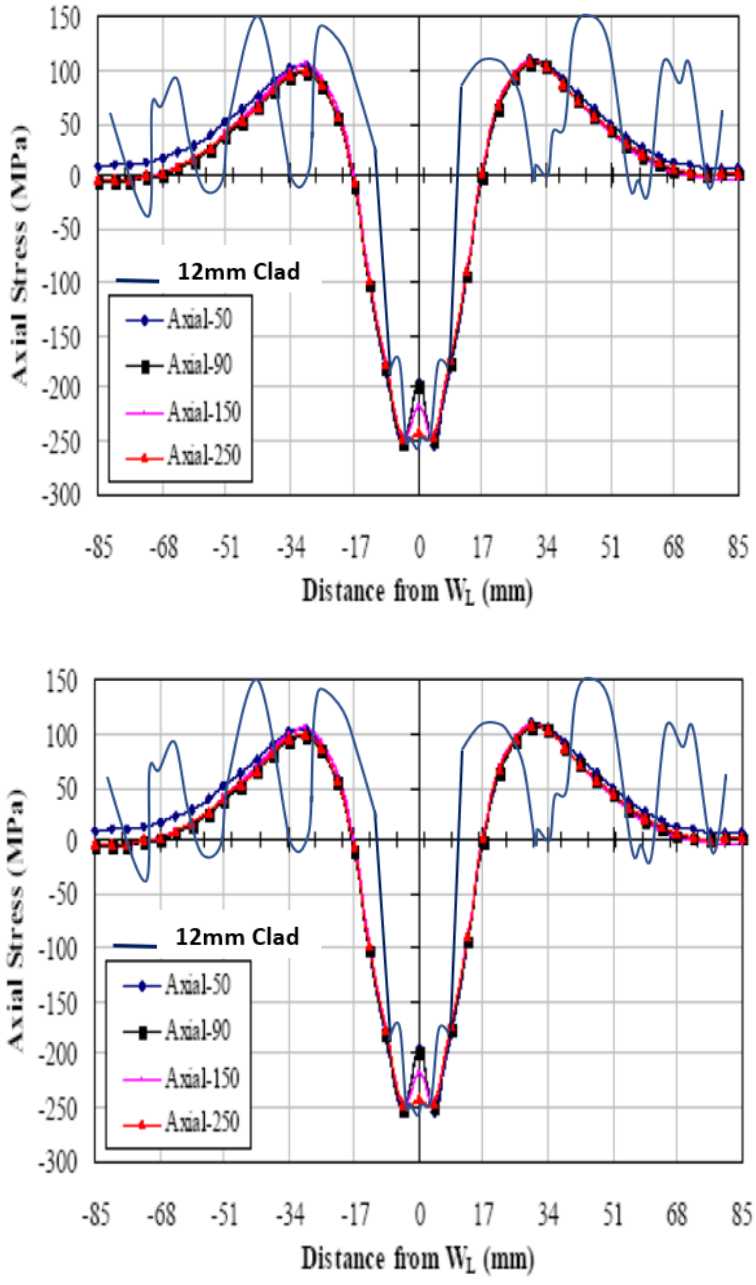

12 mm and 2mm cladded pipe – External surface. Residual stress validated with (Sinha et al., 2013)

Residual stress validity of 12 mm and 2mm cladded pipe – Internal surface with (Sinha et al., 2013)

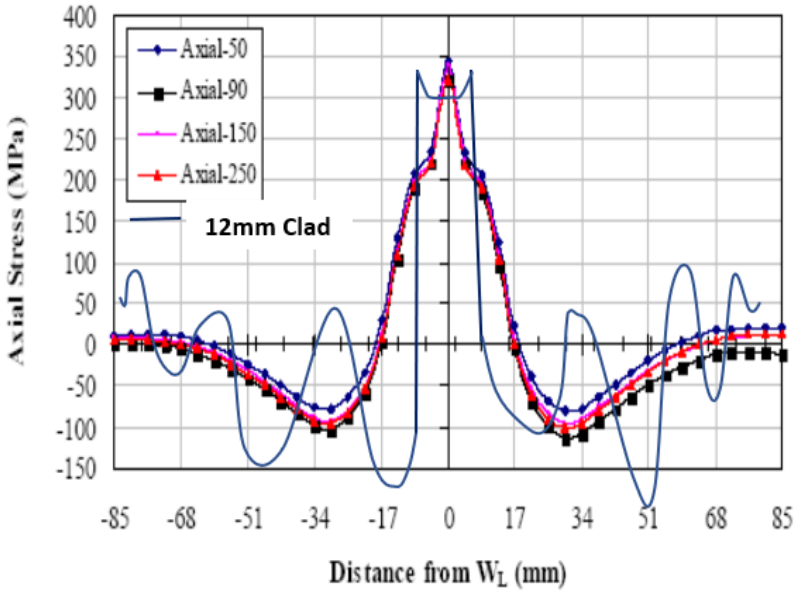

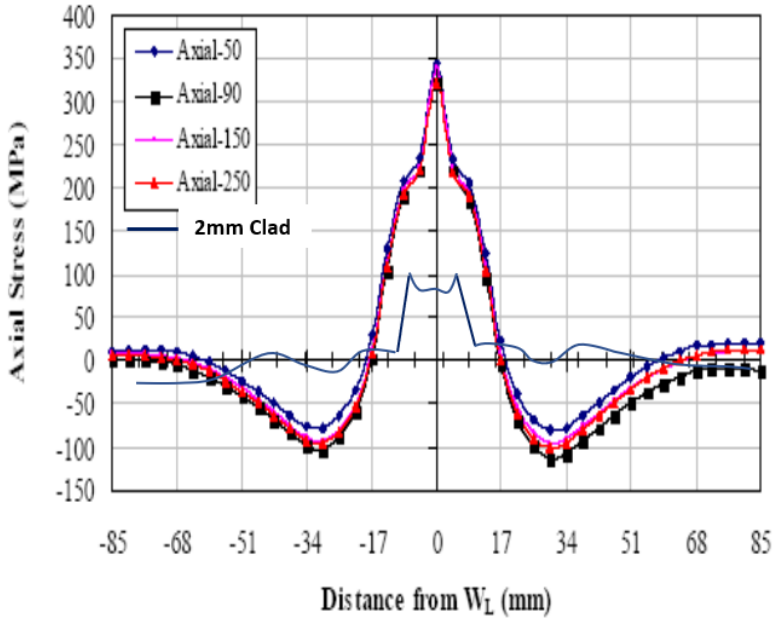

12 mm and 2mm cladded pipe – Internal surface. Residual stress validated with (Sinha et al., 2013)

Residual stress validity of 12 mm and 2mm cladded pipe – External surface by Dar et al, 2009)

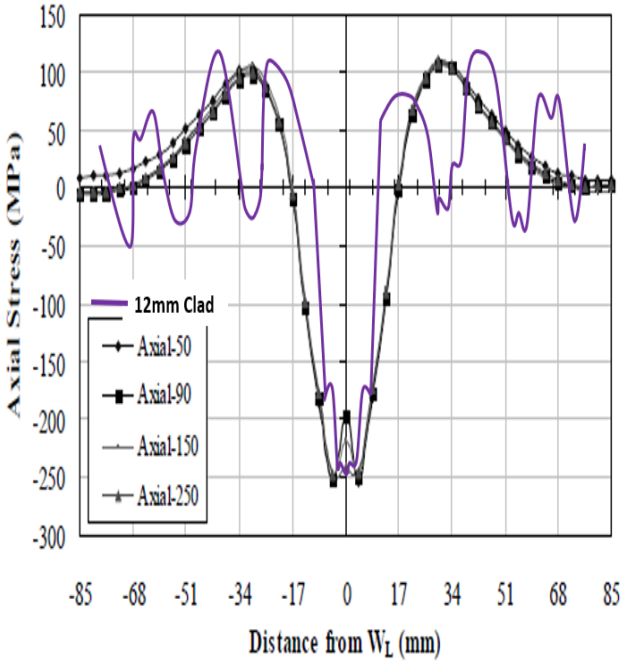

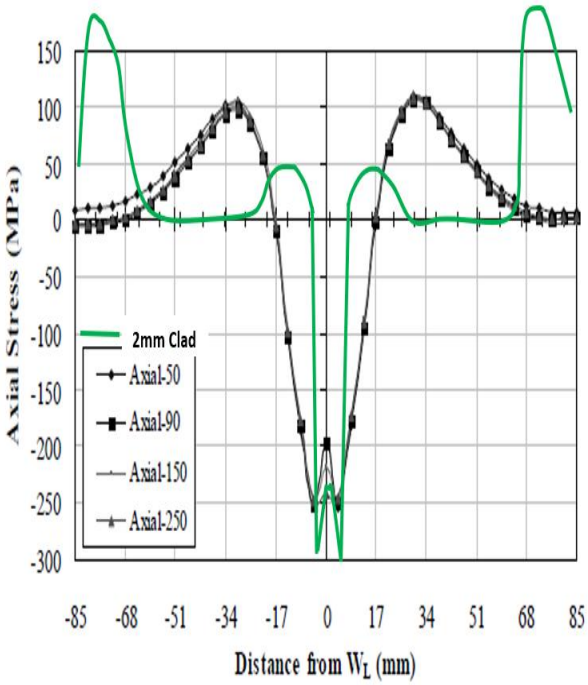

12 mm and 2mm cladded pipe – External surface. Residual stress validated by (Dar et al., 2009)

12 mm and 2mm cladded pipe – Internal surface. Residual stress validated by (Dar et al., 2009)

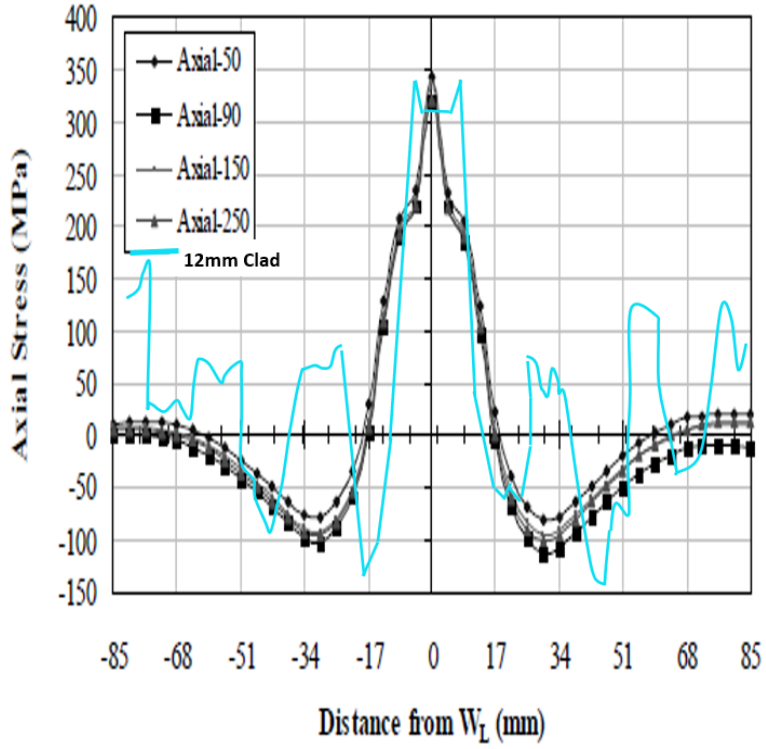

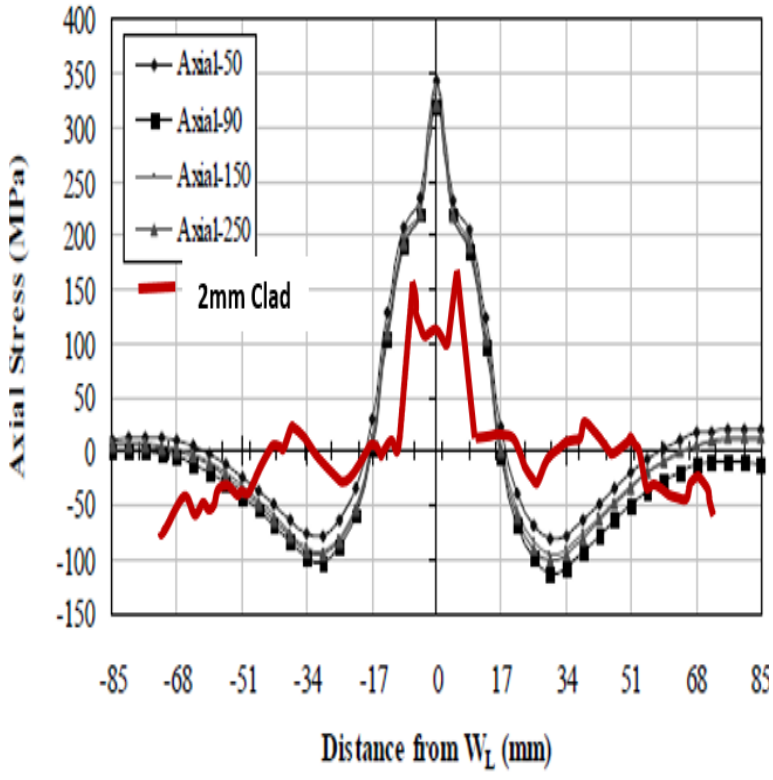

12 mm and 2mm cladded pipe – Internal surface. Residual stress validated by (Dar et al., 2009)

12 mm and 2 mm cladded pipe – External surface. Residual stress validated by (Deng & Murakawa, 2006)

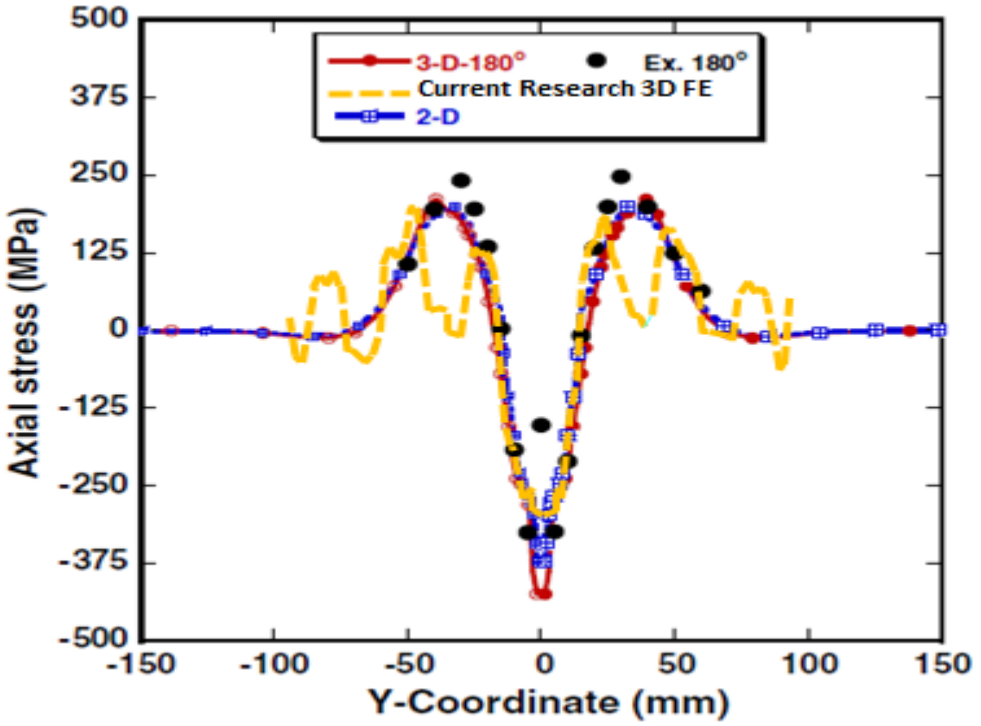

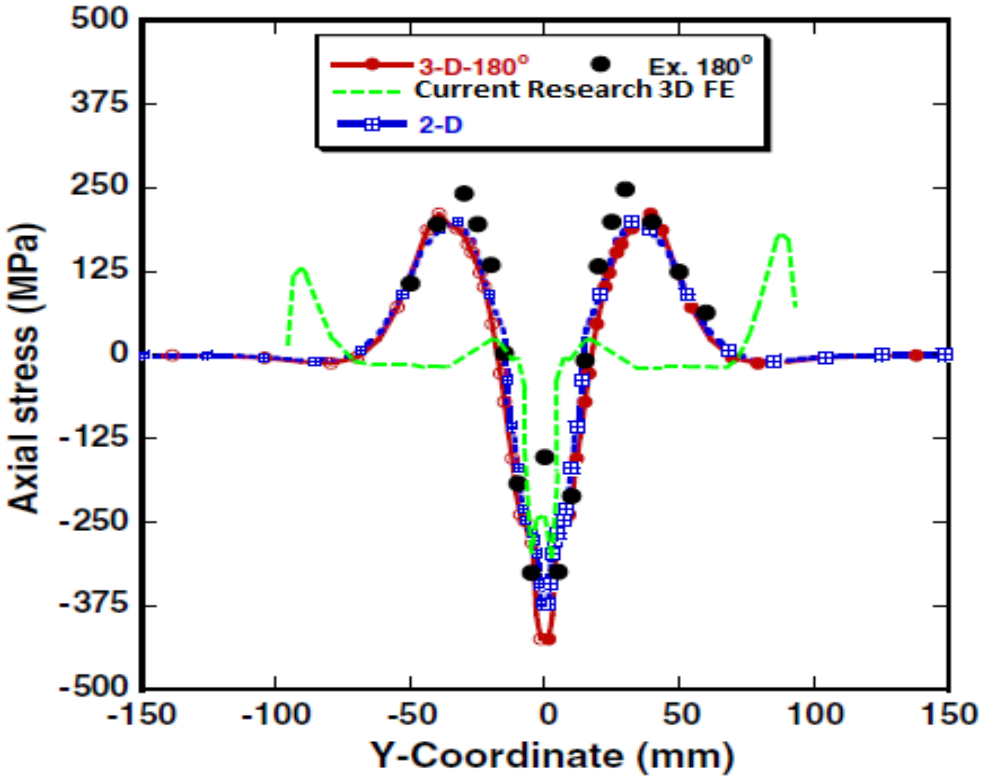

12 mm and 2mm cladded pipe – Internal surface. Residual stress validated by (Deng & Murakawa, 2006)

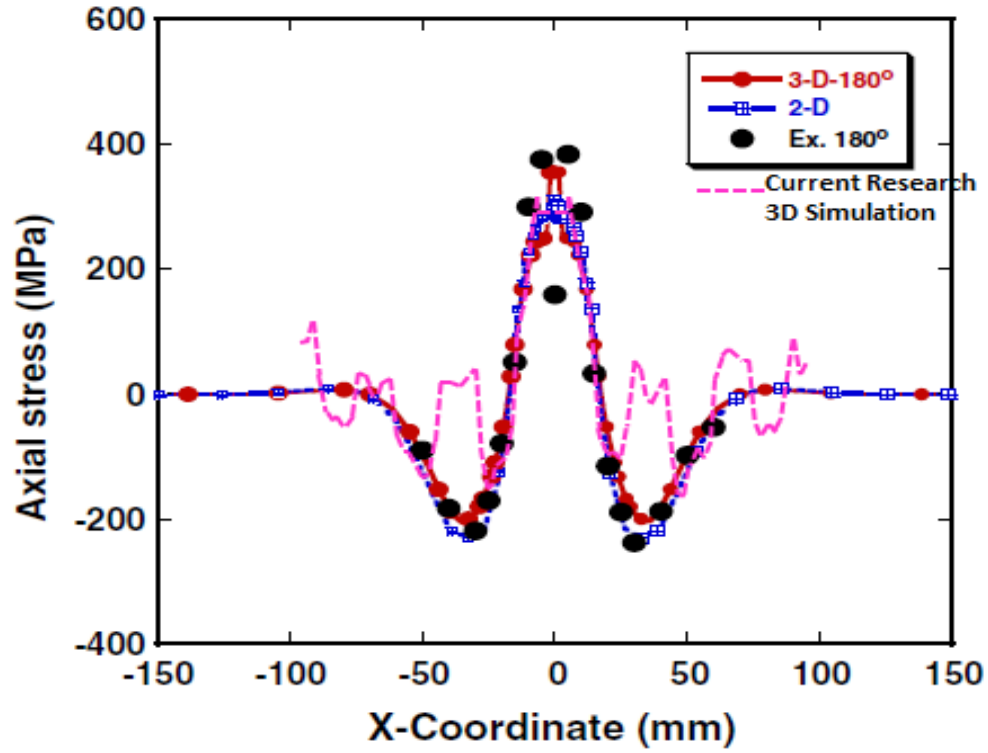

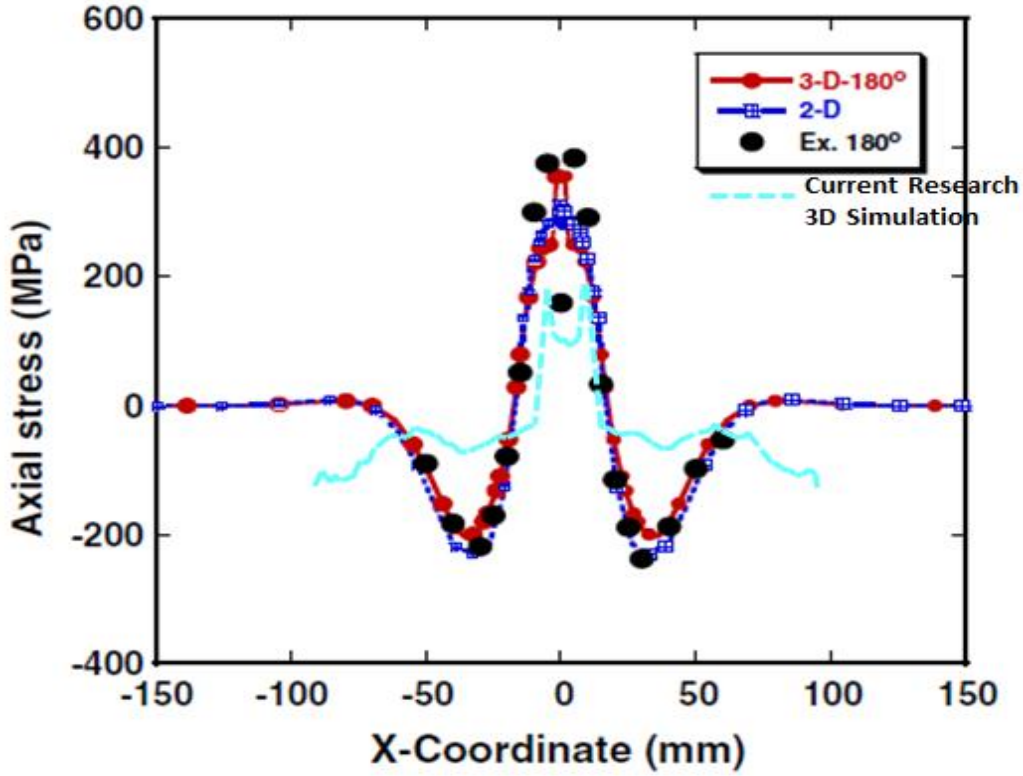

12 mm and 2mm cladded pipe – External surface. Residual stress validated by (Jonsson & Josefson, 1988)